

# STUDIA

UNIVERSITATIS BABEŞ-BOLYAI

CHEMIA

1 - 2

1995

CLUJ-NAPOCA

**REDACTOR ȘEF: Prof. A. MARGA**

**REDACTORI ȘEFI ADJUNCȚI: Prof. N. COMAN, prof. A. MAGYARI, prof. I. A. RUS, prof. C. TULAI**

**COMITETUL DE REDACȚIE AL SERIEI CHIMIE: Prof. S. GOCAN, prof. L. LITERAT, prof. S. MAGER (redactor coordonator), prof. L. ONICIU, prof. I. SILBERG, conf. N. DULĂMIȚĂ, conf. L. SILAGHI-DUMITRESCU (secretar de redacție)**

**TEHNOREDACTARE COMPUTERIZATĂ: M. TOPLICEANU**

# S T U D I A

## UNIVERSITATIS BABEȘ-BOLYAI

### CHEMIA

1 - 2

---

Redacția : 3400 CLUJ-NAPOCA str. M. Kogălniceanu nr.1 ▶ Telefon : 194315

---

#### SUMAR - CONTENTS - SOMMAIRE

E. A. CORDOS, T. FRENTIU, S. D. ANGHEL, A.M. RUSU, M. PONTA, S. NEGOESCU, Analysis of Calcium, Natrium and Lithium Using a Capacitively Coupled Argon Plasma Atomic Emission Spectrometry	1
E. A. CORDOS, T. FRENTIU, A. FODOR M. PONTA, A.M. RUSU, L. KEKEDY, Figures of Merit for a Sequential Spectrometer with Inductively Coupled Argon Plasma Source	13
A. PATRUT, C. ROSU, H. P. BECK, Heteropolyoxometalate Anions of Bismuth(III), I. Anions with pseudo-Dawson-Wells Structure	21
A. PATRUT, C. ROSU, H. P. BECK, Heteropolyoxometalate Anions of Bismuth(III), I. Anions with pseudo-Keggin Structure	29
C. ROMAN, O. BODEA, A. LEVI, N. PRODAN, E. CORDOS, I. MANOVICIU, Capacitive-Type Humidity Sensors Based on Methacrylate-Co-Polymer and Poliamide	35
M. STANCA, Z. BOCSKAI, A. MAICANEANU, Decyanidation of Industrial Waters Through Ozonization	41
F. FORGACIU, M. NEMEȘ, E.J. POPOVICI, V. URSU, D. MACAROVICI, The Influence of Precipitation Conditions on the Quality of Calcium Tungstate used in Phosphor Synthesis	47
E. J. POPOVICI, M. ANECULĂESE, V. URSU, D. MACAROVICI, Studies on the Synthesis of Silver Activated Zinc Sulphide Phosphor	55
M. ANECULĂESE, E. J. POPOVICI, V. URSU, D. MACAROVICI, Attempts on the Synthesis of Zinc Sulphide Phosphorus Activated by Lead	63
C. COSTACHE, S. GOCAN, GH. COMAN, R. ZABAVA, Studies for Detection and Quantification of Triazines Residues	71
S. GOCAN, GH. COMAN, C. COSTACHE, C. DRAGHICI, Using Affinity Chromatography in Biomolecules Separation	77
L. SILAGHI-DUMITRESCU, A. HAIDUC, Diphenylantimony(III) Diorganoarsinate and Tioarsinate Synthesis and Spectral Characterisation	83
I. SILAGHI-DUMITRESCU, I. HAIDUC, On the Geometry and Electronic Structure of $\text{XH}_2\text{SiNH}_2(\text{X}=\text{F}, \text{Cl}, \text{Br})$ Silanes. MNDO Molecular Orbital Calculations	91
M. HORN, I. GROSU, S. MAGER, Synthesis and Conformational Analysis of some 2-Alkylloxycarbonyl	

Substituted 1,3-Dioxanes .....	99
E. M. RUS, The effect of Phosphoric Acid on the Electrochemical Behaviour of Lead Acid Battery Positive Electrode .....	109
C. MURESANU, I. BALDEA, L. ONICIU, The Oxidation of Benzyl Alcohol by Cerium (IV) in Sulfuric Media .....	119
M. BUTAN, C. M. POP, M. DIUDEA, QSAR Study on a Set of Imidazole Derivates with Antimicrobial and Antimicotic Activity .....	129
S. COBZAC, T. HODIȘAN, TLC Determination of Caffeine from some Beverage Using Solid Phase Extraction .....	139
E. M. RUS, Aspects of the Electroreduction of Anodic Layers Formed on Lead in Sulphuric Acid Solutions .....	145
S. GOCAN, G. CIMPAN, Quantitative Analysis of some Benzodiazepines by Thin Layer Chromatography-Densitometry and UV spectrometry. A comparative study .....	155
L. MURESAN, I. C. POPESCU, L. ONICIU, Transition Metal Hexacyanoferrates (III) Modified Electrodes. I. characterisation of Co, Ni and Cu Hexacyanoferrate Modified Rotating Disk Electrodes .....	161
I. CRISTEA, I. PANEA Synthesis and Stereo chemistry of some 4-Arylidene-1-Pyrimidinyl-2-Pyrazolin-5-ones .....	171
T. HODISAN, C. CIMPOIU, V. HOISAN, C. SARBU, Study of Free Amino-Acids from Equisetum Extract .....	177
M. CURTUI, I. HAIDUC, C. POP, Solvent Extraction of Dioxouranium(IV) with Diisopropyldithiophosphoric Acid and Triphenylphosphine Oxide .....	183
L. MUNTEAN, I. GROSU, S. MAGER, Synthesis of 1,3-Oxathiane and Perhydro-1,3-Thiazine Derivates .....	189
F.D. IRIMIE, A. MORAR, M. BOJIN, Catalytic Antibodies .....	209
<b>Book Review .....</b>	<b>253</b>

---

**Analysis of Calcium, Sodium and Lithium Using a Capacitively Coupled Argon Plasma Atomic Emission Spectrometry**

Emil A. Cordos, Tiberiu Frentiu,  
Sorin D. Anghel, Ana-Maria Rusu,  
Michaela Ponta and Sorin Negoescu 1

A capacitively coupled argon plasma in tip-ring electrode geometry operated at 85-275 W and 27.12 MHz is used in the determination of Ca, Li, Na. The best detection limits are 15, 13 and 9 ng ml<sup>-1</sup> for Ca, Na and Li, respectively. The self-absorption effect is similar to that in the arc source. The experimental results for Ca determination in blood samples are similar to those obtained by traditionally established spectral methods.

---

**Figures of Merit for a Sequential Spectrometer with Inductively Coupled Argon Plasma Source**

Emil A. Cordos, Tiberiu Frentiu,  
Sorin D. Anghel, Ana-Maria Rusu,  
Michaela Ponta and Sorin Negoescu 13

Figures of merit for a sequential emission spectrometer with inductively coupled argon plasma source are assessed on the basis of 10 elements determination in steel certified materials. Limits of detection for Al, Co, Cr, Cu, Mn, Mo, Ni, Si, Ti and V agree with those obtained for standard inductively coupled plasma (1 kW).

---

**Heteropolyoxometalate Anions of Bismuth(III)  
I. Anions with pseudo-Dawson-Wells Structure**

A. Pătruț, C. Roșu and H. P. Beck

21

1:1 complexes were prepared through the reaction between the [H<sub>3</sub>BiW<sub>18</sub>O<sub>60</sub>]<sup>6-</sup> heteropolyoxometalate anion and transition metal cations (Mn<sup>2+</sup>, Co<sup>2+</sup> and Ni<sup>2+</sup>). The potassium salts of the starting anion and of the complexes were investigated. A pseudo-Dawson-Wells structure is proposed and discussed.

---

**Heteropolyoxometalate Anions of Bismuth(III)  
II. Anions with pseudo-Keggin Structure**

A. Pătruț, C. Roșu and H. P. Beck

29

1:1 complexes were prepared through the reaction between the [H<sub>3</sub>BiW<sub>11</sub>O<sub>38</sub>]<sup>6-</sup> heteropolyoxometalate anion and transition metal cations (Mn<sup>2+</sup>, Co<sup>2+</sup> and Ni<sup>2+</sup>). The potassium salts of the starting anion and of the complexes were investigated. A pseudo-Keggin structure is proposed and discussed.

---

**Capacitive-type humidity sensor based on methacrylate-co-polymer and capacitive-type humidity sensor using polyimide**

C. Roman, O. Bodea, A. Levi,  
N. Prodan, E. Cordoș, I. Manovicu 35

Two types of capacitive-type humidity sensors have been prepared using: (i) cross-linked poly(methyl methacrylate-co-(2-hydroxy-propyl-methacrylate)); (ii) commercially polyimide. The sensors have been prepared in a sandwich structure: alumina substrate + lower gold electrodes + thin film polymer + upper gold electrode. The sensitivity (the ratio of capacitance at "X" % RH to that at 12% RH), the hysteresis, the response type, the durability against acetone vaporous and the drift of the two sensors have been measured and compared. The characteristics of the capacitive-type humidity sensor using methacrylate-co-polymer are better than the sensor prepared using polyimide.

---

**Decyanidation of Industrial Waters Through Ozonization**

M. Stanca, Z. Bockasai, A. Maicaneanu

41

In this paper it is presented a study of the action of ozone on cyanide ion in a watery medium, to determine the consumption of ozone in a certain time and the influence of pH and of cooper ions on the reaction of oxidation.

---

**The Influence of Precipitation Conditions on the Quality of Calcium Tungstate Used In Phosphor Synthesis**

F. Forgaciu, M. Nemes, E.J. Popovici, V. Ursu, Dan Macarovici

47

Calcium tungstate used in phosphor synthesis was precipitated from  $\text{CaCl}_2$  and  $\text{Na}_2\text{WO}_4$  solutions. The influence of precipitation conditions on the quality of  $\text{CaWO}_4$  precipitate was studied. It has been ascertained that the reagent concentration, the temperature and the pH of the precipitation medium determine the purity, morpho-crystalline structure and particle size distribution of  $\text{CaWO}_4$ -precipitate thus influencing the luminescent properties of  $\text{CaWO}_4$ -phosphor samples. The optimum precipitation conditions for calcium tungstate used in phosphor synthesis were established.

---

**Studies on the Synthesis of Silver Activated Zinc Sulphide Phosphor**

E.J. Popovici, M. Aneculăese, V. Ursu, D. Macarovici

55

The zinc sulphide prepared by thiosulphate method was converted by thermal synthesis into  $\text{ZnS:Ag,Cl}$  phosphor samples. The concentration of silver activator, the nature of alkaline or alkaline-earth chloride used as a flux, as well as the calcination conditions influence on the crystalline structure, particle size distribution and luminescent properties of phosphor samples. The optimum preparation conditions were selected so that a  $\text{ZnS:Ag,Cl}$  phosphor with well defined and reproducible properties might be prepared.

---

**Attempts on the Synthesis of Zinc Sulphide Phosphorus Activated by Lead**

M. Aneculăese, E.J. Popovici, V. Ursu, D. Macarovici

63

The present paper reports some preliminary tests concerning the lead activation sulphide obtained by thiosulphate method. The  $\text{ZnS:Cl}$ ,  $\text{ZnS:Pb, Cl}$  and  $\text{ZnS:Pb}$  samples were prepared by thermal synthesis with or without alkaline or alkaline-earth chlorides as flux. The emission and excitation spectra revealed that, in our work conditions, both self activated and lead centres are formed resulting in a simultaneous blue and yellow-orange emission. The phosphor samples prepared with diferent fluxes exhibit various luminescence colours.

---

**Studies for detection and quantification of triazine residues**

In this study we used the atrazine as a hapten in order to prepare, separate, purify and label with peroxidase, specific immunoglobulins. For atrazine we established the correlation curve between its concentration and induced inhibition in a competitive ELISA. For our immunochemical system the detection limit of atrazine traces is 0.05 ng/ml.

---

Claudia Costache, S. Gocan, Gh. Coman, R. Zăbavă 71

**Using affinity chromatography in biomolecules separation**

In this study we presented in extend a method of separation based on the affinity antigen-anticorp interactions. The stationary phase is obtained by covalently binding of IgG on a matrix (Sephrose 4B). The immunoglobulins from the sample are specifically adsorbed by the complementary ligand and then eluted separated.

S. Gocan, Gh. Coman, Claudia Costache, 77  
Camelia Drăghici

**Diphenylantimony(III) Diorganoarsinate and Tioarsinate Synthesis and Spectral Characterisation**

L. Silaghi-Dumitrescu, A. Haiduc

83

Diphenylantimony(III) dimethyl -and diphenylarsinate and dimethylthioarsinate were prepared and characterised by their IR and mass spectra. Bidentate oragnoarsinic ligands are present in the synthesised compounds. The fragmentation pattern under electron impact is in agreement with a greater affinity of oxygen for arsenic than for antimony.

**On the Geometry and Electronic Structure of  $XH_2SiNH_2$  ( $X=F, Cl, Br$ ) Silanes. MNDO Molecular Orbital Calculations**

I. Silaghi-Dumitrescu, I. Haiduc

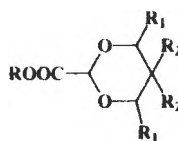
91

Full optimized geometry of the title compounds have been determined by MNDO molecular orbital calculations. As a result of the interplay between the Si( $\sigma$ )-N( $\sigma$ ) interactions and hyperconjugative effects, the Si-N and Si-H bond lengths decrease by substitution of fluorine for a heavier halogen. The energies and simmetry of the unoccupied mo's suggest that Cl(Br)H<sub>2</sub>SiNH<sub>2</sub> are better candidates for cyclodimerization than FH<sub>2</sub>SiNH<sub>2</sub>.

**Synthesis and Conformational Analysis of Some 2-Alkyloxycarbonyl Substituted 1,3-Dioxanes**

The synthesis, stereochemistry and NMR spectra of some 1,3-dioxane derivatives bearing acid or ester groups in the acetal part of the heterocycle are discussed

Mihai Horn, Ion Grosu and Sorin Mager



R=H, C<sub>2</sub>H<sub>5</sub>

R<sub>1</sub>=H, CH<sub>3</sub>

R<sub>2</sub>=H, CH<sub>3</sub>

99

**The Effect of Phosphoric Acid on the Electrochemical Behaviour of Lead Acid Battery Positive Electrode**

The effect of phosphoric acid on the PbO<sub>2</sub> electrode was examined by cyclic voltammetry. The anodic and cathodic polarization behaviour has been investigated by changing the potential range, sweeping rate and concentration of H<sub>3</sub>PO<sub>4</sub> in electrolyte.

E. M. Rus

109

---

**The Oxidation of Benzyl Alcohol by Cerium(IV) in Sulfuric Media**

C. Mureșanu, I. Bâldea, L. Oniciu

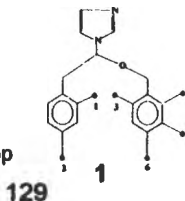
119

The kinetics of the oxidation of the benzyl alcohol to benzaldehyde has been studied in the presence of  $\text{Na}_2\text{SO}_4$  over a wide range of organic substrate and hydrogen ion concentrations. An intermediate complex having the ratio  $\text{Ce(IV)} : \text{C}_6\text{H}_5\text{CH}_2\text{OH}$  of 1:1 has been identified by spectrometrical means. The redox reaction obeys a second-order rate law at hydrogen ion concentration held constant (first order in each,  $\text{Ce(IV)}$  and  $\text{C}_6\text{H}_5\text{CH}_2\text{OH}$ ) but a rather complex dependence associated with  $[\text{H}^+]$ . The kinetics and the dependence of the experimental activation energy of the acidity of the medium indicate the involvement of different reactive  $\text{Ce(IV)}$  sulfatocomplexes in the oxidation process.

---

**QSAR Study on a Set of Imidazole Derivatives with Antimicrobial and Antimycotic Activity**

Mioara Butan, Corina Pop and Mircea V. Diudea



129

A Free-Wilson analysis on a set of 13 imidazole derivatives of general formula 1, indicated different substituent location for either antimicrobial or antimycotic activity.

---

**TLC determination of caffeine from some beverage using solid phase extraction**

Simona Cobzac, T. Hodîșan

139

The paper concerns with caffeine determination from some beverage using SPE as sample preparation. The quantitation was performed using TLC / densitometry. The wavelength was 275nm. The obtained recovery was 93.54%. Our results are comparable with those from literature.

---

**Aspects of the Electroreduction of Anodic Layers formed on Lead in Sulphuric acid Solutions**

E. M. Rus

145

Cyclic voltammetry has been used to study the electroreduction of anodically formed layers on lead electrodes under various experimental conditions. The negative potential sweep curves were recorded at different sweep rates for a range of polarization potentials and times.

---

**Quantitative analysis of some benzodiazepines by thin-layer chromatography - densitometry and UV spectrophotometry. A comparative study.**

Simion Gocan, Gabriela Cîmpan

155

Three benzodiazepines (diazepam, oxazepam, chlordiazepoxid) were quantitatively analyzed by thin layer chromatography - densitometry. A comparative study was performed between two analytical techniques: the classical spectrophotometric method and the proposed one, thin-layer chromatography and densitometry. There are no significant differences between the experimental results obtained by the two methods.



**Transition Metal Hexacyanoferrates (III) Modified Electrodes.**

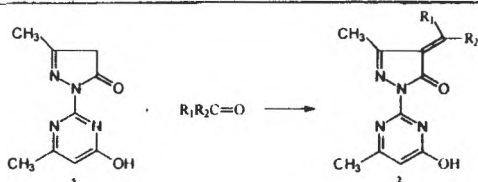
**I. Characterization of Co, Ni and Cu Hexacyanoferrate Modified rotating Disk Electrodes.**

L. Mureşan, I.C. Popescu, L. Oniciu

161

A new metod to obtain cobalt-, nickel- and cooper-hexacyanoferrate(III) modified electrodes based on the use of a rotating disk electrode is presented. The performed complexes were electrosorbed from solution during the elctrode potential scanning. An optimization study concerning the electrode material and the metal hexacyanoferrates preparation, electrochemical (scan rate) and hydrodynamic (rotation speed) conditions, was performed. Ionic selectivity testing for  $\text{Na}^+$ ,  $\text{K}^+$ ,  $\text{Li}^+$  and  $\text{NH}_4^+$  showed that glassy carbon/CoHCF-modified RDE is the most suitable for  $\text{Na}^+$  and Pt/NiHCF- modified RDE for  $\text{K}^+$ .

**Synthesis and stereochemistry of some 4-arylidene-1-pyrimidinyl-2-pyrazolin-5-ones**



Ioan Cristea and Ioan Panea

171

**Study of Free Amino-acids from Equisetum Extract**

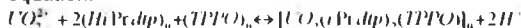
Investigation of Equisetum starting with extraction and ending with identification of the amino-acids she contained, was performed by extraction of dried material with a solution of 1% HCl and by double development bidimensional on cellulose thin layer chromatography plates.

T.Hodişan, Claudia Cimpoi, Viorica Hodişan and C.Sârbu

177

**Solvent extraction of Dioxouranium(VI) with Diisopropyldithiophosphoric Acid and Triphenylphosphine Oxide.**

The extraction equilibrium of dioxouranium(VI) with  $\text{HiPrdtp}$  and  $\text{TPPO}$  in benzenecan be described by equation:



The high solubility of the mixed ligand complex in benzen explains the sinergic increase of the distribution ratio.

M.Curtui, I.Halduc, C.Pop

183

**Synthesis of 1,3-Oxathiane and Perhydro-1,3-Thiazine Derivatives**

A review on the synthesis of 1,3-oxathiane (I) and perhydro-1,3-thiazine (II) derivatives is presented.

Luminița Muntean, Ion Grosu and

Sorin Mager



189



## ANALYSIS OF CALCIUM, NATRIUM AND LITHIUM USING A CAPACITIVELY COUPLED ARGON PLASMA ATOMIC EMISSION SPECTROMETRY

Emil A. Cordos<sup>1</sup>, Tiberiu Frentiu<sup>2</sup>, Sorin D. Anghel<sup>3</sup>, Ana-Maria Rusu<sup>1</sup>,  
Michaela Ponta<sup>1</sup> and Sorin Negoescu<sup>1</sup>

<sup>1</sup> University "Babeș-Bolyai", Dept. of Chemistry, 3400 Cluj-Napoca, Romania

<sup>2</sup> University "Babeș-Bolyai", Dept. of Physics, 3400 Cluj-Napoca, Romania

<sup>3</sup> Research Centre for Analytical Instrumentation, P.O.Box 5-717, 3400 Cluj-Napoca, Romania

**ABSTRACT:** A capacitively coupled argon plasma in tip-ring electrode geometry operated at 85-275 W and 27.12 MHz is used in the determination of Ca, Li, Na. The optimisation of plasma parameters for the analysis is described in detail. The optimum operating conditions are: 185 W, 1 l min<sup>-1</sup> Ar flow and ring electrode at 10 mm height above the tip. The detection limits of 45, 18 and 12 ng ml<sup>-1</sup> with the ring electrode at 40 mm above the tip decrease to 15, 13 and 9 ng ml<sup>-1</sup> for Ca, Na and Li, respectively, when the ring is moved down to 10 mm. The self-absorption effect is similar to that in the arc source and is a function of power level, Ar flow, system geometry and observation height. It considerably decreases as the ring electrode moves downward. The experimental results for Ca determination in blood samples are similar to those obtained by traditionally established spectral methods

### INTRODUCTION

Over the last 30 years several procedures in spectroscopy, electrochemistry, neutron activation analysis and X-ray spectrometry have been developed for the determination of elements either as a free form or in combination. Among spectroscopic methods, inductively coupled plasma atomic emission spectrometry (ICP-AES) and inductively coupled plasma mass spectrometry (ICP-MS) have been used frequently [1, 2]. In recent years radiofrequency capacitively coupled plasma (r.f.CCP) has been developed as an alternative source for ICP with several advantages [1, 3]

Blades and co-workers have reported the use of a r.f.CCP at powers between 30 and 600 W in combination with an electrothermal vaporization system for detection by atomic absorption spectrometry (AAS) and atomic emission

spectrometry (AES) or as a gas-chromatography detector (GC-CCP) for halogenate and organotin compounds [4,5]. Along this line, Platzer *et al.* [6] have also developed a r.f.CCP source with external annular electrodes for element specific detection in GC. A r.f.CCP source with coaxial electrodes has been used by Liang and Blades [7] for the direct determination of trace elements in solid samples (conducting pins). Liang and Blades [8] and Sturgeon *et al.* [9] have developed a r.f.CCP source in coaxial geometry operated at 5-100 W and 13.56-50 MHz sustained in He or Ar inside a graphite furnace. The evolution of emission spectrometry inside a graphite furnace at atmospheric pressure (FAPES) is based on the combination of high atomization and transport efficiencies in electrothermal atomizers with the high efficiency of excitation and multielement capability in plasma. The FAPES has rapidly developed and has been extensively studied with regard to spectral and spatial characteristics, thermal characteristics, influence of operating power and polarization potential, some applications and analytical performances and interferences studies.

Cordoş and co-workers have developed a r.f.CCP source with tip-ring electrode geometry adapted for pneumatically nebulized samples [10-12]. The Ar plasma is sustained at atmospheric pressure and operated at 85-275 W.

In this paper the spectral source mentioned in ref. [10] is used for the analysis of alkaline and alkaline-earth elements (Ca, Na, Li) by AES. The focus is given to the optimization of operating parameters and of coupling system geometry on analytical performances: sensitivity, signal-to-background ratio (SBR), limits of detection (LOD) and self-absorption. The emission was measured at the resonance, non-resonance and ionic lines. The optimum conditions were chosen for the analysis of Ca in blood samples by AES and the results were compared with those obtained by flame atomic absorption spectrometry (FAAS) and flame atomic emission spectrometry (FAES).

## ANALYSIS OF CALCIUM, NARIUM AND LITHIUM ..

### Experimental

**Instrumentation.** The plasma torch, r.f. generator and sample introduction system were described previously [10]. The experimental set-up is provided in Fig. 1. The atmospheric pressure plasma was generated at 27.12 MHz and operated at 85 - 275 W with Ar as support gas (*AzoMureş, Tg. Mureş*) at 0.3 - 1.8 l min<sup>-1</sup> flow rate. The torch assembly has a central water-cooled electrode with a sharp W tip connected to the r.f. high-voltage. The counter electrode connected to ground is a copper ring (25 mm diameter) at heights in the range 10 - 70 mm from the inner electrode tip. An Ar flow is used both for sample nebulization and plasma support. The plasma emission is focused onto the entrance slit of the monochromator by a 110 mm focal length fused-silica lens. A Heath EU 700 monochromator equipped with a 1P28 photomultiplier (Hamamatsu, Japan) supplied at 600 V was used in the optimization study as well as in the quantitative measurements. The photocurrent was recorded on a K 201 recorder (Zeiss Jena, Germany). The samples were nebulized using a Meinhard nebulizer and a peristaltic pump. The nebulized samples were then fed into a mixing chamber made of poly(tetrafluoroethylene). From here the samples are swept into the base of the plasma through 12 holes placed concentrically around the central electrode.

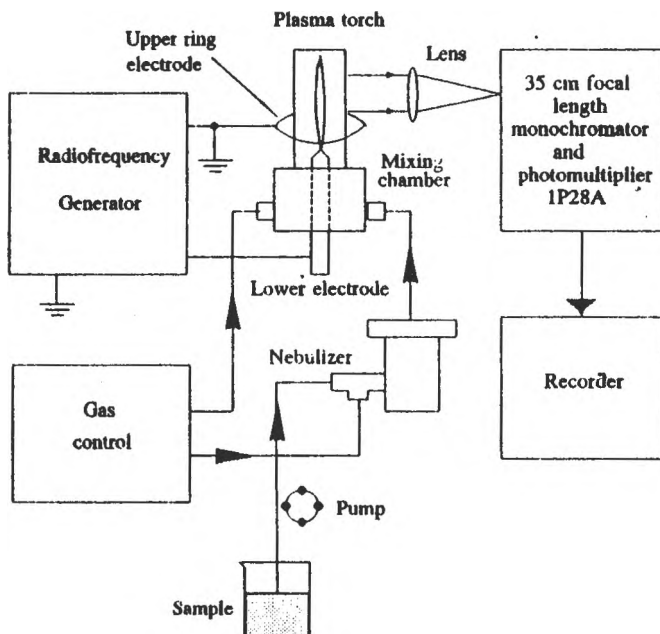


Fig. 1 Block diagram of the experimental set-up

Details of the equipment and operating conditions are given in Table 1.

Calcium in blood samples was also analysed by FAAS in air-acetylene flame and by FAES in methane-air flame with an AAS 1N atomic absorption spectrometer (Zeiss Jena).

Table 1. Instrumentation and operating conditions of plasma source and spectrometer system

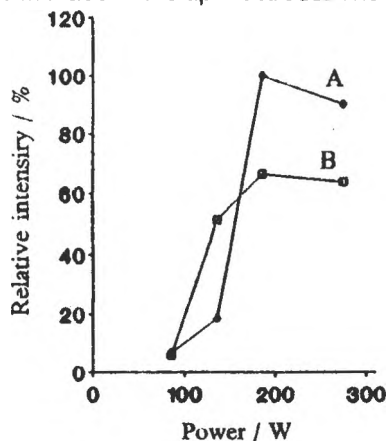
Apparatus	Model	Manufacturer
Plasma power supply r.f.-generator 27.12 MHz, 2 kW, free-running oscillator modified for capacitive coupling and for operating at 85 - 275 W (four power levels)	EOP	Research Centre for Analytical Instrumentation, Cluj-Napoca, Romania
Plasma torch lip-ring electrode geometry, ring electrode 25 mm diameter Ar-flow rate: 0.3 - 2.0 l min <sup>-1</sup>		Laboratory constructed
Nebulizer, spray chamber and desolvation system pneumatic, concentric type nebulizer 4 rolls peristaltic pump, 120 cm <sup>3</sup> glass chamber		Research Centre for Analytical Instrumentation, Cluj-Napoca, Romania
Optics scanning monochromator, 0.35 m focal length, 1200 grooves/mm grating focusing: quartz lens, 110 mm focal length slit width: 50 μm	EU 700	Heath Co., Benton Harbor, MI, USA
Photomultiplier tube	1P28A	Hamamatsu., Japan.
High-voltage power supply for photomultiplier tube (800 V)	EU 701	Heath Co., Benton Harbor, MI, USA
Recorder	K 201	Zeiss-Jena, Jena, Germany.

**Reagents.** Stock solutions ( 1000 mg ml<sup>-1</sup> ) of Li, Na and Ca were prepared by dissolution of high-purity Li<sub>2</sub>CO<sub>3</sub> and CaCO<sub>3</sub> ( Merck ) in as small as possible concentrated HCl amount and NaCl ( Merck ) in double distilled water, respectively. Single element working solutions ( 50 mg l<sup>-1</sup> ) were obtained by diluting the stock solutions with high-purity 2 % (v/v) HNO<sub>3</sub>. These solutions were used in the optimization study of the operating conditions.

**Preparation of Blood Samples.** The processing of blood samples was made according to the sampling protocol described in ref. [13]. After collection the blood samples were allowed to clot and centrifuged for 5 - 10 min at 3000 rpm to separate the serum fraction. To prevent the classical Ca-PO<sub>4</sub><sup>3-</sup> atomization interference, 3 ml of 1% La(NO<sub>3</sub>)<sub>3</sub> were added at 1 ml of serum then the sample was diluted to 25 ml with double distilled water. Standard addition method was used for Ca determination in the attempt to eliminate the ionization interferences caused by the presence of Na and K in samples. One ml of double distilled water, 1 ml Ca solution 50 mg l<sup>-1</sup> and 1 ml Ca solution 100 mg l<sup>-1</sup> were added to 3 aliquots of 4 ml sample prepared as above. These solutions were nebulized in plasma or flame and by resorting to an elementary calculation the concentration of Ca in mg l<sup>-1</sup> was obtained. The normal values are in the range 90 - 110 mg l<sup>-1</sup>.

## RESULTS AND DISCUSSIONS

**Optimization of Plasma Parameters.** To get maximum analytical performances the following parameters were optimized: r.f. power, Ar flow, observation height, coupling system geometry. The graph in Fig. 2 shows the response of emission for Ca(I) 422.673 nm to changes in r.f. power at 1 l min<sup>-1</sup> Ar and ring electrode at 10 mm and 40 mm above the tip electrode. The plasma was viewed in the core



According to Fig. 2 there is a maximum sensitivity at a power level of 185 W. The sensitivity sharply rises in the range 85 - 185 W and further decreases in the range 185-275 W. For power levels above 275 W the torch gets highly heated and is damaged. Consequently the power level of 185 W was considered as being optimum as in the case of Na and Li.

Fig. 2 Influence of r.f. power on Ca (I) 422.673 nm emission. Ar flow: 1 l/min; ring electrode at 10 mm above the tip (A) and 40 mm above the tip (B)

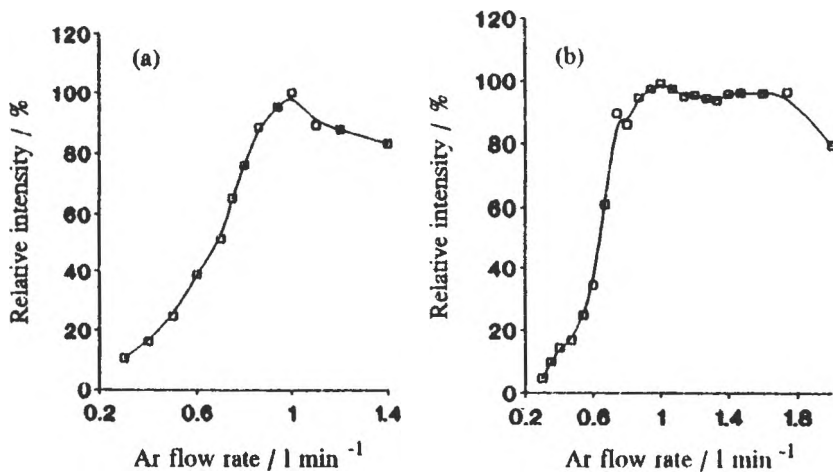


Fig. 3. Influence of Ar flow rate on emission at 185 W. a. Na(I) 588.995 nm b. Ca(I) 422.673 nm

According to the influence of Ar flow on Na(I) 588.995 nm and Ca (I) 422.673 nm emission lines ( Fig. 3 ), the maximum emission occurs for an Ar flow of  $1 \text{ l} \cdot \text{min}^{-1}$ .

The influence of observation height and coupling system geometry on Ca, Na and Li emissions at the resonance wavelengths are presented in Fig. 4.

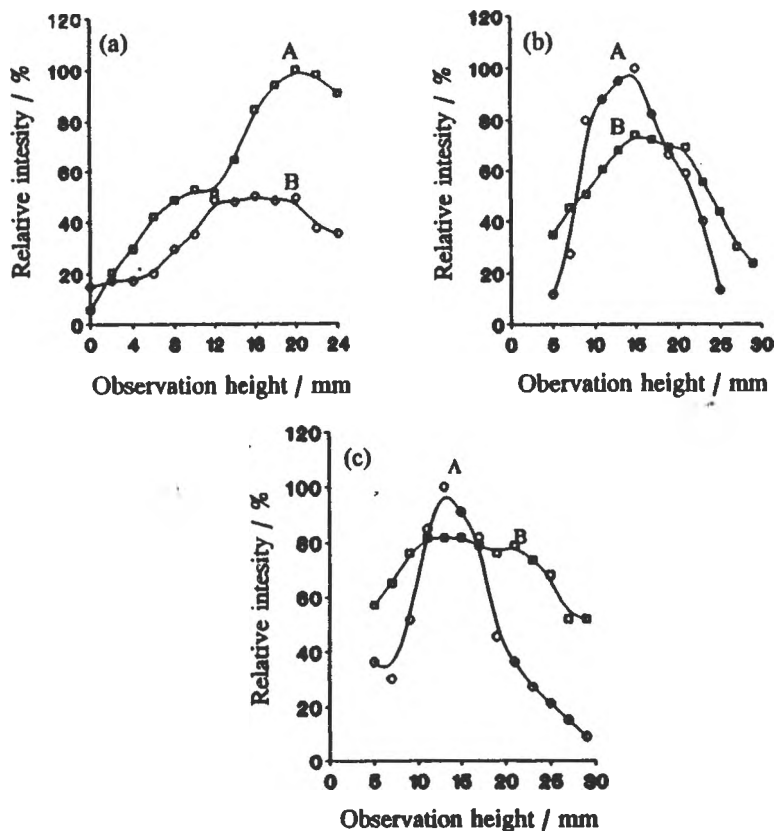


Fig. 4. Influence of observation height and coupling system geometry on emission at 185 W.  
 a. Ca(I) 422.673 nm b. Na(I) 588.995 nm c. Li(I) 670.784 nm  
 A - ring electrode at 10 mm above the tip; B - ring electrode at 40 mm above the tip.

For all 3 elements there is an enhancement in emission as the ring electrode is moved down from 40 mm (curve B) to 10 mm (curve A) above the tip and the signals



increase by 50% for Ca, 33% for Na and 12% for Li. Similar rises were previously found for other 16 elements [14] and can be explained by a diminished self-absorption and a rise both for excitation temperature and electron number density as the ring electrode is moved down [15]. The optimum observation heights were found to be 20 mm for Ca and 13 mm for both Na and Li and does not significantly change when the ring electrode is moved. The higher excitation energy of Ca than that of Na and Li as well as the formation of CaO and CaOH refractory compounds with the oxygen diffused in plasma account for the high optimum observation height for Ca. The highest sensitivity in the nearness of ring electrode or a bit over it (curves A) shows its important role in the improvement of analyte excitation efficiency. Based on this study the optimum height of the ring electrode was established to be 10 mm above the tip while the observation at maximum sensitivity.

The possibility to analyse Ca at the ionic line Ca(II) 393.366 nm was also studied. Fig. 5 provides the ratio of intensities Ca(I) 422.673 nm/ Ca(II) 393.366 nm at 20 mm observation height as a function of ring electrode height and power level. As the outer electrode is moved down from 65 mm (curve C) to 40 mm (curve B) and 10 mm (curve A) respectively, the ratio of intensities rapidly increases especially at low powers (85-135 W). This proves that the increase rate of atomic line intensity is much higher than that for ionic line as a result of a superior atomisation and atomic excitation efficiency as well as a diminished self-absorption effect. In the range 185 - 275 W

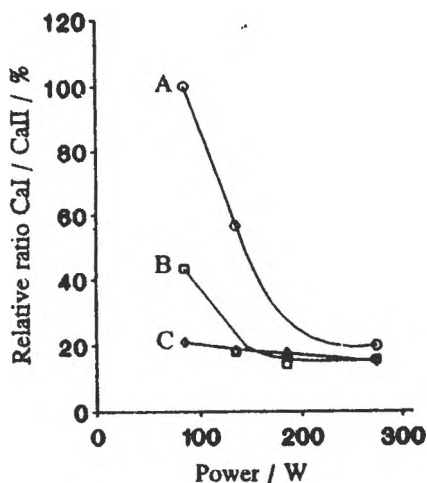


Fig. 5 Ratio of emission intensities Ca(I)422.673 nm/Ca(II)393.366 nm at 20 mm observation height as a function of power level and ring electrode height

the ratio of intensities  $\text{Ca(I)}/\text{Ca(II)}$  is less influenced by the ring electrode height and power level, perhaps as a result of plasma processes stabilisation. Sensitivities for atomic lines are up to one order of magnitude superior to that of ionic ones regardless the power level and ring electrode height. Thus, in r.f.CCP with tip-ring electrode geometry the resonance atomic lines are more evident than ionic lines and the excitation of the analyte in plasma occurs mainly by atom-electron collisions.

Because sample is swept in plasma through 12 holes placed concentrically around the tip electrode at 5 mm distance from the plasma core it is necessary to investigate the self-absorption due to atoms situated in the outer mantle. Therefore the ratio of doublet lines intensities  $D1/D2$   $\text{Na(I) } 588.995/\text{Na(I) } 589.592$  nm was calculated. This value is 1.8 in arc and 2 in spark excitation sources [16,17]. Values below 2 show the presence of self-absorption. This phenomenon was studied in the range 1 - 100  $\mu\text{g ml}^{-1}$  Na in r.f.CCP-AES. The influence of power level, gas flow and coupling system geometry on self-absorption for a solution of 50  $\mu\text{g ml}^{-1}$  is plotted in Fig. 6. Accordingly, self-absorption linearly decreases with the power level (Fig. 6a) and uniformly increases with Ar flow (Fig. 6b) The latter is explained by a higher amount of sample introduced in plasma. In the optimum range of the observation heights (11-21 mm), the self-absorption considerably diminishes as the distance between electrodes decreases (Fig. 6c curves A, B). The explanation consists in a better energy transfer, a more efficient sample excitation and consequently, an increased sensitivity. Consequently, the study established that self-absorption could be considerably suppressed by an increase in power supply and by moving down the ring electrode. The ratio of Na doublet emission intensities  $D1/D2$  at 185 W power level, 1 l  $\text{min}^{-1}$  Ar, ring electrode at 10 mm above the tip and 13 mm observation height is 1.8 as in the arc source. The ratio of 1.8 calculated for the slopes of calibration curves at doublet lines is maintained throughout the range 1 - 100  $\mu\text{g ml}^{-1}$  Na concentration.

ANALYSIS OF CALCIUM, NARIUM AND LITHIUM ..

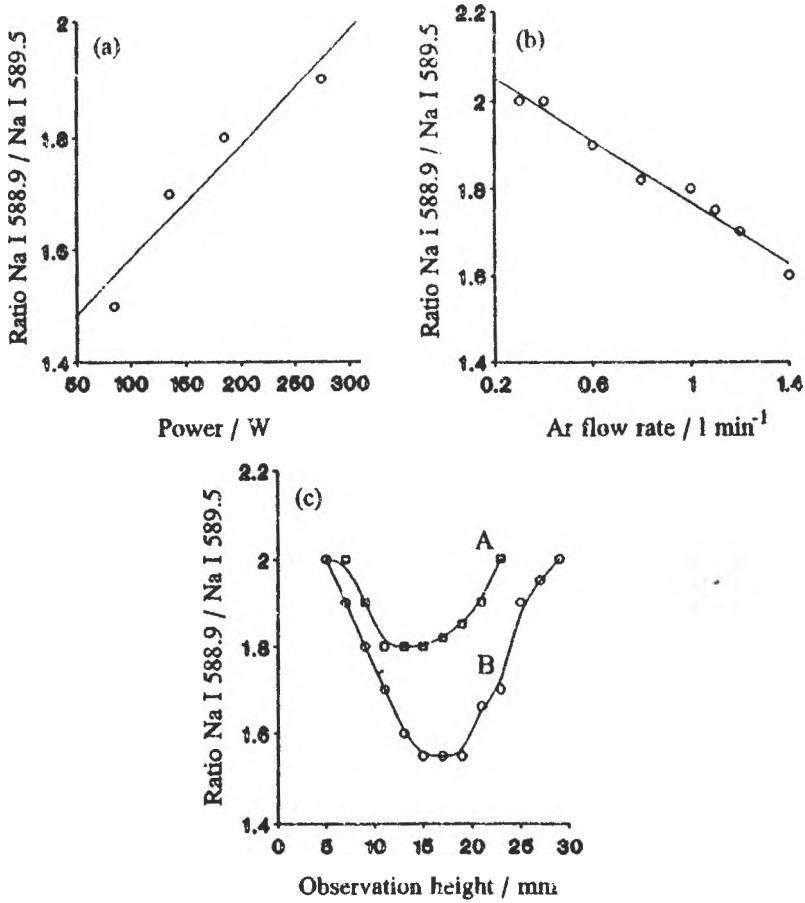


Fig. 6 Influence of power level (a), gas flow rate (b) and coupling system geometry (c) on the ratio of doublet emission D1/D2; 50<sub>μ</sub>g ml<sup>-1</sup> Na solution

**Analytical performances.** Analytical performances were expressed as signal-to-background ratio (SBR), relative standard deviation of background (RSDB) and limits of detection (LODs) calculated according " 3σ " criteria and SBR-RSDB approach of

Boumans and co-workers [18]. The plasma background was measured with double distilled water as blank. Table 2 shows the analytical performances in comparison with the LODs previously determined at 185 W and the ring electrode at 40 mm above the tip [14]. As it is shown in Table 2, LODs decrease from 45 to 15 ng ml<sup>-1</sup> for Ca, from 18 to 13 ng ml<sup>-1</sup> for Na and from 12 to 9 ng ml<sup>-1</sup> for Li. The trend could be explained by an increased sensitivity and a lower background level. The limits of detection and SBR values certify that r.f.CCP in tip-ring electrode geometry has very good analytical performances in the analysis of alkaline and alkaline-earth elements.

**Table 2** Signal-to-background ratio (SBR), relative standard deviation of background % (RSDB) and limits of detection (LODs) for Ca, Na and Li at the resonance wavelengths. Power level: 185 W; Ar flow: 1 l min<sup>-1</sup>.

Element	$\lambda$ nm	Excitation energy eV	Ring electrode height/				
			10 mm			40 mm	
			Obs.height/ mm	SBR	RSDB / %	LOD <sup>†</sup> / ng ml <sup>-1</sup>	LOD <sup>†</sup> / ng ml <sup>-1</sup>
Ca	422.673	2.94	20	100	1.0	15	45
Na	588.995	2.11	13	120	1.0	13	18
Li	670.784	1.90	13	200	1.2	9	12

\* SBR for 50 µg ml<sup>-1</sup> single element solution    † LODs calculated according 3σ criteria.

\*\* RSDB % based on 10 replicate measurements of the background

**Determination of Ca in Blood Samples.** Experimental results obtained in parallel by r.f.CCP-AES, FAAS in air-acetylene flame and FAES in methane-air flame using the standard addition method are provided in Table 3.

**Table 3** Analytical results for Ca in blood samples by r.f.CCP-AES, FAAS and FAES<sup>\*</sup>

Sample	r.f.CCP-AES		FAAS		FAES	
	mg l <sup>-1</sup>	(RSD) <sub>o</sub>	mg l <sup>-1</sup>	(RSD) <sub>o</sub>	mg l <sup>-1</sup>	(RSD) <sub>o</sub>
S1	87	2.3	85	2.4	-	-
S2	100	4.5	92	4.1	-	-
S3	92	4.3	97	4.7	91	5.8

\* Average of 3 replicate measurements.

## ANALYSIS OF CALCIUM, NARIUM AND LITHIUM ...

Experimental results are important mainly because a new emission source, the r.f.CCP in tip-ring electrode configuration is used. In addition to FAES this source allows the determination of much more elements with physiological importance (Mg, Cu, Fe) or very toxic (Pb) [10,11]. Unlike FAAS, r.f.CCP does not need hollow-cathode sources that is a major advantage for the analysis cost. Data of Table 3 show a good agreement of Ca determinations by r.f.CCP, FAAS and FAES. As the last two methods are commonly used for the determination of Ca in biological fluids they are indicative of the accuracy of r.f.CCP-AES. The precision in the range 2.3 - 4.5 % is better than in FAES and similar with FAAS.

### CONCLUSIONS

The present paper shows in detail the analytical performances in the analysis of Ca, Na and Li by r.f.CCP-AES. The argon plasma in tip-ring electrode configuration is operated at low power levels. The optimum operating conditions were established to be 185 W power level, 1 l min<sup>-1</sup> Ar flow and the ring electrode at 10 mm above the tip. The self-absorption estimated by the ratio of Na doublet lines depends on power level, Ar flow rate, system geometry, observation height and is similar to that in the arc source. The limits of detection are at the level of tens of ng ml<sup>-1</sup> and improve when the ring electrode is moved down as a result of a more efficient energy transfer. The analytical results of Ca in blood samples by r.f.CCP favourably compare with those obtained by FAAS and FAES. The r.f.CCP is an attractive source and could be used in the analysis of metals in biological fluids.

### References

1. M. W. Blades, P. Banks, C. Gill, D. Huang, C. Le Blanc and D. Liang, *IEEE Transaction on Plasma Science*, 1991, **19**, 1090.
2. P. W. J. M. Boumans, *J. Anal. At. Spectrom.*, 1993, **8**, 767.
3. M. W. Blades, *Spectrochim. Acta Part B*, 1994, **49B**, 47.

4. D. C. Liang and M. W. Blades, *Anal. Chem.*, 1988, **60**, 27.
5. D. Huang and M. W. Blades, *Appl. Spectrosc.*, 1991, **45**, 1468.
6. R. Gross, B. Platzer, E. Leitner, A. Schalk, H. Sinabell, H. Zach and G. Knapp, *Spectrochim. Acta B*, 1992, **47B**, 95.
7. D. C. Liang and M. W. Blades, *Spectrochim. Acta Part B*, 1989, **44B**, 1049.
8. D. C. Liang and M. W. Blades, *Spectrochim. Acta Part B*, 1989, **44B**, 1059.
9. R. E. Sturgeon, S. N. Willie, V. T. Luong, S. S. Berman and J. G. Dunn, *J. Anal. At. Spectrom.*, 1989, **4**, 669.
10. E. A. Cordoş, S. D. Anghel, T. Frentiu and A. Popescu, *J. Anal. At. Spectrom.*, 1994, **9**, 635.
11. E. A. Cordoş; T. Frentiu, Ana-Maria Rusu and G. Vatca, *Analyst (London)*, 1995, **120**, 725.
12. E. A. Cordoş, T. Frentiu, A. Fodor, Michaela Ponta, Ana-Maria Rusu and S. Negoescu, *A. C. H.-Models in Chemistry (Budapest)*, 1995, **132**, (3), in press.
13. I. Manta, M. Cucuianu, G. Benga and A. Hodarnau, *Metode Biochimice în Laboratorul Clinic*, Ed. Dacia, Cluj-Ńapoca, 1976, 233-239.
14. T. Frentiu, Ana-Maria Rusu, Michaela Ponta, S.D. Anghel and E. A. Cordos, *Fresenius J. Anal. Chem.*, 1996, **354**, in press.
15. S. D. Anghel, T. Frentiu, Ana-Maria Rusu, E. Darvasi and E. A. Cordos, *Fresenius J. Anal. Chem.*, 1996, **354**, in press.
16. *Tablitz Spectralinij Linij*, Izdatelstvo Nauka, Moskva, 1977, 773.
17. L. H. Ahrens and S. R. Taylor, *Spectrochemical Analysis*, Addison-Wesley Publishing Company, Inc. Reading, Massachusetts, U.S.A., sec. ed., 1961, 99-101.
18. P. W. J. M. Boumans, *Anal. Chem.*, 1994, **66**, 459.

Received: 12.12.1994

## FIGURES OF MERIT FOR A SEQUENTIAL SPECTROMETER WITH INDUCTIVELY COUPLED ARGON PLASMA SOURCE

Emil Cordoș, Tiberiu Frentiu, Alpar Fodor, Michaela Ponta, Ana-Maria Rusu and  
Ladislau Kekedy

*University "Babeș-Bolyai" Cluj-Napoca, Chemistry Department*

**ABSTRACT:** Figures of merit for a sequential emission spectrometer with inductively coupled Ar plasma source are assessed on the basis of 10 elements determination in steel certified materials. Estimated performance criteria are: background equivalent concentration, limit of detection, short-term precision and long-term reproducibility or stability. The presence of  $5000 \mu\text{g}\cdot\text{ml}^{-1}$  Fe matrix has a significant depressive effect on refractory metals (Ti, V) as well as on Co, Cu, Mo, Ni, a slightly depressive one on Mn and Si and a slightly increasing one on Al and Cr. The limits of detection are in good agreement with those obtained for standard ICP (1 kW). The analytical system has good short-term precision and stability in the elemental determination of alloyed steel. Recovery ranges within 89-112%.

**INTRODUCTION.** Performance of any analytical system strongly depends on its constructive and operating parameters. In order to reach the maximum performance, the constructive optimisation and the assessment of the main parameters influence on analytical system are required. These objectives are achieved by means of optimisation criteria or performance criteria. The main valuation criteria used in the optimisation of an analytical system include: sensitivity, detection limit, limit of determination, signal to noise ratio (SNR), short-term precision and long-term reproducibility [1-9]. Emission spectrometer with inductively coupled plasma source (ICP-AES) is very suitable for the multielemental analysis since it allows the determination of major, minor and trace elements in the same sample. Interference effects present in classical emission spectrometry (arc, spark) are greatly diminished in ICP-AES.

In the present paper, the performance of a sequential spectrometer with inductively coupled argon plasma source is estimated. Experimental results have been the basal data for a sequential analysis methodology of 10 elements (Al, Co, Cr, Cu, Mn, Mo, Ni, Si, Ti, V) in steel samples. Analytical performances are compared with those obtained by Boumans with a standard ICP source (1 kW) [10].

Estimated performance criteria are:

- background equivalent concentration (BEC);
- limit of detection ( $c_L$ );
- short-time precision and stability or long-term reproducibility.

Experimental. The main constructive and operating parameters are shown in tab.1.

**Table 1. Equipment parameters and operating conditions.**

Plasma source (ICP)	Plasma r.f. generator Model EOP 27.12±0.05% MHz, 2 kW, free-running type oscillator, two turns copper induction coil (CAA- Research Center for Analytical Instrumentation, Cluj-Napoca, Romania).
Plasma torch	Fassel type torch with 3 concentric quartz tubes, 18-20 l·min <sup>-1</sup> cooling Ar flow-rate, 1.5-2 l·min <sup>-1</sup> nebulizer Ar flow-rate, 1ml·min <sup>-1</sup> sample intake rate, 18 mm observation height above the induction coil, pneumatic concentric nebulization (CAA- Cluj-Napoca, Romania).
Optic transfer	Scanning monochromator and photocurrent measurement system Model SMS, Czerny-Turner mount, 1 m focal length, 2400 groves·mm <sup>-1</sup> grating blazed at 340 nm, spectral bandpass 25 pm, entrance and exit slits 20μm, 32±1°C thermostated, spectral range 190-800 nm with 0.02 nm increment, internal wavelength calibration with a Si hollow-cathode lamp, photomultiplier detector EMI 9781R (CAA- Cluj-Napoca).
Monochromator driving, data acquisition and processing	Telerom (IEIA Cluj-Napoca, Romania) computer, model 3P86 with 2020 DAF display (IEIA Cluj-Napoca, Romania), Control Data Fast Printer, interface laboratory constructed, 64 μs data acquisition time, in house software.

The radiofrequency generator and plasma torch were presented in detail in references [11,12] while the nebulization system in reference [13]. The plasma emission is focused onto the entrance slit of the monochromator by a 110-mm focal length fused-silica lens. The monochromator is a scanning type, each line being scanned over 15 steps at 0.02 nm increments. Both the monochromator driving and the data processing are accomplished by a Telerom computer model 3P86. The background level is measured at 0.1 nm from the spectral analytical wavelength.

**Reagents.** Stock solutions (1000 mg·ml<sup>-1</sup>) were prepared by dissolving high-purity metals (Al, Co, Cr, Cu, Mn, Mo, Ni, Ti, V) either in HCl or in HNO<sub>3</sub>. Stock solution of Si (1000 μg·ml<sup>-1</sup>) was prepared by dissolving Si high-purity powder in NaOH 40% (m/m) solution and stock solution of Fe (50000 μg·ml<sup>-1</sup>) was obtained by dissolving Fe high-purity powder in aqua regia.



## FIGURES OF MERIT FOR A SEQUENTIAL SPECTROMETER...

Single element standard solutions were prepared in  $5000 \mu\text{g}\cdot\text{ml}^{-1}$  Fe matrix or without matrix by diluting the stock solutions to establish the background equivalent concentrations and the detection limits.

For the determination of short-term precision and long-term reproducibility the following steel certified materials were used: E71CEM, E8, E16, E30, E77, E153, E161, E166 and E114. The steels (except E114) were dissolved in HCl and oxidized with  $\text{HNO}_3$ . The E114 steel certified material (18% W) was dissolved in a Speaker mixture ( $\text{H}_2\text{SO}_4$  98% :  $\text{H}_3\text{PO}_4$  85% = 1 : 1 (v/v)).

### RESULTS AND DISCUSSION

#### Background equivalent concentration and limits of detection.

Background equivalent concentration (BEC) is a measure of the sensitivity for a specific wavelength and it is closely related to the slope of the calibration curve. It is defined as the concentration of an analyte that yields a net intensity signal equal to the intensity of the background. BEC is a very useful parameter for comparing analytical systems [6, 14-16]. The reciprocal value of BEC is the normalised sensitivity. We used this mode of expression because results are more reproducible from day to day and are relatively independent from operating parameters, such as the radiofrequency power [17].

Calibration curves were drawn using single element solutions in  $5000 \mu\text{g}\cdot\text{ml}^{-1}$  Fe matrix and without Fe matrix, respectively.

$$y = x_b + m \cdot c \quad (1)$$

where:  $y$  - gross signal,  $x_b$  - background signal,  $m$  - slope of the calibration curve and  $c$  - analyte concentration. BEC values were estimated using the calculated coefficients of the most probable curves with relation (2):

$$\text{BEC} = x_b / m = 1 / S_{\text{norm}} \quad [\mu\text{g}\cdot\text{ml}^{-1}] \quad (2)$$

where  $S_{\text{norm}}$  is the normalised sensitivity.

The limit of detection ( $c_L$ ) was calculated using  $3\sigma$  criteria adopted by IUPAC [5] according SBR-RSDB or BEC-RSDB approach [14-16],

$$c_L = 3 \cdot 0.01 \cdot \text{RSDB} (\%) \cdot \text{BEC} = 3 \cdot 0.01 \cdot \text{RSDB} (\%) / S_{\text{norm}} \quad [\mu\text{g}\cdot\text{ml}^{-1}] \quad (3)$$

where SBR is signal to background ratio and RSDB is the relative standard deviation of background (%).

This method provides a realistic and practical value of the detection limit and has the advantage of using normalised or relative values.

Coefficients of the most probable calibration curves in 5000  $\mu\text{g ml}^{-1}$  Fe matrix and in the absence of Fe matrix are listed in tab. 2

**Table 2. Coefficients of the most probable calibration curves in and without 5000  $\mu\text{g ml}^{-1}$  Fe matrix \***

Element	$\lambda$ / nm	Matrix					
		H <sub>2</sub> O			5000 $\mu\text{g ml}^{-1}$ Fe		
		$x_b$	m	correlation <sup>o</sup>	$x_b$	m	correlation <sup>o</sup>
Al	396.152	8598	8946	0.997	11120	9267	0.996
Co	345.350	2376	8336	0.999	2623	6099	0.999
Cr	357.869	1620	2428	0.999	1403	2551	0.999
Cu	324.754	3196	31965	0.997	2981	24891	0.995
Mn	403.076	10142	7986	0.999	9803	7541	0.999
Mo	386.411	3773	11433	0.998	3916	8702	0.999
Ni	352.454	1211	621	0.999	1240	532	0.999
Si	288.158	4061	5343	0.999	4262	4956	0.999
Ti	334.941	3650	12166	0.993	4060	6696	0.995
V	437.920	9672	4836	0.999	10001	3175	0.999

\* - 8 calibration solutions       $x_b$  - intercept with axis (estimated concentration for blank,  $c \approx 0$ )  
 m - estimated slope of the calibration curve       $\square$  - dynamic range: 3 orders of magnitude

The linear relationship was tested over 3 orders of magnitude using 8 calibration solutions. As it is shown in tab. 2, the presence of the Fe matrix does not substantially influence the background signal level  $x_b$ . The depressive effect of 5000  $\mu\text{g ml}^{-1}$  Fe matrix is significant for refractory elements since the sensitivity decreases by 45 % for Ti and 35 % for V. The matrix yields also a decrease in sensitivity of about 25% for Co, Cu, Mo and 15% for Ni. The depressive effect on Mn and Si and the increasing one in the case of Al and Cr are insignificant. For all these elements, the dynamic range has not been affected by the 5000  $\mu\text{g ml}^{-1}$  Fe matrix as the correlation coefficients are extremely close in both cases. Percentage relative standard deviations of calibrations curves are always below 3%.

FIGURES OF MERIT FOR A SEQUENTIAL SPECTROMETER...

The figures of merit for the the sequential spectrometer ( BEC, RSDB and  $c_L$  ) are shown in tab. 3.

**Table 3. Background equivalent concentration (BEC), relative standard deviation of background (RSDB %) and detection limits ( $c_L$ ) for ICP-AES.**

Element	$\lambda$ / nm	Matrix						$c_L$ ICP-AES <sup>d</sup> Standard ng ml <sup>-1</sup>
		H <sub>2</sub> O			5000 $\mu$ g ml <sup>-1</sup> Fe			
		BEC <sup>a</sup> / $\mu$ g ml <sup>-1</sup>	RSDB <sup>b</sup> / %	$c_L^c$ / ng ml <sup>-1</sup>	BEC <sup>a</sup> / $\mu$ g ml <sup>-1</sup>	RSDB <sup>b</sup> / %	$c_L^c$ / ng ml <sup>-1</sup>	
Al	396.152	0.96	0.80	23	1.20	1.00	36	19
Co	345.350	0.28	1.00	8.5	0.43	1.10	14	8.8
Cr	357.889	0.67	0.50	10	0.55	0.60	10	15
Cu	324.754	0.10	1.00	3	0.12	0.85	3	3.6
Mn	386.411	0.33	0.80	8	0.45	0.70	9.5	6.5
Mo	403.078	1.27	0.92	35	1.30	1.00	39	29
Ni	352.454	1.95	0.60	35	2.33	0.60	42	30
Si	288.158	0.76	1.10	25	0.86	1.00	26	18
Ti	334.941	0.30	1.00	9	0.61	1.10	20	2.5
V	437.920	2.00	0.85	51	3.15	0.90	85	-

a -  $BEC = x_b / m$

b - RSDB% from 10 replicate measurements of blank

c - calculated according  $3\sigma$  criteria and SBR-RSDB method

d - data from [10]

BEC significantly increases in the case of Al, Co, Ni, Ti, V, slightly increases for Cu, Mn, Mo, Si and slightly decreases for Cr owing to 5000  $\mu$ g·ml<sup>-1</sup> Fe matrix. Generally, results agree with matrix effect.

The calculated  $c_L$  are within the range of ng·ml<sup>-1</sup> or tens of ng·ml<sup>-1</sup> as they actually are in standard ICP. The matrix of 5000  $\mu$ g·ml<sup>-1</sup> Fe affects the detection limit by its influence both on BEC and RSDB. In most cases, RSDB has slightly increased in the presence of Fe matrix but has remained below 1% and has not been affected the plasma stability. The limits of detection have significantly increased for Al, Co, Ni, Ti, V, have moderately increased for Mn, Mo, Si and have not been affected for Cr and Cu.

**Short-term precision.** Short-term precision was estimated by the relative standard deviation of concentration [3] using 10 replicate measurements of calibration solutions obtained from steel certified materials. The relative standard deviations (%) of 10 concentration levels were calculated. The accuracy of the steel materials analysis was assessed through recovery degree of the certified concentrations. Results are listed in tab. 4.

**Table 4. Precision and accuracy in the analysis of 10 elements by ICP-AES.\***

Element	Standard steel	Certified concentration/%	Concentration found by ICP-AES/%	Average recovery/%	Precision RSD/%
Al	E161.	0.033	0.033	100	7.8
Co	E114	4.71	5.19	110	2.3
Cr	E161	1.55	1.55	100	5.6
Cu	E16	0.16	0.16	100	6.3
Mn	E7ICEM	0.90	0.86	95	3.0
Mo	E8	0.42	0.44	105	7.4
Ni	E8	1.85	2.05	112	3.7
Si	E77	0.36	0.36	100	6.5
Ti	E166	0.54	0.55	102	3.7
V	E114	0.37	0.33	89	3.0

\* the working wavelengths are listed in tab. 2; observation height: 18 mm above the induction coil

As it could be seen in tab. 4, analyses show good accuracy as the determined concentration levels are very close to the certified values. The average recovery degree ranges within 89-112%, with very good results for Al, Cr, Cu, Si and Ti. The precision has been up to 8 % but sometimes it has diminished below 4 %.

**Long-term reproducibility.** The stability of an analytical system is estimated by the probability of keeping its analytical characteristics at a level as high as possible for a time as long as possible [3, 4]. Spectrometer stability insures that

## FIGURES OF MERIT FOR A SEQUENTIAL SPECTROMETER

correct wavelengths are located and maintained, that intensity measurements are precise, and provides freedom from frequent calibration [6].

For the long-term reproducibility study, Cu and Mn in E16 and E7ICEM steel certified materials, respectively, were determined every 10 minutes over a period of 1 h, 20 days after calibration. Accuracy and long-term reproducibility for Cu and Mn analysis in steel certified materials over a period of 1 h are listed in tab. 5.

**Table 5. Accuracy and long-term reproducibility of Cu and Mn determination\*.**

Element	Steel certified material	Certified concentration %	Found concentration %	Average recovery %	Long-term reproducibility RSD %
Cu	E 16	0.16	0.17	106	6.0
Mn	E7 ICEM	0.90	0.90	100	3.1

\* measurements every 10 minutes over a period of 1h, 20 days after calibration

Data from tab. 5 prove a very good reproducibility of ICP source over a period of 1 h since there is not a significant difference between recovered and certified concentrations. Short-term precision and long-term reproducibility have also close values. The validity of the calibration curve up to 20 days after an appropriate correction means that the same calibration can be used over a long time.

**CONCLUSIONS.** The presence of the Fe matrix has a strongly depressive effect on Ti, V, Co, Cu, Mo and Ni emission since the sensitivity decreases significantly. The depressive effect of the same matrix on Mn and Si and the increasing one for Al and Cr are not relevant. The detection limits depend on the matrix influence both on BEC and RSDB. These are similar with those reported in standard ICP spectrometry. The overall study on short-term precision and long-term reproducibility demonstrates that the analytical system has a good stability resulting in precise and accurate results.

### References

1. J. D. Ingle jr., *Chem. Educ.*, 1974, **51**, 4100.
2. L. A. Curie, *Anal. Chem.*, 1968 **40**, 586
3. C. Liteanu and I. Răcă, "Optimizarea proceselor analitice", Ed. Academiei R.S.R., 1985, 11-76
4. C. Liteanu and I. Răcă, "Teoria și metodologia statistică a analizei urmelor", Ed. Scisul Românesc, Craiova, 1979, 102-399.
5. Analytical Methods Committee, *Analyst*, 1987, **112**, 199.
6. S. D. Arellano, M. W. Routh and P. D. Dalager, *Int. Lab.*, 1985, Oct., 45.
7. Jane C. Miller and J. N. Miller, *Analyst*, 1988, **113**, 1351.
8. M. Thompson, *Analyst*, 1988, **113**, 1579.
9. F. Karol, *Anal. Chem. (Warsaw)*, 1990, **35**, 129.
10. P. W. J. M. Boumans, *Spectrochim. Acta Part B*, 1981, **36B**, 169.
11. S. D. Anghel, A. Popescu, F. Ratz, E. Tătaru and E. Cordoș, *Rev. Chem.*, 1989 **40**, 344.
12. E. Cordoș, L. Kekedy, T. Frentiu, "Lucrări Practice de Analiză Instrumentală", Univ. "Babeș-Bolyai", Cluj-Napoca, 1993, 174-204.
13. E. Cordoș, A. Popescu, A. Fodor și M. Cosma, *Studia Univ. Babeș-Bolyai, Chemia*, 1984, **XXIX**, 57.
14. P. W. J. M. Boumans, *Spectrochim. Acta Part B*, 1991, **46B**, 431.
15. P. W. J. M. Boumans, J.C. Ivaldi and W. Slavin, *Spectrochim. Acta Part B*, 1991, **46B**, 641.
16. P. W. J. M. Boumans, *Anal. Chem.* 1994, **66**, 459A..
17. E. Cordoș, S.D. Anghel and T. Frentiu, *J. Anal. At. Spectrom.*, 1994, **9**, 635.

Received: 12 12 1994

## HETEROPOLYOXOMETALATE ANIONS OF BISMUTH(III) I. ANIONS WITH PSEUDO-DAWSON-WELLS STRUCTURE

Adrian Pătruț<sup>x</sup>, Cristina Roșu<sup>x</sup> and Horst P. Beck<sup>xx</sup>

<sup>x</sup> Department of Chemistry, Babeș-Bolyai University, Cluj-Napoca, Romania

<sup>xx</sup> Department of Chemistry, University of Saarland, Saarbrücken, Germany

### Abstract

The starting compound was the  $[H_2BiW_{18}O_{60}]^{6-}$  heteropolyoxometalate anion, with a pseudo-Dawson-Wells structure. 1:1 complexes were prepared through the reaction between  $[H_2BiW_{18}O_{60}]^{6-}$  and transition metal cations ( $Mn^{2+}$ ,  $Co^{2+}$  and  $Ni^{2+}$ ). The potassium salts of the starting anion and of the complexes were investigated by: chemical analysis, vibrational spectroscopy, electronic spectroscopy and thermal analysis. The experimental data suggest that in the complexation reactions the ligand is the  $[H_aBiW_{17}O_{5a}]^{(13-a)}$  ( $a=2,3$ ) unsaturated heteropolyoxometalate anion. Thus, the investigated complexes have the formulae:  $[H_2BiMnW_{17}O_{5a}(H_2O)]^9-$ ,  $[H_2BiCoW_{17}O_{5a}(H_2O)]^9-$ ,  $[H_2BiNiW_{17}O_{5a}(H_2O)]^9-$  and a modified pseudo-Dawson-Wells structure.

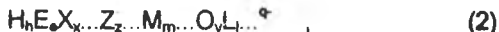
### INTRODUCTION

In the simplest form which has been used for a long time, the heteropolyanions can be written:



where:  $x \leq m$ ,  $X$ =(primary) heteroatom,  $M$ =addendum,  $O$ =oxygen (oxo).

Recent developments in heteropolyanion chemistry, especially in the last twenty years, have resulted in the synthesis of new complex and sometimes unexpected structures. Consequently, the term "heteropolyanion" was found unsatisfactory and was replaced by the term "heteropolyoxometalate anion" (HPOM-A) [1] or "metal-oxygen cluster heteroanion" [2]. In broader terms, it is possible to propose a general formula of the (HPOM-A)s of the type:



where:  $H$ =non-replaceable hydrogen,  $E$ =encrypted cation,  $X$ =primary heteroatom,  $Z$ =secondary heteroatom,  $M$ =addendum,  $O$ =oxygen (oxo),  $L$ =ligand other than oxo and ... shows the possible existence of more chemical species with the respective function [3]. The primary heteroatom, sometimes inaccurately called central heteroatom, is essential for the structure of the (HPOM-A). That is why, its removal brings about the destruction of the whole polyanion architecture. Due to the complexity of the general formula, several criteria for the classification of the

(HPOM-A)s can be envisaged. Thus, according to the electronic structure of the primary heteroatom, we have:

- (HPOM-A)s with a primary heteroatom without lone electron pairs;
- (HPOM-A)s with a primary heteroatom with lone electron pairs.

The common (HPOM-A)s have all the electrons of the primary heteroatom engaged in bonds with the ligand. At the same time, some (HPOM-A)s containing an X primary heteroatom with lone pair/s are also known. Their study is in full development, suggesting promising prospects for the future. The structure and the formulae of the (HPOM-A)s with a heteroatom possessing lone pair/s are markedly different from those of the corresponding common (HPOM-A)s. The configuration of the  $XO_n$  primary group, around which the entire anion is built, must allow the accommodation of the lone pair/s. One of the post-transition elements which can act as a primary heteroatom in such polyanions is bismuth(III). Two (HPOM-A)s with Bi(III) as a primary heteroatom, isolated as salts from weakly acidic solution, which were formulated as  $[H_3BiW_{11}O_{36}]^{6-}$  [4] and  $[H_3BiW_{18}O_{60}]^{6-}$  [5], are mentioned in the literature. Recently, some results suggest the existence of other two (HPOM-A)s of Bi(III). One of the anions was formulated as  $[BiW_9O_{33}]^{9-}$  [6].

The only (HPOM-A) of Bi(III) whose crystal structure has been determined by X-ray diffraction is  $[H_3BiW_{18}O_{60}]^{6-}$  [5], isostructural with  $[H_2AsW_{18}O_{60}]^{7-}$  [7], which is an anion of As(III). The common (HPOM-A)s, with similar formula, i.e.  $[X_2M_{18}O_{62}]^{6-}$ , have a Dawson-Wells structure [8,9]. Unlike this, the  $[H_3BiW_{18}O_{60}]^{6-}$  and  $[H_2AsW_{18}O_{60}]^{7-}$  (HPOM-A)s, with a heteroatom with lone pair, exhibit the following characteristics:

- a) the structure is built up with two  $B-W_9O_{33}$  trilacunary Keggin units, sharing six oxygen atoms;
- b) the two  $B-W_9O_{33}$  units are different: one contains the  $X=Bi(III)$  or  $As(III)$  heteroatom and the other contains two protons (non-replaceable hydrogens);
- c) in the primary group, the X heteroatom is coordinated by three oxygen atoms, forming an  $XO_3$  trigonal pyramid.

The unsaturated (HPOM-A)s with lacunary structure can act as multidentate ligands toward cations of very different elements (transitional, post-transitional, lanthanides, actinides), forming complexes with various stoichiometries. The metal cation/s is/are coordinated as secondary heteroatom/s by oxygen atoms, which delimit the cavity/cavities due to the absence of the addendum/addenda. In certain very particular cases, even saturated (HPOM-A)s, with complete structure, can act as ligands, forming similar complexes. In these cases, the cation/s is/are coordinated by terminal oxygen atoms. The forming complexes are themselves (HPOM-A)s, with the structure derived from those of the ligand (HPOM-A), which can be considered as parent structure.



Our attention was focused upon  $[\text{H}_3\text{BiW}_{18}\text{O}_{60}]^{6-}$ , i.e. (3-hydrogen)-18-tungsto-1-bismuthate(III), according to the nomenclature proposed by us [3]. The research undertaken by Ozawa and Sasaki [5] only had in view the synthesis of the (HPOM-A), as tetramethylammonium salt, with the formula  $[(\text{CH}_3)_4\text{N}]_6[\text{H}_3\text{BiW}_{18}\text{O}_{60}]$  and the determination of the structure. The possibility of the parent (HPOM-A), i.e.  $\text{L}_{(1)}=[\text{H}_3\text{BiW}_{18}\text{O}_{60}]^{6-}$ , saturated and with complete structure, to react with transition metal cations ( $\text{Mn}^{2+}$ ,  $\text{Co}^{2+}$ ,  $\text{Ni}^{2+}$ ) was explored in this work and 1:1 complexes were obtained, according to a formal reaction of the type:



where:  $\text{Z}=\text{Mn}^{2+}$ ,  $\text{Co}^{2+}$ ,  $\text{Ni}^{2+}$  and  $\text{L}_{(1)}=[\text{H}_3\text{BiW}_{18}\text{O}_{60}]^{6-}$ .

The aim of the present paper is further characterization of the  $[\text{H}_3\text{BiW}_{18}\text{O}_{60}]^{6-}$  (HPOM-A), as well as the synthesis and the characterization of the possible derivatives.

## RESULTS AND DISCUSSION

**Chemical analysis.** The results of the chemical analysis are presented in Table 1.

**Vibrational spectra (IR spectra).** The absorption bands and their assignment are presented in Table 2. The assignment of the absorption bands was done on the basis of studies upon IR spectra of (HPOM-A)s with Keggin-type or derived structures (including the Dawson-Wells structure) [10-13], respectively upon the recorded IR spectra of  $\text{Bi}_2\text{O}_3$ . The characteristic absorption band is  $\nu_{\text{as}}$  Bi-O<sub>(1)</sub> antisymmetric stretching vibration, which indicates the presence of the Bi(III) primary heteroatom inside the polyanion. The IR spectra are very similar for the four (HPOM-A)s. This proves that the building structure of the parent (HPOM-A) is not affected to a significant degree by the complexation reaction.

**Electronic spectra (UV/VIS spectra).** The absorption bands and their assignment are presented in Table 3. The assignment of the absorption bands was done on the basis of the studies upon the electronic spectra of the (HPOM-A)s, in general, and of those with Keggin and Dawson-Wells structure, in particular [14-18], respectively upon the aquaions of the transition metal cations which are coordinated as a secondary heteroatom [19].

**UV spectra (51 350 – 28 000  $\text{cm}^{-1}$ ; 194.5 – 360 nm).** The UV spectra contain charge-transfer (CT) bands, characteristic of the polyanionic structure. The  $\nu_2$  CT band, unique to anions with Keggin structure, is split in two large shoulders, as in the case of anions with Dawson-Wells structure. The CT bands reveal the polyoxometalate character of the investigated anions. Thus, the nature of the primary and secondary heteroatom/s, the complete, lacunary and modified

character of the structure and, partially, the nature of the addenda have only a limited influence upon the UV spectra. This explains the slight differences between the UV spectra of the investigated (HPOM-A)s.

TABLE 1. Analytical results

Compound	Found / calculated % w/w						
	K	Bi	Mn	Co	Ni	W	H <sub>2</sub> O
L <sub>(1)</sub>	5.02/4.88	4.70/4.35	—	—	—	67.45/68.86	1.80/1.87
MnL	6.71/7.20	4.53/4.29	1.23/1.13	—	—	66.03/64.24	3.71/3.70
CoL	6.85/7.23	4.51/4.31	—	1.30/1.21	—	65.80/64.13	3.20/3.34
NiL	6.67/7.25	4.60/4.31	—	—	1.13/1.21	66.14/64.10	3.28/3.34

TABLE 2. IR absorption bands of L<sub>(1)</sub>, MnL, CoL and NiL

Assignment	Wavenumber $\bar{\nu}$ (cm <sup>-1</sup> )			
	$\nu_{as}$ W-O <sub>(6)</sub>	950	945	950
$\nu_{as}$ W-O <sub>(2)</sub> -W	890	895	890	890
$\nu_{as}$ Bi-O <sub>(1)</sub>	844	845	848	845
$\nu_{as}$ W-O <sub>(3)</sub> -W	830-680	830-680	830-680	830-680
$\delta$ W-O <sub>(2)</sub> -W	540	530	535	530
Compound	L <sub>(1)</sub>	MnL	CoL	NiL

VIS spectra (28 000 – 11 100 cm<sup>-1</sup> ; 360 – 900 nm). The (HPOM-A)s without secondary heteroatom/s and/or reduced addenda have no absorption bands in the visible (and in the near IR) domain. This can also be noticed in the spectrum of L<sub>(1)</sub>.

The d-d and f-f electronic transitions, characteristic of this domain, are, however, observed when cations of transition metals, lanthanides or actinides, as secondary heteroatom/s, are present. In the spectra of CoL and NiL the expected d-d transition bands are found. This proves the coordination of Co(II) and Ni(II) as a secondary heteroatom in the polyanionic structure. The (HPOM-A)s with Mn(II) as a secondary heteroatom, including MnL, are a particular case without the d-d bands resolved in the visible spectrum. The expected d-d bands in this case have a very low intensity, being forbidden by the Laporte and spin selection rules. They are totally masked by the  $\nu_1$  CT band, prolonged from the UV into the visible [16-18].

Anions with Pseudo-Dawson-Wells Structure

TABLE 3. UV/VIS absorption bands of  $L_{(1)}$ , MnL, CoL and NiL

Assignment	Wavenumber / Wavelength $\bar{\nu}$ ( $\text{cm}^{-1}$ ) / $\lambda$ (nm) [ $\epsilon(\text{L}\cdot\text{mol}^{-1}\cdot\text{cm}^{-1})$ ]			
	(CT) $\nu_2$ : W-O <sub>(6)</sub>	48 100/208 [141 400]	48 800/205 [124 000]	49 300/203 [122 300]
(CT) $\nu_1$ : W-O-W	40 800/245 sh 34 500/290 sh	41 300/242 sh 34 500/290 sh	41 700/240 sh 34 500/290 sh	41 700/240 sh 34 700/288 sh
(ET) $\nu_3$ : ${}^4T_{1g(F)} \rightarrow {}^4T_{1g(P)}$	-	-	18 500/540 [100]	-
(ET) $\nu_2$ : ${}^3A_{2g(F)} \rightarrow {}^3T_{1g(F)}$	-	-	19 700/508 sh	14 400/693 sh 13 400/745 [12]
Compound	$L_{(1)}$	MnL	CoL	NiL

**Thermal analysis.** The thermal effects and their interpretation are presented in Table 4.

TABLE 4. Thermal analysis data of  $L_{(1)}$ , MnL, CoL and NiL

Temperature , T (°C)				Effect	Interpretation
115	122	120	121	endothermic	loss of water
180	210	218	220	endothermic	loss of water
315	320	313	325	endothermic	decomposition of the anion
338	341	343	340	endothermic	decomposition of the anion
365	382	379	369	exothermic	crystallization of $\text{WO}_3$
780	782	781	783	exothermic	phase transformation of $\text{WO}_3$
829	824	826	824	endothermic	melting of $\text{Bi}_2\text{O}_3$
840	838	840	839	endothermic	phase transformation of $\text{WO}_3$
858	859	860	859	endothermic	sublimation of $\text{Bi}_2\text{O}_3$
$L_{(1)}$ (K salt)	MnL (K salt)	CoL (K salt)	NiL (K salt)	Compound	

The interpretation of the thermal effects was done by comparison with other thermal analyses of the (HPOM-A)s [20,21]. The recorded thermal effects can be divided into three categories: the loss of (lattice and constitutional) water (40–220°C), the decomposition of the compound through destruction of the polyanionic structure (300–350°C) and physical transformations of the resulted oxides (350–900°C). The thermal effects are identical and occur at close temperature for the

four investigated (HPOM-A)s, revealing their similar structures and the similar nature of the primary heteroatom and addenda.

**Formula and structure.** The formula and the structure of the parent (HPOM-A), which we noted with  $L_{(1)}$ , are well established through single crystal X-ray diffraction [5]. The  $L_{(1)}$  anion has the formula  $[H_3BiW_{18}O_{60}]^{6-}$  and a pseudo-Dawson-Wells structure. According to chemical analysis, the potassium salt synthesized by us has the formula  $K_6[H_3BiW_{18}O_{60}] \cdot 5H_2O$ .

On the other hand, the determination of the formula and structure of the ZL complexes, which are also (HPOM-A)s, raise some problems. Theoretically, the ZL complexes can be:

i) complexes of the saturated  $L_{(1)}=[H_3BiW_{18}O_{60}]^{6-}$  (HPOM-A), in which the transition metal cation would rather be a pseudo-secondary heteroatom, coordinated in a bridge by three oxygen atoms, each from two  $L_{(1)}$  anions. In order to respect the 1:1 metal:ligand stoichiometry, complexes should be polymeric structures of the type  $(ZL_{(1)})_n$ . In this case, the formula of the ZL complex anions would be  $(H_aBiZW_{18}O_{60}^{(7-a)})_n$ , where  $a=2,3$ .

ii) complexes of an unsaturated (HPOM-A), derived from the  $L_{(1)}$  parent structure. This hypothetically unsaturated (HPOM-A) should be the corresponding anion with a monolacunary pseudo-Dawson-Wells structure, i.e.  $[H_aBiW_{17}O_{59}]^{(13-a)-}$ , ( $a=2,3$ ), resulting from the removal of a  $WO^{4+}$  unit from the complete structure. Thus, the Z transition metal cation would be coordinated as a secondary heteroatom by five oxygen atoms (from the  $O_{(5)}$  cavity generated by the absence of an addendum) and by a constitutional water molecule. In this case, the formula of the ZL complex anions would be  $[H_aBiZW_{17}O_{59}(H_2O)]^{(11-a)-}$ , ( $a=2,3$ ), with a modified pseudo-Dawson-Wells structure. It remains to establish the way in which the complete  $[H_3BiW_{18}O_{60}]^{6-}$  anion is degraded to the monolacunary  $[H_aBiW_{17}O_{59}]^{(13-a)-}$ , ( $a=2,3$ ) anion. As of today, the hypothetical monolacunary (HPOM-A) has not yet been isolated.

In the absence of a crystal structure determination, a categorical option for one of the two possibilities, to which perhaps others could be added, should be unwise. And yet, the pronounced resemblance of certain experimental results for  $L_{(1)}$  and for the ZL complexes does not suggest a polymeric structure for the ZL complexes. In our view, the experimental data, especially the thermal analysis (in the case of polymeric structure for the complex (HPOM-A)s, the destruction temperature of the polymeric anion should have been significantly higher than for the parent monomeric anion), rather suggest the second possibility mentioned. According to the chemical analysis, the three complex anions have the formulae:  $[H_2BiMnW_{17}O_{59}(H_2O)]^{9-}$ ,  $[H_2BiCoW_{17}O_{59}(H_2O)]^{9-}$  and  $[H_2BiNiW_{17}O_{59}(H_2O)]^{9-}$ , with a

modified pseudo-Dawson-Wells structure and the formulae of their potassium salts are:  $K_9[H_2BiMnW_{17}O_{59}(H_2O)] \cdot 9H_2O$ ,  $K_9[H_2BiCoW_{17}O_{59}(H_2O)] \cdot 8H_2O$  and  $K_9[H_2BiNiW_{17}O_{59}(H_2O)] \cdot 8H_2O$ .

## EXPERIMENTAL

**Synthesis of  $L_{(1)}=H_3BiW_{18}O_{60}^{6-}$  (K salt)**. The  $[H_3BiW_{18}O_{60}]^{6-}$  parent (HPOM-A), abbreviated as  $L_{(1)}$ , was prepared as potassium salt, according to the procedure described by Ozawa and Sasaki [5]  $H_2WO_4$  (142 g, 0,570 mol) and NaOH (45 g, 1,125 mol) were dissolved in 1000 mL hot water (60-70°C). Acetic acid was added to adjust to pH 4.  $Bi(NO_3)_3 \cdot 5H_2O$  (25 g, 0,0515 mol) was dissolved in  $CH_3COOH/CH_3COONa$  buffer solution (200 mL, pH 4) and was added to the tungstate solution. The mixture became pale yellow after heating on a water bath (90°C) for 4 hours. To the solution obtained was added solid  $KNO_3$  (50 g). After a few days, slow evaporation led to the formation of white-very slightly yellowish crystals, which were purified by several recrystallizations from acidulated water (pH 4). Yield: 65 g (43%).

**Synthesis of MnL, CoL and NiL (K salts)**. The complexes of the parent (HPOM-A) ( $L_{(1)}=H_3BiW_{18}O_{60}^{6-}$ ) with transition metal cations ( $Z=Mn^{2+}, Co^{2+}$  and  $Ni^{2+}$ ), which are themselves (HPOM-A)s, were prepared as follows:

**Synthesis of MnL (K salt)**.  $K_6[H_3BiW_{18}O_{60}] \cdot 5H_2O$  (40 g) was dissolved in  $CH_3COOH/Na$  citrate buffer (50 mL, pH 6.7).  $MnCl_2 \cdot 4H_2O$  (2 g) was also dissolved in water (10 mL) and was added to the first solution. The resulting mixture was heated on a water bath (60-70°C), with stirring, diluted with water (150 mL) and then slowly acidified to pH 4-5 with  $CH_3COOH$ . The heating was continued for 30-40 min, until the solution volume was reduced to half. After cooling, solid  $KNO_3$  (20 g) was added. After a few days, slow evaporation led to the formation of pale brown-yellowish crystals, which were purified by several recrystallizations from acidulated water (pH 4-5). Yield: 29 g (73%).

**Synthesis of CoL (K salt)**. The procedure of MnL is followed.  $CoCl_2 \cdot 6H_2O$  (2.4 g) was used instead of  $MnCl_2 \cdot 4H_2O$ . Red-purple crystals were obtained. Yield: 28 g (70%).

**Synthesis of NiL (K salt)**. The procedure of MnL is followed.  $NiCl_2 \cdot 6H_2O$  (2.4 g) was used instead of  $MnCl_2 \cdot 4H_2O$ . Pale green-yellowish crystals were obtained. Yield: 28 g (70%).

**Chemical analysis**. K was directly determined in solution, by atomic emission spectrophotometry.

Bi was determined gravimetrically, as  $BiI_3$ . The compound was decomposed by boiling with NaOH 11 mol.L<sup>-1</sup> (120°C, 30 min). The resulting solution was neutralized and then acidulated with  $HNO_3$ . Solid KI was added, after which the solution was diluted, heated and filtered.

Mn, Co and Ni were determined spectrophotometrically. The compound was decomposed by boiling with NaOH 11 mol.L<sup>-1</sup> (120°C, 30 min). The resulting solution was neutralized and slightly acidulated with HCl. The extinction was measured at  $\lambda = 475$  nm (for Mn), 515 nm (for Co) and 649 nm (for Ni) (owing to the very weak absorption bands of  $[Mn(H_2O)_6]^{2+}$ , Mn was determined as  $MnO_4^-$ , after oxidation with  $H_5IO_6$ , in the presence of heat).

W was determined spectrophotometrically. The compound was decomposed by boiling with NaOH 11 mol.L<sup>-1</sup> (120°C, 30 min). The resulting solution was neutralized with diluted HCl and  $H_3PO_4 + NaVO_3$  reagent was added. The extinction was measured at  $\lambda = 400$  nm.

$H_2O$  was determined by thermal analysis, from mass loss at 220°C.

**Vibrational spectra (IR spectra)**. The vibrational spectra were recorded in the IR range 1 200-500 cm<sup>-1</sup>, with an IR Perkin Elmer 580 B spectrophotometre.

**Electronic spectra (UV/VIS spectra)**. The electronic spectra were recorded in the UV/VIS range 51 300-11 100 cm<sup>-1</sup> (194.5 - 900 nm), with an UV/VIS Perkin Elmer 550 SE spectrophotometre.

**Thermal analysis**. The thermal analysis was carried out on a Nietzsche STR 409 simultaneous thermoanalyser (Parametres: temperature range 20-900°C, heating rate 5°C.min<sup>-1</sup>).

## REFERENCES

1. M.T.Pope, "*Heteropoly and Isopoly Oxometalates*", Springer, Berlin, Heidelberg, New-York, Tokyo, 1983.
2. M.T.Pope and A Müller, *Angew. Chem.*, 1991, **103**, 56.
3. A.Pătruț, G.Marcu, A.Botar and A.Naumescu, *Studia Univ. Babeș-Bolyai, Ser. Chem.*, 1989, **34(2)**, 46.
4. P.Souchay, M.Leray and G.Hervé, *C. R. Acad. Sci. Paris, Ser. C.*, 1970, **271**, 1337.
5. Y.Ozawa and Y.Sasaki, *Chem. Lett.*, 1987, **5**, 923.
6. A.Botar, *Private communication*, 1994.
7. Y.Jeannin and J.Martin-Frère, *Inorg. Chem.*, 1979, **18**, 3010.
8. B.Dawson, *Acta Cryst.*, 1953, **6**, 113.
9. A.F.Wells, "*Structural Inorganic Chemistry*", 4th. ed., Oxford University Press, 1975.
10. T.J.R.Weakley, *Struct. Bonding(Berlin)*, 1974, **18**, 131.
11. C.Rocchiccioli-Deltcheff, R.Thouvenot and R.Franck, *Spectrochim. Acta*, 1976, **32 A**, 587.
12. C.Rocchiccioli-Deltcheff and R.Thouvenot, *J. Chem. Res.(M)*, **1977**, 546.
13. C.Tourné, A.Ravel and G.Tourné, *Rev. Chim. Min.*, 1977, **14**, 537.
14. G.M.Varga, E.Papaconstantinou and M.T.Pope, *Inorg. Chem.*, 1970, **9**, 662.
15. E.Papaconstantinou and M.T.Pope, *Inorg. Chem.*, 1970, 667.
16. C.Tourné and G.Tourné, *Bull. Soc. Chim. France*, **1969**, 124.
17. C.Tourné and G.Tourné, *J. Inorg. Nucl. Chem.*, 1970, **32**, 3875.
18. A.Pătruț, *Ph.D.Thesis*, Chemistry Institute, Cluj-Napoca, Romania, 1986.
19. R.Micu-Semeniuc, "*Structura combinațiilor anorganice*", (lithographic textbook) Babeș-Bolyai University, Cluj-Napoca, 1978.
20. G.A.Tsigdinos, *Bulletin Cdb-12a*, Climax Molybdenum Co., Ann Arbor, MI, 1969.
21. H.J.Lunk and S.Schönherr, *Z. Chem.*, 1987, **27**, 158.

Received: 5.11.1994

## HETEROPOLYOXOMETALATE ANIONS OF BISMUTH(III)

### II. ANIONS WITH PSEUDO-KEGGIN STRUCTURE

Adrian Pătruț<sup>x</sup>, Cristina Roșu<sup>x</sup> and Horst P. Beck<sup>xx</sup>

<sup>x</sup> *Department of Chemistry, Babeș-Bolyai University, Cluj-Napoca, Romania*

<sup>xx</sup> *Department of Chemistry, University of Saarland, Saarbrücken, Germany*

#### Abstract

The starting compound was the  $[\text{HBiW}_{11}\text{O}_{36}]^{6-}$  heteropolyoxometalate anion with a pseudo-Keggin structure. 1:1 complexes were prepared through the reaction between  $[\text{HBiW}_{11}\text{O}_{36}]^{6-}$  and transition metal cations ( $\text{Mn}^{2+}$ ,  $\text{Co}^{2+}$  and  $\text{Ni}^{2+}$ ). The potassium salts of the starting anion and of the complexes were investigated by: chemical analysis, vibrational spectroscopy, electronic spectroscopy and thermal analysis. Thus, the investigated complexes have the formulae:  $[\text{BiMnW}_{11}\text{O}_{36}(\text{H}_2\text{O})]^{5-}$ ,  $[\text{BiCoW}_{11}\text{O}_{36}(\text{H}_2\text{O})]^{5-}$ ,  $[\text{BiNiW}_{11}\text{O}_{36}(\text{H}_2\text{O})]^{5-}$  and a modified pseudo-Keggin structure.

## INTRODUCTION

Bismuth(III) is a post-transition element which can act as a primary heteroatom in heteropolyoxometalate anions (HPOM-A)s with one lone electron pair. Part one of the study was dedicated to the anions with pseudo-Dawson-Wells structure [1]. But, the first (HPOM-A) of Bi(III), isolated from weakly acidic solution by Souchay, Leray and Hervé was formulated as  $[\text{HBiW}_{11}\text{O}_{36}]^{6-}$ , corresponding to a monolacunary Keggin structure [2]. Some authors expressed doubt concerning the fact that a cation as large as  $\text{Bi}^{3+}$  (ionic radius ca. 1.1 Å) could generate an authentic Keggin structure, occupying a tetrahedral site at the centre of the anion [3,4]. The structure of  $[\text{HBiW}_{11}\text{O}_{36}]^{6-}$ , i.e. (1-hydrogen)-11-tungsto-1-bismuthate(III), according to the nomenclature proposed by us [5], has not yet been clarified in the absence of a crystal structure determination. In view of the controversies concerning the formula, the structure and even the existence of  $[\text{HBiW}_{11}\text{O}_{36}]^{6-}$ , which has so far been investigated relatively summarily, we decided to continue its investigation. Michelon and Hervé have shown that  $[\text{HBiW}_{11}\text{O}_{36}]^{6-}$  can coordinate metal cations, forming 1:1 complexes, which they briefly characterized [6].

We also verified the possibility that the basic (HPOM-A), i.e.  $L_{(2)}=[\text{HBiW}_{11}\text{O}_{38}]^{6-}$  considered unsaturated and with a monolacunary structure, could function as ligand toward transition metal cations ( $\text{Mn}^{2+}$ ,  $\text{Co}^{2+}$ ,  $\text{Ni}^{2+}$ ) according to a formal reaction of the type:



where:  $Z=\text{Mn}^{2+}$ ,  $\text{Co}^{2+}$ ,  $\text{Ni}^{2+}$  and  $L_{(2)}=[\text{HBiW}_{11}\text{O}_{38}]^{6-}$ .

## RESULTS AND DISCUSSION

**Chemical analysis.** The results of the chemical analysis are presented in Table 1.

TABLE 1. Analytical results

Compound	Found / calculated % w/w						
	K	Bi	Mn	Co	Ni	W	H <sub>2</sub> O
$L_{(2)}$	7.30/7.17	6.53/6.38	—	—	—	61.11/61.79	6.17/6.05
$\text{Mn}L_{(2)}$	5.92/5.89	6.44/6.32	1.54/1.66	—	—	62.43/61.20	6.70/6.54
$\text{Co}L_{(2)}$	6.10/5.94	6.26/6.35	—	1.90/1.79	—	60.61/61.43	6.22/6.02
$\text{Ni}L_{(2)}$	5.95/5.88	6.40/6.28	—	—	1.88/1.76	61.15/60.81	7.20/7.04

**Vibrational spectra (IR spectra).** The absorption bands and their assignment are presented in Table 2. For the assignment of the absorption bands see part one of the study [1]. The characteristic absorption band is  $\nu_{\text{as}}$  Bi-O<sub>(1)</sub> antisymmetric stretching vibration, which indicates the presence of the Bi(III) primary heteroatom inside the polyanion. The vibrations are specific for the parent structure and for its derivatives. Thus, the IR spectra are very similar for the four (HPOM-A)s. This proves that the polyanionic building is not affected to a significant degree by the coordination of the metal cation as a secondary heteroatom.

**Electronic spectra (UV/VIS spectra).** The absorption bands and their assignment are presented in Table 3. For the assignment of the absorption bands see part one of the study [1].

**UV spectra (51 350 – 28 000  $\text{cm}^{-1}$  ; 194.5 – 360 nm).** The UV spectra contain charge-transfer (CT) bands, which reveal the polyoxometalate character of



the investigated anions. This explains the slight differences between the UV spectra of the four (HPOM-A).

VIS spectra ( $28\ 000 - 11\ 100\ \text{cm}^{-1}$  ;  $360 - 900\ \text{nm}$ ). The (HPOM-A)s without secondary heteroatom and/or reduced addenda have no absorption bands in the visible (and in the near IR) domain. This can be observed in the spectrum of  $\text{L}_{(2)}$ . But the d-d and f-f electronic transitions are observed when cations of transition metals, lanthanides and actinides, as secondary heteroatom/s, are present. Thus, in the spectra of  $\text{CoL}_{(2)}$  and  $\text{NiL}_{(2)}$  appear the expected d-d bands. This demonstrates the coordination of Co(II) and Ni(II) as a secondary heteroatom in the polyanionic structure. The (HPOM-A)s with Mn(II) as a secondary heteroatom, including  $\text{MnL}_{(2)}$ , are without the d-d bands resolved in the visible spectrum. The expected d-d bands have a very low intensity and are totally masked by the  $\nu_1$  CT band prolonged from the UV into the visible.

TABLE 2. IR absorption bands of  $\text{L}_{(2)}$ ,  $\text{MnL}_{(2)}$ ,  $\text{CoL}_{(2)}$  and  $\text{NiL}_{(2)}$

Assignment	Wavenumber $\bar{\nu}$ ( $\text{cm}^{-1}$ )			
$\nu_{\text{as}} \text{W-O}_{(4)}$	955	955	950	955
$\nu_{\text{as}} \text{W-O}_{(2)}\text{-W}$	895	695	895	895
$\nu_{\text{as}} \text{Bi-O}_{(1)}$	840	842	840	841
$\nu_{\text{as}} \text{W-O}_{(3)}\text{-W}$	820-700	820-700	820-700	820-700
$\delta \text{W-O}_{(2)}\text{-W}$	540	540	540	540
Compound	$\text{L}_{(2)}$	$\text{MnL}_{(2)}$	$\text{CoL}_{(2)}$	$\text{NiL}_{(2)}$

TABLE 3. UV/VIS absorption bands of  $\text{L}_{(2)}$ ,  $\text{MnL}_{(2)}$ ,  $\text{CoL}_{(2)}$  and  $\text{NiL}_{(2)}$

Assignment	Wavenumber / Wavelength $\bar{\nu}$ ( $\text{cm}^{-1}$ ) / $\lambda$ (nm) [ $\epsilon$ ( $\text{L}\cdot\text{mol}^{-1}\cdot\text{cm}^{-1}$ )]			
(CT) $\nu_2 : \text{W-O}_{(4)}$	48 100/208 [86 400]	48 300/207 [80 500]	48 500/208 [81 000]	49 000/204 [80 000]
(CT) $\nu_1 : \text{W-O-W}$	37 000/268 sh	37 000/268 sh	37 000/268 sh	37 000/268 sh
(ET) $\nu_3 : \text{T}_{1g(\text{F})} \rightarrow {}^4\text{T}_{1g(\text{F})}$	-	-	18 500/540 [60] 19 600/510 sh	-
(ET) $\nu_2 : {}^3\text{A}_{2g(\text{F})} \rightarrow {}^3\text{T}_{1g(\text{F})}$	-	-	-	14 900/671 sh 13 500/740 [12]
Compound	$\text{L}_{(2)}$	$\text{MnL}_{(2)}$	$\text{CoL}_{(2)}$	$\text{NiL}_{(2)}$

**Thermal analysis.** The thermal effects and their interpretation are presented in Table 4. For the interpretation of the thermal effects see part one of the study [1]. The thermal effects are identical and occur at close temperature for the four investigated (HPOM-A)s, revealing their similar structures and the similar nature of the primary heteroatom and addenda.

TABLE 4. Thermal analysis data of  $L_{(2)}$ ,  $MnL_{(2)}$ ,  $CoL_{(2)}$  and  $NiL_{(2)}$ 

Temperature, T (°C)				Effect	Interpretation
106	115	125	120	endothermic	loss of water
185	194	210	208	endothermic	loss of water
312	310	318	313	endothermic	decomposition of the anion
348	349	350	350	endothermic	decomposition of the anion
384	379	375	382	exothermic	crystallization of $WO_3$
780	783	782	781	exothermic	phase transformation of $WO_3$
828	830	825	824	endothermic	melting of $Bi_2O_3$
840	838	839	840	endothermic	phase transformation of $WO_3$
858	860	859	860	endothermic	sublimation of $Bi_2O_3$
$L_{(2)}$ (K salt)	$MnL_{(2)}$ (K salt)	$CoL_{(2)}$ (K salt)	$NiL_{(2)}$ (K salt)	Compound	

**Formula and structure.** Our investigations are in accordance with the formula advanced by Souchay et al. [2], for the parent (HPOM-A), which we noted with  $L_{(2)}$ , i.e.  $[HBiW_{11}O_{38}]^{6-}$ . According to the chemical analysis, the prepared potassium salt has the formula  $K_6[HBiW_{11}O_{38}].11H_2O$ . Also Souchay et al. [2] did not explicitly refer to the structure of the anion, it is clear that they had in view a monolacunary Keggin structure, with an  $BiO_4$  primary group. In this sense, the reserves of those who doubted that a cation as large as  $Bi^{3+}$  can accommodate such a configuration are probably not groundless. Certain research with single crystal X-ray diffraction have shown that Bi(III) and As(III) generate (HPOM-A)s with an  $XO_3$  trigonal pyramid group ( $X=Bi(III)$ ,  $As(III)$ ) [7,8]. Thus, it is probable that the  $[HBiW_{11}O_{38}]^{6-}$  anion is also built around a  $BiO_3$  primary group. In our opinion, this structure could be called monolacunary pseudo-Keggin structure.

In the  $ZL_{(2)}$  complexes, the Z transition metal cation is coordinated as a secondary heteroatom by five oxygen atoms (from the  $O_{(5)}$  cavity generated by the absence of the addendum from the theoretically complete structure) and by a

constitutional water molecule. According to the chemical analysis, the three complex anions have the formulae:  $[\text{HBiMnW}_{11}\text{O}_{38}(\text{H}_2\text{O})]^{5-}$ ,  $[\text{BiCoW}_{11}\text{O}_{38}(\text{H}_2\text{O})]^{5-}$ ,  $[\text{BiNiW}_{11}\text{O}_{38}(\text{H}_2\text{O})]^{5-}$  and a modified pseudo-Keggin structure. According to the same chemical and thermal analysis, the formulae of their potassium salt are:  $\text{K}_5[\text{BiMnW}_{11}\text{O}_{38}(\text{H}_2\text{O})] \cdot 11\text{H}_2\text{O}$ ,  $\text{K}_5[\text{BiCoW}_{11}\text{O}_{38}(\text{H}_2\text{O})] \cdot 10\text{H}_2\text{O}$  and  $\text{K}_5[\text{BiNiW}_{11}\text{O}_{38}(\text{H}_2\text{O})] \cdot 12\text{H}_2\text{O}$ .

## EXPERIMENTAL

**Synthesis of  $\text{L}_{(2)} = \text{HBiW}_{11}\text{O}_{38}^{6-}$  (K salts).** The  $[\text{HBiW}_{11}\text{O}_{38}]^{5-}$  parent (HPOM-A), abbreviated as  $\text{L}_{(2)}$ , was prepared as potassium salt, according to the procedure described by Souchay [2]:  $\text{Bi}(\text{NO}_3)_3 \cdot 5\text{H}_2\text{O}$  (22 g) was dissolved in  $\text{HNO}_3$  11 mol.L<sup>-1</sup> (60 mL) and diluted to 200 mL.  $\text{Na}_2\text{WO}_4 \cdot 2\text{H}_2\text{O}$  (165 g) was dissolved in hot water (60-70°C) to obtain 500 mL solution 1 mol.L<sup>-1</sup>. The first solution was progressively added to the second solution, which has been previously brought to boiling and buffered with 200 mL  $\text{CH}_3\text{COOH}/\text{CH}_3\text{COONa}$  (pH 4). A slightly yellowish solution was obtained, which was further boiled for 2 hours. After cooling, solid  $\text{KNO}_3$  (50 g) was added. After a few days, slow evaporation led to the formation of white crystals, which were purified by several recrystallizations from acidulated water (pH 4). Yield: 81 g (56%).

**Synthesis of  $\text{MnL}_{(2)}$ ,  $\text{CoL}_{(2)}$  and  $\text{NiL}_{(2)}$  (K salts).** The complexes of the parent and ligand (HPOM-A) ( $\text{L}_{(2)} = \text{HBiW}_{11}\text{O}_{38}^{6-}$ ) with transition metal cations ( $\text{Z} = \text{Mn}^{2+}$ ,  $\text{Co}^{2+}$  and  $\text{Ni}^{2+}$ ), which are themselves (HPOM-A)s, were prepared as follows:

**Synthesis of  $\text{MnL}_{(2)}$  (K salt).**  $\text{K}_6[\text{HBiW}_{11}\text{O}_{38}] \cdot 11\text{H}_2\text{O}$  (34 g) was partially dissolved in acidulated water (30 mL, pH=4.5).  $\text{MnCl}_2 \cdot 4\text{H}_2\text{O}$  (2 g) was also dissolved in water (10 mL) and was added to the first solution. The pH of the resulting mixture was adjusted to 4.7 with  $\text{CH}_3\text{COOH}/\text{CH}_3\text{COONa}$  buffer (60 mL). Then, the mixture was heated on a water bath (60-70°C), with stirring, until the solution volume was reduced to half. After cooling, solid  $\text{KNO}_3$  (15 g) was added. After a few days, slow evaporation led to the formation of brown-yellowish crystals, which were purified by several recrystallizations from acidulated water (pH 4.7). Yield: 28 g (82%).

**Synthesis of  $\text{CoL}_{(2)}$  (K salt).** The procedure of  $\text{MnL}_{(2)}$  is followed.  $\text{CoCl}_2 \cdot 6\text{H}_2\text{O}$  (2.4 g) was used instead of  $\text{MnCl}_2 \cdot 4\text{H}_2\text{O}$ . Dark red crystals were obtained. Yield: 25 g (71%).

**Synthesis of  $\text{NiL}_{(2)}$  (K salt).** The procedure of  $\text{MnL}_{(2)}$  is followed.  $\text{NiCl}_2 \cdot 6\text{H}_2\text{O}$  (2.4 g) was used instead of  $\text{MnCl}_2 \cdot 4\text{H}_2\text{O}$ . Green yellowish crystals were obtained. Yield: 26 g (77%).

**Chemical analysis.** K was directly determined in solution, by atomic emission spectrophotometry.

Bi was determined gravimetrically, as  $\text{BiI}_3$ . The compound was decomposed by boiling with  $\text{NaOH}$  11 mol.L<sup>-1</sup> (120°C, 30 min). The resulting solution was neutralized and then acidulated with  $\text{HNO}_3$ . Solid  $\text{KI}$  was added, after which the solution was diluted, heated and filtered.

Mn, Co and Ni were determined spectrophotometrically. The compound was decomposed by boiling with  $\text{NaOH}$  11 mol.L<sup>-1</sup> (120°C, 30 min). The resulting solution was neutralized and slightly acidulated with  $\text{HCl}$ . The extinction was measured at  $\lambda = 475$  nm (for Mn), 515 nm (for Co) and 649 nm (for Ni) (owing to the very weak absorption bands of  $[\text{Mn}(\text{H}_2\text{O})_6]^{2+}$ , Mn was determined as  $\text{MnO}_4^-$ , after oxidation with  $\text{H}_2\text{O}_2$ , in the presence of heat).

W was determined spectrophotometrically. The compound was decomposed by boiling with  $\text{NaOH}$  11 mol.L<sup>-1</sup> (120°C, 30 min). The resulting solution was neutralized with diluted  $\text{HCl}$  and  $\text{H}_3\text{PO}_4 + \text{NaVO}_3$  reagent was added. The extinction was measured at  $\lambda = 400$  nm.

$\text{H}_2\text{O}$  was determined by thermal analysis, from mass loss at 220°C.

**Vibrational spectra (IR spectra).** The vibrational spectra were recorded in the IR range 1 200-500  $\text{cm}^{-1}$ , with an IR Perkin Elmer 580 B spectrophotometer.

**Electronic spectra (UV/VIS spectra).** The electronic spectra were recorded in the UV/VIS range 51 300-11 100  $\text{cm}^{-1}$  (1945 - 900 nm), with an UV/VIS Perkin Elmer 550 SE spectrophotometer.

**Thermal analysis.** The thermal analysis was carried out on a Nietzsche STR 409 simultaneous thermoanalyser (Parameters: temperature range 20-900°C, heating rate 5°C.min<sup>-1</sup>).

REFERENCES

1. A Pătruț, C.Roșu and H.P.Beck, *Studia Univ. Babeș-Bolyai, Ser. Chem.*, 1995,, **40(1-2)**, 23.
2. P.Souchay,M.Leray and G.Hervé, *C. R. Acad. Sci. Paris, Sec. Ç.*, 1970, **271**, 1337.
3. T.J.R.Weakley, *Struct. Bonding (Berlin)*, 1974, **18**, 131.
4. M.T.Pope, *"Heteropoly and Isopoly Oxometalates"*, Springer, Berlin, Heidelberg, New-York, Tokyo, 1983.
5. A.Pătruț, G.Marcu, A.Botar and A.Naumescu, *Studia Univ. Babeș-Bolyai, Ser. Chem.*, 1989, **34(2)**, 46.
6. M.Michelon and G.Hervé, *C. R. Acad. Sci. Paris, Ser. C.*,1972, **274**, 209.
7. Y.Ozawa and Y.Sasaki, *Chem. Lett.*,1987, **5**, 923.
8. Y.Jeannin and J.Martin-Frère, *Inorg. Chem.*, 1979, **18**, 3010.

Received: 5.11.1994

## CAPACITIVE-TYPE HUMIDITY SENSOR BASED ON METHACRYLATE-CO-POLYMER AND POLYIMIDE

Cecilia Roman, Olimpiu Bodea, Andrei Levi, Nicolae Prodan,  
Emil Cordoș\*, Ionel Manovicu\*\*

*Research Center for Analytical Instrumentation, PO Box 717,  
Of. Post 5, 3400 Cluj-Napoca, ROMANIA*

*\*Dept. of Chemistry, University "Babes-Bolyai",  
Arany Janos 11, 3400 Cluj-Napoca, ROMANIA*

*\*\*Technical University Timișoara,  
Bocșei 6-8, 1900 Timișoara, ROMANIA*

### ABSTRACT

Two types of capacitive-type humidity sensors have been prepared using: (i) cross-linked poly[methyl methacrylate-co-(2-hydroxypropyl-methacrylate)]; (ii) commercially polyimide. The sensors have been prepared in a sandwich structure: alumina substrate + lower gold electrodes + thin film polymer + upper gold electrode. The sensitivity (the ratio of capacitance at  $x\%$  RH to that at 12% RH), the hysteresis, the response time, the durability against acetone vapours and the drift of the two sensors have been measured and compared. The characteristics of the capacitive-type humidity sensor using methacrylate-co-polymer are better than the sensor prepared using polyimide.

### INTRODUCTION

Humidity sensing is an important parameter in the control of relative humidity (RH) in industrial processes where the efficiency of drying operation can be improved. Due to the widespread applications of humidity sensors, the demands made on the characteristics of the device, such as sensitivity, response time, reproducibility, etc., are specific for the field of application.

An impressive number of humidity sensing systems are based on physical methods. Many sensors, which make use of the dependence of electrical properties (e.g. resistance [1, 3], capacitance [4, 8] or conductivity [9, 11]) of different materials (e.g. porous ceramics, organic polymers) on humidity, can be found in the literature and some of them are commercially available. In recent years, organic polymers have been investigated for their sensor properties. The water content of many polymers depends on the partial pressure of water in air. Only a few polymers show this effect with reproducibility and sensitivity without too much hysteresis.

There are two main families, depending on whether a variation occurs essentially in capacitance or essentially in the resistance. The advantage of using a variation in capacitance is the good specificity of the physical phenomenon used (high dielectric constant of water).

Until the early 1980s the polymer generally used by manufactures belonged to the cellulose acetate butyrate family [12, 16], but these materials were unsatisfactory in practical application with respect to hysteresis, stability, reversibility, etc. To overcome this disadvantages the sensing material must have low hygroscopicity and rigid structure.

Polyimide (PI) and poly(methyl methacrylate) (PMMA) are an attractive material for use as a humidity sensor because they have high mechanical strength, chemical stability, low hygroscopicity and low solubility to common organic solvents [17].

In the present study the sensing characteristics of a capacitive-type humidity sensor using polyimide and methacrylic copolymers are examined.

## EXPERIMENTAL

The polymers were used in solutions, prepared as follows:

(i) the poly(methyl methacrylate-co-(2-hydroxy-propyl-methacrylate)) solution was prepared by polymerization of a mixture of methyl methacrylate (Merck) and 2-hydroxy-propyl methacrylate (Merck), both previously distilled under reduced pressure in a 4:1 mol ratio, with 1% mol benzoyl peroxide ("Reactivul" București) as initiator, at 80 °C.

When an appropriate viscosity was yielded, the polymeric solution was cooled and 5% mol of di-vinyl-benzene (Merck), previously distilled under reduced pressure, were added as cross-linking reagent. After casting on support, the polymeric film were thermally treated at 120 °C for 24 h.

(ii) A 5% polyimide solution was prepared by dissolving polyimide powder P84 (LENZING AG) in N-methylpyrrolidone (Reactivul București).

The detailed structure of the sensor is displayed in Fig. 1.

The solutions above, were cast by spin-coating onto a pair of gold electrodes (3,4) evaporated on a 10 x 6 x 0.8 mm alumina plate (IPEE Curtea de Argeș) (5). The upper gold electrode (10 - 20 nm) (1) was deposited by vacuum evaporation (IEV 80, IFA București) to obtain two serial connected capacitors with the polymers as dielectric (2).

A low-frequency generator type E0502M (IEMI București) was used to measure capacity at 100 kHz. To obtain a constant controlled RH atmosphere, solutions of saturated salts at 20 °C in closed space were used [18] (see Table 1)

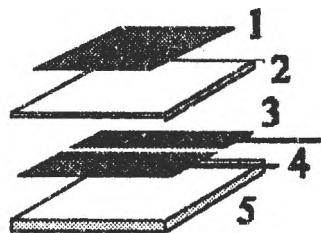


Fig.1 The structure of the sensor

Table 1

Salts	LiCl x H <sub>2</sub> O	CaCl <sub>2</sub> x 6 H <sub>2</sub> O	NaHSO <sub>4</sub> x H <sub>2</sub> O	NaNO <sub>2</sub>	NaClO <sub>3</sub>	KBr	ZnSO <sub>4</sub> x 7 H <sub>2</sub> O	Na <sub>2</sub> SO <sub>4</sub> x10 H <sub>2</sub> O
RH (%)	12	32.3	52	66	75	84	90	93

**RESULTS AND DISCUSSIONS**

Fig. 2 illustrates the relationship between the sensitivity (the ratio of capacitance at "x"% RH to that at 12% RH) and relative humidity over the humidity range of 12 - 95% RH. From this figure we can see that the two sensors have a good linearity over the humidity range of 12 - 90% RH and these are preferable characteristics of a humidity sensor. Among the prepared sensors, the sensitivity *S* (capacitance at 95% RH/capacitance at 12% RH ratio) of the methacrylic copolymer sensor was  $S_{PMMA} = 1.21$  and it has a value of  $S_{PI} = 1.14$  for polyimide sensor. The increase of sensitivity of PMMA sensor seems to arise from the hydrophilic groups of HPMA affecting the hygroscopic characteristics.

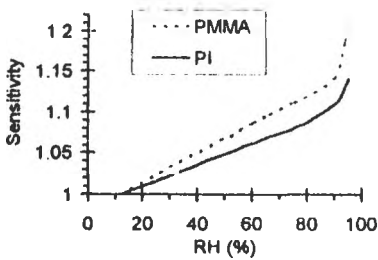


Fig.2 Sensitivity of the sensors at 100 kHz and 20 °C

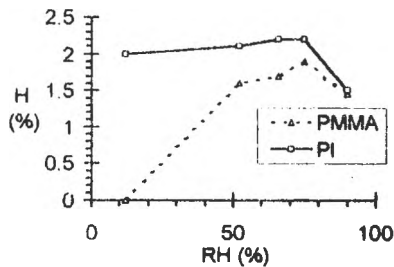


Fig.3 Hysteresis for PMMA and PI at 100k Hz and 20 °C

The hysteresis, *H* [defined as :  $(C_i - C_i)/C_i$  where  $C_i$  - the value of capacitance at RH% (RH increases);  $C_i$  - the value of capacitance at the same RH% (when RH decreases)] of the sensors is shown in Fig. 3. The values of hysteresis for the two sensors are:  $H_{PMMA} < 2\%$ ;  $H_{PI} \sim 2.2\%$ . The sorption sites of the water are the free spaces around the polar sites of the polymer. The density of the polymer increased as the result of the crosslinked and polymerization reactions and the available spaces of the water molecules sorption and diffusion decreased.

Hysteresis was detected having small values, because the amount of sorbed water is small and the formation of clusters of sorbed water are prevented.

The drift at 95% RH (D) is defined as the difference between the asymptotic value of capacitance at saturation and the value after 1 h at 95% RH. The drift values are  $D_{PMMA} = 2,1 \%$  and  $D_{PI} = 2,8 \%$ .

The response time of the sensors to sharp changes in RH was measured by rapidly transferring the sensor from the vessel in which it had equilibrated at high RH (using a saturated salt solution) into relatively low RH (50%) in the atmosphere from the laboratory on the day of experiment. (In ref. 18 the response time was defined as that taken to reach 63% of the final values.) Returning the sensor to the 95% RH (vessel) caused the capacitance to return to the 95% RH "baseline" value.

The response was very fast. The response time was within ~ 1 min for the sensor based on PMMA, and ~ 5 min for the sensor based on PI.

The effect of acetone vapours was tested since acetone is a good organic solvent for PMMA and PI. After exposure to saturated acetone vapours for 15 min in a closed vessel (0% RH) the sensors were rapidly transferred to the vessel in which the humidity was controlled. The sensitivity at various humidities was measured. The capacitance was quite stable showing a small effect by acetone vapours. This means that the acetone vapours are simple absorbed without permanent deformation of the thin film.

## CONCLUSIONS

We have prepared two capacitive-type humidity sensors using methacrylate copolymer and polyimide. The characteristics of the sensors were as follows:

1. Methacrylic copolymer and polyimide have a hydrophobic character and the water molecules did not form clusters. That explains the small hysteresis.
2. The sensors have a good sensitivity and linearity ( $S_{PMMA}=1.21$ ;  $S_{PI} = 1.14$ ).
3. The sensor composed of crosslinked PMMA exhibits durability against acetone vapour
4. The sensor based on methacrylic copolymer is superior with respect to hysteresis and the drift ( $H_{PMMA} < 2\%$ ,  $H_{PI} = 2.2\%$ ;  $D_{PMMA} = 2.1\%$   $D_{PI} = 2.8\%$ ).



The authors consider that clarifying the relation between the density of polymer and sorption behaviour leads to the development of a reliable humidity sensor.

#### REFERENCES

1. K.H.Murata, O.S.Kitso, T.S.Okabe, US Patent No. 4 442 422 (10 Apr. , 1984)
2. T.Yamamoto, H.Shimizu, Trans IECE of Japan, J64, 9 (1981)
3. T.Yamamoto, H.Shimizu, in "Program and Abstracts of 2nd Int.Conf. Solid-State Sensors and Actuators" (Delft, the Netherlands) , 1983, p. 126
4. N.Kinjo, S.Ohara, T.Sugawara, S.Tuchitani, *Polymer J.* **15** (1983) 621
5. T.Yamamoto, H.Shimizu, "Proc. 4th Sensor Symp." (Tsukuba, Japan), 1984, p. 119
6. K.L.Rauen, D.A.Smith, W.R.Heineman, *Sensors and Actuators B*, **17** (1993) 61
7. H.H.Seidel, *Wiss.Z. TH Karl-Marx-Stadt*, **4** (1985) p. 3
8. Boltshauser, H.Baltes, *Sensors and Actuators A*, **25-27** (1991) 509
9. S.V. Silverthorne, C.W. Watson, R.D.Baxter, *Sensors and Actuators B*, **19** (1989) 371
10. D.E.Williams, P.McGeelin "Solid-State Gas Sensors and Monitors", AERE, Harwell, 1985, UK
11. Y.Shimizu, H.Okada, H.Asai "Proc. 2nd Int. Meet. Chem. Sensors", Bordeaux, France, July 7-10, 1989, p. 380
12. K.Katayama, H.Hasegawa, T.Noda, T.Akiba, *Sensors and Actuators B*, **2** (1990) 143
13. T.Seyiama (ed.) "Chemical Sensors Technology", vol. 2, Kodansha, Tokyo/Elsevier, Amsterdam, 1989, p. 99
14. Y.Sadaoka, M.Matsuguchi, Y.Sakai, *Sensors and Actuators*, **26** (1991) 489
15. Y.Sadaoka, M.Matsuguchi, Y.Sakai, *J.Electrochem.Soc.*, **138** (1991) 489
16. G.Kampfrath, D.Duschi, C.Hamann, *Acta Polym.*, **38** (1987) 389
17. C.Hamann, G.Kampfrath, M.Mueller, *Sensors and Actuators, B1* (1990) 142
18. K.Goette "Feuchtemesstechnicke", Verlag Technik, Berlin, 1966, p.24

Received:12.12.1994



## DECYANIDATION OF INDUSTRIAL WATERS THROUGH OZONIZATION

Maria Stanca \* , Zoltan Bocsikai \*\* , Andrada Măicăneanu \*

*\* Department of Technological Chemistry , " Babeș - Bolyai " University ,  
Cluj - Napoca 3400 , Romania*

*\*\* Institute of Research and Design for Electrical Engineering ,  
Bistrița 4400 , Romania*

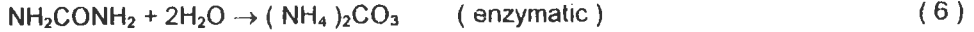
### ABSTRACT

In this paper it is presented a study of the action of ozone on cyanide ion in a watery medium , to determine the consumption of ozone in a certain time and the influence of pH and of copper ions on the reaction of oxidation .

### INTRODUCTION

The ozone (  $O_3$  ) is a strong oxidizer which being used in a correct way may contribute on a large scale to the maintaining of the quality of the environment . Comparing it with other oxidizing agents , for example chlorine , the ozone oxidation of the cyanides will not produce any toxic residue before being eliminated from the aqueous medium . In the process of oxidation of the cyanide with chlorine may appear the chlorcyan (  $CNCl$  ) which is a very toxic substance . This is not the single advantage . It may also decrease the time of each reaction , it may produce the ozone at the very place of its use , it may improve the organic qualities of the water , etc . In principle  $O_3$  reacts quickly and completely with the cyanides .

In the speciality works we find different ways of oxidation with ozone of the cyanide ion in a aqueous medium . Cr. Fafian considers that the oxidation can be expressed by the reaction sequence ( 1 - 7 ) [ 1 ] :



W. Zaban considers that the oxidation follows the equation (8) [3].



S. Kustanov and his co-workers determine the ozone mole consumption for the oxidation of the cyanide showing that there is necessary to use 0,5 O<sub>3</sub> moles for the oxidation of 1 gram-ion CN<sup>-</sup>, suggesting the following reaction (9) [4].



## EXPERIMENTAL

In order to study the oxidation we used an experimental equipment consisting of an ozone-generator from the air, an oxidation tower made of Pyrom glass and a reaction vessel with KI 1% used for the determination of the unreacted ozone. The experimental equipment is drawn in figure 1.

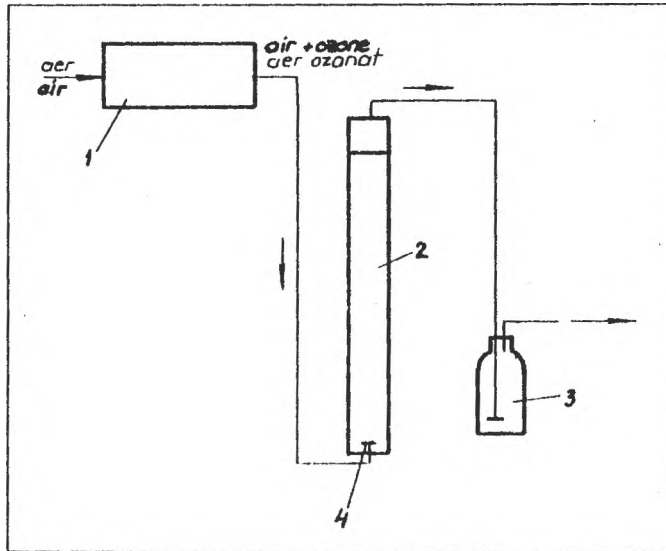


FIGURE 1. The experimental equipment of oxidation with ozone of the aqueous solutions of cyanide. 1-ozone generator ; 2-oxidation tower ; 3-reaction vessel for the determination of the unreacted-ozone ; 4-ceramics spreading .

## Decyanidation of Industrial Waters Through Ozonization

The generator of ozone has supplied ozonized air with a concentration of  $20\text{gO}_3/\text{m}^3$  and a flow rate of  $0,25\text{ m}^3/\text{h}$ . The aqueous solutions of cyanide being oxidated in the oxidation tower had the initial concentrations as follows : 60 , 100 , and  $130\text{mgCN}^-/\text{l}$ .

The gas phase contacted the liquid phase through the bubbling of gas in the aqueous solutions of the cyanide under the conditions of  $\text{pH} = 10$  and  $t = 18^\circ\text{C}$ .

The influence of the pH values in the case of oxidation with ozone has been studied in particular cases of  $\text{pH} : 5,5 ; 7,0 ; 10$ .

The effect of the copper ions during the oxidation reaction with ozone has been studied through the comparison of variation of cyanide concentration in a definite period of time , both in solutions containing copper ions and without copper ions .

At the end of the oxidation we made copper ions analysis according to STAS 7795-67 . The cyanides has been through the colour - test according to STAS 7685-66 .

## RESULTS AND DISCUSSION

The variation of cyanide concentrations in a certain time is shown in figure 2 .

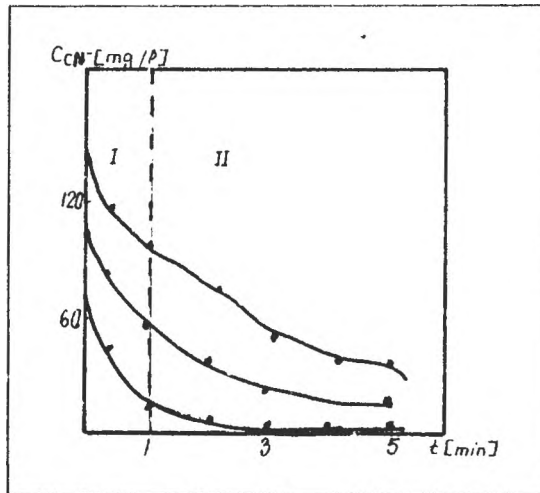


FIGURE 2. The variation of  $\text{CN}^-$  concentration during a certain period of time .

The experimental results prove the fact that during the first minute of the oxidation , when the concentration of oxidation product is at a low level , the ozone quantity consumed is about  $0,7\text{gO}_3/1\text{gCN}^-$  , corresponding approximately to  $0,35\text{molesO}_3/1\text{gram-ionCN}^-$  , these experimental figures corresponding to the reaction ( 8 ) given by W. Zaban . This reaction mainly takes place in the first zone . For the entire destroy of the cyanide ions from the aqueous solution we recorded an average consumption of  $0,96\text{gO}_3/1\text{gCN}^-$  .

The experimental results show that in the environment conditions the ozone reacts not only with  $CN^-$  but also with the oxidation products resulting in the oxidation process of cyanide ion. According as the concentration of oxidation products increases the ozone is consumed in the solution both for oxidation of the existing reaction products and for the oxidation of the cyanide ion according to the reaction sequence ( 1 - 7 ) prevalent in the second zone .

The influence of copper ions on the oxidation reaction show in figure 3. points out the fact that the copper ions increase the speed of the oxidation reaction with ozone of the cyanide .

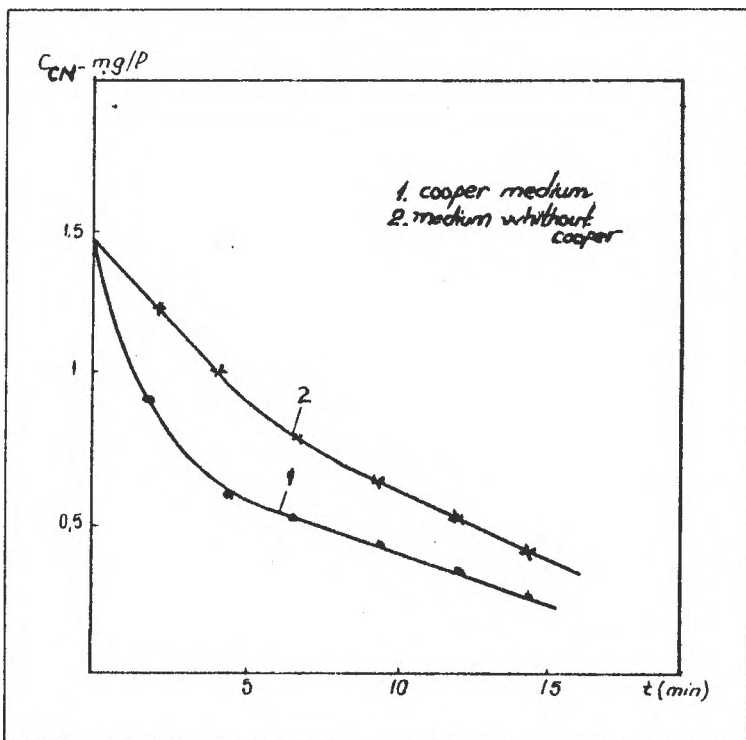


FIGURE 3. The influence of copper ions on the oxidation reaction with ozone of the cyanide . 1-copper ions medium ; 2-medium without copper ions .

The copper ions find again in the aqueous solution at the end of the oxidation reaction pointing out the fact that the copper ions have a catalytic effect in the

## Decyanidation of Industrial Waters Through Ozonization

oxidation reaction accelerating the transmission of the active oxygen to the cyanide group .

The influence of the pH on the oxidation reaction showed in figure 4. proves that the most favourable medium of the reaction is the low level alkaline medium of a pH = 10 .

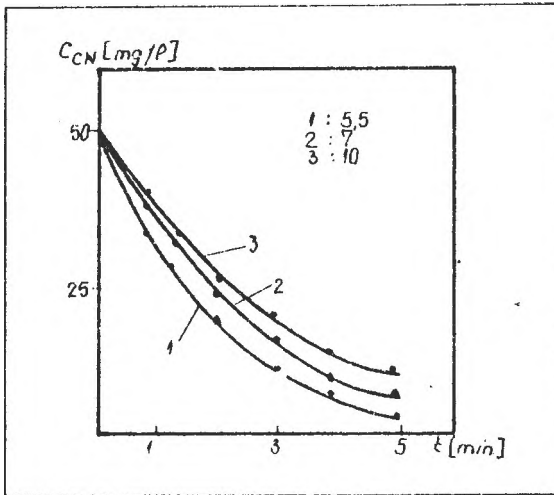


FIGURE 4. The influence of the pH during the reaction with ozone of the CN<sup>-</sup>.

As the pH goes lower , the speed of the reaction also decreases , only the times of the reaction being increases .

### CONCLUSIONS

One may draw the conclusion that during the first minutes of the oxidation reaction of the cyanide the reaction follows mainly the reaction ( 8 ) and the supplementary consumption of ozone comparative with the stoichiometric estimation is due to the equations 1 - 7

The most favourable medium of the oxidation reaction from the kinetic point of view is the low level alkaline medium of pH = 10

Copper ions have a catalyst role in the oxidation reaction with ozone of the cyanide .

REFERENCES

1. Cr. , Fabian , *Galvanotechnik* , 1975 , **66** , 100
2. T. , Bober , *Ozonation of Photographic Processing Waster* , *Journal W.C.P.F.* , 1975 august , 2114
3. W. , Zaban , *Palting and Surface Zinishing* , 1980 august
4. S. , Kustanov , *Ucrancki Himicesechii Journal* , 1978 , **44** , 1287
5. H. , Eisenhauer , *Journal W.P.C.F.* , 1968 , **40** , 1887
6. V , Caprio , A. , Insola , *La chimica i L' industria* 1975 , **57** , 311
7. D. , Negoiu , *Tratat de chimie anorganică* , Editura Tehnică , București , 1972
8. \* \* \* \* \* *Cqlecție STAS* , Editura Tehnică , București , 1979 .

Received:20.12.1994



## THE INFLUENCE OF PRECIPITATION CONDITIONS ON THE QUALITY OF CALCIUM TUNGSTATE USED IN PHOSPHOR SYNTHESIS

Flavia Forgaciu<sup>a</sup>, Miloslava Nemes<sup>a</sup>, Elisabeth J.Popovici<sup>a</sup>, Veronica Ursu<sup>b</sup> and Dan Macarovici<sup>a</sup>

*a. Institute of Chemistry "Raluca Ripan", Str.Fântânele 30, 3400- Cluj-Napoca*

*b. Institute of Physical Chemistry of the Romanian Academy, Spl. Independenței 202, Bucharest, ROMANIA*

### ABSTRACT

Calcium tungstate used in phosphor synthesis was precipitated from  $\text{CaCl}_2$  and  $\text{Na}_2\text{WO}_4$  solutions. The influence of precipitation conditions on the quality of  $\text{CaWO}_4$  precipitate was studied. It has been ascertained that the reagent concentration, the temperature and the pH of the precipitation medium determine the purity, morpho-crystalline structure and particle size distribution of  $\text{CaWO}_4$ -precipitate thus influencing the luminescent properties of  $\text{CaWO}_4$ -phosphor samples. The optimum precipitation conditions for calcium tungstate used in phosphor synthesis were established.

### INTRODUCTION

The  $\text{CaWO}_4$  can be excited by X-rays, short wavelength ultraviolet radiation, cathode rays etc. and are used especially for the manufacture of X-ray intensifying screens. The luminescent emission is correlated with certain electronic transitions which take place inside of some native defects (self-activated phosphor) or rare earths ions which are uniformly distributed into the well-formed crystalline structure of calcium tungstate. The nature of the self-activated luminescence centres and the luminescence process have not been entirely elucidated yet, so, tungstate phosphors still arise a lot of interest [1-3].

The phosphor synthesis implies both the preparation of the host crystalline substance (i.e. tetr- $\text{CaWO}_4$ ) and the formation of luminescence centres (i.e. some imperfect tetrahedral  $\text{WO}_4$ -groups) [4]. Generally, the self-activated phosphor could be obtained by the calcination of the  $\text{CaWO}_4$ -precipitate. The earlier literature gave, in majority of cases, rather incomplete technical information (under patent cover) on phosphor preparation. The indicated precipitation conditions vary to a large extent

and the information about the influence of the  $\text{CaWO}_4$ -precipitate quality on the resulting phosphor are missing. The precipitation is carried out from calcium chloride (or nitrate) and sodium (or ammonium) tungstate solutions which are sequentially or simultaneously added. The reagent concentration is 0.5-2.0 mol/l and the precipitation pH is 8.0-10.0 [5-7]. The  $\text{CaWO}_4$ -precipitate undergoes a thermal treatment so that luminescence centres are created and the  $\text{CaWO}_4$ -phosphor is synthesised. The phosphor thermal synthesis takes place at 700-900°C, with or without mineralising agent into the synthesis mixture [8,9].

The self-activated  $\text{CaWO}_4$  is one of the most sensitive phosphors to the variations of the synthesis conditions which might affect the concentration of the native lattice defects. One can mention that, attempts have been recently made at controlling the defect concentration by addition of donor or acceptor impurities so that a new way in phosphor synthesis has been opened [10,11].

Our preliminary tests concerning the synthesis of self-activated  $\text{CaWO}_4$ -phosphor gave no reproducible results. Despite the thermal synthesis conditions were kept constant, the luminescent intensity of various  $\text{CaWO}_4$ -phosphor samples showed differences with up to 20%. This could be explained only by the different quality of the various  $\text{CaWO}_4$  precipitate samples.

The objective of this paper is to study the way in which the precipitation conditions can affect the quality of the precipitated calcium tungstate and consequently, the properties of the self-activated phosphor. Actually, this study has enabled us to establish the optimum precipitation conditions for calcium tungstate used in phosphor synthesis.

## EXPERIMENTAL

Luminescent grade (i.g)  $\text{CaWO}_4$  is prepared from highly purified solutions of  $\text{CaCl}_2$  and  $\text{Na}_2\text{WO}_4$ . Equal volumes of reagent solutions with equal concentrations were simultaneously added to a bottom solution containing a small  $\text{Na}_2\text{WO}_4$  amount. The precipitation pH was adjusted to a domain between 7.0 and 10.0 by using small quantities of diluted solutions of  $\text{CH}_3\text{COOH}$  or  $\text{NaOH}$ . The precipitation was conducted at 20°C or 60°C and was followed by a maturation stage (1 hr) taking place at 20°C or 95°C, respectively. The precipitate batches were filtered, well washed and dried at 105°C.

In order to synthesise the corresponding phosphor samples, all  $\text{CaWO}_4$  precipitate batches were calcinated at 900°C, in air, for 1 hr. The precipitate batches were analysed by electronic microscopy, thermal analysis, X-ray diffraction and particle size analysis (Coulter Counter method). The luminescence of phosphor samples was estimated on the basis of emission spectra which were registered on a Perkin Elmer Spectrofluorimeter, with a 254 nm UV excitation, in comparison with a  $\text{CaWO}_4$ -phosphor taken as an internal standard.

## Calcium Tungstate for Phosphor Synthesis

### RESULTS AND DISCUSSION

Calcium tungstate was prepared according to the following reaction equation :



The preliminary precipitation tests with  $\text{CaCl}_2$  and  $\text{Na}_2\text{WO}_4$  solutions having initial pH-values of 6,5 - 6,9 and 8,5 - 9,0, respectively, indicated some fluctuations of the medium pH which might affect the quality of calcium tungstate used in phosphor synthesis. In order to check out the validity of this supposition and to find the optimum precipitation pH, four batches of  $\text{CaWO}_4$ -precipitate were prepared at pH equal to 7.0; 8.0; 9.0 and 10.0 and subsequently converted into four phosphor samples.

The emission spectra, depicted in figure 1, illustrate the fact that all phosphor samples exhibit the characteristic blue luminescence with emission maximum at the same wavelength (400 nm) but with very different emission intensities. The highest value is presented by the phosphor sample synthesised from  $\text{CaWO}_4$ -precipitate obtained at pH=8.0. The other samples show much lower emission intensities which might be explained as follows.

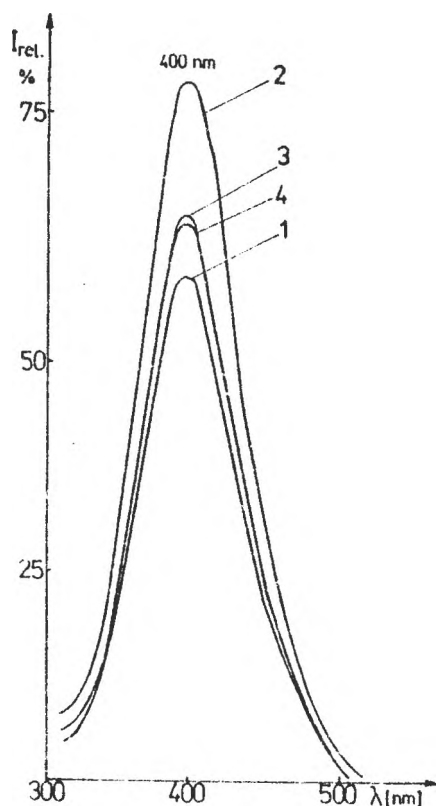


Fig. 1. Emission spectra of phosphor samples prepared from  $\text{CaWO}_4$  precipitated in different pH conditions ( $c = 0.5 \text{ mol/l}$ ;  $T = 60^\circ \text{C}$ ):  
1) pH= 7.0; 2) pH = 8.0;  
3) pH = 9.0, 4) pH = 10.0.

The precipitation product formed at pH -values, lower or higher than 8.0, might contain small quantities of tungstic acid or calcium hydroxide, respectively. Consequently, the corresponding phosphor samples obtained by calcination would contain even tungstic trioxide or calcium oxide, both determining the decrease in the luminescence yield (CaO absorbs the exciting UV radiation and  $\text{WO}_3$  absorbs the blue luminescent emission of  $\text{CaWO}_4$  - phosphor).

The X-ray diffraction spectra confirm the  $\text{WO}_3$  presence into the  $\text{CaWO}_4$  - phosphor sample corresponding to pH = 7.0. It must be also noted that all  $\text{CaWO}_4$  -precipitate batches exhibit the characteristic crystalline structure of scheelite (tetragonal). The calcination process, generating the phosphor samples, only enhances the crystallinity degree of the calcium tungstate lattice.

The different quality of  $\text{CaWO}_4$  batches precipitated in various pH conditions was also confirmed by the thermal analysis. Although the weight-loss values are small and the thermal effects are of low intensity, the precipitate batches could be differentiated from one another (fig.2). The thermogravimetric curves of  $\text{CaWO}_4$  precipitates obtained at pH = 8.0 and pH = 9.0 indicate a weight-loss of about 2.5% which might be explained by the removal of both the remanent humidity and the constitutional water. The differential thermogravimetric (DTG) curves suggest that the dehydration effect is more intense at 250-350 °C and is completed at 600-700 °C. For  $\text{CaWO}_4$  - precipitate prepared at pH = 7.0 and pH = 10.0, one can observe additional dehydration processes which could be correlated with the presence of tungstic acid ( $\text{H}_2\text{WO}_4 \cdot \text{H}_2\text{O}$ ) or calcium hydroxide, respectively. For these two  $\text{CaWO}_4$  -batches, the weight-loss is slightly higher, namely 3.2%. The mentioned dehydration processes are confirmed by the thermal effects which are observed on the differential thermal analysis (DTA) curves.

The microscopical analysis of the  $\text{CaWO}_4$ -precipitate particles indicates that the pH of the precipitation medium exerts an influence on their morpho-crystalline structure. The precipitate formed at pH = 8.0 consists mostly of individual rhomboedric crystals, 8-13  $\mu\text{m}$  in size. At higher pH-values, conglomerates of irregular particles are also formed whereas, at a lower pH-value only conglomerates of small spherical particles are observed. This morpho-crystalline structure of precipitate particles might influence the formation of luminescence

## Calcium Tungstate for Phosphor Synthesis

centres during the thermal treatment stage for phosphor synthesis. Consequently, the diminished emission intensities of phosphor samples prepared from  $\text{CaWO}_4$  precipitated at pH values lower or higher than 8.0 could be explained by both the presence of some impurities and the irregular appearance and size of precipitate particles.

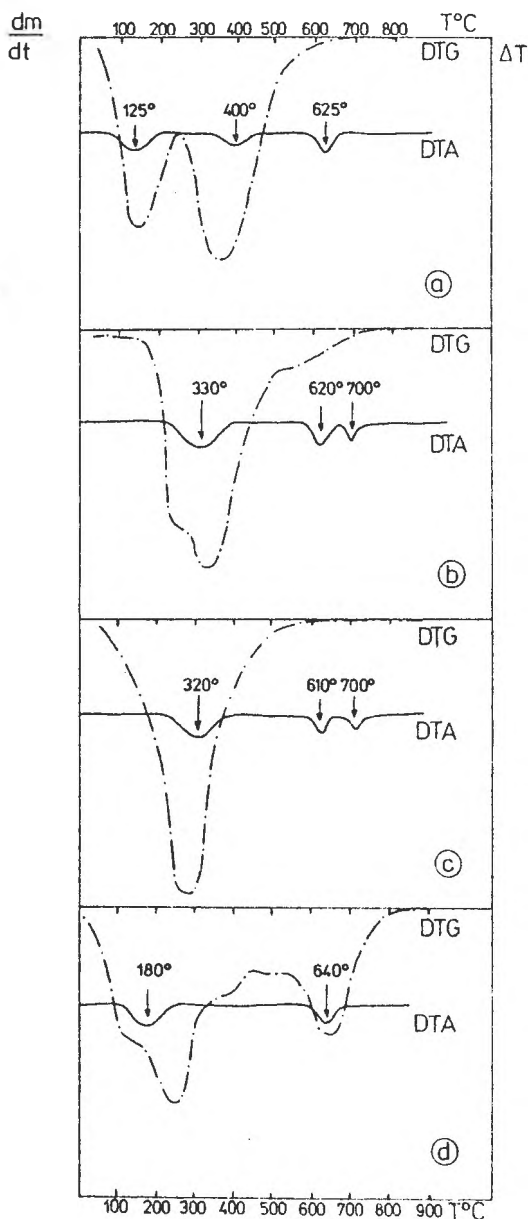


Fig.2. Differential thermogravimetric curves (DTG) and differential thermal analysis curves (DTA) of  $\text{CaWO}_4$  precipitated in different pH conditions ( $c=0.5 \text{ mol/l}$ ;  $T=60^\circ\text{C}$ ):

- a) pH= 7.0;  $\Delta m=-3.2 \%$
- b) pH= 8.0;  $\Delta m=-2.5 \%$
- c) pH= 9.0;  $\Delta m=-2.5 \%$
- d) pH=10.0;  $\Delta m=-3.2 \%$

The reagent concentration could also influence the quality of  $\text{CaWO}_4$ -precipitate and consequently that of  $\text{CaWO}_4$ -phosphor. In order to study this influence, three precipitate batches were prepared from  $\text{CaCl}_2$  and  $\text{Na}_2\text{WO}_4$  solutions of 0.25 ; 0.50 and 1.0 mol / l concentrations. The registered emission spectra indicate that all phosphor samples exhibit the same luminescence colour (emission maximum at 400 nm ) but rather different luminescence brightness (various emission intensities). The strongest blue luminescence is shown by phosphor sample corresponding to  $\text{CaWO}_4$  precipitated from 0.5 mol / l solutions ( fig.3).

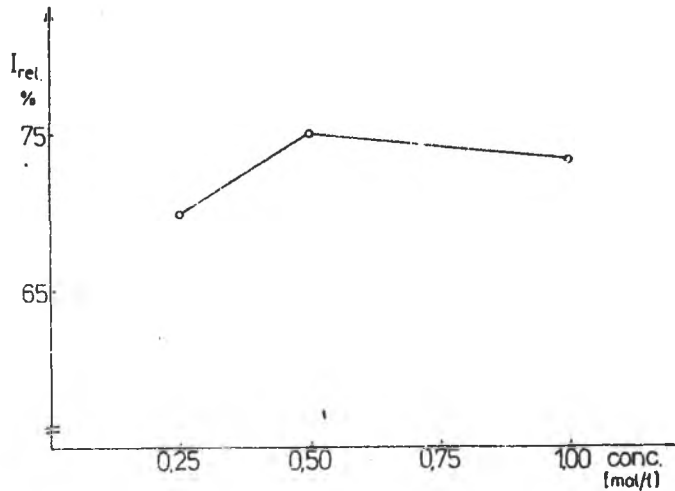


Fig . 3 . Variation of emission intensity of phosphor samples with the reagent concentration used in  $\text{CaWO}_4$  precipitation ( pH = 8.0; T = 60°C )

The rather small variation of the emission intensity with the reagent concentration could come from some small morpho-crystalline differences between the three corresponding precipitate batches, as it was in fact proved by the microscopical analysis. Moreover, the tendency of particle size diminution, simultaneously with the increase in reagent concentration was also observed. From 0.50 mol/l solutions, individual crystals of size 8 -13  $\mu\text{m}$  are formed whereas from 1.0 mol/l solutions crystalline agglomerates of 5 -10  $\mu\text{m}$  are obtained.

The influence of the thermal conditions of precipitation-maturation on the quality of  $\text{CaWO}_4$ -precipitate and consequently, on the quality of the corresponding phosphor samples, was also studied. In this respect, two  $\text{CaWO}_4$ -precipitate batches were prepared in warm and cold precipitation medium respectively, and were converted

## Calcium Tungstate for Phosphor Synthesis

into corresponding phosphor samples. The two phosphor samples show no difference in their luminescence colour, but a slight one in their emission intensity ( $I_{rel}$ ). They are essentially different in their particle size distribution (table nr.1).

The temperature of precipitation - maturation medium strongly influences the particle size distribution of the  $\text{CaWO}_4$  -precipitate batches. The precipitate powders obtained in cold and warm precipitation medium exhibit homogenous particle size distribution with different median diameter ( $d_{50\%}$ ), namely 30  $\mu\text{m}$  and 16  $\mu\text{m}$ , respectively.

Table 1. Some characteristics of  $\text{CaWO}_4$  precipitate A obtained in different precipitation conditions and of the corresponding phosphor samples B

Nr.	$\text{CaWO}_4$ -type	Precipitation conditions*	$I_{rel}$ (%)	$d_{50\%}$ ( $\mu\text{m}$ )
1 A	Precipitate	pH = 8.0 - 8.2 c = 0.5 mol / l	—	16
1 B	Phosphor	T = 60°C / 95°C	78	6.5
2 A	Precipitate	pH = 8.0 - 8.2 c = 0.5 mol / l	—	30.0
2 B	Phosphor	T = 20° / 20°C	81	23.0

\* T = 60° / 95°C represents the precipitation / maturation temperature ;

By synthesising the phosphor samples, significant modifications of particle size distribution appear. The precipitate batches are disaggregated and consequently smaller phosphor particles are generated. The disaggregation effect is stronger for  $\text{CaWO}_4$  obtained in warm precipitation medium, thus generating the smallest phosphor particles ( $d_{50\%} = 6.5 \mu\text{m}$ ). However, in this case, the particle size distribution becomes nonhomogenous, presenting two maxima, at about 3  $\mu\text{m}$  and 16  $\mu\text{m}$ ; during the thermal treatment, the natural process of particle growing arises and acts in opposite direction. The various luminescent intensities of the two samples might be explained partially through the different particle size distribution.

## CONCLUSIONS

The reagent concentration, the temperature and the pH of the precipitation medium determine the purity, the morpho-crystalline structure and the particle size distribution of  $\text{CaWO}_4$ -precipitate thus influencing the properties of the resulting phosphor samples. Under our working conditions, the recommended precipitation parameters are a medium pH equal to about 8.0, a reagent concentration of about 0.50 mol/l and a precipitation temperature of 20°C.

## REFERENCES

1. R.Grasser and A.Scharmann, *Phys. Status Sol. (a)* **1990** , 130, K 99-K105;
2. G.Blasse, "Luminescent centres in insulators" in "Solid State Luminescence. Theory, Materials and Devices", (ed A.K.Kitai), Chapman Hall, London, **1993**, p 48;
3. E.V.Sokolenko and V.V.Gavrilov in " Abstracts of the VII All Union International Meeting. "Physics, Chemistry and Technology of Phosphors", Stavropol, **1992**, p119
4. A.M.Gurvich , " Vvedenie v fizicheskuyu himiyu kristallofosforov ", Moskva, ed. 2, **1982** , 119;
5. V.I.Krivobok , M.V.Mohosoev and A.P.Nahodnova , *Ukr.Khim.Zh.*, **1971** , 37, 992 -998;
6. G.W.Luckey , *Brit. Pat.* , 1.254.272 (25 Aug. 1971); *Chem.Abstr.* **1971** , 76, 52855
7. G.W.Luckey , *Ger. Pat.* 1.592.870 (13 Jul. 1972); *Chem.Abstr.* **1972** , 77, 20685
8. A.M.Gurvich , *Sb.Nauch.Tr.VNII. Lyuminoforov i Osobo Chist.Veshchestv.*, Stavropol, **1971** , 5, 133 - 143;
9. A.M.Gurvich, A.A.Mihalev and M.I.Tombak , *Sb.Nauch.Tr.VNII. Lyuminoforov i Osobo Chist. Veshchestv.* , Stavropol, **1972** , 7, 18 - 26;
10. I.G.Kaplenov, V.G.Krongauz, *Sb.Nauch.Tr.VNII Lyuminoforov i Osobo Chist. Veshchestv.*, Stavropol **1983**, 25, 33-38;
11. E.V.Sokolenko, V.V. Gavrilov, O.K.Tischenko and A.I.Ishkova, *Sb.Nauch.Tr.VNII Lyuminoforov i Osobo Chist.Veshchestv.*, Stavropol, **1989**, 37, 9-12;

Received: 20.12.1994



## STUDIES ON THE SYNTHESIS OF SILVER ACTIVATED ZINC SULPHIDE PHOSPHOR

Elisabeth-Jeanne Popovici<sup>a</sup>, Maria Aneculăese<sup>a</sup>, Veronica Ursu<sup>b</sup> and D. Macarovici<sup>a</sup>

*a. Institute of Chemistry "Raluca Ripan", Str. Fântânele 30, 3400 Cluj-Napoca*

*b. Institute of Physical-Chemistry of Romanian Academy, Spl Independenței 202,*

*Bucharest, ROMANIA*

### ABSTRACT

The zinc sulphide prepared by thiosulphate method was converted by thermal synthesis into ZnS:Ag,Cl phosphor samples. The concentration of silver activator, the nature of alkaline or alkaline-earth chloride used as a flux, as well as the calcination conditions influence on the crystalline structure, particle size distribution and luminescent properties of phosphor samples. The optimum preparation conditions were selected so that a ZnS:Ag,Cl phosphor with well defined and reproducible properties might be prepared

### INTRODUCTION

The simultaneous incorporation of silver ( activator ) and chlorine ( coactivator ) into the crystalline lattice of luminescent grade zinc sulphide ( host lattice ) generates a ZnS:Ag,Cl phosphor which, being excited by UV light or cathode rays, shows an intensive blue luminescence. The ZnS:Ag,Cl phosphor is especially used in the manufacture of screens for different cathode rays tubes, a fact which assumes well defined granulometric characteristics and superior luminescent properties.

Usually, the zinc sulphide used in phosphor processing is prepared by the H<sub>2</sub>S - method and consequently, the literature data refer especially to the conversion of this ZnS-type into the corresponding phosphors. For preparing the starting luminescent-grade zinc sulphide, we selected the more convenient Na<sub>2</sub>S<sub>2</sub>O<sub>3</sub> -method which is seldom used in the manufacture of luminescence substances.

In order to study the manner in which both the zinc sulphide quality and the conditions of phosphor thermal synthesis influence on the luminescent properties of ZnS:Ag,Cl phosphor, an extensive study has been recently initiated. Our previous papers revealed that the luminescence ability of ZnS prepared by thiosulphate method is determined by factors such as the surface area, particle

size distribution or desulphuration degree and structure of the crystalline lattice [1-3]. The objective of this paper is to establish the way in which the composition of the synthesis mixture and the calcination conditions influence the crystalline structure, particle size and luminescent properties of the ZnS:Ag,Cl samples corresponding to the zinc sulphide prepared by the thiosulphate-route.

## RESULTS AND DISCUSSION

The incorporation of silver and chlorine into ZnS crystalline lattice determines the formation of a phosphor with blue luminescence whose spectrum, registered under UV excitation, consists of only one emission band. The position of the emission maximum and the luminescence intensity are finally established during the thermal synthesis of phosphor samples.

In order to establish the optimum conditions of thermal treatment, some samples of ZnS:Ag ( $1 \times 10^{-2}$  %), Cl (2.5% MgCl<sub>2</sub>) were prepared by calcination at 800-1050°C, for one or two hours. The emission spectra of phosphor samples show that, *the calcination temperature* influences both the luminescence colour and the emission intensity (fig. 1). The change of the firing temperature from 800°C to 1050°C produces a shift of the emission maximum from 445 nm to 435 nm and a continuous increase of the emission intensity. The shift toward shorter wavelengths could be correlated with a change of the ZnS-crystalline structure from cubic -sphalerit- to hexagonal -würtzit [6]. The X-ray diffraction patterns confirm that the samples obtained at 1050°C are hexagonal whereas the other ones are cubic in structure. Mention must be made that the starting sulphide is about 90% cubic in structure [2]. The emission intensity of phosphor samples increases simultaneously with the increase of the firing temperature. According to the literature data referring to the phosphor samples prepared by the H<sub>2</sub>S-route, the increase in the firing temperature should have brought about the increase in the luminescent emission up to a maximum value and afterwards the gradual decrease of this one; for ZnS:Ag,Cl samples [7], the maximum intensity should have been reached at about 800-900°C. The decrease taking place at higher temperatures was explained by the presence of some lattice defects (i.e. vacancies or interstitial atoms) which act as extinguishing centres for luminescence of phosphor samples. Taking into account our results, one can say that, for ZnS:Ag,Cl samples obtained by Na<sub>2</sub>S<sub>2</sub>O<sub>3</sub>-route, the formation of such unfavourable defects is somehow "inhibited".

## Synthesis of Silver Activated Zinc Sulphide Phosphor

The emission intensity is also affected by the calcination time; a long firing process is favourable only for phosphor samples calcinated below 1000°C. Above this temperature, a long calcination process contributes to the increase of the number of extinguishing centres.

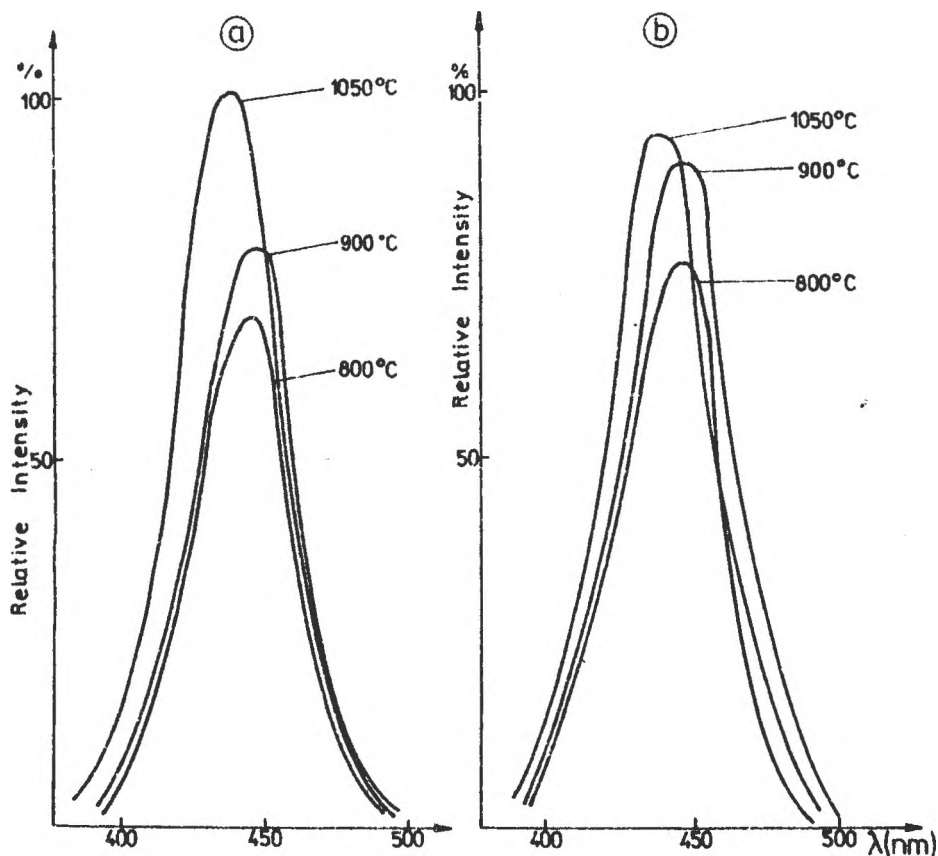


Fig.1 Emission spectra of  $\text{ZnS:Ag}(1 \cdot 10^{-2}), \text{Cl}(2.5\% \text{MgCl}_2)$  samples prepared in different calcination conditions: a) 1 hr calcination; b) 2 hrs calcination

The incorporation of silver activator into the ZnS-crystalline lattice is facilitated by the presence of alkaline or alkaline earth chlorides which act as a *flux*. In order to select the optimum mineralising agent, some ZnS:Ag,Cl samples were prepared by using 2.5% NaCl or  $\text{MgCl}_2$  or  $\text{BaCl}_2$  and  $1 \times 10^{-2}\%$  silver as activator. The calcination was conducted for 0.5; 1.0; 1.5 and 2.0 hrs at 900°C. The

relative intensities of phosphor samples were evaluated from the corresponding emission spectra and were plotted versus the firing time (fig.2a).

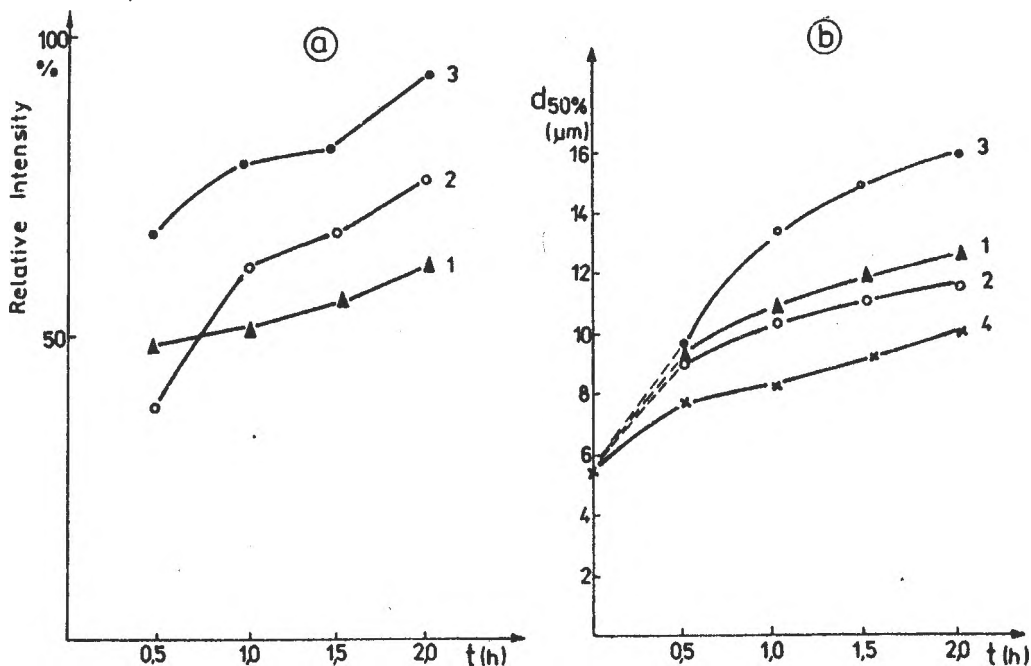


Fig.2. Variation of the emission intensity (2a) and of the median diameter ( $d_{50\%}$ ) of phosphor particles (2b) for ZnS:Ag ( $1 \cdot 10^{-2}$  %) samples prepared with different flux versus the firing time:  
 1 - NaCl; 2 - BaCl<sub>2</sub>; 3 - MgCl<sub>2</sub>; 4 - no flux used;

One can note that, irrespective of the flux nature used during the thermal synthesis, the luminescence intensity increases with the firing time. Moreover, the luminescence intensity is stronger for samples prepared with MgCl<sub>2</sub> and weaker for those obtained in the presence of NaCl as a flux. It appears that, MgCl<sub>2</sub> ensures the best activator incorporation, which is in good agreement with the literature data [8].

The alkaline and alkaline-earth chlorides could also contribute to the growth of phosphor particles. The particle size distribution of all phosphor samples was determined and the median diameter ( $d_{50\%}$ ) was plotted versus the firing time (fig.2b). The variation of the median diameter of the starting ZnS particles ( $d_{50\%} = 5.6 \mu\text{m}$ ) with the firing time is also represented; no flux was used in this case. As it was expected, the particle size increases continuously with the firing time. According to our results, MgCl<sub>2</sub> assures the formation of the largest

## Synthesis of Silver Activated Zinc Sulphide Phosphor

phosphor particles whereas  $\text{BaCl}_2$  that of the smallest ones. In the presence of magnesium chloride, the phosphor particles obtained by a two hours calcination are about three times larger than the initial ZnS particles

The different effects observed for the above mentioned chlorides could be explained by their various manner of acting. At a firing temperature of  $900^\circ\text{C}$ ,  $\text{NaCl}$  acts in liquid state,  $\text{BaCl}_2$  in solid state and  $\text{MgCl}_2$  through gaseous phase. Under our working conditions, magnesium chloride undergoes a high temperature hydrolysis resulting in a  $\text{HCl}$  generation; this one is responsible for both the good silver incorporation and the significant particle growth. Another reason for the observed different mineralising action could be the size of the cations which are implied in the transport process ( $\text{Mg}^{2+} = 0.79 \text{ \AA}$ ;  $\text{Na}^+ = 0.89 \text{ \AA}$ ;  $\text{Ba}^{2+} = 1.33 \text{ \AA}$ ) [ 9].

As it was postulated in our previous paper<sup>3</sup>, the incorporation of activator ions is influenced by the quality of the starting sulphide and consequently, the silver concentration which generates the proper number of luminescence centres should be determined. The optimum activator concentration was established by comparing the luminescence intensities of some phosphor samples which were prepared with a variable amount of silver, i.e. between  $4.5 \times 10^{-5}$  and  $45.0 \times 10^{-5}$  mol/mol ZnS. The calcination was conducted at  $900^\circ\text{C}$ , in the presence of 2.5 %  $\text{MgCl}_2$  as a flux, for 1 hr. The relative intensities of phosphor samples were evaluated from the corresponding emission spectra and were plotted versus the silver concentration ( fig.3).

The silver concentration increase brings about a monotonous rise in the emission intensity up to a maximum value and afterwards, a continuous decrease. This variation is in good agreement with the literature data [7, 10]. Generally, the luminescence brightness is determined by the ratio between the number of luminescence centres and the extinguishing ones. However, at high silver concentrations there are too many luminescence centres so that a reciprocal interaction might appear which results in a decrease of the luminescence intensity (concentration quenching).

The zinc sulphide prepared by  $\text{Na}_2\text{S}_2\text{O}_3$ -method, in the described procedure, permits the optimum incorporation of about  $1.35 \times 10^{-4}$  mol / mol silver atoms.

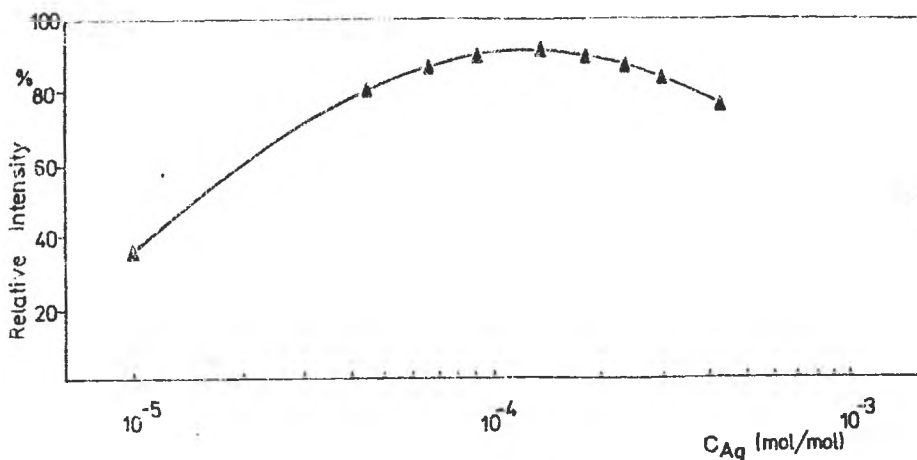


Fig.3. Variation of the emission intensity of ZnS:Ag,Cl (2.5% MgCl<sub>2</sub>) samples with the silver concentration.

## CONCLUSIONS

The calcination time and temperature, the nature of flux used in preparing the synthesis mixture and the silver concentration influence not only the luminescence colour and brightness but also the crystalline structure and particle size distribution of phosphor samples

The performed studies enabled us to establish the optimum conditions for the "conversion" of the zinc sulphide prepared by Na<sub>2</sub>S<sub>2</sub>O<sub>3</sub>-method into a ZnS:Ag,Cl phosphor with well-defined characteristics : cubic crystalline structure, uniform particle size distribution with a median diameter of 14-16 μm and an intense blue luminescence with the emission maximum at 445 nm. The recommended silver concentration is of about  $1.35 \times 10^{-4}$  mol / mol and magnesium chloride could be used as a flux

## EXPERIMENTAL

ZnS used in phosphor synthesis is luminescent grade (1 g) and was prepared from highly purified solutions of zinc sulphate and sodium thiosulphate [4]. The preparation procedure developed in two stages, namely precipitation and pre-calcination [5]. The precipitation took place at 100°C, at a molar ratio of ZnSO<sub>4</sub> : Na<sub>2</sub>S<sub>2</sub>O<sub>3</sub> equal to 1 : 2 and the pre-calcination developed at 900°C, in a protective N<sub>2</sub>-atmosphere, for 1 hr. The procedure of ZnS preparation was thoroughly described in a previous paper [2]

## Synthesis of Silver Activated Zinc Sulphide Phosphor

The ZnS:Ag,Cl samples were prepared in the usual manner of phosphor synthesis. The desired amount of ZnS was wet-mixed with a determined quantity of AgNO<sub>3</sub> and 2.5% alkaline or alkaline earth chloride. The mixture was dried at 105-110°C and subsequently fired at 800-1050°C, for 0.5-2.0 hrs, in a protective N<sub>2</sub>-atmosphere. Special quartz ampoules were used by cautiously introducing them into the preheated furnace. After completing the thermal treatment, the samples were taken out into a special designed cooling device. All phosphor powders were washed, coated with a protective layer of Zn<sub>3</sub>P<sub>2</sub>O<sub>7</sub>, dried and sieved.

The phosphor powders were characterised by crystalline structure (X-Ray Diffraction), particle size distribution (Coulter Counter method) and luminescent properties. The emission spectra were registered with 365 nm UV excitation on a Perkin Elmer 204 Spectrofluorimeter. In all cases, a ZnS:Ag phosphor sample Lumilux Blau F (Riedel-de Haen) was taken as a standard.

### REFERENCES

1. E.J. Popovici, M. Aneculăeșe, V. Ursu and D. Macarovici, *Roum. Chem. Quart. Rev.*, **1993**, 1(3), 233-238;
2. E.J. Popovici, V. Ursu and D. Macarovici, *Roum. Chem. Quart. Rev.*, **1993**, 1(3), 239-244;
3. E.J. Popovici, V. Ursu and D. Macarovici, *Rev. Roum. Chimie*, (in press);
4. E.J. Popovici, M. Aneculăeșe and D. Macarovici, *Rom. Pat.*, 96 826 (September, 5, 1988);
5. E.J. Popovici, M. Aneculăeșe and D. Macarovici, *Rom. Pat.*, 98 116 (March 29, 1989);
6. W. Lehmann, *J. Electrochem. Soc.*, **1966**, 113 (8), 788-792;
7. A.A. Cherepnev, *Izv. A.N. SSSR, Ser. Fiz.*, **1959**, 23 (11), 1334-1340;
8. A.M. Gurvich, *Zh. Fiz. Him.*, **1962**, 36 (4), 1678-1684;
9. H. Hawai, T. Abe and T. Hoshina, *Jap. J. Appl. Phys.*, **1981**, 20(2), 313 - 320;
10. L. A. Gromov and V. A. Trofimov, *Zh. Prikl. Him.*, **1979**, 52 (10), 2165-2169;

Received: 20.12.1994





## ATTEMPTS ON THE SYNTHESIS OF ZINC SULPHIDE PHOSPHORS ACTIVATED BY LEAD

Maria Aneculăese<sup>a</sup>, Elisabeth-Jeanne Popovici<sup>a</sup>, Veronica Ursu<sup>b</sup> and D. Macarovici<sup>a</sup>

a. *Institute of Chemistry "Raluca Ripan", Str. Fântânele 30, 3400 Cluj-Napoca*

b. *Institute of Physical Chemistry of the Romanian Academy, Spl. Independenței 202,  
Bucharest, ROMANIA*

### ABSTRACT

The present paper reports some preliminary tests concerning the lead activation of zinc sulphide obtained by thiosulphate method. The ZnS:Cl, ZnS:Pb,Cl and ZnS:Pb samples were prepared by thermal synthesis with or without alkaline or alkaline-earth chlorides as flux. The emission and excitation spectra revealed that, in our work conditions, both self-activated and lead centres are formed resulting in a simultaneous blue and yellow-orange emission. The phosphor samples prepared with different fluxes exhibit various luminescence colours.

### INTRODUCTION

The incorporation of small amounts of foreign elements into zinc sulphide often gives rise to luminescent emissions characteristic of the activating elements. Most activators determine the occurrence of a strong luminescence in the green spectral region, and only few of them give light emission in the yellow-red part of the spectrum. Among the latter, the group IV elements (as Pb and Sn) could be quoted [1].

The preparation and luminescent properties of lead activated zinc sulphide have already been reported by a number of investigators [2-4]. The phosphor preparation takes place by the high temperature calcination of the synthesis mixture consisting of luminescent-grade zinc sulphide, lead salts and sometimes, alkaline and/ or alkaline-earth halides.

Usually, the zinc sulphide used in phosphor processing is prepared by the H<sub>2</sub>S-method and consequently, the literature data refer particularly to the conversion of this ZnS-type into the corresponding phosphor. In order to synthesise ZnS -type phosphor we selected the more convenient Na<sub>2</sub>S<sub>2</sub>O<sub>3</sub>-method for preparing the

starting luminescent-grade zinc sulphide. In some previous papers we brought evidence that this zinc sulphide can be successfully used in phosphor synthesis [5,6]. Taking into account that the luminescent properties of lead activated phosphors depend strongly on the preparation conditions [7,8], a study has been initiated in order to establish the most convenient conditions for the conversion of zinc sulphide ( $\text{Na}_2\text{S}_2\text{O}_3$ -method) into the corresponding phosphors. The present paper reports some experimental results concerning the synthesis of lead activated zinc sulphide phosphors.

## RESULTS AND DISCUSSION

Luminescent-grade zinc sulphide obtained by  $\text{Na}_2\text{S}_2\text{O}_3$ -method is about 90 % cubic in structure and presents a good luminescence ability. As it was already shown, this starting material could be transformed into good silver activated phosphor samples [10]. In order to prepare ZnS:Pb,Cl phosphor samples, a similar procedure was applied namely, the calcination at  $950^\circ\text{C}$ , of some homogenous mixtures consisting of zinc sulphide, lead nitrate and alkaline or alkaline-earth chlorides as flux; the added lead concentration was 0.01% and the flux content was 5%. Two more samples were prepared namely ZnS:Cl, containing  $\text{NH}_4\text{Cl}$  as a flux and no lead activator (sample 1) and ZnS:Pb, with lead as activator but without chlorides flux (sample 6, table 1).

The obtained ZnS:Cl, ZnS:Pb,Cl and ZnS:Pb phosphor samples display mainly the cubic crystalline structure of sphalerite and different luminescent properties. Table 1 includes some of their luminescence characteristics: the apparent luminescence colour -fluorescence (Fl) and phosphorescence (Ph) - and the emission intensity values at 450 nm and 580 nm, which were evaluated from the correspondending emission spectra registered under 365 nm excitation.

As it was expected, the ZnS:Cl sample shows a strong self-activated SA-luminescence due to some structural defects and the zinc sulphide host lattice. The lead incorporation should determine the diminution of this blue SA-luminescence and the generation of the characteristic yellow-orange luminescence. For the lead activated samples prepared with equal flux concentrations, SA-luminescence is more or less diminished by the use of  $\text{NaCl}$ ,  $\text{BaCl}_2$  or  $\text{MgCl}_2$  and rather intensified by the  $\text{NH}_4\text{Cl}$  flux.

## Lead Activated Zinc Sulphide Phosphorus

TABLE 1. Some luminescence characteristics of phosphor samples prepared with 0.01% lead and different fluxes.

No.	Phosphor sample	Luminescence colour		$I_{450}$ (a.u.)	$I_{650}$ (a.u.)
		Fl.	Ph.		
1.	ZnS:Cl (NH <sub>4</sub> Cl)	blue	blue-green	63.0	1.0
2.	ZnS:Pb,Cl (MgCl <sub>2</sub> )	pink	orange	61.5	3.0
3.	ZnS:Pb,Cl (NaCl)	white-blue	blue-green	46.5	1.5
4.	ZnS:Pb,Cl (BaCl <sub>2</sub> )	blue	green	56.5	1.5
5.	ZnS:Pb,Cl (NH <sub>4</sub> Cl)	blue	green	64.5	1.0
6.	ZnS:Pb	pink	pink	44.0	4.0

Regarding the lead characteristic luminescence, this could be observed in the case of MgCl<sub>2</sub> when the apparent luminescence becomes pink.

The incorporation of lead into the ZnS host lattice could be also realized in the absence of halogenide ions. In the case of ZnS:Pb sample, the blue luminescence due to the host lattice is diminished with about 30% as compared to the ZnS:Cl sample and the lead luminescent contribution becomes evident. In order to explain the different results obtained with various fluxes, the emission and excitation spectra are presented and analysed.

According to the literature data [11], in cub-ZnS phosphors, the lead ion determines two apparent emission bands situated in the green and yellow-orange part of the spectrum. These two bands are composed of at least four subbands situated at about 500, 580, 630 and 760 nm. Moreover, the characteristic emission could be accompanied by the blue SA-luminescence. The excitation spectrum of the characteristic yellow-orange emission is also of composed nature, some of the bands being situated at about 345, 365, 470, 480 and 500 nm.

The emission spectra of the prepared phosphor samples, some of them being depicted in figure 1, reveal that the yellow-orange emission band at about 580-600 nm, assigned to lead, appears only in ZnS:Pb and ZnS:Pb,Cl(MgCl<sub>2</sub>) samples.

The expected green emission band cannot be noticed because it was probably covered by the strong blue SA-luminescence at 450-455 nm, which appeared in all cases.

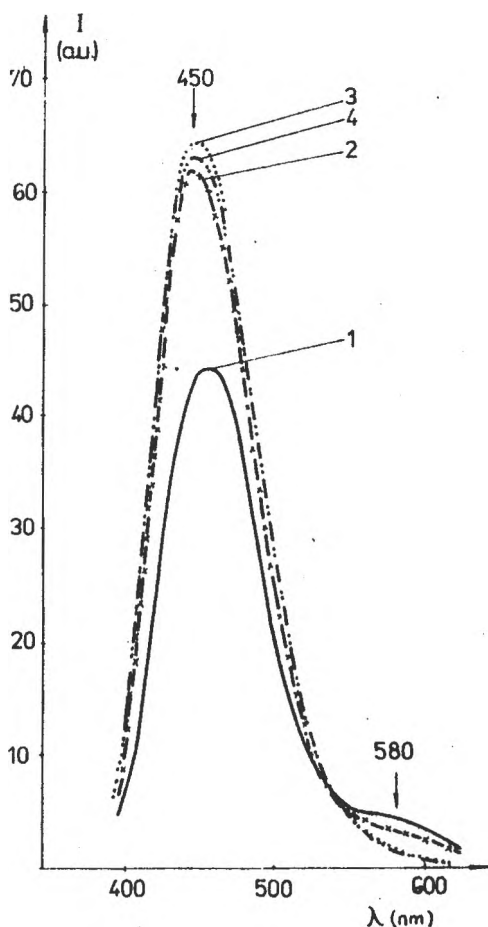


Fig. 1. The emission spectra of some phosphor samples prepared with different fluxes ( $\lambda_{exc} = 365 \text{ nm}$ ):  
 1 - ZnS:Pb;  
 2 - ZnS:Pb,Cl(MgCl<sub>2</sub>);  
 3 - ZnS:Pb,Cl(NH<sub>4</sub>Cl);  
 4 - ZnS:Cl(NH<sub>4</sub>Cl).

The excitation of the blue emission band (450 nm) proceeds mainly with UV radiation of 360-365 nm ( fig. 2A ). For ZnS:Pb and ZnS:Pb,Cl(MgCl<sub>2</sub>) samples the excitation peak is slightly shifted towards longer wavelengths as compared to ZnS:Pb and ZnS:Pb,Cl(NH<sub>4</sub>Cl) samples. The excitation spectra corresponding to the yellow-orange emission band (580 nm) are different for all the phosphor samples (fig. 2B). For ZnS:Pb,Cl (NH<sub>4</sub>Cl) the excitation takes place especially in the 354 nm band, which is very similar to the case of the self-activated ZnS:Cl sample.

## Lead Activated Zinc Sulphide Phosphorus

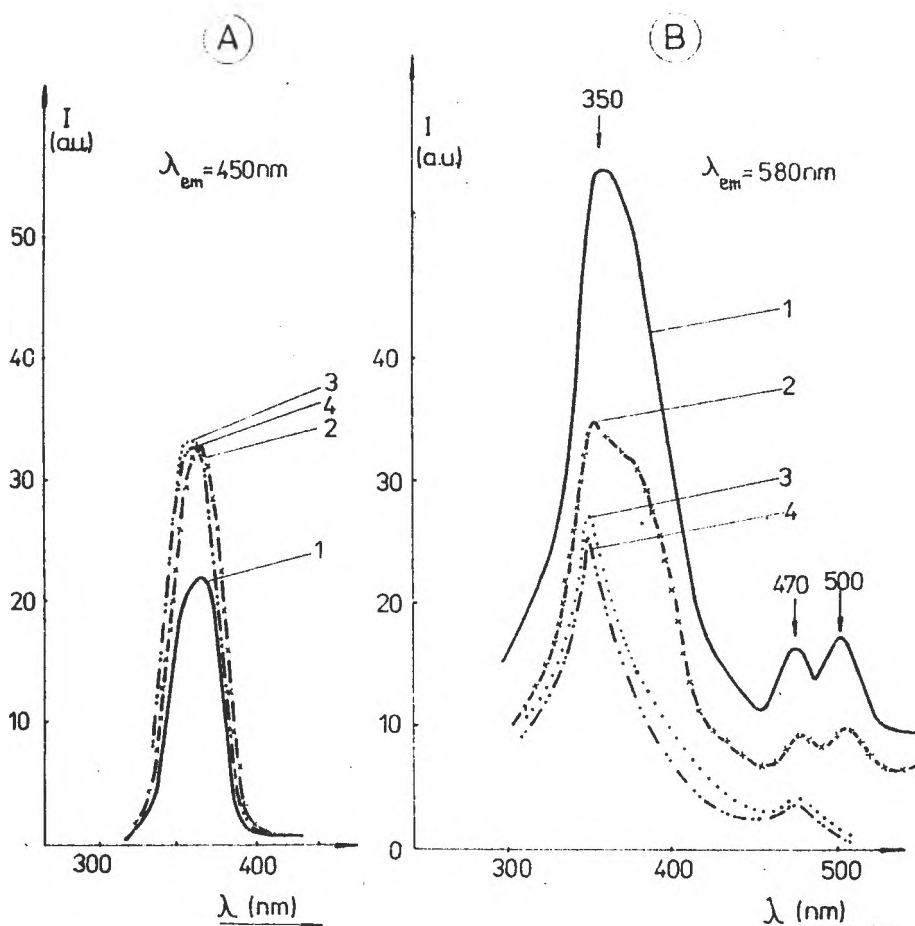


Fig.2. The excitation spectra of some phosphor samples prepared with different fluxes: 1-ZnS:Pb; 2-ZnS:Pb,Cl(MgCl<sub>2</sub>); 3-ZnS:Pb,Cl(NH<sub>4</sub>Cl) ;4-ZnS:Cl(NH<sub>4</sub>Cl).

For ZnS:Pb,Cl(MgCl<sub>2</sub>) sample four excitation peaks were observed namely at about 347 nm and 370 nm (ultraviolet), 470 nm (blue) and also 500 nm (green). For ZnS:Pb sample, the two UV excitation bands cannot be distinguished from one another and apparently, the excitation spectrum consists only in three peaks situated at about 350, 470 and 500 nm.

Taking into account that the apparent shape of spectra with composite nature depends on the sample preparation and measurement conditions, our results could be considered as being in good agreement with the literature data. The emission

and excitation spectra also confirmed that in ZnS:Pb,Cl sample prepared with 5%  $\text{NH}_4\text{Cl}$ , there is no lead contribution to the observed luminescence. Moreover, the characteristic lead emission band situated in the yellow-orange part of the spectrum, is very weak in comparison with the self-activated band.

The different results obtained for ZnS:Pb,Cl samples prepared in the presence of various fluxes could be explained by both the variable amount of lead centres and the different concentration of structural defects generating SA-luminescence. In our preparation conditions, the ammonium chloride undergoes an abrupt thermal decomposition and consequently, the most part of the activator is washed out from the host lattice. The ZnS:Pb,Cl( $\text{NH}_4\text{Cl}$ ) sample becomes in fact a ZnS:Cl( $\text{NH}_4\text{Cl}$ ) sample so that no lead contribution to the apparent luminescence can be observed. On the other hand, the various fluxes contribute, in a different extent, to the creation of SA-centres.

Mention must be made that the incorporation of lead in the presence of ammonium chloride could be also achieved in other experimental conditions. Indeed, at high  $\text{NH}_4\text{Cl}$  concentrations (12.5%), we obtained a ZnS:Pb,Cl sample with a SA-luminescence diminished with about 50% but with equal contribution of yellow-orange band, by comparison with the emission of the ZnS:Pb,Cl( $\text{MgCl}_2$ ) sample; the apparent luminescence was bright pink.

## CONCLUSIONS

In our work conditions, the zinc sulphide prepared by thiosulphate method could be transformed into ZnS:Pb or ZnS:Pb,Cl phosphor samples, presenting a strong blue SA-luminescence and a weak yellow-orange lead luminescence. The apparent luminescence is different in colour (from blue-green to pink) depending on the nature of the flux used in the phosphor synthesis.

The study might be continued in order to obtain a lead activated zinc sulfide phosphor with superior luminescent properties.

## EXPERIMENTAL

Zinc sulphide used in phosphor synthesis is luminescent-grade (l.g.) and was prepared from highly purified solutions of  $\text{ZnSO}_4$  and  $\text{Na}_2\text{S}_2\text{O}_3$ ; the preparation procedure developed in two stages, namely, precipitation and pre-calcination [9]. The precipitation took place at  $100^\circ\text{C}$ , at a molar ratio of  $\text{ZnSO}_4:\text{Na}_2\text{S}_2\text{O}_3$  equal to 1:2 and the pre-calcination developed at  $900^\circ\text{C}$ , in a protective  $\text{N}_2$ -atmosphere. The procedure was thoroughly described in previous papers [5,6].

## Lead Activated Zinc Sulphide Phosphorus

The ZnS:Pb,Cl samples were prepared in the usual manner of phosphor synthesis. The desired amount of ZnS was wet-mixed with 0.016 %  $Pb(NO_3)_2$  and 5 % alkaline or alkaline-earth chlorides. The mixtures were dried at  $105^\circ C$ , and subsequently fired at  $950^\circ C$  for 1 hr., in a protective  $N_2$ -atmosphere. Special quartz ampoules were used by cautiously introducing them into the preheated furnace. After completing the thermal treatment, the samples were taken out into a special designed cooling device. All phosphor powders were washed, dried and sieved.

The apparent luminescence was checked out by irradiating the samples with UV lamp. The emission and excitation spectra were registered by means of a Perkin-Elmer 204 Spectrofluorimeter. The registrations were performed by using  $UG_1$  and  $UG_2$  filters before the samples and  $WG_1$  filter after them; no filters were used for the excitation of the 580 nm emission band.

### REFERENCES

1. Y.Mita and K.Sugibuchi in "Proceedings of the International Conference on Luminescence 1966" (G.Szigeti Editors), vol.1, Akademiai Kiado, Budapest, 1966, 1158-1163.
2. Y.Mita, *J.Phys.Soc.Japan*, 1965, 20, 1822-26
3. Y.Uehara, *J.Chem.Phys.*, 1969, 51, 4401-4413.
4. A.Schermann, D.Schwabe and D.Weyland in "Proceedings of the 1975 International Conference on Luminescence" (Ed. Shionoya-Nagakura-Sugano), North Holland Publishing- Amsterdam, 1976, 479-483.
5. E.J.Popovici, M.Aneculăese, V.Ursu and D.Macarovici, *Roum. Chem. Quart. Rev.*, 1993, 1(3), 233-238.
6. E.J.Popovici, V.Ursu and D.Macarovici, *Roum. Chem. Quart. Rev.*, 1993, 1(3), 239-244.
7. N.W.Smit and F.A.Kroger, *J. Opt. Soc. Am.*, 1949, 39, 661-663.
8. E.I.Boev, A.A.Mikhalev and G.D.Guseva, *Optica i Spektroskopiya*, 1967, 22, 662-663.
9. E.J.Popovici, M.Aneculăese and D.Macarovici, *Rom. Pat.*, 98116 (March 29, 1969)
10. E.J.Popovici, M.Aneculăese, V.Ursu and D.Macarovici, *This Journal*, (in press).
11. Y.Uehara, *J.Chem.Phys.*, 1969, 51, 4385-4400.

Received: 20.12.1994





## STUDIES FOR DETECTION AND QUANTIFICATION OF TRIAZINES RESIDUES

Claudia Costache\*, S. Gocan\*\*, Gh. Coman\*, R. Zăbavă\*\*\*

\**Centrul de Medicină Preventivă, Cuza Vodă 20, 2200 Brașov*

\*\* *Universitatea "Babeș-Bolyai", Facultatea de Chimie și Inginerie Chimică,  
Arany Janos 11, 3400 Cluj-Napoca*

\*\*\**Institutul Pasteur, Stejeriș 8, 2200 Brașov.*

### **Abstract**

In this study we used the atrazine as a hapten in order to prepare, separate, purify and label with peroxides, specific immunoglobulins. For atrazine we established the correlation curve between its concentration and induced inhibition in a competitive ELISA. For our immunochemical system the detection limit of atrazine traces is 0,05ng/mL.

### **INTRODUCTION**

In the last few years the problems of the mankind of being protected against epidemics, of increasing the quality of food with less efforts, have imposed some rules to maintain under control some species of plants and animals. In the same time the chemical pollution of the food, water, air, soil and biological systems increased, and the need for some strategies all over the world become more necessary. Recently there have been taken, at global level, different measures to regulate the maximum levels of chemical products, and to control the obey of them by the mean of precise analytical methods.

The most common chemicals used as pesticides are herbicides, insecticides, fungicides and disinfectants. The analytical methods used for determination of pesticides residue are accurate and can detect quantities as mg/kg and even

$\mu\text{g}/\text{kg}$ . Among the methods used to detect pesticides residues are : biological methods [1] consisting in inhibition of an enzyme activity, chromatographic methods : paper chromatography [2], thin layer chromatography [3], gas chromatography [4], high performance liquid chromatography [5], spectrochemical methods [6], radiometric methods [7]. Because of their high specificity and sensitivity, immunochemical methods have been widely used for detection and quantification of pesticides residues [8,9].

Pesticides are compound with a small molecular weight they cannot induce specific antibody synthesis. Covalently coupling of pesticides and some macromolecules like ovalbumin, bovine serum albumin (BSA), human albumin, hemocyan, followed by inoculation of these new structures into distant taxonomical mammals [10], induces biosynthesis of immunoglobulins specific to the pesticide and also to the macromolecule used to bind it [11,12].

These antibodies can be used after purification or can be labelled with enzymes in a diagnostic kit for detection of the pesticide which induced their biosynthesis.

#### **Experimental**

Atrazine is one of the most used pesticide in agricultural practices. For preparation of atrazine - BSA antigen we used Atlas atrazine (Italy) and BDH - BSA (England) [13]. The resultant antigenic was inoculated intradermic to goats for specific antibody synthesis. After the separation and purification of goat IgG anti antigenic complex, the goat immunoglobulins were labelled with Merck peroxidase [14]. The resulted goat IgG anti atrazine - BSA labelled with peroxidase was used to detect and quantify the pesticides residues through a competitive ELISA.

#### **RESULTS AND DISCUSSION**

In ELISA the concentration of the atrazine - BSA complex was  $5\mu\text{g}/\text{mL}$  and the dilution of immunoenzymatic conjugate was 1/200. We used as substrate for peroxidase 5 amino salicylic acid, 7,68 mM in phosphate buffer pH = 6,95.

We added to the conjugate various quantities of atrazine as shown in table 1.

## Detection and Quantification of Triazines Residues.

Table 1 Variation of the optical density at 450 nm versus of the atrazine concentration in ELISA, by competition mode.

Nr.crt.	Atrazine (mg/mL)	$\overline{OD}$ (450 nm)	ELISA inhibition (%)
1	0,00	0,489	0,00
2	0,02	0,475	2,86
3	0,05	0,470	3,88
4	0,075	0,468	4,32
5	0,15	0,456	6,80
6	0,30	0,440	8,60
7	0,75	0,425	11,90
8	1,50	0,410	16,25
9	3,00	0,395	19,34
10	5,00	0,382	21,90
11	10,00	0,379	22,50

In a semilogarithmical representation of the means of OD and the atrazine concentration added to the system, we obtained a correlation curve of these parameters (Fig.1), and the values give a straight line between the atrazine concentrations 0,075 - 5 ng/mL. Out of this range the variation is not linear.

We noticed that at high level of atrazine concentration the inhibition is maintained around 20%. The explanation of this fact is the low solubility of the atrazine in the reaction medium. The detection limit of the atrazine is 0,05 ng/mL, comparable with other reports for pesticides.

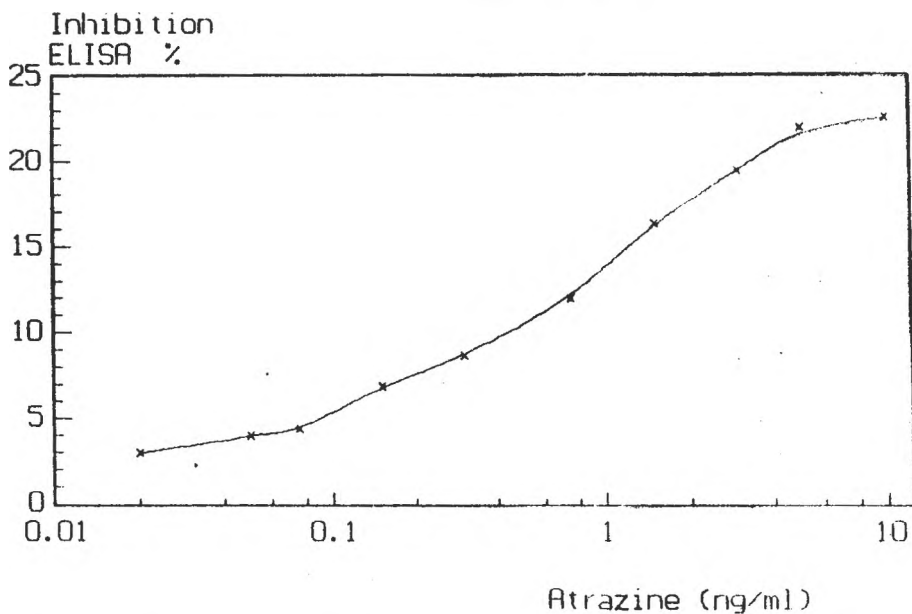


Figure 1. The procentual ELISA inhibition versus of the atrazine concentration.

## CONCLUSION

In this study we demonstrated that the ELISA technique can be used to detect and quantify atrazine and some other triazine pesticides. The immunochemical reaction of the antigen with specific antibodies make possible to use same system in ordre to quality a class of substances or a group with same chemical structure, with a high specificity and sensitivity, in a short time through a modern and accessible technique.

REFERENCES

1. F. Geike, *J. Chromatogr.*, 53, 296 (1970).
2. J.A. Bates, *The Analyst*, 90, 453 (1965).
3. C.E. Mendoza, *J.Chromatogr.*, 50, 92, (1970).
4. Qing Xiao Li, *Anal.Chem.*, 61, 819 (1989).
5. C.A. Bake, *Anal.Chem.*, 43, 950 (1971).
6. H.A. Maye, *J.Agric.Food Chem.*, 13, 516 (1965).
7. J.F. Lawrence, *Anal.Chem.*, 44, 2046 (1972).
8. J.van Emon, *Anal.Chem.*, 58, 1666 (1986).
9. R.J. Bushway, *J.of AOAC International*, 75 (2) 323 (1992).
10. Lucia Andrieş, A. Olinescu, *Compendiu de imunologie fundamentală*, Ed. Ştiinţa, Chişinău, 1992, p.459.
11. B. Dumbar, *J. Agric.Food Chem.*, 38 (2) 433 (1990).
12. E.M. Thurman, *Anal.Chem.*, 62, 2043 (1990).
13. Gh. Coman, Claudia Costache, S. Gocan, R. Zăbavă, *Bull.of the Transilvania University of Braşov*, 35, 72 (1993).
14. Gh. Coman, S. Gocan, R. Zăbavă, Pompilia Szabo, *Stud.Univ.Babeş-Bolyai Chem.*, 37 (1-2) 45 (1992).

Received:15.05.1995



## USING AFFINITY CHROMATOGRAPHY IN BIOMOLECULES SEPARATION

S. Gocan\*, Gh. Coman\*\*, Claudia Costache\*\*, Camelia Drăghici\*\*\*

\* *Universitatea "Babeș - Bolyai", Facultatea de Chimie și Inginerie Chimică, Arany Janoš 11, 3400 Cluj-Napoca.*

\*\**Centrul de Medicină Preventivă, Cuza Vodă 20, 2200 Brașov.*

\*\*\**Universitatea Transilvania, Fac. SIM, Cibinului 3, 2200 Brașov.*

### Abstract

In this study we presented in extend a method of separation based on the affinity antigen-antibody interaction. The stationary phase is obtained by covalently binding of IgG on a matrix (Sephacrose 4B). The immunoglobulins from the sample are specifically adsorbed by the complementary ligand and then eluted separated.

### INTRODUCTION

Affinity chromatography is a type of adsorption in which the molecule to be purified is specifically adsorbed by a complementary binding substance (ligand) covalently attached to an insoluble support matrix. This type of chromatography is the only technique for the purification of almost any biomolecule on the basis of its biological function [1,2]. At molecular level, the specificity of reaction is a characteristic of the biological processes, their replication in vitro being used in the affinity chromatography in order to separate and purify some of the components [3,4]. The development of affinity chromatography and applications in macromolecules purification are based on Axen's work [5] in which Sepharose is activated with bromocyanide. Using this technique he obtained activated polysaccharides matrix capable of interaction with peptides and proteins through their free amino groups along polipeptidic chains.

## EXPERIMENTAL

The matrix used was Sepharose and the binding substance (ligand) immunoglobulin G purified by steric exclusion chromatography and ion exchange chromatography.

### Preparation of stationary phase

Sepharose 4B gel (10g) was washed with distilled water for several times on G<sub>3</sub> fritte suspended in 2,5 mL phosphate buffer 5 M, pH = 11,9. After that was added distilled water up 20 mL and 1 mL BrCN 100mg/mL in cold and stirring. The resulting mixture was stirred for 6 minutes and then washed with a HCl solution 1 mM (60mL/g gel) to prevent the dislocation of active sites. The gel was balanced in borate buffer saline 0,1M, pH = 8,3.

The coupled immunoglobuline was suspended in the same buffer at room temperature and added to the activated gel (10 mg IgG/mL gel) in order to be covalently coupled with the polysaccharide matrix. After the coupling reaction was finished 2 hours of slow stirring, the excess immunoglobuline was washed up with the coupling buffer (check at 280 nm). The active sites uncoupled with IgG were annihilated by washing with a large amount of deactivation buffer tris - HCl 0,2 M, pH = 8.

The blocking agent in excess was washed up for a several times with coupling buffer pH = 8,3 and acetate buffer 0,2 M, pH = 4.

### Separation using affinity chromatography

We used this technique to separate rabbit IgG anti bovine IgG [9]. Rabbit serum anti bovine IgG (4 mL) were put in a 100 x 12 mm column and the stationary phase was bovine IgG - Sepharose 4B.

The column and the sample were previously balanced in tris - HCl buffer 0,1 M, pH=8. After the sample was introduced in the column, very slowly, for a steady diffusion, the ligand (bovine IgG) and the immune reagent (rabbit IgG anti bovine IgG) were maintained at room temperature for 16 hours for specific interaction.

Besides the specific interaction antigen-antibody these are some non-specific interactions like adsorptions due to bipolar forces or van der Waals forces.

The macromolecules adsorbed non-specifically were eluted with equilibration buffer until these are no proteins in the effluent (check at 280 nm).

The specific interactions, mainly hydrogen bonds, were annihilated by the decreasing of the pH and the increasing of the ionic strength of the eluent (in this case glycine - HCl buffer pH = 2,95 with NaCl 0,5 M) (Fig.1.).



## Using Affinity Chromatography in Biomolecules Separation

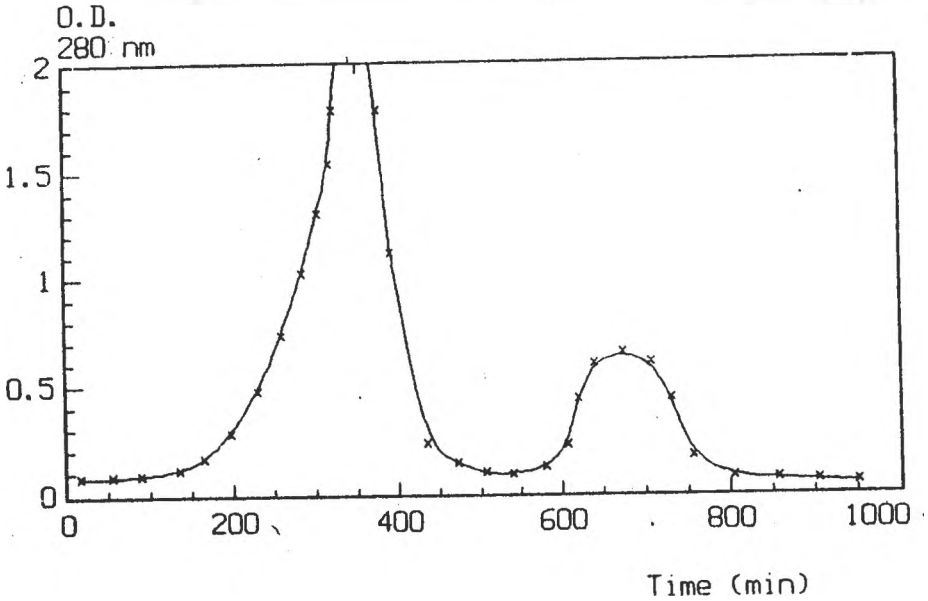


Figure 1. Affinity chromatography of rabbit serum anti bovine IgG.

The elution speed was 10mL/h and the effluent was collected in phosphate buffer 0,5 M, pH = 7,5, 1/1 volumic rapport to avoid denaturation of immunoglobulins due to sudden change of the pH.

### RESULTS AND DISCUSSIONS

We collected 25mL protein solutions and after dialyse against phosphate buffer 0,1 M, pH = 7,3 remained 4,6 mL. From 250 mg total protein in the rabbit anti bovine IgG, 50 mg were gammagolbulins, 35 mg IgG and finally we obtained 9 mg total protein.

The immunoelectrophoresis of the product corresponding to second peak (Fig.2) showed signals characteristic to non-specific interactions.

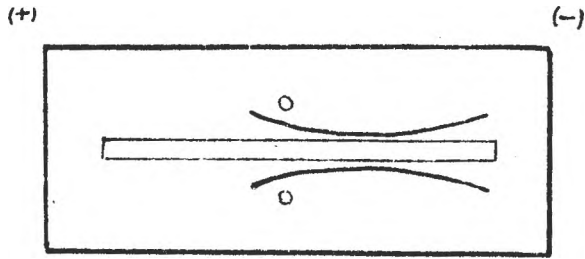


Figure 2. The immunoelectrophoresis of the product corresponding to second peak of affinity chromatography.

The proteic fractions corresponding to the first peak contained macromolecules specific to all seric proteins. The presence of IgG in these fractions (Fig.3.) led to some suppositions :

- the proteic excess in our sample compared with the maximum specific capacity.
- the non-specific interaction of IgG with stationary phase, besides the specific interaction.
- incubation time too short.
- ionic strength of elution buffer tris - HCl, pH = 8 to high.

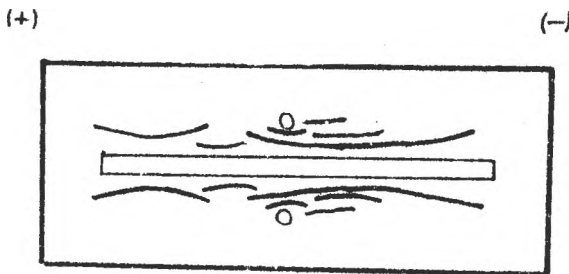


Figure 3. The immunoelectrophoresis of the product corresponding to first peak of affinity chromatography.

## Using Affinity Chromatography in Biomolecules Separation

Even the parameters of interaction - elution were modified (incubation in cold up 48 hours, incubation at 37°C up to 24 hours, decrease of NaCl up to elimination from the elution buffer, decrease of the sample quantity up to 1 mL) we could eliminate the IgG from the proteic fractions corresponding to the first chromatographic peak, neither could we increase the recovering degree of IgG in the fraction corresponding to the second peak over 30%. The explanation for this low recovery was the non-specific interactions between IgG and stationary phase.

### CONCLUSIONS

Using this chromatographic method of separation based on specific interaction antigen - antibody type, we obtained a purified Igg which can be enzyme labelled in order to prepare a diagnostic kit.

### REFERENCES

1. Eva Szondy, *Immunobiol.*, 157, 414 (1980).
2. A. Ștefan, *Șt. Cer. Biochim.*, 29 (1) 52 (1986).
3. K.W. Goding, *Monoclonal antibodies*, 2-nd ed., Academic Press, New York, 1986, p.108.
4. M. Elliqasson, *J. Immunol.*, 142, 575, (1982).
5. R. Axen, *Nature*, 214, 1302 (1967).
6. R.G. Wittaker, *Australian Vet. J.*, 59, 4, 125 (1982).
7. Td. Nguen, *Ann. Rech. Vet.*, 18, 25 (1987).
8. A.E. Clarke, *J. Biochem.*, 121, 811 (1971).
9. Gh. Coman, S. Gocan, R. Zăbavă, *A XI-a Conferință de chimie analitică*, Cluj-Napoca, sept. 1992.

Received: 5.12.1995



## DIPHENYLANTIMONY(III) DIORGANOARSINATE AND THIOARSINATE. SYNTHESIS AND SPECTRAL CHARACTERISATION

Luminita Silaghi-Dumitrescu and Adrian Halduc

*Department of Chemistry, Babes-Bolyai University Cluj-Napoca, Romania*

### Abstract

Diphenylantimony(III) dimethyl- and diphenylarsinate and dimethylthioarsinate were prepared and characterised by their IR and mass spectra. Bidentate organoarsenic ligands are present in the synthesised compounds. The fragmentation pattern under electron impact is in agreement with a greater affinity of oxygen for arsenic than for antimony.

### INTRODUCTION

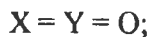
The synthesis and structural characterisation of antimony(III), phenylantimony(III) and diphenylantimony(III) derivatives containing diorganodithioarsinato groups were reported in recent years [1,2]. Two different structures have been found for  $\text{Ph}_2\text{SbS}_2\text{AsMe}_2$  [2] and  $\text{Ph}_2\text{SbS}_2\text{AsPh}_2$  [1]: the first one is polymeric with bridging bidentate organoarsenic groups, while the other is dimeric, with basically monodentate ligands. The same dimeric structure was found for diphenyldithiophosphinato analogue [2]. Polymeric structures are reported for diphenylantimony(III) diphenylphosphinate and diphenylthiophosphinate [3]. In view of the comparing the oxygen and sulfur affinity it is of interest to prepare the antimony(III) and organoantimony(III) diorganoarsinate and thioarsinate.

In the present paper we report the synthesis and characterisation of  $\text{Ph}_2\text{SbO}_2\text{AsMe}_2$ ,  $\text{Ph}_2\text{SbO}_2\text{AsPh}_2$  and  $\text{Ph}_2\text{SbSOAsMe}_2$ .

### RESULTS AND DISCUSSION

Diphenylantimony(III) arsenate,  $\text{Ph}_2\text{SbO}_2\text{AsR}_2$  (R= Me, Ph) and dimethylthioarsinate,  $\text{Ph}_2\text{SbSOAsMe}_2$  have been prepared as white solids from diphenylantimony(III) chloride

and the corresponding sodium diorganoarsinate and thioarsinate, as depicted in the following equation:



The compounds are air stable, and can be stored for a long period. Sodium dimethylthioarsinate was prepared by bubbling hydrogen sulfide through a solution of sodium dimethylarsinate.

### Infrared spectra

Bands characteristic of phenyl groups were observed in the expected spectral regions for the title compounds. For the dimethyl- and diphenylarsinato ligands the most important region is  $900\text{-}700\text{ cm}^{-1}$  where arsenic-oxygen stretchings are located [4]. There is another region between  $2500\text{-}2200\text{ cm}^{-1}$ , where a broad band is found in the IR spectra of diorganoarsinic acids assigned to the presence of  $\text{AsO}_2\text{H}$  units [4]. The position of arsenic - oxygen stretchings was compared with the bands found in the spectra of dimethyl- and diphenylarsinic acids and the corresponding sodium salts. As it can be seen in Table 1, the arsenic-oxygen single bond stretching is shifted as a result of coordination to lower values. The same behaviour was observed for arsenic-oxygen double bond stretching (Table 1). A structure with both oxygen atoms involved in coordination can be postulated, but the data are not enough to distinguish between a monomeric, cyclic or polymeric structure.

Table 1. The AsE (E=O,S) bond stretching frequencies ( $\text{cm}^{-1}$ )

Compound	$\nu_{\text{As-O}}$	$\nu_{\text{As=O}}$	$\nu_{\text{As-S}}$
$\text{Me}_2\text{AsO}_2\text{H}$	736i	890i	-
$\text{Me}_2\text{AsO}_2\text{Na}$	760i	860i	-
$\text{Ph}_2\text{SbO}_2\text{AsMe}_2$	730i	843i	-
$\text{Me}_2\text{AsSONa}$	-	865i	432mi
$\text{Ph}_2\text{SbSOAsMe}_2$	-	845i	417mi
$\text{Ph}_2\text{SbO}_2\text{AsPh}_2$	740	855	-

The infrared spectrum of  $\text{Ph}_2\text{SbSOAsMe}_2$  was compared with the spectra of starting materials. To the best of our knowledge there are no literature data concerning the infrared spectra of dimethylthioarsinic acid or its derivatives, so we present here in some

## Diphenylantimony(III) Diorganoarsinate and Tioarsinate.

detail the spectrum of sodium dimethylthioarsinate. Two spectral regions are of interest: 500 - 400  $\text{cm}^{-1}$  for arsenic - sulfur stretchings [5] and 850 - 700  $\text{cm}^{-1}$  for arsenic - oxygen stretchings [4]. The possibility of thion - thiol equilibrium for monothioarsinate derivatives has to be taken into account when the bands in the IR spectrum are assigned. The band at 432  $\text{cm}^{-1}$  was assigned to arsenic-sulfur stretching. This value ranges, according the literature data [5,6,7], between the values for the single and double arsenic-sulfur bond stretchings. There is a strong band at 865  $\text{cm}^{-1}$  which was assigned to arsenic - oxygen stretching. The value is lower than those reported for an arsenic-oxygen double bond, but higher than the values for arsenic-oxygen single bond stretchings [4]. Thus, we can assume that the  $\pi$ - electrons are delocalised over the SAsO system as found for dimethyldithioarsinato species [8]. In the spectrum of diphenylantimony(III) dimethylthioarsinate both , arsenic - sulfur and arsenic - oxygen bond stretchings are shifted to lower values by coordination, suggesting the presence of a bidentate ligand. However it is difficult to asses the relative degree of the involvement in bonding of the two donor atoms.

### Mass spectra.

For diphenylantimony(III)dimethylarsinate both FAB and EI mass spectra were recorded. The relative intensities of the main fragments containing antimony and arsenic in the two mass spectra are given Table 2.

The spectra show the molecular ion peak ( $m/z=412$ ) with a higher abundance in the FAB spectrum. The base peak is, in the FAB spectrum,  $m/z=154$   $[\text{Ph}_2]^+$ , while the EI spectrum exhibits the base peak at  $m/z=335$  corresponding to  $[\text{PhSbO}_2\text{AsMe}_2]^+$  formed by loss of a phenyl group from the parent ion. The same base peak was reported earlier for  $\text{Ph}_2\text{SbS}_2\text{AsMe}_2$  [2]. In spite of this resemblance, the fragmentation scheme for dimethylarsinic (Scheme 1) and dimethylthioarsinic (Scheme 2) derivatives are not similar .

The loss of two methyl groups leads to the next fragment containing both antimony and arsenic  $[\text{PhSbO}_2\text{As}]^+$ ,  $m/z=305$  (15.0). Monophenylantimony  $\text{PhSb}^+$ , is formed by further fragmentation. The diphenylantimony,  $\text{Ph}_2\text{Sb}^+$  is a result of the loss of dimethylarsinic group from the parent ion. Diphenylantimony is partially transformed in  $\text{C}_{12}\text{H}_{10}\text{Sb}^+$  stibonium heterocycle.

**Table 2. Relative intensities of the antimony and arsenic containing fragments in the FAB and EI mass spectra of Ph<sub>2</sub>SbO<sub>2</sub>AsMe<sub>2</sub>.**

Fragment	FAB	EI
Ph <sub>2</sub> SbO <sub>2</sub> AsMe <sub>2</sub> (M <sup>+</sup> )	412(19.0)	412(4.0)
PhSbO <sub>2</sub> AsMe <sub>2</sub> (M-Ph)	335(40.0)	335(100.0)
Ph <sub>2</sub> SbO <sub>2</sub> As (M-2Me)	305(2.6)	305(15.0)
Ph <sub>2</sub> Sb	275(40.7)	275(19.8)
C <sub>12</sub> H <sub>10</sub> Sb	273(7.9)	273(10.3)
PhSb	198(9.2)	198(71.5)
Me <sub>2</sub> AsO <sub>2</sub> H	138(26.6)	138(3.9)
Me <sub>2</sub> AsO <sub>2</sub> <sup>+</sup>	137(21.9)	137(2.2)
SbO <sup>+</sup>	137(39)	137(0)
Me <sub>2</sub> AsO <sup>**</sup>	121(0)	121(5.2)
Sb <sup>**</sup>	121(7.9)	121(5.0)
Me <sub>2</sub> As	105(13.7)	105(6.1)
AsO	91(19.1)	91(20.8)
MeAs	90(22.7)	90(1.9)
CH <sub>2</sub> As	89(33.9)	89(4.9)
As	75(11.2)	75(3.4)
Me <sub>3</sub> AsO <sup>***</sup>	136(80.7)	-
Me <sub>3</sub> As <sup>***</sup>	120(15.3)	-
(Me <sub>2</sub> AsO <sub>2</sub> ) <sub>2</sub> <sup>***</sup>	274(70.3)	274(2.0)

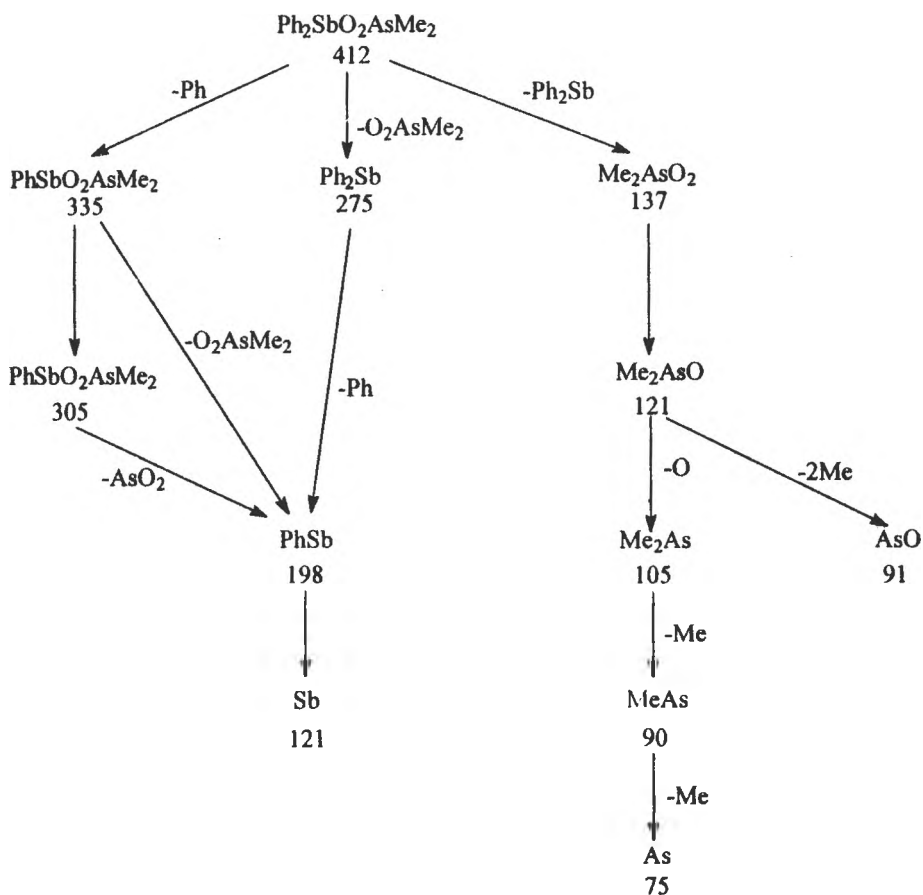
\* The peak at 137 is shared by the two mentioned ions.

\*\* The peak at m/e=123 was used to distribute the relative intensity of the peak at m/z 121 to Me<sub>2</sub>AsO and and <sup>121</sup>Sb.

\*\*\* Collision peaks



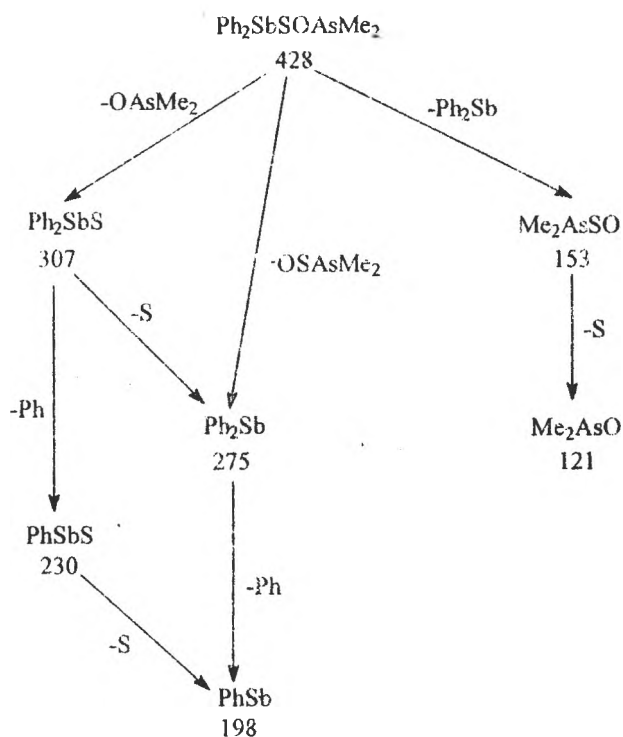
## Diphenylantimony(III) Diorganoarsinate and Tioarsinate.



Scheme 1

The loss of  $\text{Ph}_2\text{Sb}$  from the parent ion leads to the expected arsenic containing fragments. The FAB spectrum shows an intense peak at  $m/z = 137$  (21.9) assigned to  $\text{Me}_2\text{AsO}_2^+$ , and another one at  $m/z = 138$  (26.6) assigned to  $\text{Me}_2\text{AsO}_2\text{H}^+$ . Peaks of much lower intensities are found in the EI mass spectrum.

It is worth mentioning that there are no  $\text{Ph}_2\text{SbO}$  or  $\text{PhSbO}$  fragments are absent in both mass spectra discussed here, the oxygen atoms leaving together with the arsenic. A number of ions resulted from collision processes within the mass spectrometer are also listed in Table 2.



Scheme 2

The FAB mass spectrum of  $\text{Ph}_2\text{SbSOAsMe}_2$  shows a peak for the molecular ion at  $m/z = 428$  and this is the only peak containing both antimony and arsenic atoms. No loss of methyl, phenyl sulphur or oxygen is observed from the parent ion. The sulphur is shared by fragmentation between antimony and arsenic, while the oxygen is again found preferentially in the arsenic containing fragments (Scheme 2). Diphenylantimony,  $\text{Ph}_2\text{Sb}^+$  and monophenylantimony,  $\text{PhSb}^+$  are formed by successive loss of sulfur and phenyl. The formation of the heterocyclic ion  $\text{C}_{12}\text{H}_{10}\text{Sb}^+$  from  $\text{Ph}_2\text{Sb}^+$  by loss of two hydrogens is reflected in the isotopic ratios of the peaks with  $m/z = 273/275/277$  (the  $m/z$  peak at 275 is shared by the two fragments, so the relative intensity of this peak is the sum of the peaks containing  $^{121}\text{Sb}$  and  $^{123}\text{Sb}$  isotopes).

## Diphenylantimony(III) Diorganoarsinate and Tioarsinate.

### Experimental

IR spectra were recorded in Nujol mulls using a Perkin-Elmer 983 spectrometer and FAB mass spectra with an MS 902 mass spectrometer.

### Preparations

Anhydrous sodium dimethylarsinate was prepared from dimethylarsinic acid (of commercial origin) and sodium ethoxide in acetonitrile. Diphenylantimony(III) chloride was prepared according the published method [3]. Dimethylthioarsinate was prepared by bubbling  $H_2S$  through a water solution of sodium dimethylarsinate [4].

### Diphenylantimony(III) dimethylarsinate, $Ph_2SbO_2AsMe_2$

A mixture of solutions of diphenylantimony(III) chloride,  $Ph_2SbCl$  (0.62 g, 2 mmol), and anhydrous sodium dimethylarsinate,  $NaO_2AsMe_2$  (0.30 g, 2 mmol) each in acetonitrile (25 ml) was stirred at reflux for two hours. The precipitate was filtered off and the solvent evaporated slowly. The white crystals, which separated were filtered and vacuum dried. Yield 0.31 g, 38.6 %, m.p.  $214^\circ$ . Another portion of 0.27 g were extracted from the precipitate using a mixture of acetonitrile and ethanol. The product is stable up to  $350^\circ$ . The overall yield was 72.5 %.

Anal.  $C_{14}H_{18}AsSbO_2$  Found: C 53.31, H 3.91 calc.: C 53.65, H 3.72 %.

### Diphenylantimony(III) diphenylarsinate, $Ph_2SbO_2AsPh_2$

The diphenylarsinic acid (0.52 g, 2 mmol) was refluxed for 5 hours with the stoichiometric amount of  $Ph_2SbCl$  (0.62 g, 2 mmol) in acetonitrile (30 ml). The solution thus obtained was concentrated and the white solid filtered and vacuum dried. Yield 0.78 g, 73 %. The compound is stable up to  $350^\circ$ .

Anal.  $C_{24}H_{20}AsSbO_2$  Found: C 53.63, H 3.72 %

### Diphenylantimony(III) dimethylthioarsinate, $Ph_2SbSOAsMe_2$

Diphenylantimony(III) chloride (0.31 g, 1 mmol) dissolved in 10 ml  $CH_2Cl_2$  was added to the solution obtained by dissolving 0.18 g (1 mmol) in 10 ml ethanol, under stirring at room temperature. After an hour the sodium chloride precipitate was filtered off and the filtrate was concentrated in a rotary evaporator. The white crystals which separated were filtered and vacuum dried. The product decomposes over  $200^\circ$ . Yield 0.29 g (67.4 %), m.p.  $284^\circ$ .

Anal.  $C_{14}H_{16}AsSbOS$  Found: C 39.40, H 3.86; Calc.: C 39.25, H 3.73 %.

**Acknowledgement.** We are grateful to Dr.D.B.Sowerby (University of Nottingham, U.K.) for facilitating the measurements of the mass spectra and to the British Council for support of this work under the ROMLISS Program.

### REFERENCES

1. C.Silvestru, L.Silaghi-Dumitrescu, I.Haiduc, M.J.Begley, M.Nunn and D.B.Sowerby, *J.Chem.Soc., Dalton Trans.*, 1986, 1031
2. D.B.Sowerby, M.J.Begley, L.Silaghi-Dumitrescu, I.Silaghi-Dumitrescu and I.Haiduc, *J.Organometal.Chem.*, 1994, 469, 45
3. M.Begley, D.B.Sowerby, D.M.Wesolek, C.Silvestru and I.Haiduc, *J.Organometal.Chem.*, 1986, 316, 281
4. F.K.Vansant, B.J.Van der Veken and M.A.Herman, *Spectrochim Acta*, 1974, 30A, 69

L. SILAGHI-DUMITRESCU, A. HAIUC

5. R.A.Zingaro, K.J.Irgolic, D.H.O'Brien and L.J Edmonson jr., *J Amer.Chem.Soc.*, 1971, **93**, 5677
6. L.Silaghi-Dumitrescu, I.Silaghi-Dumitrescu and I.Haiduc, *Rev.Roumaine Chim.*, 1989, **34**, 305
7. I.Haiduc and L.Silaghi-Dumitrescu, *J.Organometal.Chem.*, 1982, **225**, 225
8. I.Silaghi-Dumitrescu, L.Silaghi-Dumitrescu and I.Haiduc, *Rev.Roumaine Chim.*, 1982, **27**, 8.
9. M.Nunn, D.B.Sowerby and D.M.Wesolek, *J.Organometal.Chem.*, 1983, **251**, C45

Received:5.12.1995

## ON THE GEOMETRY AND ELECTRONIC STRUCTURE OF $\text{XH}_2\text{SiNH}_2$ ( $\text{X}=\text{F}, \text{Cl}, \text{Br}$ ) SILANES. MNDO MOLECULAR ORBITAL CALCULATIONS.

Ioan Silaghi-Dumitrescu and Ionel Haiduc

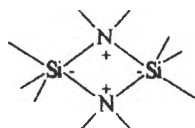
Facultatea de Chimie  
Universitatea Babeș-Bolyai, R-3400 Cluj-Napoca,  
Romania

### Abstract

Full optimized geometry of the title compounds have been determined by MNDO molecular orbital calculations. As a result of the interplay between the  $\text{Si}(\sigma)\text{-N}(\sigma)$  interactions and hyperconjugative effects, the Si-N and Si-H bond lengths decrease by substitution of fluorine for a heavier halogen. The energies and symmetry of the unoccupied mo's suggest that  $\text{Cl}(\text{Br})\text{H}_2\text{SiNH}_2$  are better candidates for cyclodimerization than  $\text{FH}_2\text{SiNH}_2$ .

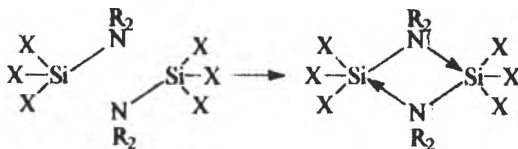
### INTRODUCTION.

Cyclodisilazanes **1** containing two silicon atoms in the five coordination environment are rare in contrast with the normal valent silicon countering four membered rings [1].



**1**

They can be obtained basically by a 2+2 cycloaddition **2** of two aminosilanes  $\text{R}_3\text{SiNH}_2$  and so far, this is the only preparation procedure reported [2-4].



**2**

I. SILAGHI-DUMITRESCU, I. HAIDUC

**Table 1**  
Valence orbital energies (eV) and the enthalpies of formation of  $\text{XH}_2\text{SiNH}_2$  (kcal/mol)

	H	F	Cl	Br
$\Delta H_{\text{formation}}$	19.344	-116.182	-66.865	-41.019
HOMO	-9.812 (5a')	-10.314 (7a')	-10.749 (7a')	-10.604 (7a')
LUMO1	2.833 (3a'')	2.322 (8a')	<u>0.818</u> (8a')	<u>0.339</u> (8a')
LUMO2	<u>2.993</u> (6a')	2.474 (4a'')	1.945 (9a')	1.866 (4a'')
LUMO3	3.118 (7a')	2.963 (9a')	1.964 (4a'')	1.946 (9a')
LUMO4	3.240 (8a')	<u>4.388</u> (10a')	2.391 (10a')	2.277(10a')

**Table 2**  
The calculated MNDO calculated geometrical parameters of  $\text{XH}_2\text{SiNH}_2$  silanes (bond lengths in angstroms, angles in degrees)

$\text{XH}_2\text{SiNH}_2$	H	F	Cl	Br
SiN	1.711	1.712	1.691	1.688
SiX	1.386	1.601	2.129	2.246
SiH	1.382	1.382	1.374	1.374
NSiX	110.42	106.48	108.42	109.33
HSiH	108.70	110.18	110.68	110.46
HNH	110.35	110.03	110.28	110.38
**SiN <sup>a</sup>	167.71	165.66	167.78	168.34

a) SiN\*\* is the angle subtended by the SiN bond and the bisector of the HNH angle.

We have shown recently [5] that the process of cycloaddition is mainly controlled by the silicon center since this will reclaim more energy to deform from the tetrahedral to the pentacoordinated state, while the potential around the nitrogen is more flat. It has been found also [5] that the barrier to the cycloaddition is much smaller for  $\text{ClH}_2\text{SiNH}_2$  than for  $\text{FH}_2\text{SiNH}_2$  and this trend might be followed by real systems too. In the present note we will examine the orbital origin of this behavior by using the semiempirical MNDO method [6] and the C.A.C.A.O package of programs for molecular orbital analysis [7].

## RESULTS AND DISCUSSION

The enthalpies of formation, the energies of the HOMO and those of some lower energy empty mo's of the  $\text{XH}_2\text{SiNH}_2$  aminosilanes are given in Table 1 and the main geometrical parameters are summarized in Table 2

Little experimental data is available for these compounds [8] so, we quote for comparison only the results of a recent ab initio (BAC-MP4) molecular orbital calculation [9] which gives a value of -11.5 kcal/mol for  $\text{H}_3\text{SiNH}_2$ . The HOMO (localized on nitrogen) of these systems is lowered by substituting H for a halogen, but in contrast to the simple predictions based on electronegativity rules [10] the bromoderivative has the lowest energy HOMO and the fluoro derivative has the highest one.

The Si-N bond lengths are within the normal range for silanes [11]; the longest SiN bond is found in the fluoroaminosilane while the shortest one in the bromoaminosilane. Note also that the XSiN bond angle is the smallest ( $106.48^\circ$ ) for the largest SiN bond and increases to  $109.33^\circ$  in  $\text{BrH}_2\text{SiNH}_2$ . The changes in the SiH bond lengths are less marked but they are still longer in  $\text{FH}_2\text{SiNH}_2$  than in the other three silanes. The coordination around the nitrogen atoms is almost planar as the  $\text{H}^*\text{SiN}$  angles show (the sum of angles at nitrogen is  $358.17^\circ$ ,  $357.51^\circ$ ,  $368.20^\circ$  and  $358.36^\circ$  for H, F, Cl and Br respectively), like in many of the N-substituted aminosilanes known [11].

One way to interpret these results would be by making use of the anomeric effect [12]. According to this concept the nitrogen lone pair interacts with Si-X antibonding orbitals and causes a SiN bond shortening as well as the lengthening of the Si-X and SiH bonds. Speaking in fragment orbitals terms, it means that when an  $\text{XH}_2\text{Si}$  fragment interact with the  $\text{NH}_2$  fragment to form  $\text{XH}_2\text{SiNH}_2$  besides the main  $\sigma$ - $\sigma$  interaction responsible for the formation of the Si-N  $\sigma$  bond

there is also a sizeable  $\pi$  overlap between the nitrogen lone pair bearing orbital and an acceptor orbital of the same symmetry localized on silicon. More lower the silicon vacant  $\sigma^*$  orbitals are [13], more important this effect would be. The trend in the Si-N bond lengths suggest that if this effect does operate, it is highest for the bromo derivative where the shortest Si-N bond length is encountered. On the other hand, the strengthening of the Si-N bond should be accompanied -as opposed to the trend shown in Table 2- by some lengthening of the Si-H bonds since a fraction of the nitrogen lone pair electrons comes in an orbital which is Si-H antibonding.

In the following we will analyze to some detail these findings by making use of the well known fragment analysis [14], frequently applied in drawing out the most important features of a given interacting set of orbitals. The fragments considered here are  $\text{XSiH}_2$  and  $\text{NH}_2$  respectively.

The  $\text{XSiH}_2$  fragment orbitals can be derived from those of the  $\text{SiH}_2$  and halogen valence orbitals. Figure 1 shows the interaction of silene radical with a fluorine and a chlorine atom. In both cases the HOMO (see scheme 3)

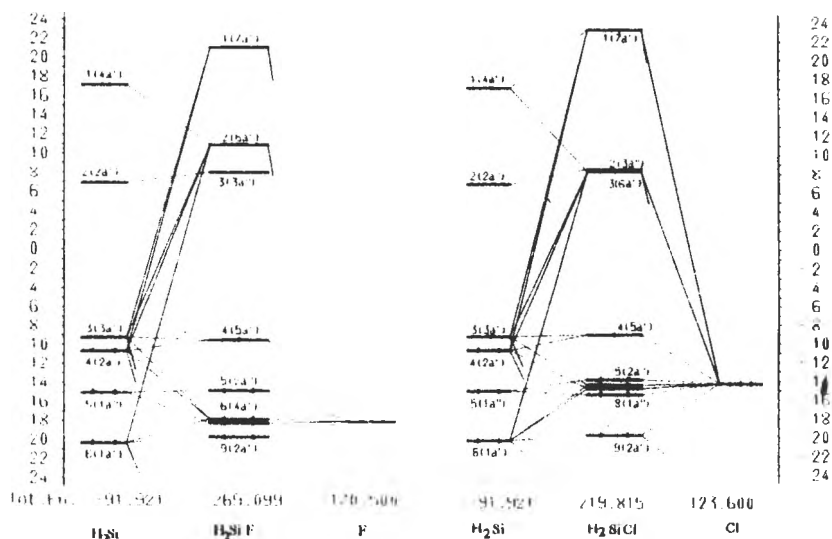
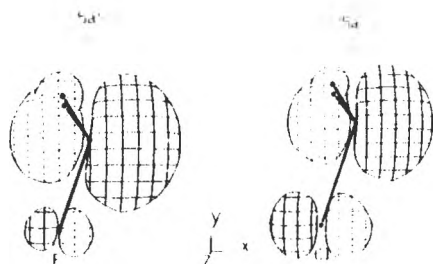


Figure 1. The orbital interaction diagrams of silene with chlorine and fluorine

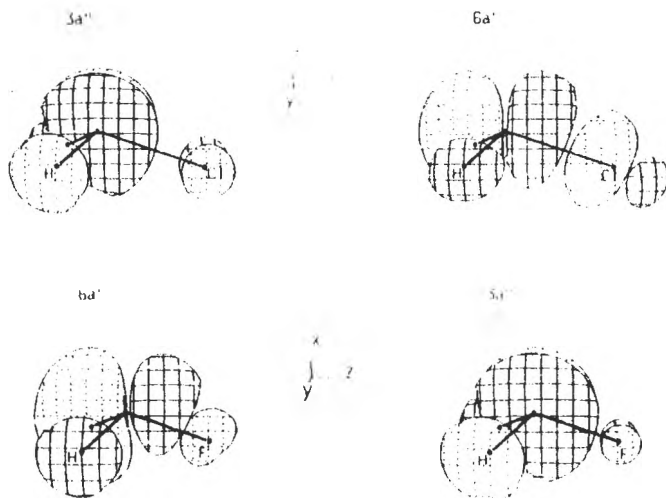


## Geometry and Electronic Structure of $\text{XH}_2\text{SiNH}_2$ ( $\text{X}=\text{F}, \text{Cl}, \text{Br}$ ) Silanes



3

is localized on silicon and consequently have almost the same energy. The next, two unoccupied mo's ( $6a'$  and  $3a''$ , 4) are related to the  $\sigma$  (degenerate antibonding orbitals of  $\text{SiH}_3$ ) and as we will see they are of key importance in determining the relative acceptor properties of  $\text{XH}_2\text{SiNH}_2$ .



4

Since  $3a''$  is composed of  $p_z$  orbitals of fluorine (chlorine) and silicon (as well as the pseudo  $\pi$  combination of the hydrogen (bound to silicon)  $s$  orbitals), they are close in energy because the  $\text{X-Si}$   $\pi$  overlap is quite similar. A major difference appears for  $6a'$  which is placed 2.5eV higher for  $\text{FSiH}_2$  than for  $\text{ClSiH}_2$ . This might sound strange since F is more electronegative than chlorine and if a

perfect parallel between the substituent effects on carbon and silicon were, it should draw  $6a'$  to a lower value than it is in  $\text{ClSiH}_2$ , and even lower<sup>15</sup> than in  $\text{H}_3\text{Si}$ . If the halogens would use only one  $\sigma$  orbital for interaction with the  $\text{SiH}_2$  moiety, than indeed, more electronegative the halogen is, more lower the energy of the correspondent of  $6a'$  is pushed. Figure 2 shows the relative energy levels of  $\text{SiH}_3$  and a hypothetical  $\text{XSiH}_2$  system where X is more electronegative than hydrogen and bears only one s orbital.

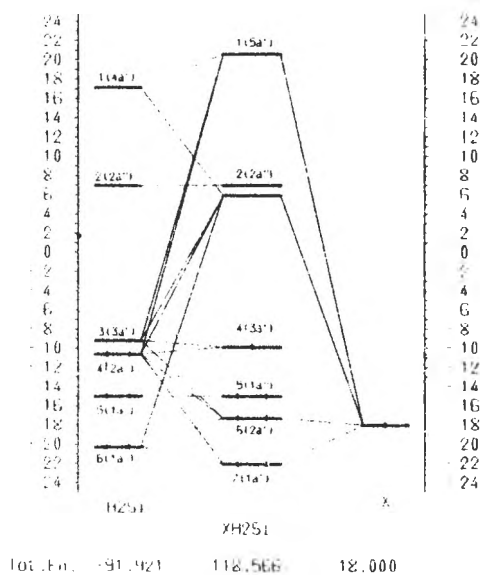


Figure 2. The orbital interaction diagram between a silene molecule and a fictive atom having  $\text{IP} = -18\text{eV}$

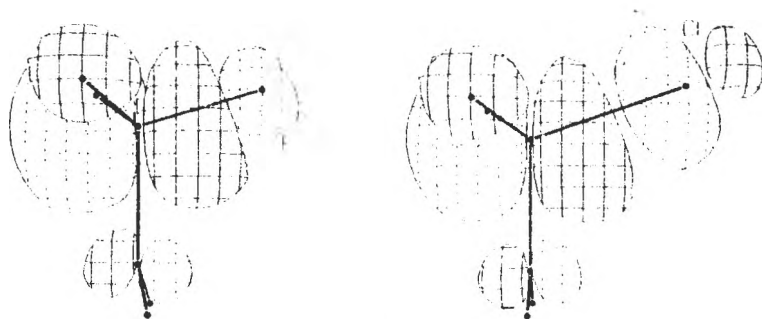
This means that the actual disposal of  $6a'$  is determined in a more complicated way, by multiorbital mixing. Since  $6a'$  is the potential acceptor of the nitrogen lone pair it is now understandable why the  $\text{he } \pi$  interaction might be stronger for  $\text{ClSiNH}_2$  (or  $\text{BrH}_2\text{Si}$ ) than for  $\text{FSiNH}_2$ .

The HOMO of  $\text{FH}_2\text{Si}$  on the other hand is slightly lower in energy than for  $\text{ClH}_2\text{Si}$  and thus the interaction with the HOMO of  $\text{NH}_2$  is slightly stronger

## Geometry and Electronic Structure of $\text{XH}_2\text{SiNH}_2$ (X=F, Cl, Br) Silanes

than for the heavier substituted silane. This means that part of the  $\sigma$  electron density coming from nitrogen goes into  $5a'$  which has Si-H bonding character. Thus, the SiN bond shortening across the  $\text{XH}_2\text{Si}$  series is the result of cooperative  $\sigma + \pi$  interactions. The SiH bond shortening on the other hand (less marked than that of SiN bond) originates in the action of opposite factors: this bond tends to be strengthened by the  $\sigma$  interactions between the  $\text{XH}_2\text{Si}$  and  $\text{NH}_2$  fragments and is weakened due to the  $\pi$  interactions (anomeric effect). Of course, for a quantitative assessment of these effects more elaborate methods of calculations are necessary.

The relative acceptor properties of the halogenosilazanes in the process of cyclodimerization can also be inferred from the above discussion. The lowest energy orbital of proper symmetry of  $\text{XH}_2\text{SiNH}_2$  resembles much  $6a'$  of the parent fragment.



5

This is situated higher for  $\text{FH}_2\text{SiNH}_2$  (due to the stronger  $\sigma$  interaction which pushes this empty orbital to higher energies - see the underlined entries in Table 2) than  $\text{ClH}_2\text{SiNH}_2$  and thus the dimerization of the former would require a higher barrier (as we found by MNDO searching of the potential surface [5]).

## REFERENCES

1. V.Klenggebiel, in *The Chemistry of Inorganic Homo- and Heterocycles*, I.Haiduc and D.B.Sowerby eds., Acad. Press, 1987, vol 1, p.221.
2. W.S.Sheldrick, W.Wolfsberger, *Z.Naturforsch.*, 1977, 173, 277.

I. SILAGHI-DUMITRESCU, I. HAIDUC

3. D.G. Anderson, D.G. Blake, A.J. Craddock, E.A.V. Ebsworth, D.W.H. Rankin, A.J. Welch, A.E. Robertson, *J. Chem. Soc. Dalton Trans.*, 1987, 3035.
4. D.G. Anderson, J. Armstrong, S. Craddock, *J. Chem. Soc. Dalton Trans.* 1987, 3029.
5. F. Lara-Ochoa, I. Silaghi-Dumitrescu, I. Haiduc, *Main Group Chemistry*, submitted for publication.
6. Dewar, M.J.S., Thiel, W. *J. Amer. Chem. Soc.*, 1977, **99**, 4999 ; the computer program written by P. Bischof and G. Friedrich, G. *Program MNDO/2*, University of Heidelberg 1988 has been transported to MS-DOS by one of the authors (ISD)
7. C. Mealli, D.M. Prosperio, *J. Chem. Educ.*, 1990, **67**, 399 .
8.  $\text{H}_3\text{SiNH}_2$  has been observed in mass spectrometrical experiments, see C.-H. Wu, *J. Phys. Chem.*, 1987, **91**, 5054 ; and also S.-S. Lin, *Electrochem. Soc.*, 1977, **124**, 1945 for  $\text{H}_{3-x}\text{F}_x\text{SiNH}_2$ .
9. C.I. Melius, P. Ho, *J. Phys. Chem.*, 1991, **95**, 1410 .
10. T.A. Albright, J.K. Burdett, M.-H. Whangbo, *Orbital Interactions in Chemistry*, Wiley, New York, 1985, chapter 6.
11. see references 3,4 and also the followings for the geometries of substituted silazanes:  
D.W.H. Rankin, *J. Chem. Soc., Dalton Trans.*, 1987, 785;  
D.W.H. Rankin, H.E. Robertson, *J. Mol. Struct.*, 1987, **158**, 339 .  
A.J. Blake, E.A.V. Ebsworth, *J. Chem. Soc. Dalton Trans.*, 1986, 91.  
G. Gunderson, R.A. Mayo, D.W.H. Rankin, *Acta Chem. Scand., Ser. A*, 1984, **A38**, 579 .
12. A.E. Reed, P.v.R. Schleyer, *Inorg. Chem.*, 1988, **27**, 3969 .
13. We assume here that the  $\sigma^*$  orbitals and not the silicon vacant 3d orbitals are involved in the interactions discussed. The question of bonding of 3d orbitals of the 3-rd row elements has been many times addressed, (for a recent account see A.E. Reed, P.v.R. Schleyer, *J. Amer. Chem. Soc.*, 1990, **112**, 1434 ) but a definitive answer is still opened.
14. L. Libit, R. Hoffmann, *J. Amer. Chem. Soc.*, 1974, **96**, 1370 ; M.-H. Whangbo, H.B. Schelegel, S. Wolfe, *J. Amer. Chem. Soc.*, 1977, **99**, 1296 .
15. L. Radom, *Structural Consequences of Hyperconjugation*, in *Theoretical Organic Chemistry*, vol 3, I.G. Csizmadia (Ed.), Elsevier, Amsterdam, 1982.

Received: 5.01.1996

## Synthesis and Conformational Analysis of Some 2-Alkyloxycarbonyl Substituted 1,3-Dioxanes

Mihai Horn, Ion Grosu and Sorin Mager\*

Universitatea "Babeș-Bolyai", Facultatea de Chimie și Inginerie Chimică, str.  
Arany Janos 11, 3400-Cluj-Napoca, România

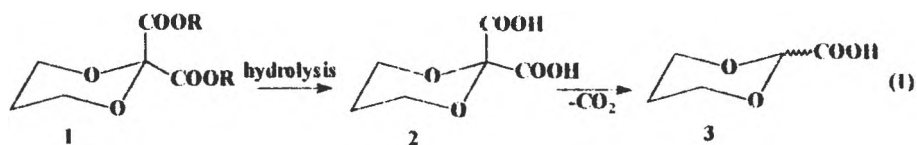
**Abstract:** The stereochemistry of some 2-carboxy and ethyloxycarbonyl 1,3-dioxanes was investigated using NMR and mass-spectrometry data. The investigations prove the anancomericity of the structures and the equatorial preference of the acid or ester groups located in the acetal part of the molecule. Several methods were tried for the synthesis of the investigated compounds, but only the transacetalization of the dialkoxyacetic ester gave the desired compounds in good yields.

### INTRODUCTION

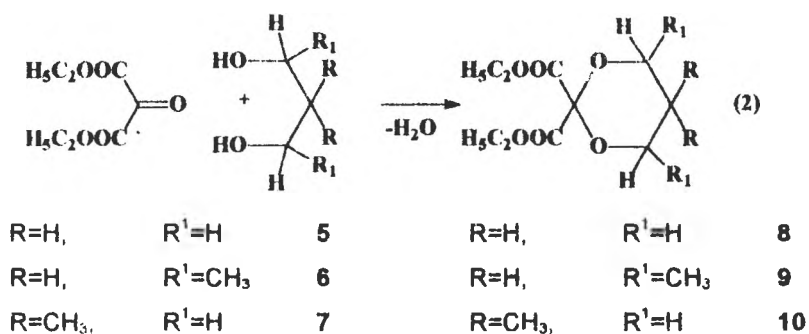
Conformational analysis of 1,3-dioxanes offers information concerning equilibration studies respectively "conformational free energies"[1], data related to 5-substituted 1,3-dioxanes with or without anancomeric substituents in position 2 (configurational and conformational equilibria, respectively) [2-6]. Few data are available for 1,3-dioxane compounds having carboxy or alkyloxycarbonyl substituents in 2 position [7], mainly because of the difficulties encountered in their synthesis [8,9]. It was considered of interest to improve the methods used in the synthesis of this type of 2-substituted 1,3-dioxanes and to develop a study concerning their stereochemistry.

### RESULTS AND DISCUSSION

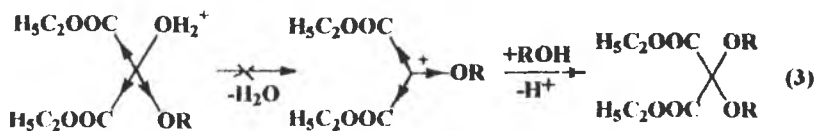
It was tried to obtain 2,2-bis(ethyloxycarbonyl)-1,3-dioxanes **1** as starting diesters for the synthesis of 2-carboxy-1,3-dioxane **3** through the hydrolysis of the diester **1** followed by monodecarboxylation (1) of the diacid **2**:



The easiest way seemed to be the synthesis by means of the general method starting from mesoxalic ester **4** and 1,3-diols (1,3-propanediol **5**, meso-2,4-pentanediol **6** or neopentylglycol **7**) in acidic catalysis by azeotropic distillation of the water (2):



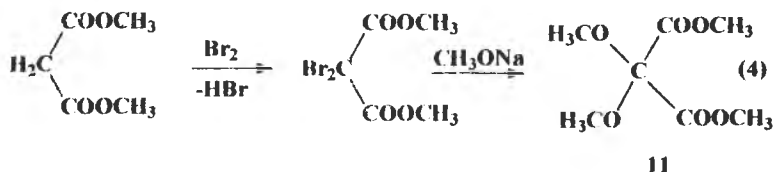
No 1,3-dioxane compound was obtained (unreacted mesoxalic ester was recovered) by this way, presumable because the direct acetalisation mechanism involving a nucleophilic substitution at the protonated hemiacetalic intermediate with a carbon atom bearing three strong withdrawing substituents, can not take place (3):



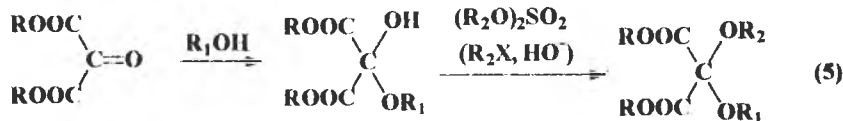
Taking into account the reported synthesis [10], of some cyclic acetals of ketoesters by means of a transacetalization reaction (which can not take place by direct acetalization), we tried to obtain the desired 1,3-dioxane starting from the dimethyldimethoxymalonate **11** obtained from dimethylmalonate by means of

## Synthesis and Conformational Analysis of some Dioxanes

the sequence reactions (4):

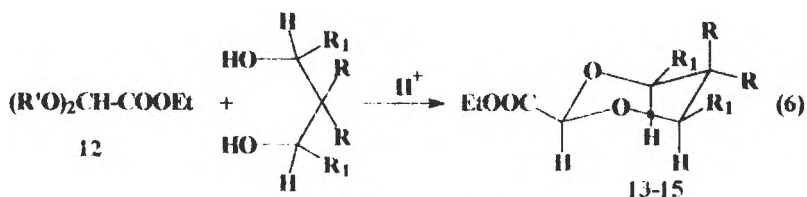


The total very poor yield of the reactions (about 10% for the compound, with 90% purity) made us to try another alternative, starting from mesoxalic ester (5). This promising method [11, 12] makes possible the synthesis of some unsymmetrical ketals, unknown in the literature [12].



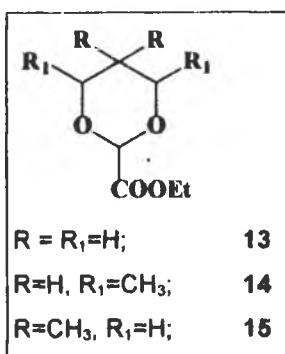
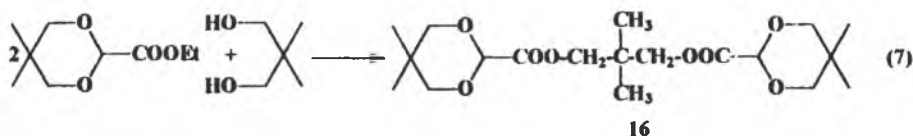
All the attempts to achieve the transacetalization reaction of the obtained diether 11 with the meso-2,4-pentanediol (run in benzene in the presence of p-toluenesulphonic acid as catalyst, without solvent in the presence of some drops of concentrated sulphuric acid or using Amberlist-15 as catalyst) failed

In order to avoid the presence of two strong electron withdrawing substituents (COOEt) at the reaction center, the synthesis of the desired 2-alkyloxycarbonyl substituted 1,3-dioxane was conceived starting from the dialkoxyacetic ester 12 by means of the transacetalisation reaction (6) with the diols 5-7.



R=H,	R <sup>1</sup> =H	5	R=H,	R <sup>1</sup> =H	13
R=H,	R <sup>1</sup> =CH <sub>3</sub>	6	R=H,	R <sup>1</sup> =CH <sub>3</sub>	14
R=CH <sub>3</sub> ,	R <sup>1</sup> =H	7	R=CH <sub>3</sub> ,	R <sup>1</sup> =H	15

In the case of the synthesis of compound 15 (obtained from neopentylglycol) a new diester 10 of the neopentylglycol with 2-carboxy-1,3-dioxane, representing a side product, was obtained as a result of the trans esterification reaction (7):



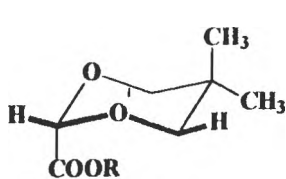
Concerning the conformational analysis of the 1,3-dioxanes 13-16, their NMR spectra prove for all of them anancomeric structures owed for compound 14 not only to the equatorial orientation of the two methyl groups, but also to the equatorial orientation of the ethyloxycarbonyl group in the position 2, the equilibrium (8) being shifted towards the left side:



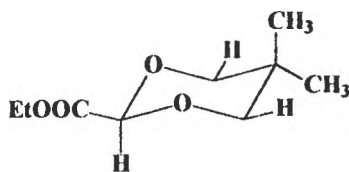
Because the assumption concerning the COOEt group based only on volumes can not be taken into account (the OR and CH<sub>2</sub>Cl groups for instance attached to the C<sup>2</sup> atoms adopt preferentially an axial orientation [13-15]), a supplementary experimental proof was necessary. Thus, the absence in the <sup>1</sup>H-NMR spectra of a long range coupling owned to a "M" (or W) arrangement of the bonds H<sub>ax</sub>-C<sup>2</sup>-O-C<sup>4(6)</sup>-H<sub>ax</sub> in the isomer 15a, with an axial ethyloxycarbonyl group, represents an argument for the equatorial orientation of the COOR group (and for an anancomeric structure) in compound 15.



## Synthesis and Conformational Analysis of some Dioxanes



15a



15

The complete interpretation of the NMR spectra was possible for dioxanes 15 and 16, only. Concerning compound 14, the extension of the signal belonging to the axial proton of the position 4 and 6 ( $\delta=3.76-3.98$  ppm) shows an ABX coupling model further splitted by three protons of the equatorial methyl group. In spite of some superposed signals, it is possible to identify the 16 peaks ( $2 \times 2 \times 4$ ) in concordance with the assumed splitting pattern (Figure 1)

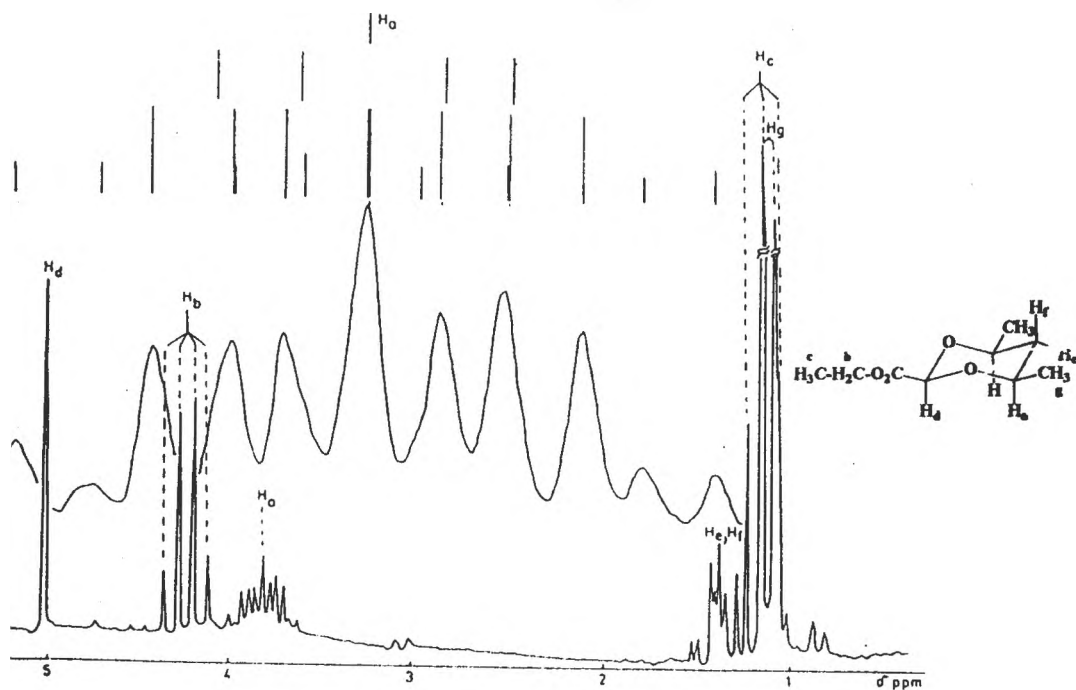
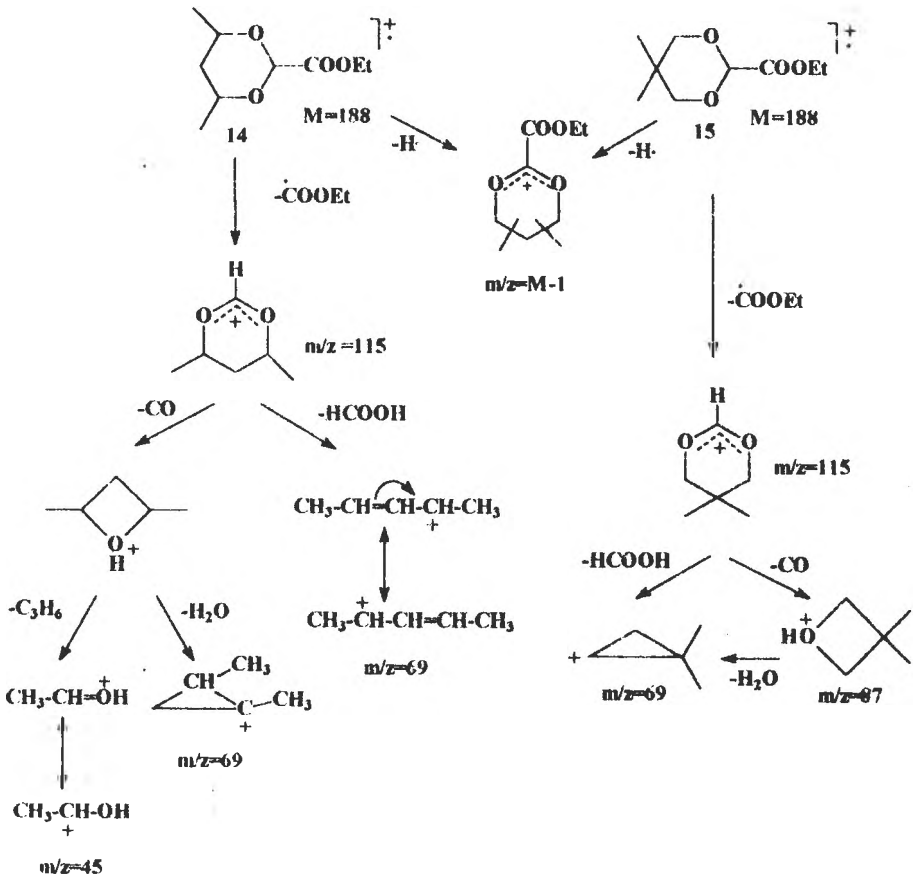


Figure 1.  $^1\text{H-NMR}$  spectrum of compound 14

In order to bring more information related to the few mass spectral studies in the field of 1,3-dioxanes [16-25], the 2-ethoxycarbonyl-1,3-dioxanes 13-15 were studied from this point of view.

The peculiar fragmentations of the 1,3-dioxanes 13-15 (Figure 2, Scheme 1), represent the loss of the ethoxycarbonyl fragment giving high peaks (90-100%) and the lack, of the molecular ion; a very small peak (less than 1 %) can be observed for the loss of a hydrogen atom (M-1).



Scheme 1

## Synthesis and Conformational Analysis of some Dioxanes

For the dimethylated 1,3-dioxanes **14** and **15** the loss of the COOEt group gives rise to the very abundant  $m/z=115$  peak (>90%) whose successive loss of carbon monoxide and water leads to the base peak  $m/z=69$  (100%). The same fragment is obtained directly by the splitting of a formic acid molecule.

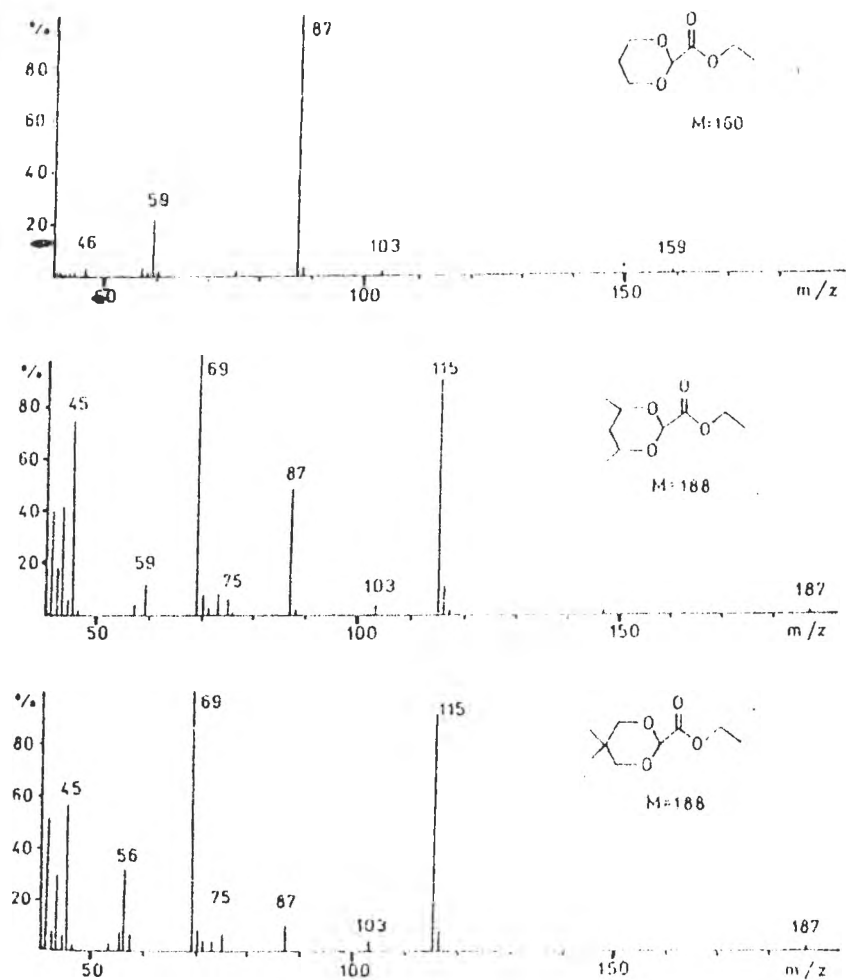
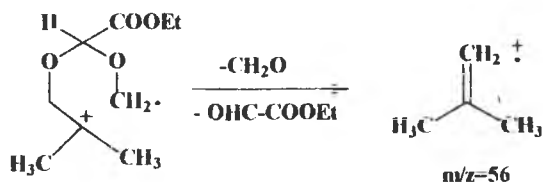
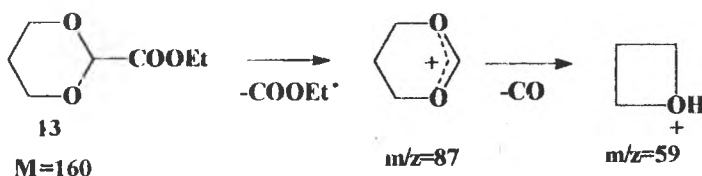


Figure 2. Mass-spectra of compounds **13**, **14** and **15**

Peculiar for the geminal dimethylated 1,3-dioxane **15** is also the fragmentation that leads to the  $m/z=56$  peak (32.5%)



The unsubstituted 2-ethyloxycarbonyl-1,3-dioxane shows a very poor fragmentation pattern with only two significant peaks:



Concerning the symmetric 1,3-dioxane diester **16**, the base peak is the same  $m/z=115$  peak, resulted from the loss of the ester part of the molecule. The main abundant peaks are presented in the experimental part.

## EXPERIMENTAL

The transacetalisation reactions at the ethyldiethoxyacetate **12** with the three diols **5-7** was run following the general procedure:

0.1 mol ester **12**, 0.1 mol of diol and 4.5g Amberlyst 15 were warmed under stirring on an oil bath between 120-150° C. After 40-45 minutes about 80-90 % of the corresponding alcohol resulted from the reaction was collected. The catalyst was filtered and the product was distilled at low pressure, obtaining about 90% purity compounds (G. C. Carbowax 20M/Cromosorb W). A new vacuum distillation with a small Vigreux column leads to pure products (G.C. > 98%). From the residue in the distillation flask, the diester **16** was obtained by crystallisation from ethanol.

Compounds **14-16** are new ones.

### 2-Ethyloxycarbonyl-1,3-dioxane **13**

MS,  $m/z$  (%): 103(2), 88(3.5), 87(100), 75(2.5), 59(22.5), 58(1.5), 57(3), 46(3), 44(2), 40(15)

### *1,2*-2-Ethyloxycarbonyl-*c*-4,*c*-6-dimethyl-1,3-dioxane **14**

Liquid, b p =103-104 ° C (10 mm col.Hg). Yield 70.8%.  $C_9H_{16}O_4$ ,  $M=188.22$ . Found: C, 57.27, H, 8.86; required C, 57.47, H, 8.57

## Synthesis and Conformational Analysis of some Dioxanes

$^1\text{H-NMR}$  ( $\text{CDCl}_3$ )  $\delta$  1.30[d, 6H,  $J=6$  Hz, 4(6)- $\text{CH}_3$ ], 1.33(t, 3H,  $J=7$  Hz,  $\text{COOCH}_2\text{CH}_3$ ), 0.86-1.65(m, 2H,  $\text{C}^5$ ), 3.76-3.98[m, 2H, 4(6)- $\text{H}_{\text{ax}}$ ], 4.27(q, 2H,  $J=7$  Hz,  $\text{COOCH}_2\text{CH}_3$ ), 5.03 ppm(s, 1H, 2- $\text{H}_{\text{ax}}$ ). MS,  $m/z$  (%): 187(0.5), 147(2), 116(11), 115(90), 103(5), 87(48), 75(8), 73(9), 71(5.5), 70(9), 69(100), 59(12.5), 57(5.5), 45(75), 44(7), 42(18), 41(39.5)

### *2-Ethylloxycarbonyl-5,5-dimethyl-1,3-dioxane 15*

Liquid, b.p.=105-106 °C (10 mm col.Hg). Yield 60.5%.  $\text{C}_9\text{H}_{16}\text{O}_4$ ,  $M=188.22$ . Found: C, 57.54; H, 8.71; required C, 57.47; H, 8.57.  $^1\text{H-NMR}$  ( $\text{CDCl}_3$ )  $\delta$  0.79[s, 3H, 5- $\text{CH}_3(\text{eq.})$ ], 1.21[s, 3H, 5- $\text{CH}_3(\text{ax.})$ ], 1.33(t, 3H,  $J=7$  Hz,  $\text{COOCH}_2\text{CH}_3$ ), 3.54[d, 2H,  $J=11$  Hz, 4(6)- $\text{H}_{\text{ax}}$ ], 3.75[d, 2H,  $J=11$  Hz, 4(6)- $\text{H}_{\text{eq}}$ ], 4.28(q, 2H,  $J=7$  Hz,  $\text{COOCH}_2\text{CH}_3$ ), 4.92 ppm(s, 1H, 2- $\text{H}_{\text{ax}}$ ). MS,  $m/z$  (%): 187(0.8), 116(8.5), 115(94), 103(4), 87(7), 75(7), 73(3.5), 71(3.5), 70(8.5), 69(100), 57(8.5), 56(32.5), 55(7), 53(3.5), 45(57.5), 44(5), 43(29), 42(7), 41(51).

### *2,2-Dimethyl-1,3-propylen-bis(2-carboxyl-5,5-dimethyl-1,3-dioxane) 16*

Solid, m.p. 102-104 °C. Yield 10.5%.  $\text{C}_{19}\text{H}_{32}\text{O}_6$ ,  $M=344.45$ . Found: C, 59.24; H, 8.15; required C, 58.74; H, 8.30.  $^1\text{H-NMR}$  ( $\text{CDCl}_3$ )  $\delta$  0.79[s, 6H, 5- $\text{CH}_3(\text{eq.})$ ], 1.01[s, 6H,  $\text{H}_2\text{C-C}(\text{CH}_3)_2\text{-CH}_2$ ], 1.20[s, 6H, 5- $\text{CH}_3(\text{ax.})$ ], 3.51[d, 4H,  $J=11$  Hz, 4(6)- $\text{H}_{\text{ax}}$ ], 3.75[d, 4H,  $J=11$  Hz, 4(6)- $\text{H}_{\text{eq}}$ ], 4.06(s, 4H,  $\text{-COOCH}_2\text{-}$ ), 4.92 ppm(s, 2H, 2- $\text{H}_{\text{ax}}$ ). MS,  $m/z$  (%) 589 (0.1), 388 (0.05), 286(1), 258(2), 257(12), 217(3.5), 216(1.5), 202(2.5), 176(1.5), 175(20.5), 147(17), 127(8.5), 119(25.5), 115(100), 91(30), 69(64), 59(15), 57(6.5), 56(15), 55(21.5), 47(55.5), 45(42.5), 44(74.5), 43(25.5), 41(30).

## REFERENCES

- [1]. E. L. Eliel, S. Wilen, "Stereochemistry of Organic Compounds", Wiley and Sons, New York, 1994, p. 695
- [2]. F. G. Riddell, "Conformational Analysis of Heterocyclic Compounds", Academic Press, New York, 1980, p.70
- [3]. S. Mager, E. L. Eliel, Rev. Roum. Chim., (1973), **18**, 1379
- [4]. S. Mager, E. L. Eliel, Rev. Roum. Chim., (1973), **18**, 2097
- [5]. G. Binsch, E. L. Eliel, S. Mager, J. Org. Chem., (1974), **38**, 4079
- [6]. M. Kaloustian, N. Dennis, S. Mager, S. Evans, F. Aicudia, E. L. Eliel, J. Am. Chem. Soc., (1976), **98**, 956
- [7]. W. F. Bailey, E. L. Eliel, J. Am. Chem. Soc., (1974), **96**, 1798
- [8]. H. Suemune, N. Tanaka, K. Sakai, Chem. Pharm. Bull., (1990), **38**, 3155
- [9]. C. Tschierske, H. Kohler, H. Zuschke, E. Kleinpeter, Tetrahedron, (1989), **45**, 1987
- [10]. E. Vogel, H. Schiuz, Helv. Chim. Acta, (1950), **33**, 116

- [11]. Y. Olsuji, S. Wake, E. Isuoto, *Tetrahedron*, (1970), **26**, 4293
- [12]. M. Horn, M. Bojin, S. Mager, unpublished results
- [13]. F. Nader, E. L. Eliel, *J. Am. Chem. Soc.*, (1970), **92**, 3050
- [14]. E. L. Eliel, *Pure Appl. Chem.*, (1968), **25**, 509
- [15]. E. L. Eliel, C. Giza, *J. Org. Chem.*, (1968), **33**, 3754
- [16]. M. Horn, S. Mager, N. Palibroda, M. Culea, *Org. Mass Spectr.*, (1991), **26**, 649
- [17]. S. Mager, R. Țăranu, M. Horn, N. Palibroda, *Stud. Univ. "Babeş-Bolyai" Chem.*, (1982), **27**, 45
- [18]. S. Mager, N. Palibroda, I. Grosu, M. Horn, *Stud. Univ. "Babeş-Bolyai" Chem.* (1983), **28**, 16
- [19]. D. Rakhmankulov et al., *Zh. Prikl. Khim. (Leningrad)*, (1978), **51**, 1356
- [20]. J. Collin, G. Condé, *Bull. Acad. Royal Belg.*, (1966), **52**, 978
- [21]. F. Borremans, M. Anteunis, *Bull. Soc. Chim. Belg.*, (1971), **80**, 595,
- [22]. D. Jeremic et al. a) *Bull. Soc. Chim. Beograd*, (1979), **44**, 406; b) *Idem*, (1981) **46**, 1; *ibidem*, (1981), **46**, 403
- [23]. O. Chalova et al., *Zh. Prikl. Khim. (Leningrad)*, (1981), **54**, 3691
- [24]. J. Watowska, H. Malikowska, H. Otwinowska, *Chem. Anal.*, (1985), **30**, 853
- [25]. K. Pihlaja, J. Jalonen, *Org. Mass Spectrom.* (1971), **5**, 1363

Received:21.02.1996

## THE EFFECT OF PHOSPHORIC ACID ON THE ELECTROCHEMICAL BEHAVIOUR OF LEAD ACID BATTERY POSITIVE ELECTRODE

Eleonora Maria Rus

*Department of Physical Chemistry , University "Babes-Bolyai" Cluj-Napoca  
Romania*

### **Abstract**

The effect of phosphoric acid on the  $PbO_2$  electrode was examined by cyclic voltammetry. The anodic and cathodic polarization behaviour has been investigated by changing the potential range, sweeping rate and concentration of  $H_3PO_4$  in electrolyte.

### **INTRODUCTION**

In the last decade a special attention was given to the study of the possibilities to improve the cyclic life of positive electrodes in acid batteries by strengthening the positive plate active material structure and minimizing the corrosion of the positive grids [1-10]

The exact nature of the corrosion layers formed on positive grids are dependent on the voltage range, temperature, scan rate, electrolyte composition and electrode history.

In agreement with Ruetschi's results the corrosion film will consist of a  $PbSO_4$  layer on the outer surface and successive layers of monobasic lead sulphate, tribasic lead sulphate and lead oxides inside [11].

Some additives have been proposed in order to improve low temperature performance [12-15]. The behaviour of these additives is related to the electrochemical reaction of the lead/lead sulphate electrode.

It has been found that the addition of phosphoric acid to battery electrolyte enables the batteries to be charged and discharged with increased current densities. It is thought that the presence of  $H_3PO_4$  in electrolyte modifies the morphology of  $PbO_2$  crystals on the lead grids of positive electrodes [16-17].

## E. M. RUS

As a result of the morphological changes which occur, the  $\text{PbO}_2$  films formed are more hardly reducible with  $\text{PbSO}_4$  and impedes formation of a resistive  $\text{PbSO}_4$  layer at the grid/active material interface.

It has been proved that in lead oxidation with formation of lead dioxides in the presence of  $\text{H}_3\text{PO}_4$  an intermediate lead phosphate  $[\text{Pb}_3(\text{PO}_4)_2]$  is formed which influences the sulphation rate of  $\text{PbO}_2$ . How  $\text{Pb}_3(\text{PO}_4)_2$  influences the morphology of  $\text{PbO}_2$  is not yet understood.

Among the negative effects recorded at the addition of  $\text{H}_3\text{PO}_4$  is a capacity loss in the initial cycles mainly at low temperature operation conditions and an increase of the structural instability of negative electrodes [18]. The effects are minor as compared with the beneficial action of the  $\text{H}_3\text{PO}_4$  added.

### EXPERIMENTAL

The study of the  $\text{H}_3\text{PO}_4$  effects on the electrochemical behaviour of  $\text{PbO}_2$  has been made by using the cyclic voltammetry. Pure lead electrodes have been used (99.99%). The electrolyte used consisted of a solution of 4.3 m  $\text{H}_2\text{SO}_4$  with different  $\text{H}_3\text{PO}_4$  additions. A  $\text{Hg}/\text{Hg}_2\text{SO}_4/\text{K}_2\text{SO}_4(\text{sat})$  electrode served as the reference electrode. The counter electrode was made of pure lead. All the experiments were carried out at room temperature, the cyclings being effectuated over conveniently chosen potential ranges and at various potential sweeping rates.

Before each experiment, the working electrodes were polished with abrasive paper to remove the surface layers of oxides and were subjected to some anodic polarisations at potentials characteristic for oxygen evolution. This was meant to provide some reproducible surfaces as corrosion products were concerned.

### RESULTS AND DISCUSSION

Some typical voltammograms recorded on a disk shaped lead electrode ( $1 \text{ cm}^2$ ) in 4.3m  $\text{H}_2\text{SO}_4$  solution by sweeping the potential between -2 to +2 V (vs. a  $\text{Hg}/\text{Hg}_2\text{SO}_4$ ) at the scan rate of 20 mV/s, are shown in figure 1.

The voltammograms show that the potential cyclic sweep provides proper conditions for the deploy of several redox processes each of them being of major importance over a certain potential range. Thus, with the anodic sweep started in the range of hydrogen evolution continuing until the oxygen evolution only the anodic peak  $A_1$  associated to the formation of  $\text{PbSO}_4$  was recorded. It was remarkable that in this range no anodic peak corresponding to  $\text{PbO}_2$  species formation was recorded. The  $\text{PbO}_2$  formation is still supposed to have taken place. The absence of the peak was due to simultaneous deploy of formation process with oxygen evolution.



## Phosphoric Acid on the Electrochemical Behaviour of Lead Acid Battery

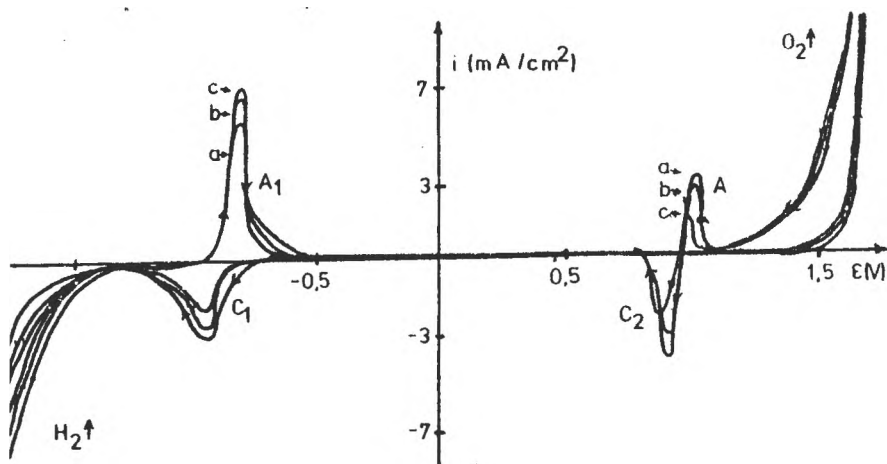


Fig.1. Cyclic voltammograms of lead in 4.3m H<sub>2</sub>SO<sub>4</sub>. Scan rate 20mV/s.  
a.- cycle 5; b.- cycle 10; c.- cycle 15

In cathodic potential sweep around the value 1V a mixt activity was recorded being characterized by the appearance of anodic peak A which precedes the cathodic peak C<sub>2</sub> associated with the electroreduction of Pb(IV) species to Pb(II) ( $\alpha$  PbO<sub>2</sub> and  $\beta$  PbO<sub>2</sub> to PbSO<sub>4</sub>). The peak A can be associated with further formation of PbO<sub>2</sub>. This process is stimulated by adsorbed oxygen on the electrodes surface in anodic sweep. This mixt activity was found to be dependent on anodic switch potential (ASP). For example peak A was not recorded when ASP was lower than 1.5V

In cathodic sweep, at negative potential values (-0.890V) peak C<sub>1</sub> was recorded associated with electroreduction of Pb(II) species to metallic lead. With the increase of the number of cycles the peak associated currents increase, in general, and shifts of peaks occur towards a more negative potential in anodic sweep, while the cathodic peaks move towards more positive potentials. Generally the peak shifts take place in directions contrary to potential scanning. One can say that peak shifts take place in directions contrary to potential scanning. One can say that overpotentials of processes decrease with the

increase of number of cycles. It is to remark that the shifting of these peaks was significantly influenced both by the anodic and cathodic switch potential values (ASP and CSP). The effect of these switching potentials proved to be smaller in the case of relatively reversible processes (see  $A_1$  and  $C_1$ ) and much greater in the case of less reversible processes.

Limiting the potential sweeping range between 0 and +2 V, in the positive going potential scan two peaks corresponding to  $\alpha$ - $PbO_2$  ( $A_2$ ) and  $\beta$ - $PbO_2$  ( $A_2'$ ) formation progressively developed with increasing cycle number, figure 2.

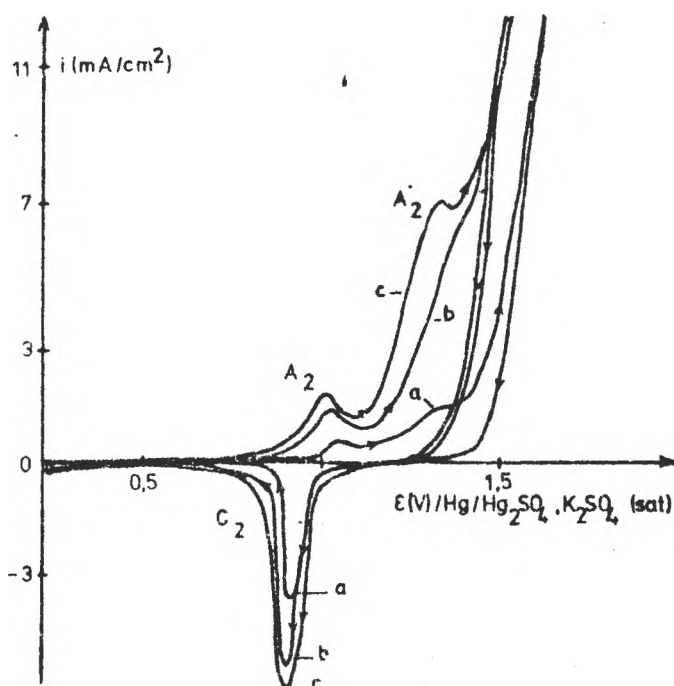


Fig.2. Cyclic voltammograms of pure lead in 4.3m  $H_2SO_4$ . Scan rate 10mV/s.

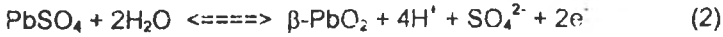
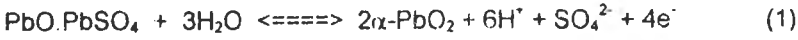
a.- cycle 5; b.- cycle 10, ASP - 1.75V; c.- cycle 10, ASP - 1.85 V.

The height of peak current due to  $\beta$ - $PbO_2$  formation increased with increasing cycle number (curves a and b - figure 2.) and the peak potential

## Phosphoric Acid on the Electrochemical Behaviour of Lead Acid Battery

shifted with the ASP (curves b and c - figure.2). The higher the ASP, the greater were the current densities corresponding to the two peaks ( $A_2$  and  $A_2'$ ).

It is supposed that  $\alpha$ - $PbO_2$  is formed in the conditions of reduced acidity inside the  $PbSO_4$  and  $\beta$ - $PbO_2$  is formed at the  $PbSO_4$ / electrode interface. In this case, the peaks  $A_2$  and  $A_2'$  are ascribed to equations [10] :



The addition of phosphoric acid in electrolyte shifts the anodic peaks of phase formation  $\alpha$  and  $\beta$   $PbO_2$  towards more positive potential values concomitantly with the decrease of their area, figure 3

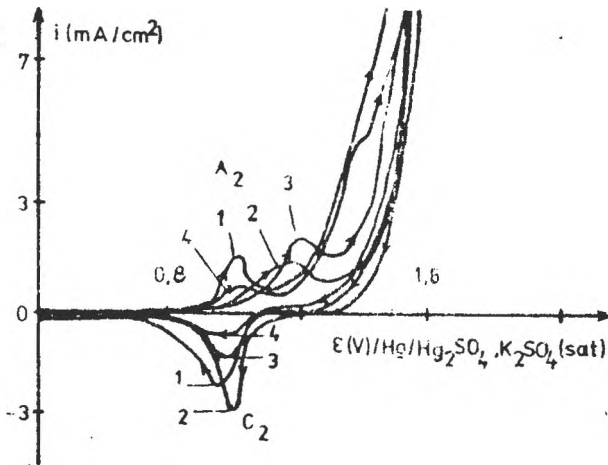


Fig. 3 Cyclic voltammograms of lead in 4.3 m  $H_2SO_4$  containing  $H_3PO_4$  : 1- 0%; 2-0.3%; 3-0.65% 4-0.85% Scan rate: 10mV/s.

With the gradual increase of  $H_3PO_4$  concentration added to  $H_2SO_4$  solution peak  $A_2$  corresponding to phase  $\alpha$ - $PbO_2$  almost disappeared (curves 3 and 4, figure3). Like the oxidation peaks, the reduction peaks of  $PbO_2$  to  $PbSO_4$

moved in anodic direction, a decrease of their area taking place. This result would suggest that  $\text{H}_3\text{PO}_4$  decreases the rate of sulfation. The greater the cathodic peak shift the greater the anode peak  $A_2$  and the more it moves towards more positive potentials (towards the range of oxygen evolution)

This decrease in peak area is supposed to be closely related to the thickness of corrosion layers formed during anodic sweep, at the metal grid / $\text{PbSO}_4$  layer interface [16]. In the presence of  $\text{H}_3\text{PO}_4$  the formation of soluble phosphate species causes the decrease of corrosion layer thickness (but this corrosion layers can not stopped to form). The addition of more than 0.85 %  $\text{H}_3\text{PO}_4$  to electrolyte did not cause significant changes of voltammograms. The beneficial effect of  $\text{H}_3\text{PO}_4$  is only manifested at concentrations of 0.65 %  $\text{H}_3\text{PO}_4$  when the electrode surface is saturated with  $\text{PO}_4^{3-}$  ions being adsorbed on the  $\text{PbO}_2$  layer. This fact is also supported by a decrease of electrochemical processes rates, with the increase of cycles number, figure 4.

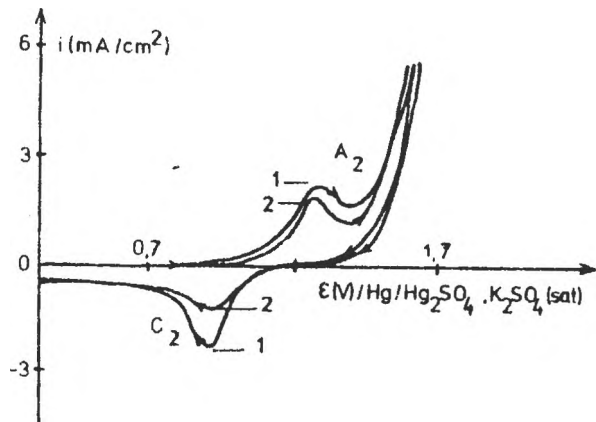


Figure 4 . Cyclic voltammograms of Pb in 4.3 m  $\text{H}_2\text{SO}_4$  containing 0.65%  $\text{H}_3\text{PO}_4$ . Scan rate 10mV/s 1-cycle 10; 2-cycle 20;

The potential sweeping rate does not significantly change the form of the voltammogram curves, figure 5

Higher concentrations of  $\text{H}_3\text{PO}_4$  negatively affect the behaviour of the electrodes higher potentials being required for the oxidation of  $\text{PbSO}_4$  to  $\text{PbO}_2$ ,

## Phosphoric Acid on the Electrochemical Behaviour of Lead Acid Battery

when the rate of oxygen evolution is also higher. As a result the charging efficiency of electrode is consequently lower.

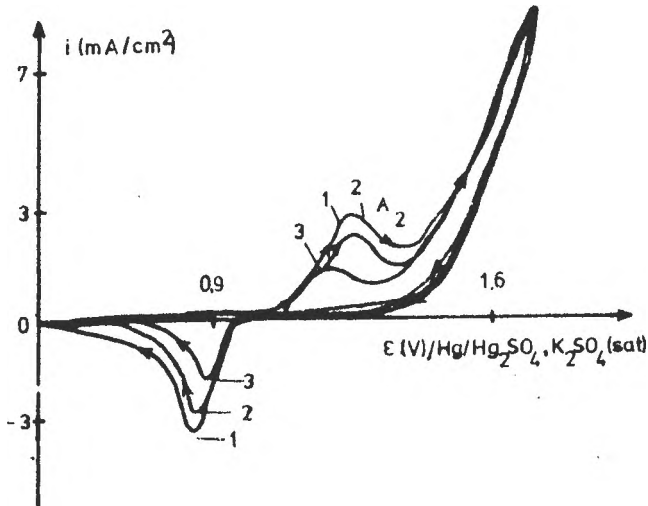


Figure 5. Cyclic voltammograms of Pb in 4.3 M  $\text{H}_2\text{SO}_4$  containing 0.65%  $\text{H}_3\text{PO}_4$ . Scan rate : 1-10mV/s; 2-33mV/s, 3-66mV/s.

It is to remark that with high concentration of  $\text{H}_3\text{PO}_4$  the electrolyte became opaque. This fact can be explained by the increase, in electrolyte, of insoluble lead phosphate species concentration. Based on these experimental observations, formation of  $\text{Pb}_3(\text{PO}_4)_2$  as an intermediate in the corrosion of Pb to  $\text{PbO}_2$  seems reasonable.

### CONCLUSIONS

In general one can say that the addition of  $\text{H}_3\text{PO}_4$  in small quantities to the electrolyte modifies the kinetics of processes at the  $\text{PbSO}_4/\text{PbO}_2$  interface. This becomes evident with the shifting of oxidation peaks towards higher positive values and the decrease of reduction peaks heights. In the presence of phosphate ions the lead dioxide formed during electrode oxidation is more difficult to reduce to  $\text{PbSO}_4$  resulting in lower rate grid corrosion.

On the basis of these results one can say that  $H_3PO_4$  increases the rate of  $\alpha$  and  $\beta$   $PbO_2$  formation in the corrosion layers and reduces the amount of sulfate on the grid

Although the cyclic voltammetry enables us to accurately identify the changes in the kinetics of electrode reactions, the method does not lend itself to an intimate study of these processes.

## REFERENCES

1. K. R. Bullok and D. Pavlov (Editors), *Advances in Lead-Acid Batteries*, The Electrochemical Society Inc, Pennington, New Jersey 1984.
2. Y. Guo, *J. Electrochem. Soc.*, 1993, **140**, (12), 3369.
3. D. Pavlov, B. Monahov, G. Sundholm and T. Laitinen *J. Electroanal. Chem.* 1991, **305**, 57.
4. F. E. Varela, L. M. Gassa and J. R. Vilche, *J. Appl. Electrochem.* 1995, **25**, 364.
5. Y. Yamamoto, K. Fumino, T. Ueda and M. Nambu, *Electrochim Acta*, 1992, **37**, 199.
6. K. Kanamura and Z. Takehara, *J. Electrochem. Soc.* 1992, **139**, 345.
7. D. Pavlov, *J. Power Sources*, 1995, **9**, 53.
8. A. F. Hollenkamp, K. K. Constanti, M. J. Koop and L. Apăteanu, *J. Power Sources*, 1994, **48**, 195.
9. R. F. Nelson and D. M. Wilson, *J. Power Sources*, 1991, **33**, 165.
10. Y. Yamamoto, M. Matsuoka, M. Kimoto, M. Uemura and C. Iwakura, *Electrochem. Acta*, 1996, **41**, 439.
11. P. Ruetschi and R. T. Angstad, *J. Electrochem. Soc.*, 1964, **111**, 1323.
12. M. P. J. Brenann and N. A. Hampson, *J. Electroanal. Chem.*, 1973, **48**, 465.
13. C. Lazarides, N. A. Hampson and G. M. Bulman, *J. Appl. Electrochem.*, 1981, **11**, 655.

## Phosphoric Acid on the Electrochemical Behaviour of Lead Acid Battery

14. A. G. Mateescu, A. C. Doboş and E. Comănescu , *Revista de Chimie*, 1981, **32**, 185.
15. K. R. Bullock and D. H. McClelland, *J. Electrochem. Soc.* 1977, **124**, 1478
16. K. R. Bullock, *J. Electrochem. Soc.* , 1979, **126**, 360.
17. K. R. Bullock, *J. Electrochem. Soc.* , 1979, **126**, 1848.
18. A. Mateescu , D. Mateescu and Gh. Alexandru, *Revista de Chimie*, 1986, **37**, 906.

Received:24.02.1996





## THE OXIDATION OF BENZYL ALCOHOL BY CERIVM ( IV ) IN SULFURIC MEDIA

Claudia Mureșanu , Ioan Bâldea and Liviu Oniciu  
*Faculty of Chemistry and Chemical Engineering , " Babeș-Bolyai " University of Cluj ,  
11 Arany Janos Str. , Cluj-Napoca , Romania*

### Abstract

The kinetics of the oxidation of the benzyl alcohol to benzaldehyde by ceric sulfate has been studied in the presence of  $\text{Na}_2\text{SO}_4$  over a wide range of organic substrate and hydrogen ion concentrations. An intermediate complex having the ratio  $\text{Ce(IV)} : \text{C}_6\text{H}_5\text{CH}_2\text{OH}$  of 1 : 1 has been identified by spectrophotometrical means. The redox reaction obeys a second-order rate law at hydrogen ion concentration held constant ( first-order in each ,  $\text{Ce(IV)}$  and  $\text{C}_6\text{H}_5\text{CH}_2\text{OH}$  ) , but a rather complex dependence associated with  $[\text{H}^+]$  . The kinetics and the dependence of the experimental activation energy on the acidity of the medium indicate the involvement of different reactive  $\text{Ce(IV)}$  sulfatocomplexes in the oxidation process .

### INTRODUCTION

Cerium (IV) is an efficient one-electron oxidizing agent and has been frequently used to oxidize various classes of organic substances as aromatic hydrocarbons [1-3] , aliphatic [4-8] and aromatic alcohols [9-12] , aldehydes [13-16] or organic acids [17-18] . The redox couple  $\text{Ce(IV)/Ce(III)}$  was recently used as a mediator for electrochemical oxidation of aromatic hydrocarbons [10] . The oxidation of benzyl alcohol and its derivatives by cerium ammononitrate , used in excess in aqueous-acetic ( 50% ) media, leads to benzaldehyde or the corresponding carbonyl compounds , with yields between 55 and 94% [9] .

The kinetics of benzyl alcohol oxidation by cerium ammononitrate has been studied in acetonitrile-water mixture [10] and in aqueous perchloric acid media [11,12] . A second order rate law ( first order in each reactant ) has been found , and an activation energy of 83.7 and 89.5  $\text{kJ.mol}^{-1}$  has been determined in acetonitrile-water and aqueous perchlorate media , respectively . Various second-order rate constant values have been reported [10-12,20] depending on the conditions employed . An isotopic effect has also been noticed , using  $\text{Ce(NH}_3)_2(\text{NO}_3)_6$  as oxidising agent [21]

The proposed mechanism involves a fast formation of an intermediate 1 : 1 complex between  $\text{Ce(IV)}$  and benzyl alcohol , followed by its depletion , as an one-electron rate determining-step [10,11] , yielding  $\text{Ce(III)}$  and a hemi-oxidized intermediate . An additional  $\text{Ce(IV)}$  ion finishes the oxidation in a fast subsequent step to form

benzaldehyde .

The kinetics of benzyl alcohol oxidation by cerium sulfate has been less studied . Saiprakash and Sethuram [20] found that the active species is  $Ce(SO_4)_2$  under certain conditions . Because of the fact that the sulfate ion is bound to  $Ce(IV)$  , the formation of  $Ce(IV)$ -benzyl alcohol complex seems to be diminished compared to perchlorate media, and new aspects of the reaction mechanism arise .

It is the purpose of the present investigation to study kinetic behaviour of the reacting system  $Ce(IV)$ - $C_6H_5CH_2OH$  in aqueous sulfuric acid medium

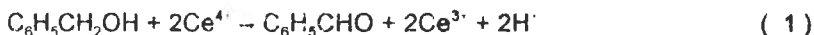
## RESULTS AND DISCUSSIONS

**The solubility check** The solubility of benzyl alcohol was reported only for pure water or for solutions with a relative high sulfuric acid concentration [22,23] .

We have checked its solubility in the range of diluted sulfuric acid solutions , up to  $0.7 \text{ mol.dm}^{-3}$  , containing  $Na_2SO_4$  (  $0.55\text{-}0.00 \text{ mol.dm}^{-3}$  ) at  $20$  ,  $40$  and  $60^\circ C$  . We found that at  $20^\circ C$  the solubility increases slowly with increasing content of  $H_2SO_4$  . The solubility is increased at  $40$  and  $60^\circ C$  , compared to lower temperatures , but less affected by the acid concentration .

The solutions of benzyl alcohol up to  $1.4 \cdot 10^{-2}$  (  $20^\circ C$  ) and  $3.5 \cdot 10^{-2} \text{ mol dm}^{-3}$  (  $40^\circ C$  ) are the upper limits of solubility .

**Stoichiometry** The reaction stoichiometry has been established in the literature [9] . Our spectral measurements , under a large excess of organic substrate, confirmed that the major product is benzaldehyde



Under the experimental conditions employed , benzoic acid , a product of a subsequent oxidation of benzaldehyde has not been detected .

**Complex formation** Because various sulfato-complexes  $CeSO_4^{2+}$  ,  $Ce(SO_4)_2$  ,  $Ce(SO_4)_3^{2-}$  and some protonated species , which are formed [24-28] , we have measured the absorbance values at acidity and ionic strength held constant , and varying  $Ce(IV)$  concentration between  $3.1 \cdot 10^{-5}$  and  $4.0 \cdot 10^{-4} \text{ mol.dm}^{-3}$  . A good linearity, with a correlation coefficient of  $0.9992$  , was obtained by plotting " A " as a function of  $Ce(IV)$  concentration . A molar absorption coefficient of  $2470 \pm 30 \text{ dm}^3 \text{ mol}^{-1} \text{ cm}^{-1}$  has been found

The major species of  $Ce(IV)$  under the condition employed is  $Ce(SO_4)_3^{2-}$

## The Oxidation of Benzyl Alcohol

( 91.3 - 99.2% ) [24-26].

When benzyl alcohol is present in the reaction mixture , a small decrease of initial absorbance has been noticed . Thus , both the extrapolated values of absorbance at 370 nm to the start of the kinetic runs at 60°C , as well as separate absorbance measurements at 25°C , showed decreased values with increasing concentration of benzyl alcohol , compared to the values measured in the absence of the organic substrate . Figure 1 shows absorption spectra recorded immediatly after mixing , at 25°C.

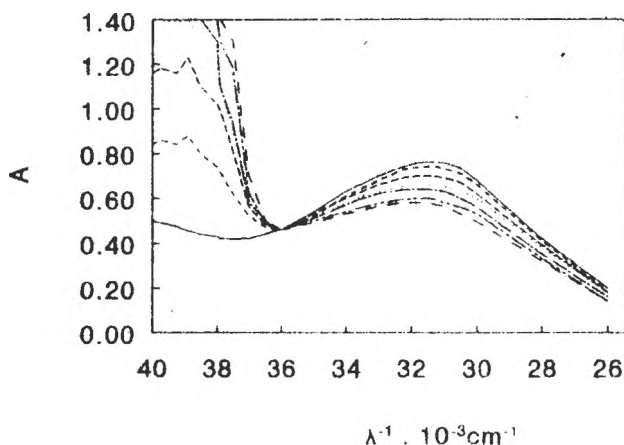
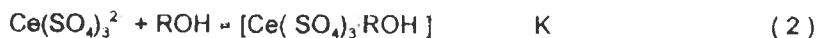


Fig. 1 Absorption spectra of Ce( IV ) - benzyl alcohol mixture ;  
 1. — Ce(IV)  $1.6 \cdot 10^{-4} \text{ mol} \cdot \text{dm}^{-3}$  ; 2. - - - Ce(IV)  $1.6 \cdot 10^{-4}$  - ROH  $1.74 \cdot 10^{-3} \text{ mol} \cdot \text{dm}^{-3}$  ; 3. --- Ce(IV)  $1.6 \cdot 10^{-4}$  - ROH  $3.47 \cdot 10^{-3} \text{ mol} \cdot \text{dm}^{-3}$  ; 4. — — — Ce(IV)  $1.6 \cdot 10^{-4}$  - ROH  $5.2 \cdot 10^{-3} \text{ mol} \cdot \text{dm}^{-3}$  ;  
 5. — — — — Ce(IV)  $1.6 \cdot 10^{-4}$  - ROH  $6.94 \cdot 10^{-3} \text{ mol} \cdot \text{dm}^{-3}$  ; 6. — — — — — Ce(IV)  $1.6 \cdot 10^{-4}$  - ROH  $8.67 \cdot 10^{-3} \text{ mol} \cdot \text{dm}^{-3}$  ; 7. - - - - - Ce(IV)  $1.6 \cdot 10^{-4}$  - ROH  $9.37 \cdot 10^{-3} \text{ mol} \cdot \text{dm}^{-3}$  ;  $t = 25^\circ\text{C}$  .

The moderate decrease of the absorbance could be attributed to the formation of an 1:1  $\text{Ce}(\text{SO}_4)_3^2$  - ROH complex . The occurrence of an isosbestic point at 277 nm on the absorption spectra proves that only two absorbing species are involved . By analogy with the complex formed in perchlorate media [11, 12] or with the complex formed with mercaptoacids in sulfuric medium [27] we consider the following pre-equilibrium :



The binding of alcohol to Ce(IV) brings about a diminution of absorption coefficients in the range of 240-400 nm .

To determine the equilibrium constant  $K$  for (2), a method described by Ardon [5] was applied. The equation which correlates the equilibrium constant and absorbance is:

$$\frac{1}{A_0 - A_m} = \frac{1}{(\epsilon_0 - \epsilon)[Ce(IV)]_t} + \frac{1}{K(\epsilon_0 - \epsilon)[Ce(IV)]_t [ROH]} \quad (3)$$

where  $A_0$  and  $A_m$  stand for the measured absorbance of  $Ce(IV)$  and  $Ce(IV)$ -benzyl alcohol mixtures respectively,  $\epsilon_0$  and  $\epsilon$  are the absorptivity coefficients for  $Ce(IV)$  and complex. By plotting  $\Delta A^{-1}$  versus  $[ROH]^{-1}$  a straight line was obtained and  $K$  calculated from the ratio intercept/slope. Table 1 contains absorbance measurements at three different wavelengths. Using a least-square method, correlation coefficients of 0.9975-0.9999 were obtained. A mean value of  $K = 8.4 \pm 2.0 \text{ dm}^3 \cdot \text{mol}^{-1}$  at  $25^\circ\text{C}$ ,  $[H^+] = 0.307$

Table 1 Absorbance values of mixtures containing  $Ce(IV) = 1.6 \cdot 10^{-4}$ ,  $[H_2SO_4] = 0.25 \text{ mol} \cdot \text{dm}^{-3}$ ,  $\mu = 0.37 \text{ mol} \cdot \text{dm}^{-3}$  and benzyl alcohol

ROH · 10 <sup>3</sup> mol · dm <sup>-3</sup>	A		
	315 nm	320 nm	330 nm
0.00	0.758	0.756	0.682
1.74	0.727	0.725	0.651
3.47	0.699	0.695	0.621
5.20	0.668	0.668	0.590
6.94	0.640	0.639	0.564
8.67	0.618	0.607	0.534
9.37	0.598	0.593	0.523

and  $\mu = 0.37 \text{ mol} \cdot \text{dm}^{-3}$  has been considered. This relative small value of the formation constant  $K$  (even smaller at higher temperatures) suggested that no extensive complex formation has taken place, which has been proved by the dependence of the first-order rate constant on the benzyl alcohol concentration (see next paragraph).

**Kinetics of the oxidation process** In all experiments, conditions were chosen with a 35-90 fold excess of ROH present. This ensured that only the oxidation to benzaldehyde took place as well as first-order conditions. Semilogarithmic plots

$$\ln(A - A_\infty) - \ln(A_0 - A_\infty) = k_{obsd} \cdot t \quad (4)$$

were linear to more than 90% completion. Here  $A$ ,  $A_0$  and  $A_\infty$  stand for absorbance at various values of time, at the beginning and the end of run respectively. Table 2

## The Oxidation of Benzyl Alcohol

contains some results . The data were reproducible to within  $\pm 5\%$  .

Table 2 First order rate constants at various ROH concentrations at 60°C ,  
 $[H^+] = 0.307 \text{ mol-dm}^{-3}$  ,  $\mu = 0.37 \text{ mol-dm}^{-3}$   $[Ce(IV)] = 4 \cdot 10^{-4} \text{ mol-dm}^{-3}$

$[ROH] \cdot 10^2$ $\text{mol-dm}^{-3}$	$k_{\text{obsd}} \cdot 10^2$ ( $\text{min}^{-1}$ )	$\bar{k}_{\text{obsd}} \cdot 10^2$ ( $\text{min}^{-1}$ )
1.35	0.532	0.521
	0.519	
	0.502	
	0.532	
1.74	0.685	0.680
	0.667	
	0.67	
2.12	0.830	0.866
	0.877	
	0.89	
2.7	1.16	1.11
	1.08	
	1.1	
	1.18	
3.09	1.30	1.26
	1.24	
	1.28	
	1.23	
3.47	1.53	1.45
	1.53	
	1.45	
	1.38	
	1.34	

When observed first-order rate constants were plotted versus alcohol concentration , a straight line , passing trough the origin was obtained , proving also a first-order dependence with respect to the organic substrate , at acidity held constant . An extensive formation of the complex should lead to some curvature on this plot , which

has not been observed, proving that the formation of the intermediate complex between reacting compounds is not indicated by the kinetic data. Therefore, a second-order rate law, first-order in each is obeyed by the oxidation process. Second-order rate coefficients could be obtained by dividing  $k_{\text{obsd}}$  by  $2[\text{ROH}]$ . The factor 2 accounts for the stoichiometry. An average value of  $k_2 = (3.60 \pm 0.18) \cdot 10^{-3} \text{ dm}^3 \cdot \text{mol}^{-1} \cdot \text{s}^{-1}$  has been obtained under the conditions employed. The values are shown in table 2.

In order to search for the effect of ionic strength upon the rate, several measurements were performed at  $60^\circ\text{C}$  by adding different amounts of  $\text{Na}_2\text{SO}_4$ ,  $\text{H}_2\text{SO}_4$  and  $\text{NaClO}_4$  to the reaction mixture, such that the sum  $[\text{SO}_4^{2-}] + [\text{HSO}_4^-]$  was maintained the same. The data, as mean of 2-3 individual kinetic runs, are given in table 3.

Table 3 The effect of ionic strength on the rate at  $60^\circ\text{C}$ ,  $[\text{Ce(IV)}] = 4 \cdot 10^{-4} \text{ mol/dm}^3$ ,  $[\text{ROH}] = 2.7 \cdot 10^{-2} \text{ mol/dm}^3$

$[\text{H}^+]$ $\text{mol} \cdot \text{dm}^{-3}$	$[\text{SO}_4^{2-}]$ $\text{mol} \cdot \text{dm}^{-3}$	$[\text{HSO}_4^-]$ $\text{mol} \cdot \text{dm}^{-3}$	$\mu$ $\text{mol} \cdot \text{dm}^{-3}$	$k_{\text{obsd}} \cdot 10^3$ $\text{min}^{-1}$	$k_2 \cdot 10^3$ $\text{dm}^3 \cdot \text{mol}^{-1} \cdot \text{s}^{-1}$
0.228	0.028	0.172	0.26	5.16	3.19
0.237	0.037	0.163	0.67	4.80	2.95
0.240	0.040	0.160	0.88	5.00	3.09
0.242	0.042	0.158	1.08	5.14	3.17

The second order rate constant is practically unchanged within this range of ionic strength, as long as the total sulfate concentration ( $\text{SO}_4^{2-} + \text{HSO}_4^-$ ) is constant, ensuring almost the same distribution of cerium among the various sulfato-complexes. The effect of hydrogen ion concentration on the rate has been examined within the limits of  $1.8 \cdot 10^{-2}$  and  $7.5 \cdot 10^{-1} \text{ mol} \cdot \text{dm}^{-3}$  using  $\text{H}_2\text{SO}_4$  and  $\text{Na}_2\text{SO}_4$ . Within this range of hydrogen ion concentration, there is a variation of ionic strength. Nevertheless, we maintained the total sulfate and bisulfate concentration constant. Hydrogen ion concentration was calculated, considering the second dissociation step of the sulfuric acid.



Its dependence on the ionic strength was calculated with the relation given by Reynolds and co-workers [28]. A rather complicated dependence of the second-order rate coefficient on the hydrogen ion concentration has been found, as shown in figure 2. Towards low hydrogen ion concentration there appears an increase of the rate. Over

## The Oxidation of Benzyl Alcohol

a minimum value of  $k_2$  attained around  $[H^+] = 0.065$ , the rate increases steadily, to reach even larger values towards higher acidities. It is quite difficult to describe this behavior by a single equation having a rational kinetic significance.

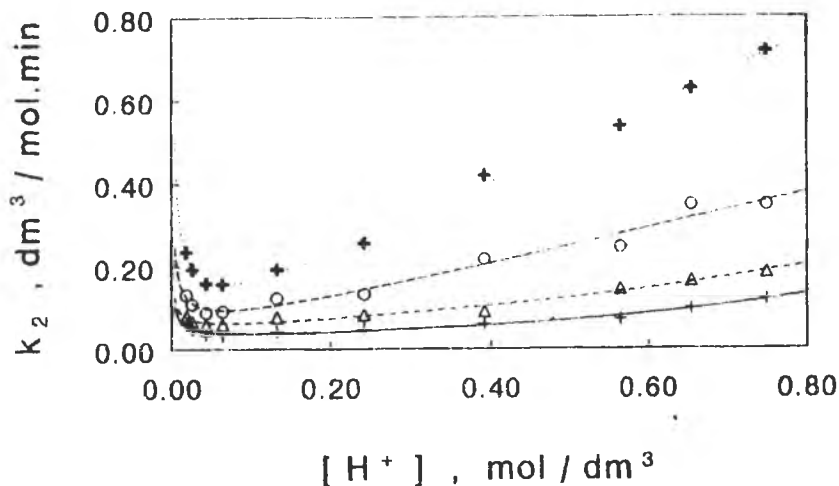


Fig. 2 The  $[H^+]$  dependence of second order rate constant at four temperatures. 1. +  $t = 50^\circ\text{C}$ , 2.  $\Delta$   $t = 60^\circ\text{C}$ , 3. o  $t = 65^\circ\text{C}$ ; 4. +  $t = 75^\circ\text{C}$ .

As Calvaruso and his co-workers pointed out [29,30] in the case of Ce(IV) oxidation of lactic, atrolactic or glycolic acid, three simultaneous pathways contribute to the process with different number of hydrogen ions involved. On the other hand, there is no possibility to establish kinetically which of the two ions  $\text{HSO}_4^-$  and  $\text{SO}_4^{2-}$ , present in the mixture, forms Ce(IV) complexes, or whether all of these complexes combines to substrate to build transition state for electron transfer. The extent of these contributions to the oxidation process depends markedly on hydrogen ion or bisulfate concentration. Consequently, some assumption have to be made to account for the dependence of second-order rate constant on the acidity.

Using a curve fitting algorithm included in the computer programm called SlideWrite 2.0, we found that within the limits  $0.0185 \leq [H^+] \leq 0.065$  the best fit of the experimental data is of the form

$$k_2 = \alpha_1 + \frac{\beta_1}{[H^+]} + \gamma_1 \cdot [H^+]^2 \quad (6)$$

The correlation coefficients were between 0.995 and 0.998 for the four examined temperature values examined . It suggests , by its second term , that some hydroxy-complex of Ce(IV) should be involved with an important contribution .

For the domain of increasing tendency of  $k_2$  with  $[H^+]$  , the equation describing the dependence is of the form:

$$k_2 = \alpha_2 + \frac{\beta_2 \cdot [H^+]}{1 + \delta_2 \cdot [H^+]} + \gamma_2 \cdot [H^+]^2 \quad (7)$$

with correlation coefficients of 0.993-0.999 . The second term in (7) suggests that some protonated cerium(IV)-sulfate complex  $H\text{Ce}(\text{SO}_4)_3$  is involved . The third term of both equations suggests that the involvement of more than one hydrogen ion could give an efficient path for the electron transfer .

Table 4 Estimated parameters of equations (6) and (7)

t (°C)	$\alpha_1 \cdot 10^3$	$\beta_1 \cdot 10^4$	$\gamma_1$	$\alpha_2 \cdot 10^2$	$\beta_2$	$\delta_2$	$\gamma_2 \cdot 10$
50	9.1	9.57	2.193	1.835	1.207	55.505	1.335
60	28.7	12.29	4.244	3.6	1.535	42.636	2.028
65	40.2	16.6	6.158	7.58	0.266	0.325	2.203
75	77.4	28.8	8.605	10.6	0.654	0.055	2.49
$E_{aa1} = 81.668$ kJ/mol.K		$E_{ay1} = 53.257$ kJ/mol.K		$E_{aa2} = 66.909$ kJ/mol.K		$E_{ay2} = 24.467$ kJ/mol.K	

Because the extent of these contributions to the overall second-order rate coefficient is changing with the temperature and the acidity ( or  $\text{HSO}_4^-$  concentration ) we cannot compute the activation energy for each pathway . However using the variation of  $\alpha$ 's and  $\gamma$ 's with temperature change , we calculated values of activation energy . For the two domains of the acidity  $E_{aa}$  have high values compared to  $E_{ay}$  , where there appears the catalytic effect of hydrogen ion .

The other alternative to see the effect of temperature upon the rate is to calculate experimental activation energy , based on the dependence of observed second-order rate constant , at any chosen hydrogen ion concentration . Values are presented in table 5



## The Oxidation of Benzyl Alcohol

Table 5 Activation energies calculated from second-order rate constants

$[H^+] \cdot 10^2$ mol·dm <sup>-3</sup>	$E_a$ kJ·mol <sup>-1</sup>
1.85	53.4±3.1
2.59	54.1±3.1
4.34	60.2±3.5
6.42	60.2±3.0
13.3	59.2±3.1
24.2	64.0±3.5
39.2	77.6±4.2
56.5	78.6±4.5
65.5	74.3±3.8
74.4	70.4±3.8

The confidence limit is derived from error estimates for the rate constant and temperature ( error propagation ) An important variation of these experimental activation energy is obtained over the range of hydrogen ion concentration , proving the change contribution of various Ce(IV)-sulfato-complexes to the overall oxidation rate .

It can be concluded that the oxidation of the benzyl alcohol to benzaldehyde by Ce(IV) in sulfate media follows a succession of two one-equivalent steps , by the formation of an 1 : 1 Ce( IV )-ROH complex in a small extent . Various forms of Ce(IV)-sulfate ( or bisulfate ) complexes , even a hydroxy complex at low acidity , contribute to the reaction process

### Experimental

The chemicals employed in the study were from commercial sources , of reagent grade purity , and used without further purification except of benzaldehyde which was purified by distillation prior to the experiments. Solutions were prepared using twice distilled water . Sulfuric acid and sodium sulfate were used to adjust desired acidity and ionic strength respectively .

The solubility of benzyl alcohol in water and H<sub>2</sub>SO<sub>4</sub> - Na<sub>2</sub>SO<sub>4</sub> solutions was checked spectrophotometrically covering all the concentration range used in the kinetic experiments

The stoichiometry of the reaction was also determined by spectrophotometrical means , by recording the spectra of the reaction products quantitatively extracted into diethylether , and compared to the spectra of benzaldehyde solution having the same concentration as those expected to be formed by oxidation . An UVVIS Zeiss spectrophotometer was used .

The formation of cerium(IV) - benzyl alcohol complex was measured recording the absorbance of mixture containing Ce(IV) and increasing amounts of benzyl alcohol , within the range of 240 - 400 nm . At 25°C by low Ce(IV) and alcohol concentration the redox reaction was extremely slow and did not affect the absorbance measurements .

The kinetics of the reaction was followed spectrophotometrically at 370 nm by means of a Spekol Zeiss

spectrophotometer, provided with a temperature jacket surrounding the cells in the cell holder. At 370 nm, either benzyl alcohol or benzaldehyde were transparent, the only coloured species being Ce(IV). The reaction was started by mixing Ce(IV) solution of appropriate concentration with alcohol solution containing H<sub>2</sub>SO<sub>4</sub> and Na<sub>2</sub>SO<sub>4</sub> in a flask maintained in the temperature bath of a Wobser U - 10 thermostat. Temperature was kept constant within  $\pm 0.2^\circ\text{C}$ . Aliquots were extracted from time to time transferred into spectrophotometer cell with an 1 cm path length, and absorbance values were measured. To be sure this method is appropriate, we verified that Lambert - Beer law held over the range of concentration used in the kinetic measurements.

## REFERENCES

1. W.S.Trahanovsky, L.B.Young, *J. Org. Chem.*, 1966, **31**, 2033
2. L.Syper, *Tetrahedron Letters*, 1963, **37**, 4493
3. E.Baciocchi, c.Rol, G.V.Sebastiani, *J. Chem. Research( Synopsis)*, 1983, **9**, 232
4. M.Ignaczak, J.Dziegiec, M.Markiewicz, *Pol. J. Chem.*, 1980, **54**, 1121
5. M.Ardon, *J. Chem. Soc.*, 1957, 1811
6. G.Gopal Rao, B.Madhava Rao, *Anal. Chim. Acta*, 1972, **59**, 461
7. B.Sethuram, S.S.Muhammad, *Acta Chim. Acad. Sci. Hung.*, 1965, **46**, 115
8. B.Sethuram, S.S.Muhammad, *Acta Chim. Acad. Sci. Hung.*, 1965, **46**, 125
9. W.S.Trahanovsky, L.B.Young, G.L.Brown, *J. Org. Chem.*, 1967, **32**, 3865
10. M.P.Doyle, *J. Chem. Educ.*, 1974, **51**, 131
11. D.Paquette, M.Zador, *Canadian J. Chem.*, 1968, **46**, 3507
12. M.Rangaswamy, M.Santappa, *Current Sci*, 1966, **35**, 332
13. M.Melicherik, L.Treindl, *Chem. Zvesti*, 1981, **35**, 153
14. J.Shorter, *J. Chem. Soc.*, 1950, 3425
15. P.Singh Sankhla, R.Narain Mehrotra, *J. Inorg. Nucl. Chem.*, 1972, **34**, 1050
16. K.B.Wiberg, P.C.Ford, *J. Amer. Chem. Soc.*, 1969, **91**, 124
17. S.B.Hanna, S.A.Sarac, *J. Org. Chem.*, 1977, **42**, 2063
18. V.K.Grover, Y.K.Gupta, *J. Inorg. Nucl. Chem.*, 1969, **31**, 1403
19. K.Kramer, P.M.Robertson, N.Ibl, *J. Appl. Electrochem.*, 1980, **10**, 29
20. P.K.Saiprakash, B. Sethuram, *Indian J. Chem.*, 1971, **9**, 226
21. H.Kwart, T.J.George, *J. Org. Chem.*, 1979, **44**, 162
22. S.Bitterlich, Dissertation, Darmstadt, 1988, 25
23. Landolt-Börnstein Tabellen, II, 2b, 3-421, 3-422, Springer, 1962
24. T.N.Bondareva, V.F.Barkovskii, *Zh. Neorg. Khimii*, 1965, **10**, 127
25. T.J.Hardwick, E.Robertson, *Canadian J. Chem.*, 1951, **29**, 828
26. S.B.Hanna, R.R.Kessler, A. Mehrbach, S. Ruzicka, *J. Chem. Educ.*, 1976, **53**, 8, 524
27. J.Hill, A.McAuley, *J. Chem. Soc.*, 1968 A, 156
28. L.Reynolds, S.Fukushima, *Inorg. Chem.*, 1963, **2**, 117
29. G.Calvaruso, F.P.Cavasino, C.Sbriziolo, *Int. J. Chem. Kinet.*, 1981, **13**, 135; *Int. J. Chem. Kinet.*, 1984, **16**, 1201
30. G.Calvaruso, F.P.Cavasino, C.Sbriziolo, R.Triolo, *Int. J. Chem. Kinet.*, 1983, **15**, 417

Received:26.02.1996

## QSAR STUDY ON A SET OF IMIDAZOLE DERIVATIVES WITH ANTIMICROBIAL AND ANTIMICOTIC ACTIVITY

Mioara Butan<sup>1</sup>, Corina M. Pop<sup>2</sup> and Mircea V. Diudea<sup>2</sup>

<sup>1</sup>Chemical-Pharmaceutical Research Institute, Cluj, Fabricil Str. 126, 3400 Cluj

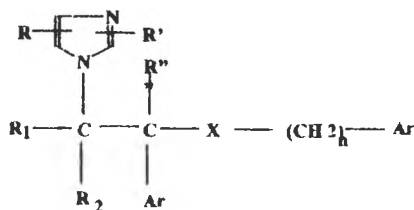
<sup>2</sup>Department of Chemistry, "Babeș-Bolyai" University, 3400 Cluj, Romania

### ABSTRACT

A Free-Wilson analysis performed on a set of 13 imidazole derivatives showing antimicrobial and antitumor activity showed that both of the two phenyl rings of the common structure must be substituted for increasing the antimicrobial activity. Conversely, the antitumor activity needs low substituted phenyl rings and shows other ordering of the substituted positions.

### 1. INTRODUCTION

From the literature data, [1] it is known that the oxygen and nitrogen derivatives of  $\alpha$ -phenyl-imidazole-1-ethanol and their ethers, as well as the 1-( $\beta$ -aminophenyl)-imidazole derivatives show antitumor activity. The general formula of 1-( $\beta$ -aryl)-ethyl-imidazole and their ethers and amines is:



where: R, R<sub>1</sub>, R<sub>2</sub> = H; inferior alkyl

X = O or NH

n = 0, 1, 2

Ar = phenyl, alkyl substituted phenyl,  
inferior alkoxy

Ar' = phenyl, halogen substituted, alkyl,  
phenyl, inferior alkoxy, CN, NO<sub>2</sub>, NH<sub>2</sub>

R' = H, CH<sub>3</sub>, CH<sub>2</sub>-CH<sub>3</sub>

R'' = H, CH<sub>3</sub>

In this study, the following structures, synthesised as in ref [1,2] , were considered:

1. 1-[2-(phenyl)-2-((4-chlorophenyl)-methoxy)-ethyl]-1H-imidazole nitrate
2. 1-[2-(phenyl)-2-((2,4-dichlorophenyl)-methoxy)-ethyl]-1H-imidazole nitrate
3. 1-[2-(4-methoxyphenyl)-2-((4-chlorophenyl)-methoxy)-ethyl]-1H-imidazole nitrate
4. 1-[2-(4-methoxyphenyl)-2-((2,4-dichlorophenyl)-methoxy)-ethyl]-1H-imidazole nitrate
5. 1-[2-(4-methoxyphenyl)-2-((2,3,6-trichlorophenyl)-methoxy)-ethyl]-1H-imidazole nitrate
6. 1-[2-(4-chlorophenyl)-2-((phenyl)-methoxy)-ethyl]-1H-imidazole nitrate
7. 1-[2-(4-chlorophenyl)-2-((2,4-dichlorophenyl)-methoxy)-ethyl]-1H-imidazole nitrate
8. 1-[2-(4-chlorophenyl)-2-((2,3,6-trichlorophenyl)-methoxy)-ethyl]-1H-imidazole nitrate
9. 1-[2-(2,4-dichlorophenyl)-2-(phenyl)-methoxy)-ethyl]-1H-imidazole nitrate
10. 1-[2-(2,4-dichlorophenyl)-2-(4-chlorophenyl)-methoxy)-ethyl]-1H-imidazole nitrate
11. 1-[2-(2,4-dichlorophenyl)-2-(2,4-dichlorophenyl)-methoxy)-ethyl]-1H-imidazole nitrate
12. 1-[2-(2,4-dichlorophenyl)-2-(2,6-dichlorophenyl)-methoxy)-ethyl]-1H-imidazole nitrate
13. 1-[2-(2,4-dichlorophenyl)-2-(2,3,6-trichlorophenyl)-methoxy)-ethyl]-1H-imidazole nitrate

The synthesis of compounds 1,2 and 6-13 has followed the finding of influence of the chlorine atom band on the phenyl rings Ar and Ar' , respectively, on their antimicrobial activity. The compounds 3-5 bear methoxy-groups on the ring Ar and chlorine on Ar' ring. From literature, [3] it is known that methoxy groups bring a higher lipophilicity in vivo. The microbial species were as follows: Staphylococcus Aureus (Y<sub>1</sub>), Staphylococcus Epidermidis (Y<sub>2</sub>), Bacillus Subtilis (Y<sub>3</sub>), Escherichia Colli (Y<sub>4</sub>) and Candida Albicans (Y<sub>6</sub>), and the methodology was as indicated in [4-6]. The inhibitory activity is given in Table 1.

## QSAR Study on a Set of Imidazole Derivates

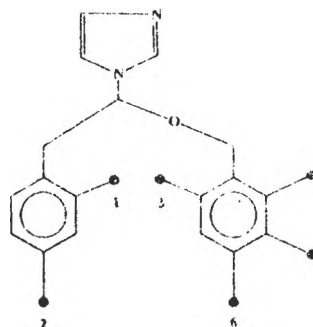
The biological screening showed that the structures 1,2,6,9 have both antimicrobial and antimicotic good activity. The antimicotic activity is lower for the compounds 3,11 and 13 whereas the compound 5 is quite inactive vs. the *Candida Albicans*

Table 1 suggests that structures with low number of chlorine atoms on aryl rings show both antimicrobial and antimicotic activity. The antifungal activity decreases as the number of chlorine atoms increases. Alkoxy groups do not increase these biological activities

**Table 1. Antimicrobial and antimicotic activities in the set of 13 molecules.**

	Y1	Y2	Y3	Y4	Y5
1	28	38	28	22	38
2	24	30	22	16	32
3	22	30	20	16	16
4	18	25	16	12	28
5	10	12	12	10	10
6	32	38	32	26	40
7	16	20	14	10	30
8	12	17	12	10	30
9	30	38	30	26	40
10	16	26	18	10	26
11	10	14	10	10	20
12	14	18	14	10	26
13	10	12	10	10	18
$Y_{\text{med}}$	18.6154	24.4615	18.3077	14.4615	27.2308

For the above listed compounds (Table 1) the following hypermolecule was built:



A molecular structure bearing several substituent can be investigated by the **Free-Wilson** method. This model looks the biological activity as a sum of contribution of the substituents bounded in positions  $j$  ( $j = 1, 2, \dots$ ) of a common structure, in the considered set of molecules [7--10]:

$$\text{Activity} = \sum_j a_{ij} X_{ij} + c$$

where  $a_{ij}$  represents the contribution to the biological activity of the substituent bounded in position  $j$ , and  $X_{ij}$  is the binary counter (1 if there is substituent in position  $j$  and 0 otherwise).

A pseudo **Free-Wilson** analysis applied on the considered set of molecules (Table 2) will be presented in the followings.

**Table 2. Free-Wilson parameters (positions 1-6 in Hipermolecule).**

Molecule	1	2	3	4	5	6
1	0	0	0	0	0	1
2	0	0	0	1	0	1
3	0	1	0	0	0	1
4	0	1	0	1	0	1
5	0	1	1	1	1	0
6	0	1	0	0	0	0
7	0	1	0	1	0	1
8	0	1	1	1	1	0
9	1	1	0	0	0	0
10	1	1	0	0	0	1
11	1	1	0	1	0	1
12	1	1	1	1	0	0
13	1	1	1	1	1	0

## 2. SINGLE VARIABLE REGRESSION

None of the substituted positions explains satisfactorily the biological activity, in monosubstituted molecule. The activity induced by substituents lowers in the following order: 4 > 3 > 5 > 2 > 1 > 6 ( see hypermolecule and Table 3) for all the tested activities, except  $Y_5$ , for which the position 5 is decisive.

**Table 3. Single variable correlations.**

Position	Y1	Y2	Y3	Y4	Y5
1	0.2742	0.2404	0.2063	0.1653	0.1086
2	0.4176	0.4322	0.3903	0.3207	0.3696
3	0.6291	0.6880	0.5752	0.4930	0.4635
4	0.7323	0.8013	0.7886	0.7257	0.4207
5	0.5774	0.6283	0.5225	0.4050	0.4826
6	0.0756	0.1930	0.0032	0.1338	0.0106

## 3. MULTIVARIABLE REGRESSION

The finding of multivariate regression was performed by following the idea: the newly introduced substituen must explain the best the residual  $Y_{obs} - Y_{calc}$  (see Table 4).

**Table 4. Checking for the optimal regression; two and three variables.**

res 4.Y1	X2	r	res 2;4.Y1	X3	r
2.40	1	0.4296	-3.40	1	0.2976
9.75	2	0.5045	3.40	3	0.2778
-3.60	3	0.3571	-2.15	5	0.3312
3.75	5	0.3825	4.66	6	0.2207
-4.25	6	0.0060	-3.34		
6.40			7.85		
1.75			2.65		
2.25			-1.34		
4.40			5.85		
-9.60			-8.14		
-4.25			-3.34		
-0.25			0.65		
-4.25			-3.34		

3.1. Two variable regression (Table 5); a second substituent brings an improvement of correlation of about 7 %. In the followings, a decreasing order of hypothetical molecular structures is presented:

Y1 : (4,2) > (4,1) > (4,5) > (4,3) > (4,6)

Y2 : (4,2) > (4,3) > (4,5) > (4,1) > (4,6)

Y3 : (4,2) > (4,1) > (4,5) > (4,3) > (4,6)

Y4 : (4,2) > (4,6) > (4,1) > (4,3) > (4,5)

Y5 : (5,2) > (5,1) > (5,3) > (4,1)

Note that only the first two structures are reliable; Y<sub>5</sub> can not be explained satisfactorily by two variables.

Table 5. Two variable regression.

Y1					
Position	4; 6	4; 3	4; 5	4; 1	4; 2
r	0.7323	0.7862	0.7872	0.7886	0.8097
Y2					
Position	4; 6	4; 1	4; 5	4; 3	4; 2
r	0.8096	0.8428	0.8500	0.8601	0.8756
Y3					
Position	4; 6	4; 3	4; 5	4; 1	4; 2
r	0.7927	0.8106	0.8138	0.8204	0.8481
Y4					
Position	4; 5	4; 3	4; 1	4; 6	4; 2
r	0.7327	0.7373	0.7486	0.7543	0.7671
Y5					
Position	-	4; 1	5; 3	5; 1	5; 2
r	-	0.4372	0.4967	0.503	0.5502



QSAR Study on a Set of Imidazole Derivates

**3.2. Three variable regression** (Table 6): the third introduced substituent increases the correlation with about 4%. Structures with three substituents show satisfactory correlation with the investigated activities. In addition to the correlation coefficient,  $r$ , the variation coefficient,  $cv = s / Y_{obs. \text{ med}} * 100$  is presented, it indicates the dispersion of  $Y_{calc}$  values vs. the mean of observed values

Y1 : (4,2,5) > (3,5,6) > (4,2,6) > (4,2,3) > (4,2,1)

Y2 : (4,2,5) > (4,2,3) > (4,2,1) > (4,1,3) > (4,3,5)

Y3 : (4,2,5) > (4,2,1) > (4,2,3) > (4,5,6) > (3,5,6)

Y4 : (3,5,6) > (4,2,6) > (4,5,6) > (4,2,1) > (4,2,3)

Y5 : (5,2,6) > (5,3,6) > (5,1,6) > (5,4,6) > (4,2,3)

Note that the structure (4,2,5) explains better the activities  $Y_1 - Y_3$ , whereas the structure (5,3,6) correlates better with the activities  $Y_4$  and  $Y_5$ . However, the experimental data for the last two activities are quite non-selective

**Table 6. Three variable regression.**

Y1					
Position	4; 2; 6	4; 1; 2	4; 2; 3	3; 5; 6	4; 2; 5
r	0.826	0.8307	0.8338	0.8384	0.8392
cv	27.7297	27.1012	26.8702	26.535	26.4727
Y2					
Position	4; 3; 5	4; 1; 3	4; 1; 2	4; 2; 3	4; 2; 5
r	0.8672	0.8835	0.8882	0.9040	0.9087
cv	23.068	21.6626	21.2456	6.7658	6.3038
Y3					
Position	3; 5; 6	4; 5; 6	4; 3; 2	4; 1; 2	4; 2; 5
r	0.8369	0.8536	0.8548	0.8576	0.8593
cv	26.2676	25.0059	24.9021	24.6836	24.5470
Y4					
Position	4; 2; 3	4; 2; 1	4; 5; 6	4; 2; 6	3; 5; 6
r	0.7698	0.7743	0.8059	0.8343	0.8590
cv	32.0022	31.7325	29.636	27.6458	25.8050
Y5					
Position	4; 2; 3	5; 4; 6	5; 1; 6	5; 3; 6	5; 2; 6
r	0.5710	0.6269	0.6623	0.7021	0.7303
cv	32.4779	30.824	29.6392	28.366	27.0245

**3.3. Four variable regression** (Table 7) gave the following ordering

(2,3,5,6) > (2,4,5,6) in  $Y_1, Y_3, Y_4$  and  $Y_5$

(2,4,5,6) > (2,3,5,6) in  $Y_2$

**Table 7. Four variable regression.**

	Y1	Y1	Y2	Y2	Y3
Position	2; 3; 5; 6	2; 4; 5; 6	2; 3; 5; 6	2; 4; 5; 6	2; 3; 5; 6
r	0.9387	0.9038	0.9087	0.935	0.9392
cv	4.8025	22.1000	20.4730	4.7994	4.4735
	Y3	Y4	Y4	Y5	Y5
Position	2; 4; 5; 6	2; 3; 5; 6	2; 4; 5; 6	2; 3; 5; 6	2; 4; 5; 6
r	0.9362	0.9510	0.8865	0.812	0.7413
cv	4.8886	3.4367	24.6033	24.5200	28.293

**3.4. Five and Six regression** (see below) suggested that the positions (2,3,4,5,6) are important in enlarging the spectrum of action of the drugs belonging to this class.

**Five variable regression:** X = 2,3,4,5,6 ;

r = 0.9604 ; Y1 cv = 2.3797  
 r = 0.9622 ; Y2 cv = 1.2755  
 r = 0.983 ; Y3 cv = 10.4000  
 r = 0.9728 ; Y4 cv = 13.429  
 r = 0.8325 ; Y5 cv = 26.053

**Six variable regression:** X = 1,2,3,4,5,6;

r = 0.9861 ; Y1 cv = 9.8934  
 r = 0.9788 ; Y2 cv = 11.6048  
 r = 0.9955 ; Y3 cv = 5.5933  
 r = 0.9797 ; Y4 cv = 12.2982  
 r = 0.838 ; Y5 cv = 27.9533

#### 4. CONCLUSIONS

1. Structures with at least three substituents satisfactorily explain the antimicrobial and antimicotic tested activities.
2. Structure (4,2,5) explains better the activities  $Y_1$ - $Y_3$ , whereas the structure (5,3,6) correlates better with the activities  $Y_4$  and  $Y_5$ .
3. The screening for the activities  $Y_4$  and  $Y_5$  are not enough selective.
4. It is important that both phenyl rings to bear substituents, in the view of improvement of their activity.

Our results do not infirm the literature data. However in vivo tests one imposes in the view of their validation.

#### ACKNOWLEDGEMENT

This work is supported by Grant 194, 1994 (B12)

#### REFERENCES

1. E.F. Godefroi, J. Heeres, *J. Med. Chem.*, 1969, **12**, 784.
2. A. Tienpont, *Arz. Forsch.* 1975, **25**, 224.
3. E. Bolgberg, *Brit. J. Clin. Pharm.*, 1983, **15**, 341.
4. F.C. Odds, *J. Antimicrob. Chemother.*, 1980, **6**, 749.
5. J.B. Cope, *J. Gen. Microbiol.*, 1980, **119**, 245.
6. J. de Louvois, *J. Antimicrob. Chemother.*, 1980, **6**, 760.
7. S.M. Free, Jr, J.W. Wilson, *J. Med. Chem.*, 1964, **7**, 395.
8. H. Kubinyi, *J. Med. Chem.*, 1977, **20**, 1991.
9. H. Kubinyi, *Struct.-Act. Relat.*, 1988, **7**, 121.
10. M.V. Diudea, O. Ivanciuc, "Topologie Moleculară", Ed. COMPREX, Cluj, 1995.

Received.11.03 1996



## TLC DETERMINATION OF CAFFEINE FROM SOME BEVERAGE USING SOLID PHASE EXTRACTION

**Simona Cobzac, T. Hodișan**

*"Babeș-Bolyai" University, Faculty of Chemistry and Chemical Engineering, 11 Arany Janos, 3400 Cluj-Napoca*

### ABSTRACT

The paper concerns with caffeine determination from some beverage using SPE as sample preparation. The quantitation was perform using TLC / densitometry. The wavelenghi was 275nm. The obtained recovery was 93.54%. Our results are comparable with those from literature

### INTRODUCTION

1,3,7-trimethylxantine or caffeine is an alkaloid which is found in coffee grains (cca. 1%), in tea leaves (cca. 5%), kola nuts and in other tropical plants. The structure of caffeine is shown in Fig.1.

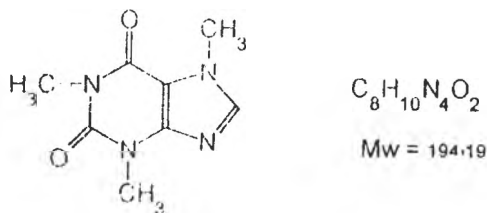


Figure 1. Structure, fomula and molecular weight of caffeine

Caffeine is a crystalline substance which sublimate at 236°C. Despite his basic character, caffeine has not the possibility to form salts which metals. Caffeine is used in medicine due to its heart stimulation property and brain activation. Caffeine is also used in the preparation of some common foods and beverage

A wide type of analytical methods was used for caffeine determination : amperometry [1], potentiometry [2], colorimetry [3], spectrometry [4,5], chromatographic technic - GI. [6], HPLC [7,8], TLC [9,10]; electrophoresis [11]. In most cases liquid-liquid extraction [5,8] for sample preparation was used

Solid phase extraction: (SPE) is an alternative technic for liquid-liquid extraction that involves the analyt transfer from a liquid to a solid phase. The technique is consist of four steps : solvation - is a process for sorbent wetting and create an environment suitable to selective retention ; sample application - when the components are retained on the sorbent surface , rinsing or washing - when some matrix components are removed from sorbent ; elution - when whit a suitable solvent the analyt and other co-retained components are desorbed from solid phase.

The importance of this steps and further information of its optimisation are treated in detail in [12,13]

#### EXPERIMENTAL

**Chemicals** acetone, chloroform, methanol, toluene from Reactivul Bucharest, caffeine from Roth, Sil G F<sub>254</sub> precoated plates from Macherey Nagel, instant coffee Amigo,russian tea and coca-cola.

**Solutions** carfeine standard solution (5.65mg caffeine/10mL CH<sub>3</sub>OH), russian tea stock solution (1 595 g leave/100 mL H<sub>2</sub>O infusion), instant coffee stock solution (0.7059 g coffee/100 ml H<sub>2</sub>O), coca-cola (used undiluted)

**Sample preparation** The cartidge used for SPE is consist of a polyethylene syringe (L=50mm, D=10mm) packed with 1cm<sup>3</sup> home made C-18 modified silica as sorbent. The solvation of solid phase was made with 5 mL CH<sub>3</sub>OH and 10 mL H<sub>2</sub>O. The standard and stock solutions was prepared in the same way as follows : 1 mL solution was diluted (at approx 70 mL) with H<sub>2</sub>O and passed through the sorbent bed with a flow rate of 10mL/min. After retention the sorbent was desolvated by drying 3 min. with air and then caffeine was eluted with 3 mL CH<sub>3</sub>OH. The resulted solution was evaporated to dryness and redissolved in 1 mL CH<sub>3</sub>OH

**Sample application** The samples were applied with a Carnag automated applicator as spots on Sil G F<sub>254</sub> precoated plates. Spots with varying volumes (1-10 $\mu$ L) from caffeine standard solution were applied to the plate in order to perform the calibration curve. For recovery, two 10  $\mu$ L spots were applied from both standard and processed (SPE) standard caffeine solutions. For quantitation, 20 $\mu$ L spots from instant coffee, russian tea and coca-cola stoke and processed (SPE) solution were applied to the plate.

**TLC conditions** The plates were developed in normal chromatographic chamber with CHCl<sub>3</sub> - (CH<sub>3</sub>)<sub>2</sub>CO (17: 3, v/v) and scanned in reflectance mode at 275 nm with a Shimadzu CS-9000 dual-wavelength flying-spot scanner. The obtained fotodensitograms are shown in figure 2-4.

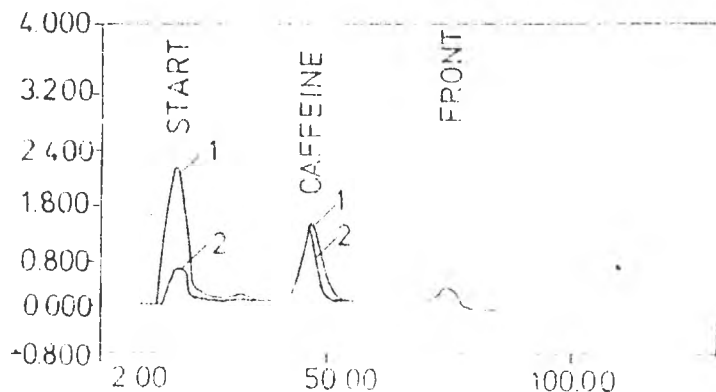


Figure 2. Fotodensitograms for 20  $\mu$ L spots for instant coffee stock and processed SPE standard solution

## TLC Determination of Caffeine Using Solid Phase Extraction

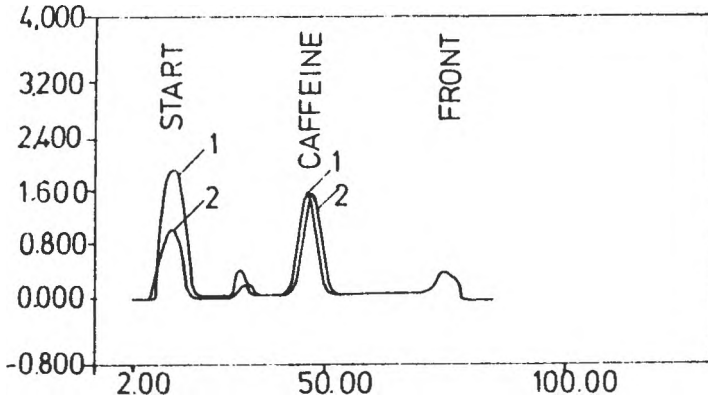


Figure 3. Fotodensitogram for 20 µL spots for russian tea stock and processed SPE standard solution.

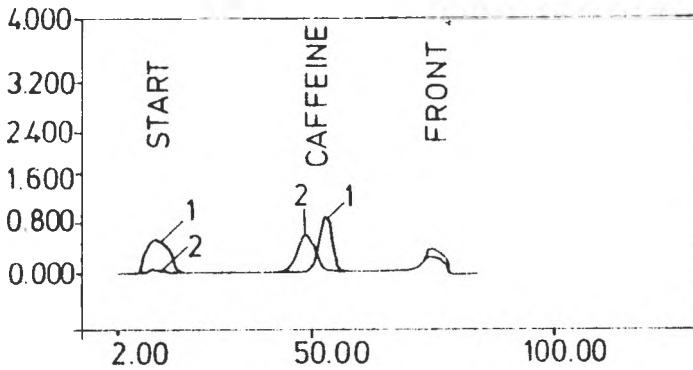


Figure 4. Fotodensitogram for 20 µL spots for coca-cola stock and processed SPE standard solution.

## RESULTS AND DISCUSSION

The equation for the calibration curve is :

$$Y = 16941 + 23316 x$$

where Y is area of chromatographic peak and x is the amount of caffeine. The calibration curve for caffeine is shown in figure 5.

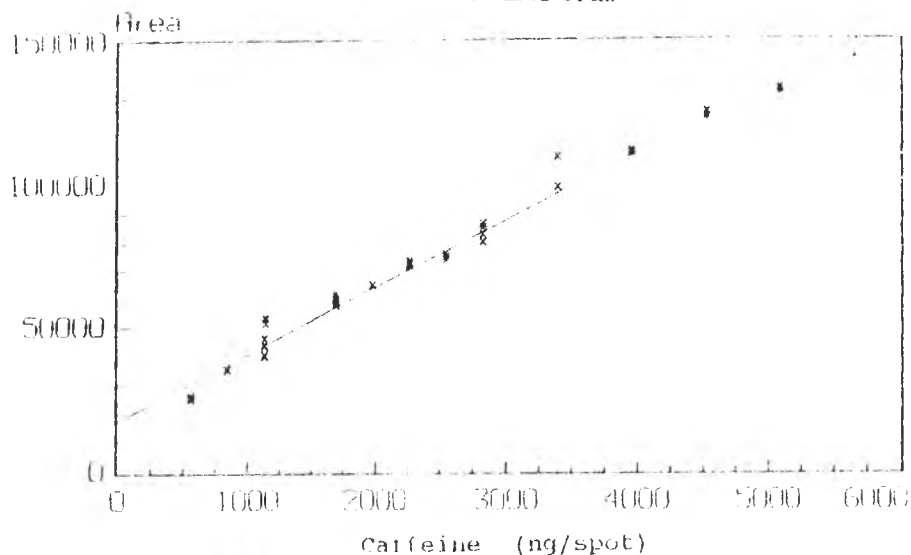


Figure 5 Calibration curve for caffeine

The recovery was calculated as ratio between corresponding areas to 10  $\mu\text{L}$  spots of processed (SPE) and standard caffeine solutions. As shown in Table I the recovery was 93.54%.

Table I Obtained experimental data used for recovery determination after the SPE processing

Solution	Volume applied ( $\mu\text{L}/\text{spot}$ )	Area	Recovery (%)
standard	10	150723	---
		151617	
		149975	
processed (SPE)	10	141442	93.54
		141136	
		140537	

The amount of caffeine in some beverage was calculated as shown in Table II.



## TLC Determination of Caffeine Using Solid Phase Extraction

Table II. Obtained experimental data used for caffeine contain in some beverage sample.

Sample	Area (impulse)	Amount* (µg/spot)	Amount** (µg/spot)	Caffeine (%)
Coca-cola	66042 66881 66448	2.12	2.12	10.6
Coca-cola (SPE)	61921 61557 62405	1.93	2.06	10.3
Tea	141610 143369 143811	5.043	5.043	1.69
Tea (SPE)	139360 137168 139811	5.22	5.58	1.75
Instant coffee	124004 125243 125598	4.63	4.63	3.28
Instant coffee (SPE)	117905 117764 118325	4.33	4.629	3.28

\* Calculated amount of caffeine from calibration curve

\*\* Corrected amount of caffeine using the recovery grade

The calibration curve is linear between 600-6000 ng/spot, and quantitative analysis can be performed. The results obtained from both methods (unprocessed and SPE processed sample) are similar. This can be predicted due to the high recovery (93.54%). Our obtained results are in good accordance with those from literature. The reported method can be successfully applied for routine determination of caffeine in different natural samples.

### REFERENCES

1. F. Slango, M. Subbajam, *Bull. Electrochem.* 1991, **7(6)**, 286
2. A. Abdennabi, N. Ullan, *Electroanalysis*, 1993, **5**, 709, *Analyt. Abstract.* 1993, **55** 6H250
3. M. Karawya, A. Diale, H. Z. Swelam, *Anal. Lett.* 1984, **17**, 77
4. E. Sell, *Chem. Anal.*, 1993, **38(3)**, 365
5. S. Li, J. Berger, S. Hartland, *Anal. Chim. Acta.* 1990, **232(2)**, 409

S. COBZAC et al.

6. B.Guo, H.Wan, *J. Chromatogr.*, 1990, **505(2)**, 435
7. F.G.Muhtadi, S.S. El Hawary, S.M. Sifaraway, *J. Liq. Chromatogr.*, 1990, **1315**, 1013
8. T.E.B.Leakey, *J. Chromatogr.*, 1990, **507**, 199
9. M.El Sadek, A. El Shanaway, A. Klier, G. Ruecker, *Analyst*, 1990, **115(9)**, 1181
10. T.Li, Yaowu Fenxi Zazhi, 1990, **10**, 366; *Analyt. Abstract*, 1991, **53**, 5H191
11. I.Z. Atamna, M. Janini, G. Musckik, *J. Liq. Chromatogr.*, 1991, **14(3)**, 427.
12. L. Liska, J. Krupcik, P.A. Leclercq, *J. High Res. Chromatogr.*, **13**, 1989
13. D.D. Blevins, M.F. Burke, T.J. Good, P.A. Harris, K.C. Van Home, L.S. Lago, *Sorbent Extraction Technology*, edited by K.C. Van Home, USA, 1985

Received: 11.03.1996

## ASPECTS OF THE ELECTROREDUCTION OF ANODIC LAYERS FORMED ON LEAD IN SULPHURIC ACID SOLUTIONS

Eleonora Maria Rus

*Department of Physical Chemistry, University "Babes-Bolyai" Cluj-Napoca  
Romania*

### Abstract

Cyclic voltammetry has been used to study the electroreduction of anodically formed layers on lead electrodes under various experimental conditions. The negative potential sweep curves were recorded at different sweep rates for a range of polarization potentials and times

### INTRODUCTION

The charging and discharging characteristics of the lead-acid batteries have been and still are extensively investigated in order to improve their performances [1-5].

Lead electrode reactions in  $H_2SO_4$  solutions have been studied by using different stationary and transient techniques. In spite of the many researches and the large number of publications regarding this system, the kinetics and mechanism of the electroreduction processes are still open to discussion. The cathodic reactions taking place during the charging stages of lead electrodes have been given considerably less attention. For this reason, conclusions concerning the exact nature and structure of reaction products are more difficult to draw.

The electroreduction of  $PbSO_4$  has been investigated in order either to examine the effect of some additives on the nucleation and growth stage in lead electrocrystallization process or to analyse the reduction of lead sulphate grown anodically on smooth and porous electrodes through potentiostatic step techniques [6-8].

According to Pavlov et al, based on X-ray diffraction and electrochemical methods, the composition of the anodic layers, formed on lead in  $H_2SO_4$  solution can be as follows [9-11]:

1. A corrosion layer, consisting of  $\text{PbSO}_4$  crystals, formed at potentials from -0.95 to -0.30 V (vs  $\text{Hg}/\text{Hg}_2\text{SO}_4$ ) 2. A film of  $\text{PbSO}_4$  and an inner layer of  $\text{PbO}$  which builds up beneath the initially grown  $\text{PbSO}_4$  porous film, at -0.3 to 0.95 V. 3. At potentials higher than 0.95 V, the predominant anodic surface products are  $\alpha$ - $\text{PbO}_2$  and  $\beta$ - $\text{PbO}_2$ .

Recently, F.E. Varela et al. have pointed out that in the electroreduction of anodic layers, three well-defined processes could be distinguished [12] a. The electroreduction of the primary  $\text{PbSO}_4$  layer which involves mainly an instantaneous nucleation and three-dimensional growth mechanism under diffusion control. b. The electroreduction of the  $\text{PbO}$  layer, consists of two current contributions: one term can be associated with an instantaneous nucleation and two-dimensional growth under diffusion control and the other one, which is the main current contribution, can be related to a progressive nucleation and three-dimensional growth mechanism under charge transfer control. c. The electroreduction of composite  $\text{PbSO}_4$ - $\text{PbO}$  layer which can be successfully described in accordance with a complex mechanism by taking into account the simultaneous influence of the two single surface layer constituents.

The present paper presents the results of investigation obtained by using cyclic voltammetry method on electroreduction of  $\text{Pb(II)}$  containing surface layers generated on lead in sulphuric acid solution under rigorously controlled conditions.

## EXPERIMENTAL

The working electrode was a disk of 99.99% pure lead ( $1 \text{ cm}^2$ ) which was press-fitted into a teflon holder. Before each experiment, the lead electrode was mechanically polished with abrasive paper, thoroughly rinsed with distilled water and cathodically polarized (for 3 minutes i.e.) in the range of hydrogen evolution potential, to provide a reproducible electroreduced lead surface. The electrolyte solution was prepared from analytical grade reagents. Aqueous solutions of sulphuric acid were used as electrolyte. Potentials were measured and referred to in the text with respect to  $\text{Hg}/\text{Hg}_2\text{SO}_4, \text{K}_2\text{SO}_4(\text{sat.})$  as reference electrode. The counter electrode was a platinum sheet of  $5 \text{ cm}^2$  in area. The experiments were carried out using a H-type glass cell, at room temperature. The cyclic voltammograms were obtained by sweeping the potential linearly in a positive direction from a certain starting negative potential to a maximum, at different sweeping rates and then the direction was reversed.

## Electroreduction of Anodic Layers Formed on Lead

### RESULTS AND DISCUSSION

In the potential region lying between the potential of hydrogen evolution and the potential of oxygen evolution a complex anodic film with a multilayer structure is formed on a lead electrode in  $\text{H}_2\text{SO}_4$  solution. The typical curves of a cyclic voltammogram for the lead electrode in 1N  $\text{H}_2\text{SO}_4$  solution are shown in figure 1, as a function of cycles number. Such voltammogram in steady-state could be obtained after several tens of cycles over the whole potential range (-2 to +2V).

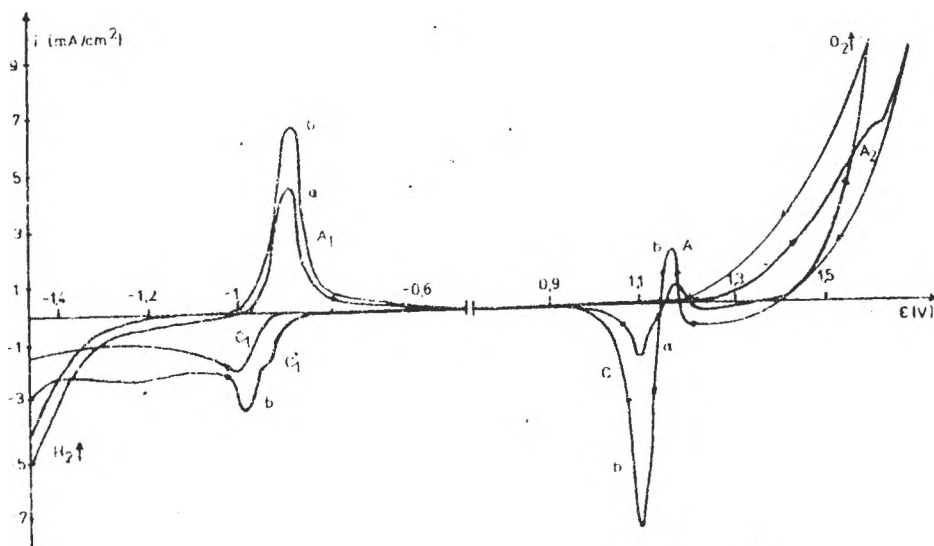


Figure 1. Cyclic voltammograms of a lead electrode in 1N  $\text{H}_2\text{SO}_4$  solution. Sweep rate 20 mV/s. a) cycle 2; b) cycle 32

In this voltammogram (curve a) the four peaks which occur are related to the main forms of active materials of the lead electrode. Thus, the well defined peak  $A_1$  corresponds to oxidation of Pb to  $\text{Pb(II)}$  species at about -0.96 V, appeared during the anodic scan potential. The peak  $A_1$  is followed by a wide passive region until the oxygen evolution occurred. Then, the irregular and sharp oxidation peak A ( $\text{Pb} + \text{PbO}_2 \rightarrow \text{PbSO}_4 + \text{PbO}_2$ ) appeared abnormally on reversing the potential sweep direction.

## E. M. RUS

The negative potential scan exhibits a well defined cathodic current peak C (which appears after the oxidation peak A), corresponding to reduction processes  $\alpha\text{-PbO}_2$  and  $\beta\text{-PbO}_2$  to  $\text{PbSO}_4$ .

At about -1.1 V an asymmetric complex cathodic peak,  $C_1$ , appeared related to the electroreduction of Pb(II) containing species to Pb.

It is to remark that the oxidation peak corresponding to  $\alpha\text{-PbO}_2$  and  $\beta\text{-PbO}_2$  formation was not clearly visible (curve a, figure 1.). Consequently,  $\text{PbO}_2$  phase formation and oxygen evolution occurred simultaneously during the positive potential scan in a few cycles. After the thirtieth cycle, in the positive potential sweep, poorly defined anodic current peak  $A_2$ , corresponding to  $\beta\text{-PbO}_2$  formation was detected (curve b, figure 1.), because the oxygen evolution potential shifted positively.

It is noticeable that all the anodic potential peaks became more negative and the cathodic potential peaks became more positive with the increase of the number of cycles. Thus, from this voltammograms it is clear that a minimum of 30 cycles are required to obtain the steady-state condition and a proper reversibility of system.

In accordance with F. Varela et al., the complex cathodic current peak  $C_1$  corresponds to two distinguished processes having, as reactants, the primary porous  $\text{PbSO}_4$  layer and the more compact PbO layer which builds up beneath the initially grown  $\text{PbSO}_4$  layer [12].

According to many authors, the tetragonal PbO is a dominant component of the inner compact layer which is formed at potentials more positive than that potential the initial  $\text{PbSO}_4$  layer was grown [13-15]. The formation of tetragonal PbO becomes the main process in the growth of anodic film at a potential above 0V[16]. Therefore, the electrochemical behaviour of the tetra-PbO films plays an important role in the anodic corrosion of lead and in determining the performances of lead acid batteries.

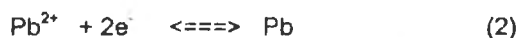
The formation of PbO layer was found to be a consequence of the local alkalization of the Pb/ $\text{PbSO}_4$  interface[17]. During the anodization of the lead, pores are formed between the  $\text{PbSO}_4$  crystals and the penetration of electrolyte solution in these pores ensure the current flow through the  $\text{PbSO}_4$  layer which is gradually transformed into a semipermeable membrane. This passive layer

## Electroreduction of Anodic Layers Formed on Lead

hinders the diffusion of sulphate ions into the pores and causes an increase of the Pb(II) ion concentration and a decrease of the H<sup>+</sup> ion concentration at the metal/film interface. Thus an alkaline medium is formed in the inner layer and at potentials more positive than -0.55V (v.s. Hg/Hg<sub>2</sub>SO<sub>4</sub>) PbO can be formed underneath PbSO<sub>4</sub> layer [17].

The formation current peak for the PbO does not appear in the positive sweep of the lead electrode and for this reason only the reduction peaks, obtained in the negative sweep can be used for studying its electrochemical behaviour.

The electroreduction of PbO can be formally represented by the following equations [14]:



The overall reaction is:



The current peak associated with PbO electroreduction,  $C_1^*$  has been clearly recorded during cathodic sweep only with cyclings effectuated over narrow potential ranges (-2 to 0 V), after the electrode was polarized for defined times (e.g.  $t_{\text{pol}} = 20$  min.) at a polarization potential,  $E_{\text{pol}} = 0.2$  V.

The voltammograms presented in figure 2, recorded in 4.3mH<sub>2</sub>SO<sub>4</sub> solution at a potential sweep rate  $v = 10$  mV/s, showed that the peak current value  $C_1^*$ , is greatly dependent on the anodic switch potential (ASP). Thus with values lower than -0.5 V the peak  $C_1^*$  was not recorded (curve a, figure 2). One can thus conclude that the formation of PbO, during anodic sweep on the electrode surface occurs only at potentials more positive than -0.5 V, when it becomes one of the main constituents of the passive layer which is formed on the lead surface (see curves b and c, figure 2).

The value of peak current for the PbO electroreduction proved to be dependent on the electrode polarization time, figure 3

With low values of polarization time, peak  $C_1^*$  was not recorded (curve a, figure 3), a fact which suggests that the anodic oxidation formation of PbO is rather slow and is dependent on the previously formed PbSO<sub>4</sub> layer structure and properties.

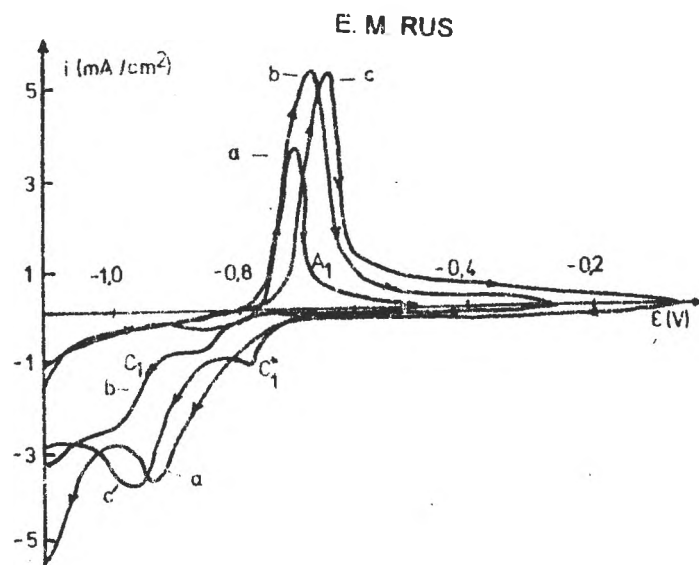


Figure 2. Cyclic voltammograms for a lead electrode in 4.3 m H<sub>2</sub>SO<sub>4</sub>,  $v=10$  mV/s,  $E_{pol} = 0.2$ V,  $t_{pol} = 20$  min., ASP: a) -0.5V; b) -0.3V; c) 0V.

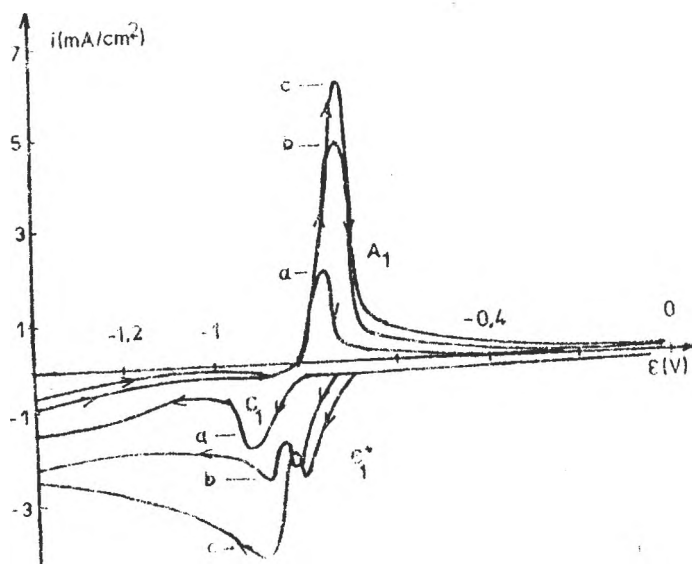


Figure 3. Cyclic voltammograms for a lead electrode in 4.3 m H<sub>2</sub>SO<sub>4</sub>, ASP 0 V,  $v=10$  mV/s,  $E_{pol} = 0.2$  V, polarization time: a) 10 min.; b) 30 min.; c) 40 min.



## Electroreduction of Anodic Layers Formed on Lead

For various sweeping rates the form of voltammograms changes slightly. The peak current height increases with the increase of sweep rates and the peak potential slightly shifts towards more negative values, (figure 4)

The increase of the peak height  $C_1^*$  may be explained by the growth of PbO amount formed in the passive layer during anodic sweep while the peak potential shift illustrates a withdrawal from process reversibility.

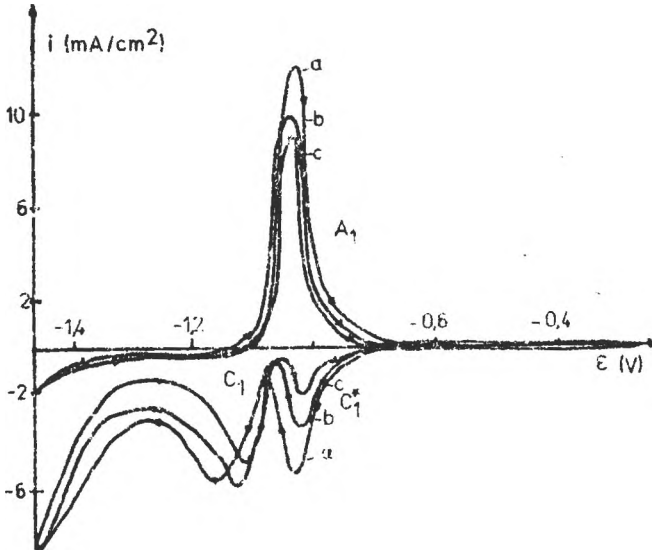


Figure 4. Cyclic voltammograms for a lead electrode in 4.3M  $H_2SO_4$ .  $E_{pol} = 0.2$  V;  $t_{pol} = 20$  min; ASP 0 V. Sweep rate a) 20 mV/s, b) 10 mV/s, c) 3.33 mV/s.

It is worth noticing that after a significant number of cycles the peak current value decreases in accordance with the PbO reduction, figure 5

On the other hand a reactivation of anodic processes in cathodic sweep was observed on the increase of number of cycles (peak  $A_1^*$ , figure 5). This reactivation process of lead oxidation in cathodic sweep may be explained by the appearance of some cracks in the anodic film induced by internal strains due to the volumic alterations of the products formed. In this context part of the anodic film is detached from the electrode surface and the metallic lead oxidised being exposed to direct contact with the electrolyte

Such phenomena called "local depassivation" have been detected, so far, only by IR-reflexion-adsorbition spectroscopy; they could not, so accurately set into evidence by voltammetric techniques, [5].

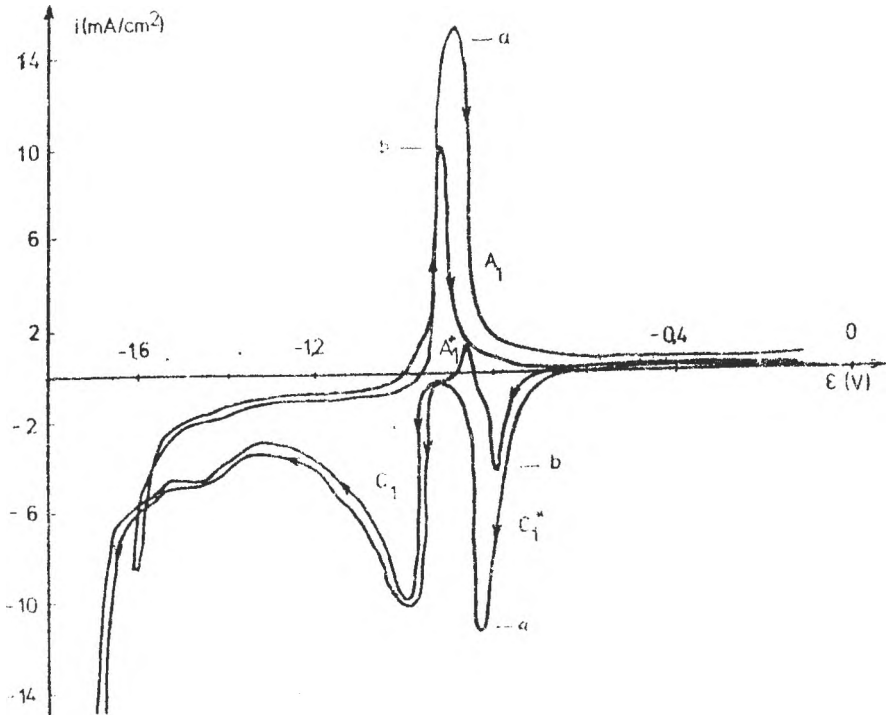


Figure 5. Cyclic voltammograms for a lead electrode in 4.3m  $H_2SO_4$ . Sweep rate 20mV/s;  $t_{pot} = 20$  min.;  $E_{pot} = 0.2V$ ; a) cycle 30; b) cycle 50.

Analysing the results obtained the following conclusions could be drawn:

a) For studying the  $PbO$  electroreduction processes in  $H_2SO_4$  solutions, by means of cyclic voltammetry the selection of cycling potential sweep range is greatly significant. During cathodic sweep the peaks corresponding to  $Pb(II)$  species electroreduction, from the  $PbSO_4$  surface layer and  $PbO$  layer formed beneath could be set in evidence.

b) The decrease of peak current with the number of cycles in  $PbO$  electroreduction processes demonstrates that an amount of hardly reducible oxide is accumulated on the electrode surface resulting in a low efficiency of electrode in acid batteries.

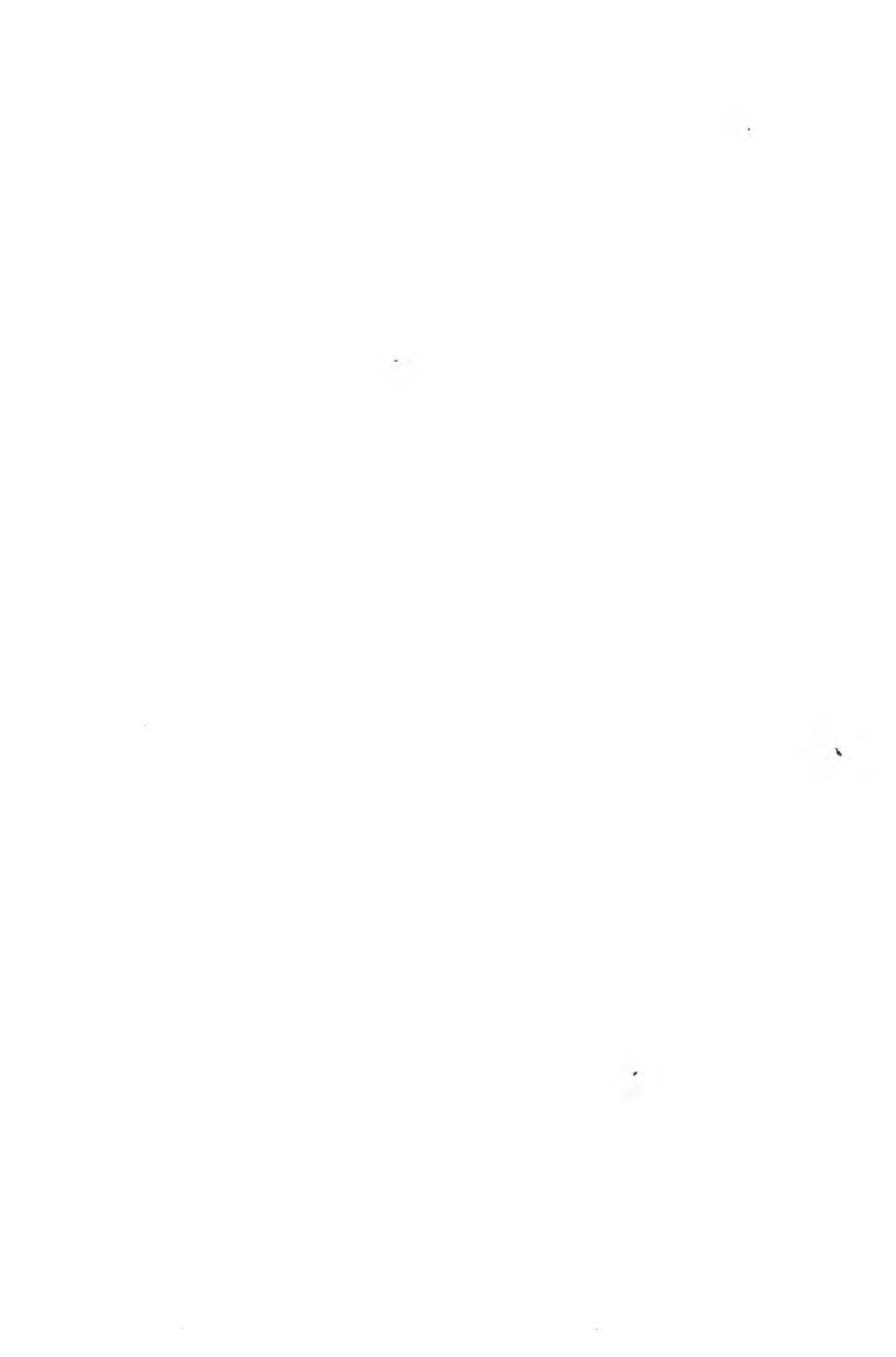
## Electroreduction of Anodic Layers Formed on Lead

c) The reactivations of anodic processes during cathodic scanning set into evidence the volumic changes accompanying the formation of anodic films at the grid/electrolyte solution interface. The mechanical deterioration of this layer due to the increased internal strains (stress) stimulates the grid corrosion processes.

### REFERENCES

1. F. E. Varela, L. M. Gassa and J. R. Vilche, *J. Electroanal. Chem.* 1993, **353**, 147.
2. K. Kanamura and Z. Takehara, *J. Electrochem. Soc.*, 1992, **139**, 345.
3. Y. Guo, *J. Electrochem. Soc.*, 1993, **140**, 3369.
4. Y. Yamamoto, K. Fumino, T. Ueda and M. Nambu, *Electrochim. Acta*, 1992, **37**, 199.
5. D. Pavlov, *J. Electrochem. Soc.*, 1992, **139**, 3075.
6. N. A. Hampson and J. B. Lakeman, *J. Electroanal. Chem.*, 1980, **108**, 347.
7. Y. Guo, J. Yue and C. Liu, *Electrochim. Acta*, 1993, **38**, 1131.
8. F. E. Varela, L. M. Gassa and J. R. Vilche, *J. Appl. Electrochem.*, 1995, **25**, 364.
9. D. Pavlov, C. N. Poulieff, E. Klaja and N. Jordanov, *J. Electrochem. Soc.*, 1969, **116**, 316.
10. D. Pavlov and N. Jordanov, *J. Electrochem. Soc.*, 1970, **117**, 1103.
11. D. Pavlov, S. Zanova and G. Papazov, *J. Electrochem. Soc.*, 1977, **124**, 1522.
12. F. E. Varela, L. M. Gassa and J. R. Vilche, *Electrochim. Acta*, 1992, **37**, 1119.
13. K. R. Bullock, G. M. Trischan and R. G. Burrov, *J. Electrochem. Soc.*, 1983, **130**, 1283.
14. Y. Guo, *J. Electrochem. Soc.*, 1991, **138**, 1222.
15. L. A. Avaca, E. R. Gonzales and G. Tremiliosi, *J. Power Sources*, 1990, **30**, 161.
16. D. Pavlov, I. Balkanov and P. Rachev, *J. Electrochem. Soc.*, 1987, **134**, 2390.
17. D. Pavlov, *Electrochim. Acta*, 1978, **23**, 845.

Received: 11.03 1996



## QUANTITATIVE ANALYSIS OF SOME BENZODIAZEPINES BY THIN LAYER CHROMATOGRAPHY - DENSITOMETRY AND UV SPECTROPHOTOMETRY. A COMPARATIVE STUDY.

**Simion Gocan, Gabriela Cimpan**

*"Babes-Bolyai" University, Analytical Chemistry Department, 11 Arany Janos street, 3400 Cluj-Napoca, Romania.*

### **Abstract**

Three benzodiazepines (diazepam, oxazepam and chlordiazepoxid) were quantitatively analyzed by thin layer chromatography - densitometry. A comparative study was performed between two analytical techniques: the classical spectrophotometric method and the proposed one, thin-layer chromatography and densitometry. There are no significant differences between the experimental results obtained by the two methods applied for the commercial pharmaceutical formulas.

### **INTRODUCTION**

In the last few years, the interest for the quantitative analysis of barbiturates has shown an increased impact in analytical quality control and also as a method associated with clinic treatments [1]. Benzodiazepines are minor tranquillisers drugs and have widespread applications in medicine. The quantitation of benzodiazepines in biological fluids is faced with the complex matrices and with the difficulties to isolate the compounds from them.

Spectrophotometry is a powerful technique very useful for purity tests of compounds. For a spectrophotometric analysis a sample can be processed in a relative easy way, especially for pharmaceutical forms, but could raise serious problems for complex matrices as biological fluids are. Due to the great capacity of separation, different chromatographic techniques were used in quantitative analysis of benzodiazepines from complex matrices: gas-chromatography (GC), high-performance liquid chromatography (HPLC) and thin-layer chromatography (TLC). Diazepam and its metabolites were extracted in benzene from biological fluids and then analyzed by gas-chromatography

[2]. Gas-chromatography was also used for identification and routine determination of different barbiturates in biological samples [3, 4]. This method is very simple but cannot be applied for all kinds of benzodiazepines (e.g. oxazepam) because degradation can occur at high temperatures. High performance liquid chromatography (HPLC) has widespread applications in clinical chemistry; some methods are available for benzodiazepines [5] and the studies were performed on different columns: -CN, -C<sub>18</sub>, -C<sub>6</sub>H<sub>5</sub>, using normal phase or reversed phase chromatography [6].

Thin-layer chromatography (TLC) was also used for the separation and identification of barbiturates and their metabolites. Klimes and Kasiner [7] have organized in a review the TLC analysis of benzodiazepines presenting a great number of eluents and spraying reagents. There are shown a lot of different situations: the separation and identification of benzodiazepines as references substances, the analysis of benzodiazepines from pharmaceutical products and the densitometry of benzodiazepines. The identification and the "in situ" quantitative analysis of compounds by thin-layer chromatography and densitometry combines the great separation power of chromatographic methods with a simple, rapid and relative cheap technique. Reversed-phase thin-layer chromatography (RPTLC) was also used for the analysis of benzodiazepines [8, 9].

The purpose of the present work is the separation and the quantitative analysis by thin-layer chromatography and densitometry of three benzodiazepines with widespread applications in medication: diazepam, oxazepam and chlordiazepoxid.

## EXPERIMENTAL

Standard substances (diazepam, oxazepam and chlordiazepoxid) were of chromatographic purity. The studied pharmaceutical forms were commercially available. All other reagents were of analytical grade and were purchased from "Chimopar", Bucharest.

### a). Spectrophotometry

The quantitative analysis of the studied benzodiazepines by spectrophotometry was performed following the routine analysis from the pharmaceutical industry.

#### Diazepam

The Diazepam tablets have an average weight of 0.188 - 0.212 g/tablet and contain 0.009 - 0.011 g of active substance per tablet. 0.4 g powder of pharmaceutical form were extracted with 80 mL acidulated ethanol (2.8 mL concentrated sulfuric acid for 1000 mL anhydrous ethanol) in a 100 mL volumetric flask.

## Quantitative Analysis of some Benzodiazepines

The mixture was vigorously shaken for 5 minutes and completed to 100 mL with acidulated ethanol. 7 mL from the filtrate were diluted to 100 mL with acidulated ethanol in a volumetric flask (Solution A). The absorptivity of a 1% (w/v) diazepam standard solution, measured in a 1 cm cell, at 285 nm, is  $\epsilon_1 = 0.437$ . The reference solution was acidulated ethanol.

### Oxazepam

The Oxazepam tablets have an average weight of 0.180 - 0.220 g/tablet, each of them containing 0.009 - 0.011 g of active substance. 0.4 g tablet powder were shaken with 150 mL of acidulated methanol (0.85 mL concentrated hydrochloric acid for 1000 mL anhydrous methanol) in a 250 mL volumetric flask. After 35 minutes of shaking the mixture was diluted to 250 mL with acidulated methanol. 5 mL of the filtrate were diluted to 100 mL with acidulated methanol in a volumetric flask (Solution B). The absorptivity of a 1% (w/v) oxazepam standard solution, measured in a 1 cm cell, at 235 nm, is  $\epsilon_2 = 1.100$ . The reference solution was acidulated methanol.

### Chlordiazepoxid

For the quantitative analysis of active substance in Chlordiazepoxid sugar-coated tablets, 1.0 g powder of pharmaceutical form (sugar-coated tablets) were shaken with 80 mL hydrochloric acid 0.1N in a 100 mL volumetric flask. The mixture was vigorously shaken for 15 minutes, diluted to 100 mL with HCl 0.1N. 3 mL of filtrate were diluted with HCl 0.1N in a 100 mL volumetric flask (Solution C). The absorptivity of a 1% (w/v) chlordiazepoxid standard solution, measured in a 1 cm cell, at 308 nm, is  $\epsilon_3 = 0.328$ . The entire determination have to be performed in 30 minutes from the first adding of hydrochloric acid because the substance suffers a rapid degradation.

### **b). Thin-layer chromatography and densitometry**

All the experiments were performed on thin-layer silica plates (10 x 10 cm, 0.25 mm layer width) including fluorescence indicator for 254 nm from Macherey-Nagel (Germany). Solutions A, B and C were applied to the plates as spots (10  $\mu$ L/spot) using a Desaga automated applicator. The mobile phase was chloroform - methanol (9 : 1, v/v). The densitometry was fulfilled by a Shimadzu CS-9000 dual-wavelength flying-spot scanner, in reflection and zigzag mode (zigzag width, 10 mm), at 254 nm. The concentration of reference standard solutions are shown in Table 1. The corresponding calibration curves were obtained by applying to the plate different volumes of the reference standard solutions (1 - 6  $\mu$ L/spot).

## **RESULTS AND DISCUSSION**

The quantitative evaluation of a thin-layer chromatogram by densitometry is based on the measurement of the light beam reflected (or transmitted) by the layer alone and by the layer and the sample spot. In this special situation, the Beer's law cannot be directly applied because the light is scattered by the thin-layer and this process is not simple. The proper relation which describes the complex process of reflection and transmission

in scattering media is the Kubelka-Munk equation [10]. The concentration of the benzodiazepines reference solutions and the corresponding quantities applied to the plates are shown in Table 1 and Table 2.

**Table 1.** The concentrations of the reference standard solutions

Compound	Concentration ( $\mu\text{g}/\mu\text{L}$ )
1. Diazepam	1.11
2. Oxazepam	1.04
3. Chlordiazepoxid	1.22

**Table 2.** The quantities of benzodiazepines applied to the plates

Plate nr	Applied volume ( $\mu\text{L}/\text{spot}$ )	Benzodiazepines ( $\mu\text{g}/\text{spot}$ )		
		1.	2.	3.
1.	1	1.11	1.04	1.22
2.	2	2.22	2.08	2.44
3.	3	3.33	3.12	3.66
4.	4	4.44	4.16	4.88
5.	5	5.55	5.20	6.10
6.	6	6.66	6.24	7.32

Usually, in reflection mode a logarithmic curve is obtained by plotting the absorption versus the amount of substance in the spot. The curve is more close to linearity in transmission, but this mode is limited by the transparency of the layer and the plate.

The results obtained by densitometry from calibration curves are shown in Table 3.

Following average weights were obtained for the series of investigated tablets and sugar-coated tablets:

- |                    |                              |
|--------------------|------------------------------|
| 1. DIAZEPAM        | 0.1922 g/tablet              |
| 2. OXAZEPAM        | 0.2975 g/tablet              |
| 3. CHLORDIAZEPOXID | 0.1932 g/sugar-coated tablet |

The corresponding results obtained by spectrophotometry and thin-layer chromatography are shown in Table 4.



## Quantitative Analysis of some Benzodiazepines

For both calibration curve (first and second order) the value of correlation coefficient is close to unit and the experimental results obtained by thin-layer chromatography can be compared with those obtained by spectrophotometry.

**Table 3.** The calibration curves obtained by densitometry

Substance	Applied quantity (mg/spot)	Area
1. DIAZEPAM	1,11	59253
	2,22	102110
	3,33	149500
	4,44	202383
	5,55	229397
	6,66	245381
The regression equation: $y = A + B \ln x$		A = 32827
The correlation coefficient, r		B = 109787
		r = 0,98
2. OXAZEPAM	1,04	45916
	2,08	69751
	3,12	94416
	4,16	105994
	5,20	124254
	6,24	127970
The regression equation: $y = A + Bx$		A = 36181
The correlation coefficient, r		B = 16081
		r = 0,98
3. NAPOTON	1,22	75678
	2,44	92658
	3,66	123722
	4,88	134546
	6,10	150792
	7,32	175274
The regression equation: $y = A + B \ln x$		A = 55778
The correlation coefficient, r		B = 53780
		r = 0,97

**Table 4.** The comparison between the experimental results obtained by the classical spectrophotometric method and the proposed one by thin-layer chromatography.

Compound	Analysis by spectrophotometry g/tablet	Analysis by thin-layer chromatography (TLC)	
		µg/spot	g/tablet
1. Diazepam	0,0100	2,40	0,0108
2. Oxazepam	0,0109	0,87	0,0110
3. Napoton	0,0096	4,77	0,0093

**CONCLUSION**

The proposed method for quantitative analysis of benzodiazepines from pharmaceutical forms by thin-layer chromatography and densitometry is accurate and comparable with the classical method by spectrophotometry.

**REFERENCES**

1. A.H.Stead, A.R.Allan, R.E.Ardrey, T.S.Bal, T.M.Callaghan, R.Gill, A.C.Moffat and M.C.H.Oon, *J. Forens. Sci. Soc.*, 1981, **21**, 41.
2. E.Arnold, *Acta pharmacol. et toxicol.*, 1975, **36**, 335.
3. F.Vincent, C.Feuerstein, M.Gavend and J.Faure, *Clinica Chimica Acta*, 1979, **93**, 391.
4. W Butte, *Ärztl. Lab.*, 1979, **25**, 189.
5. P.M.Klockowski and G.Levy, *J. Chromatogr.*, 1987, **422**, 334.
6. S.H.Y.Wong, *J.Pharm. & Biomed. Analysis*, 1989, **7(9)**, 1011.
7. J. Klimes and P.Kastner, *J.Planar Chromatogr.-Mod.TLC*, 1993, **6**, 168.
8. M.Marichy and C.Gonnet, *Chromatographia*, 1986, **21(2)**, 105.
9. W Bress, K Ziriniski, W Long, T.Manning and L.Lukash, *Clinical Toxicology*, 1980, **16(2)** 219.
10. \* \* \*. Quantitative Thin-Layer Chromatography and Its Industrial Applications, Chromatographic Science Series Vol. 30, Marcel Dekker (Editor), New York, 1987.

Received 14.03 1996

**TRANSITION METAL HEXACYANOFERRATES (III) MODIFIED ELECTRODES.  
I. CHARACTERIZATION OF Co, Ni and Cu HEXACYANOFERRATE MODIFIED  
ROTATING DISK ELECTRODES<sup>1</sup>**

Liana Mureșan, Ionel Cătălin Popescu and Liviu Oniciu

*"Babeș-Bolyai" University, Department of Physical Chemistry, 3400 Cluj-Napoca,  
Romania*

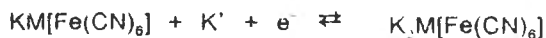
**ABSTRACT**

A new method to obtain cobalt-, nickel- and copper- hexacyanoferrate (III) modified electrodes based on the use of a rotating disk electrode is presented. The preformed complexes were electroadsorbed from solution during the electrode potential scanning. An optimization study concerning the electrode material and the metal hexacyanoferrates preparation, electrochemical (scan rate) and hydrodynamic (rotation speed) conditions, was performed. Ionic selectivity testing for Na<sup>+</sup>, K<sup>+</sup>, Li<sup>+</sup> and NH<sub>4</sub><sup>+</sup> showed that glassy carbon/CoHCF-modified RDE is the most suitable for Na<sup>+</sup> and Pt/NiHCF-modified RDE for K<sup>+</sup>.

**INTRODUCTION**

The hexacyanoferrates(III) of transition metals (MHCF), with the general formula M<sub>x</sub>[Fe(CN)<sub>6</sub>]<sub>x</sub> · x H<sub>2</sub>O, where M can be Fe(II), Co(II), Ni(II), Cu(II), are an important class of insoluble mixed valence polynuclear complexes. The most important characteristics of these compounds are based on their zeolitic structure and on the presence of two redox centers, exhibiting a good reversibility [1].

In order to maintain the electroneutrality, the electrochemical oxidoreduction of the MHCF illustrated, for example, by:



should be accompanied by an ion migration through its structure [2]. So, certain group

<sup>1</sup> Partially presented at the "Electrochemical Sensors and Biosensors Conference", Cluj-Napoca, 28-29 Sept. 1995

I cations can freely migrate into or out of the film, whereas other are excluded, resulting a special kind of ionic selectivity [3].

Besides, modified electrodes with Prussian Blue  $K_4[Fe(CN)_6]$  (PB), and his analogues, such as simple metal hexacyanoferrates (III), MHCF ( $M = Co^{2+}, Ni^{2+}$  and  $Cu^{2+}$ ) [3-5] or mixed metal hexacyanoferrates (III), PB-MHCF ( $M = Ni^{2+}, Mn^{2+}, Cu^{2+}, In^{2+}, Cr^{2+}, Ru^{2+}$ ) [6], were prepared for a variety of applications including electrocatalysis, electrochromism, photoresponse and electrochemical energy conversion [1-2, 7-10].

The strategy adopted until now for the preparation of MHCF modified electrodes consisted in the modification of a stationary electrode. Thus, during a cyclic potential scanning, the preformed complex was electrosorbed on the working electrode surface from the adjacent solution [4]. An other variant starts with the metal layer electrodeposition on the electrode surface, followed by the potential cycling in a buffer solution containing  $K_3[Fe(CN)_6]$  [3].

In the present paper, in order to control the hydrodynamic conditions during electrode modification, a new method, based on the use of a rotating disk electrode (RDE) to obtain MHCF-modified electrodes by electrosorption of the preformed complex, is presented. The influence of different experimental conditions, such as electrode material, MHCF preparation conditions on the obtention of Co(II), Ni(II), and Cu(II)-HCF modified RDEs were studied. The obtained modified electrodes were tested as potentiometric sensors for some electroinactive cations such as  $K^+$ ,  $Na^+$ ,  $Li^+$  and  $NH_4^+$ .

## EXPERIMENTAL

### *Reagents*

$CoCl_2$ ,  $NiCl_2$ ,  $KCl$ ,  $NaCl$ ,  $LiCl$  and  $NH_4Cl$  (Reactivul București) and  $K_3[Fe(CN)_6]$  (Merck) were of analytical grade and were used without further purifications

### *Electrochemical experiments*

Electrochemical experiments were performed using a potentiostatic set-up consisting of a potentiostat (PS 3, Meinsberg, RDA), a signal generator (Polarograph LP 7e, Praha) and an X-Y recorder (Endim 620 02, Meinsberg).

A conventional three electrode cell was used. The working electrode was a rotating disk electrode made of Pt ( $\Phi = 1.5$  mm), glassy carbon, GC ( $\Phi = 3$  mm) or graphite, G ( $\Phi = 3$  mm). The reference electrode was a saturated calomel electrode (SCE). The Pt counter electrode was separated from the test solution by a glass frit.

### *Preparation of the MHCF-modified electrodes*

The modification of RDE with preformed different MHCF ( $M = Co(II), Ni(II), Cu(II)$ ) was achieved by adsorption, cycling the electrode potential between 0 and 1 V/SCE at different scan rates and

## Transition Metal Hexacyanoferrates (III)

different rotation speeds. The modifier was obtained by mixing a solution of  $10^{-2}$  M  $K_3[Fe(CN)_6]$  with a  $10^{-2}$  M solution of either  $CoCl_2$ ,  $NiCl_2$  or  $CuSO_4$ , in different molar ratios. In all cases, 0.5 M KCl was used as electrolytic support. All solutions were air saturated at room temperature.

In order to maintain the same coverage throughout the experiments, growth was restricted to a fixed number of cycles (50). The obtained MHCf-modified electrodes were rinsed thoroughly with distilled water and then, they could be used for testing or stored in air.

## RESULTS AND DISCUSSION

### *Influence of the electrode material*

Typical voltammograms obtained for RDEs made of Pt, G and GC dipped in a solution of CoHCF, prepared by mixing  $10^{-2}$  M  $CoCl_2$  and  $10^{-2}$  M  $K_3[Fe(CN)_6]$  in the 2:1 v/v ratio, are shown in figure 1 (a, b, c).

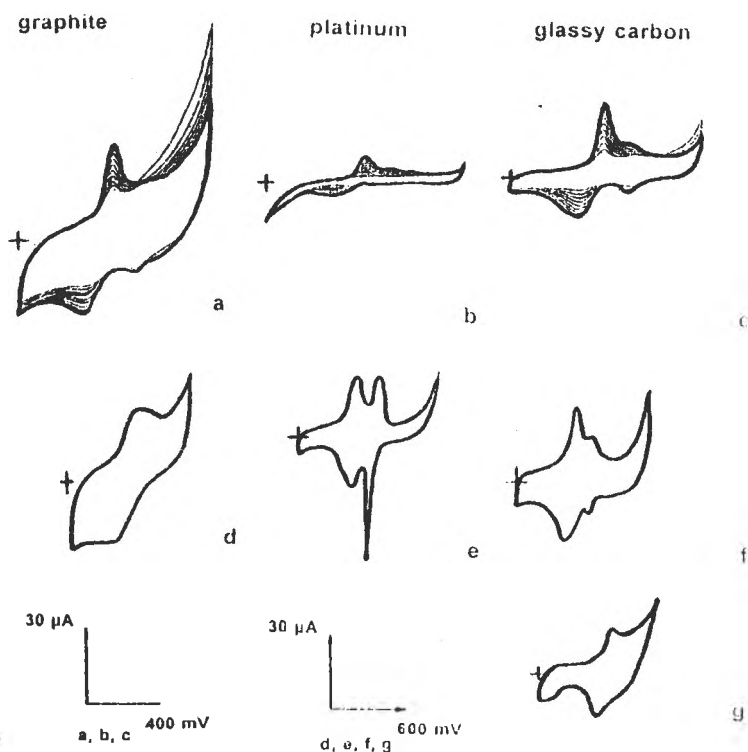


**Figure 1.** Cyclic voltammograms showing the influence of the electrode material on the MHCf- modified RDEs preparation: (a, b, c) CoHCF ; (d, e, f) NiHCF ; (g) CuHCF. Experimental conditions: scan rate, 25 mV/s for Co- and NiHCF and 60 mV/s for CuHCF; rotation speed 450 rpm; mixing ratio (A/B) 2:1 v/v for Co- and NiHCF, 1:1 v/v for CuHCF

In spite of the fact that the working electrode is not stationary, two pairs of

reversible redox peaks are observed on the cyclic voltammograms corresponding to all tested electrode materials (fig. 1 a-c). This behaviour proves the formation of an CoHCF film immobilized on electrode surface. The first redox peak, appears at a formal potential of about 0.45 V/SCE and corresponds to  $Fe^{2+}/Fe^{3+}$  redox couple, present inside of the CoHCF film. The second one, with a formal potential of about 0.67 V/SCE, corresponds to  $Co^{2+}/Co^{3+}$  couple (Table 1). These potential values and

**Table 1.** Formal standard potentials\* for MHCF-modified RDEs.

Modifier		Electrode material		
		GC	Pt	G
CoHCF	Preparation	0.46	0.44	0.44
		0.68	0.67	0.67
	Testing (0.1 M NaCl)	0.36	-	-
		0.80	-	-
NiHCF	Preparation	0.44	0.43	0.44
		0.59	0.60	no peak
	Testing (0.1 M NaCl)	0.30	0.30	0.32
		no peak	no peak	no peak
CuHCF	Preparation	0.17	-	-
		0.67	-	-
	Testing (0.1 M NaCl)	no peak	-	-
		0.55	-	-

\*estimated as the average of the anodic and cathodic peak potentials (V).

the proposed redox processes are in accordance with previous reported data for a stationary electrode [4]

The height of the two sets of redox peaks increases with the number of cycles.

### Transition Metal Hexacyanoferrates (III)

denoting an increase of the film thickness. The peak current intensity (estimated from a baseline) increases in the sequence  $Pt < G \approx GC$ . The cathodic peaks are better shaped than the anodic ones.

The cyclic voltammograms (after 50 cycles) for NiHCF modified RDEs made of Pt (fig. 1d) and GC (fig. 1e), show two reversible redox peaks more clearly defined than that recorded on G (fig. 1f). The first peak corresponds to the couple ( $Fe^{2+}/Fe^{3+}$ ) and is characterized by a formal potential of about 0.43 V/SCE. The second one belongs to the  $Ni^{2+}/Ni^{3+}$  couple and has a formal potential of about 0.6 V/SCE (table 1). Both for Pt and GC electrodes, the anodic and cathodic peaks appear at very closed potentials, proving a high degree of reversibility for the involved redox processes. On the G electrodes, only one clear redox couple can be observed at about 0.6 V/SCE, but it should be noted that the corresponding reversibility is quite low (fig. 1d), as was also reported in the literature [5].

In the case of CuHCF modified RDEs, the peaks appearing on the voltammograms for  $n = 50$  cycles, even for GC (fig. 1g), are less marked than for CoHCF- or NiHCF -modified electrodes.

Taking into account the apparent degree of reversibility, the peak resolution and the signal to background current ratio, Pt was preferred as electrode material for NiHCF- modified RDEs and GC for CoHCF and CuHCF modified RDEs.

#### *Influence of MHCF preparation conditions*

Various mixing ratios between the  $10^{-2}$  M metal salt solution (A) and the  $10^{-2}$  M  $K_3[Fe(CN)_6]$  solution (B) [ A/B = 1:1, 1:2, 2:1, 4:1, v/v] were investigated to prepare the MHCF complexes used as modifiers. The recorded cyclic voltammograms for NiHCF-modified RDE (fig. 2) show the existence of an optimum ratio (2:1) for which the film exhibits two sets of well defined, reversible redox peaks. This ratio was the same in the case of CoHCF- modified RDEs but 1:1 in the case of CuHCF- modified RDE.

For the same A/B ratio, on GC, the stability and the electrochemical activity of the films decrease in the sequence CoHCF > NiHCF > CuHCF.

#### *Influence of the scan rate and rotation speed*

For the GC/CoHCF-modified RDE cyclic voltammograms corresponding to different scan rates ( $0.4 \text{ V min}^{-1}$  -  $3.2 \text{ V min}^{-1}$ ) have been recorded at constant rotation

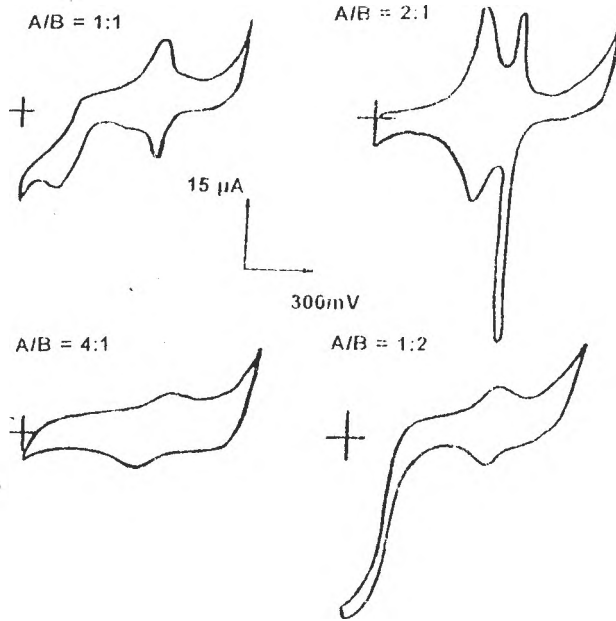


**Figure 2.** Influence of mixing ratios between the metal salt solution (A) and the  $K_3[Fe(CN)_6]$  solution (B) on the cyclic voltammograms corresponding to NiHCF modified Pt-RDE; other experimental conditions as in figure 1.

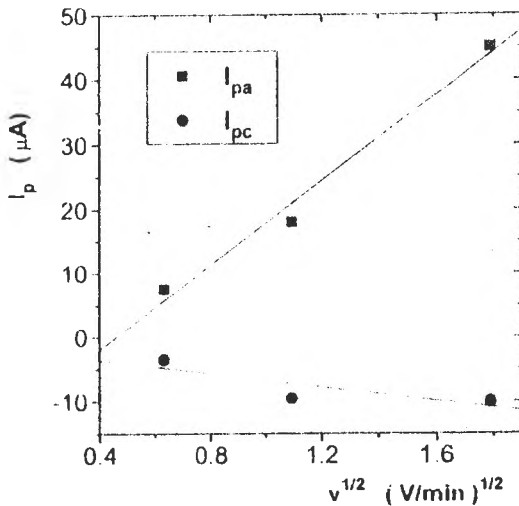


**Figure 3.** Anodic ( $I_{pa}$ ) and cathodic ( $I_{pc}$ ) peak currents vs. square root of scan rate ( $v^{1/2}$ ) corresponding to  $Fe^{2+}/Fe^{3+}$  redox couple for GC/CoHCF-modified RDE. Experimental conditions as in figure 1.

speed, in 0.5 M NaCl solution. The height of the anodic and cathodic peaks corresponding to  $Fe^{2+}/Fe^{3+}$  couple, for the CoHCF film increase linearly on  $v^{1/2}$  (fig. 3) in accordance with already reported data [3-5].

The shape and the peak potential values for the voltammograms corresponding to the GC/CoHCF-modified electrode not significantly influenced by the variation of rotation speed between 600 and 2200 rpm.



*Testing of ionic selectivity*

The MHCF-modified electrodes obtained in optimum conditions mentioned above, were tested in KCl, NaCl, LiCl and  $\text{NH}_4\text{Cl}$  solutions of various concentrations. The cyclic voltammetric responses corresponding to Co-, Ni- and CuHCF modified RDEs, dipped in KCl and NaCl are presented in figure 4.

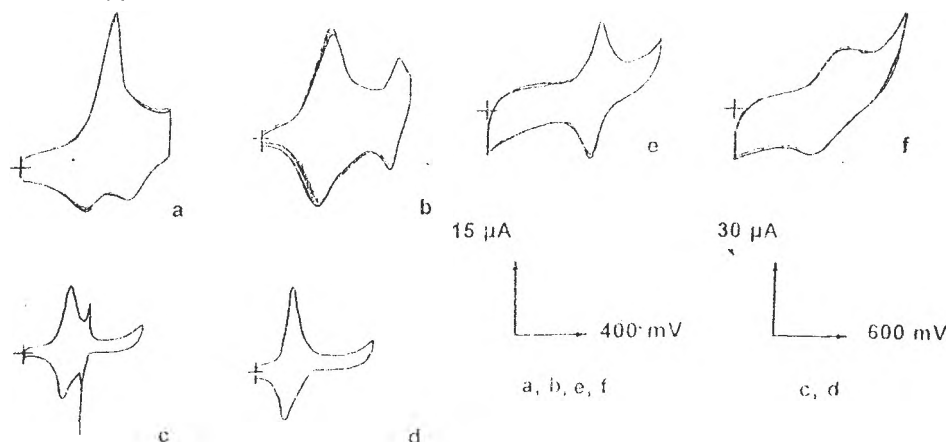


**Figure 4.** Cyclic voltammograms responses of Co-(a, b), Ni-(c, d), and Cu-(e, f)HCF-modified RDE in 0.1 M KCl (a, c, e) and 0.1 M NaCl (b, d, f). Experimental conditions: electrode material: GC for Co- and CuHCF; Pt for NiHCF; other experimental conditions as in figure 1.

The experimental results show that the electrochemical characteristics of the MHCF films deposited on RDEs are similar to those obtained on stationary electrodes reported in literature [4].

Irrespective of the MHCF nature, the electrochemical behaviour in KCl solutions (fig. 4 a, c, e) is similar to that noted during the electrode obtention (fig. 1 c, e and g), when KCl was used as electrolytic support.

Concerning the influence of  $\text{Na}^+$  ion on the response of the MHCF modified RDEs, first, it can be observed a pronounced difference between the voltammograms for the modified electrode preparation (fig. 1 c, e and g) and testing (fig. 4 b, d, f). This ionic selectivity is also reflected in the peak potentials shift induced by the replacement of  $\text{K}^+$  with  $\text{Na}^+$  inside the MHCF film (Table 1).

Second, it is worth to mention that a correlation between the nature of the ion and of the modifier can be found. Thus, the CoHCF-modified RDE shows for  $\text{Na}^+$

cyclic voltammograms with the best peak resolution and reversibility (fig. 4b) and the NiHCF-modified RDE is the most suitable for  $K^+$  (fig. 4c). For  $Li^+$ , the behaviour of GC/CoHCF-modified RDE (results not shown) is similar to that for  $K^+$ , but the value of formal standard potential for  $Fe^{2+}/Fe^{3+}$  couple inside the film is shifted toward less positive potentials (0.33 V/SCE). This is probably due to the difference between the hydrated ions radii [3]. Concerning the influence of  $NH_4^+$  on the investigated MHCF-modified electrodes it was noted (unshown results) that for this cation the electrochemical activity of the modified electrodes is very low and unstable. It was suggested that it is caused by the solubility of the ammonium substituted MHCF [6].

Third, a quasinerstian dependence ( $40 \text{ mV/pion} < \text{slope} < 66 \text{ mV/pion}$ ) between the formal standard potentials of CoHCF redox couple(s) and the  $Na^+$  and  $K^+$  concentration was found (fig. 5), recommending this kind of modified electrode as possible potentiometric sensors.

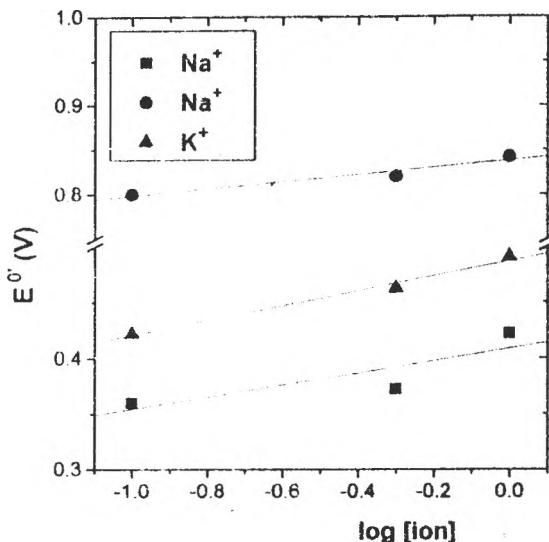


**Figure 5.** Dependence of the modifier formal standard potentials ( $E^\circ$ ) on  $\log[\text{ion}]$  for GC/CoHCF modified RDE. Experimental conditions as in figure 1.

## CONCLUSIONS

The main purpose of this work was to obtain MHCF-modified electrodes under controlled mass transfer conditions. First, it was found that no major differences between the behaviour of stationary and rotating disk modified electrodes occur,

### Transition Metal Hexacyanoferrates (III)

proving the good adherence of the modifier on the electrode surface. Second, the independence of the peaks intensity from the electrode rotating speed suggests that the ions transfer inside the modifier matrix should be the rate determining step for the charge transfer process.

For MHCF-modified RDEs, on the basis of our optimization study results, it was established the existence of a strong correlation between the nature of the electrode material, modifying agent and analyte, affecting their ionic selectivity.

In conclusion, it should be pointed out, that the presented method to obtain MHCF-modified electrodes seems to be promising to investigate the electrocatalytical properties of MHCF complexes.

### REFERENCES

1. J. A. Cox, R. K. Jaworski and P. J. Kulesza, Electroanalysis, **1991**, **3**, 869-877
2. K. Itaya, I. Uchida and V. D. Neff, Acc. Chem. Res., **1986**, **19**, 162-168
3. D. Engel and E. W. Grabner, Ber. Bunsenges. Phys. Chem., **1985**, **89**, 982-986
4. Z. Gao, G. Wang, P. Li and Z. Zhao, Electrochim. Acta, **1991**, **36** (1), 147-152
5. J. Joseph, H. Gomathi and G. P. Rao, J. Electroanal. Chem., **1991**, **304**, 263-269
6. S. Bharati, J. Joseph, D. Jeyakumar and G. P. Rao, J. Electroanal. Chem., **1991**, **319**, 341-345
7. V. Krishnan, A. L. Xidis and V. D. Neff, Anal. Chim. Acta, **1980**, **239**, 7-12
8. K. Kalcher, Electroanalysis, **1990**, **2**, 419-433
9. J. Labuda, Selective Electrode Rev., **1992**, **14**, 33-86
10. R. P. Baldwin and K. N. Thomsen, Talanta, **1991**, **38**(1), 1-16

Received: 15.03.1996



## SYNTHESIS AND STEREOCHEMISTRY OF SOME 4-ARYLIDENE-1-PYRIMIDINYL-2-PYRAZOLIN-5-ONES. PART VII.

Ioan Cristea\* and Ioan Panea

*Department of Organic Chemistry, "Babes-Bolyai" University  
11 Arany-Janos Str. 3400 Cluj-Napoca, Romania*

**Abstract.** 4-Arylidene-1-pyrimidinyl-2-pyrazolin-5-ones **2a-f** were synthesized by Knoevenagel condensation of the corresponding 1-pyrimidinyl-3-methylpyrazolin-5-one **1** with aromatic aldehydes. Chemical and spectral properties of the obtained compounds are reported.

### INTRODUCTION

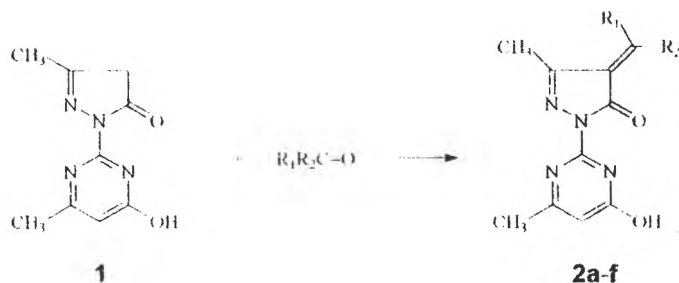
The 1-substituted-3-methylpyrazolin-5-ones which present a specific tautomerism react in the 4-position with aromatic aldehydes under acidic and basic catalysis to give 4-arylidene-pyrazolinones. The synthesis and chemistry of 4-arylidene-pyrazolinones have been of interest for some time [1,2]. These compounds are very useful intermediates in organic syntheses by their reactive conjugated system ( $C=C-C=O$ ).

Thus pyranopyrazoles [3] and pyrazolodiazepines [4], compounds with potent biological activity, were prepared by Michael cyclocondensation of 4-arylidene-pyrazolinones with various nucleophiles. Styryl dyes for color photography [5] or complexes with Co, Ce, Sa, Y [6,7] are also prepared from 4-arylidene-pyrazolinones. Some heterocyclic spirooxiranes have been used as intermediates in the synthesis of natural products [8] or labil antibiotics [9]. The stereochemistry of the 4-alkylidene- and 4-arylidene-pyrazolinones [10,11] by various methods have been reported.

### RESULTS AND DISCUSSION

1-(2-Pyrimidinyl)-3-methylpyrazolin-5-one **1**, obtained by an one pot synthesis [12] using aminoguanidine salts and ethylacetoacetate, was reacted with *p*-substituted aromatic aldehydes to give 4-benzylidene-1-(2-pyrimidinyl)-3-methyl-2-

pyrazolin-5-ones **2a-f**. This Knoevenagel condensation was studied under various conditions of acidic and basic catalysis (Scheme 1).



Compd.	<b>2a</b> (Z)	<b>2b</b> (E)	<b>2c</b> (Z)	<b>2d</b> (Z)	<b>2e</b> (Z)	<b>2f</b> (Z)
R <sub>1</sub>	H	C <sub>6</sub> H <sub>5</sub>	H	H	H	H
R <sub>2</sub>	C <sub>6</sub> H <sub>5</sub>	H	p-HO-C <sub>6</sub> H <sub>4</sub>	p-MeO-C <sub>6</sub> H <sub>4</sub>	p-Me-NC <sub>6</sub> H <sub>4</sub>	p-NO <sub>2</sub> C <sub>6</sub> H <sub>4</sub>

Scheme 1

The compounds **2a,b** were prepared by heating of **1** with benzaldehyde, at 140°C for 15 min. This reaction was monitored by TLC, and two diastereoisomers **2a** (Z) and **2b** (E) in ratio 3:1 were obtained and separated using preparative Merck plates and ethylacetate: i-propanol 9:1 as eluent [13,14]. The other compounds **2c-f** were obtained as a single stereoisomer (Z configuration) under the same reaction conditions. This reaction was also performed with various solvents as: MeOH, EtOH, dioxane, DMF under acidic or basic catalysis.

The best results were obtained using EtOH as solvent and AcOH as acidic catalyst for the compounds **2e,f** and Et<sub>3</sub>N as basic catalyst for the compounds **2c,d**. It can be observed that in the Knoevenagel condensation, benzaldehyde gives two stereoisomers whereas the p-substituted benzaldehydes give only one stereoisomer (Z-configuration). The Z-isomer is more stable energetically, because the phenyl ring is *anti* to the methyl group from the position 3 of the pyrazolinone ring (steric hindrances are minimized).

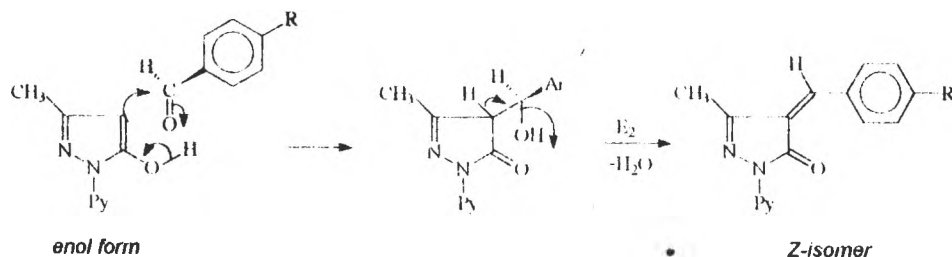
## Synthesis and Stereochemistry of some 4-Arylidene-1-Pyrimidinyl-2-Pyrazolin-5-ones

The experimental results are given in Table 1.

Table 1. Physico-chemical constants of the compounds **2a-f**

Compound	M.P. °C	Solvent recryst.	Yield %	Analysis calcd.	%N found
<b>2a</b>	192	EtOH	20	19.04	18.8
<b>2b</b>	175	EtOH	58	19.04	18.8
<b>2c</b>	297	MeOH	79	18.06	17.9
<b>2d</b>	245	i-Pr-OH	82	17.28	17.1
<b>2e</b>	273	DMF	87	20.77	20.5
<b>2f</b>	270	EtOH	72	20.83	20.7

In acid-catalyzed condensation, the pyrazolinone **1** reacts in the enol form with the *p*-substituted benzaldehyde which is oriented with phenyl ring in *anti* to the methyl group, thus affording the *Z*-isomer (see Scheme 2)



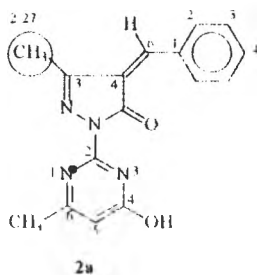
Scheme 2

The stereochemistry of exocyclic double bond in the 4-arylidene-pyrazolinones **2a-f** has been studied by <sup>1</sup>H-NMR spectroscopy. <sup>1</sup>H-NMR spectral data for the 4-arylidene-pyrazolinones **2a-f** and the reference compound **1** are summarized in Table 2. The assignments made are based on the chemical shift of the CH<sub>3</sub> group from the position 3 of the pyrazolinone ring, in the compounds **1**, **2a** and **2b**. Thus the chemical shift of the CH<sub>3</sub> group was found at 1.55 ppm in the *E*-isomer **2b**, upfield shift created by the shielding anisotropy of the *syn* phenyl ring, whereas the same chemical shift in *Z*-isomer **2a** was found at 2.27 ppm identical with that from

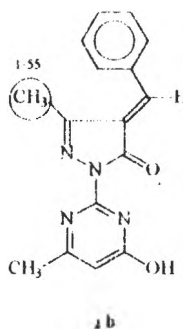
pyrazolinone **1**. This observation provides additional confirmations for the Z- and E-configuration of the exocyclic double bond in arylidene compounds **2**.

Table 2.  $^1\text{H-NMR}$  spectral data of the compounds **2a-f** and **1**. ( $\delta$  ppm)

Compd	Pyrazolinone ring		Pyrimidine ring		Benzene ring			Vinylic proton
	$\text{CH}_3(\text{C}_3)$	$\text{H}(\text{C}_4)$	$\text{H}(\text{C}_5)$	$\text{CH}_3(\text{C}_6)$	$\text{H}_2$	$\text{H}_3$	$\text{R}(\text{C}_4)$	$\text{H}(\text{C}_6)$
<b>1</b>	2.30	5.41	6.15	2.40				
<b>2a</b> (Z)	2.27		6.10	2.46	7.18 - 8.05 (m)			7.21
<b>2b</b> (E)	1.56		6.05	2.28	7.00 - 7.89 (m)			7.05
<b>2c</b> (Z)	2.25		6.12	2.42	6.48 (u)	8.42 (d)		7.32
<b>2d</b> (Z)	2.27		6.10	2.40	8.95 (d)	8.30 (d)	3.90	7.60
<b>2e</b> (Z)	2.30		6.14	2.37	6.80 (d)	8.45 (d)	3.10	7.35
<b>2f</b> (Z)	2.25		6.21	2.31	6.90 (d)	8.10 (d)		7.45



Z-isomer



E-isomer

## EXPERIMENTAL

Melting points were determined in capillaries and are uncorrected.  $^1\text{H-NMR}$  spectra were measured in  $\text{CDCl}_3$  on a 80 Mhz Tesla BS 487C spectrometer. TLC was performed with Merck Kieselgel 60F 254

### Synthesis of compounds **2a,b**

A mixture of the pyrazolinone **1** (0.2 g, 0.001 mol) and benzaldehyde (0.1 g, 0.001 mol) was heated to  $140^\circ\text{C}$  for 15 min using two boiling sticks to assist in the evolution of water. Dilution with an equal volume of methanol of the red syrup gave a mixture of two diastereoisomers **2a, b** which were separated using preparative Merck plates and ethylacetate : *n*-propanol 9:1 as eluent. The experimental data are given in Table 1.



## Synthesis and Stereo chemistry of some 4-Arylidene-1-Pyrimidinyl-2-Pyrazolin -5-ones

### General procedure for synthesis of compounds 2 c-f

A mixture of the pyrazolinone 1 (0.01 mol), *p*-substituted benzaldehydes (0.01 mol) in 20 ml EtOH and 1.5 ml AcOH (for compounds 2e, f) and 1.2 ml Et<sub>3</sub>N (for compounds 2c, d) was heated under reflux for 3 hrs. After cooling the coloured precipitate was filtered off, washed with EtOH and recrystallized (see Table 1).

### REFERENCES

1. J.De Ruiter, D.A Carter, W.S.Arledge and P.J.Sullivan, *J.Heterocycl.Chem.* 1987, **24**, 149
2. G.Cellerino, G.Desimoni, P.P.Righetti and G.Tacconi, *Gazz.Chim.Ital.*, 1973, **103**, 1247.
3. G.Tacconi, G.Gatti and G.Desimoni, *J.Prackt.Chem.*, 1980, **322**, 831.
4. A.El.Sayed, A.A.Fatty and S.Momduoh, *Z.Naturforsch.* 1980, **35**, 1313, C.A. 1981, **94**, 139754h.
5. Oriental Photo Ind.Co.Ltd.Japn.Kokai Tokkyo Koho, 1980, 80155055, C.A., 1981, **94**, 176695k.
6. F.A.Adam, *Bull.Sci.Assiut Univ.* 1988, **17**, 65, C.A., 1990, **112**, 190867q.
7. S.N.Ege, C.I.Tien, A.Diesk, B.E.Potter and B.K.Eagleson, *J.Chem.Soc. Chem.Commun.*, 1972, 682.
8. A.G.Schultz and C.K.Sha, *Tetrahedron*, 1980, **36**, 1757.
9. N.N.Gotra and N.L.Wendler, *Tetrahedron Lett.*, 1979, 4793.
10. S.N.Ege, A.D.Adams, E.I.Gress, K.S.Ragone, B.I.Kober and M.B.Lampert, *J.Chem.Soc. Perkin Trans* , 1983, 325.
11. K.Kirschke, P.Huber, G.Lutze, E.Grundemann and M.Ramm, *Liebigs Ann.Chem.*, 1994, 159.
12. I.Cristea and V.Farcasan, *Rev.Chim. (Bucharest)*, 1987, **38**, 674, C.A, 1987, **109**, 128937x.
13. S.Gocan, L.Olenic and I.Cristea, *Rev.Roum.Chim.*, 1990, **35**, 49.
14. S.Gocan, L.Olenic and I.Cristea, *Rev.Roum.Chim.*, 1989, **34**, 1509.

Received: 19.03.1996



## STUDY OF FREE AMINO-ACIDS FROM EQUISETUM EXTRACT

**T.Hodișan<sup>\*</sup>, Claudia Cimpoiu<sup>\*</sup>, Viorica Hodișan<sup>\*\*</sup> and C.Sârbu**

<sup>\*</sup> *Faculty of Chemistry and Chemical Engineering, "Babeș-Bolyai" University Cluj-Napoca, România*

<sup>\*\*</sup> *Faculty of Pharmacy, "Iuliu Hațieganu" University Cluj-Napoca, România*

### **Abstract**

Investigation of some representative medicinal plants starting with extraction and ending with identification of the amino-acids they contained, was performed by extraction of dried material with a solution of 1% hydrochloric acid and by double development: bidimensional on cellulose thin layer chromatography plates. The main advantage of thin layer chromatography for the analysis of plant extracts is its high sample throughput, since sample preparation requirements are minimal and multiple sample can be separated simultaneously. In this paper we are presenting the analysis of Equisetum extract containing the extraction, the separation and the identification of the free amino-acids by thin layer chromatography.

### **INTRODUCTION**

Throughout history people have been using the plants as drugs. Even at present the preparations based on plant extracts are used very often.

The isolation and the identification of active components from plants with biological activity are interesting for study of the structure-activity relationship.

The bioactivity materials can be tested by different analytical methods and procedea. The chromatographic methods allow the localisation of some active compounds such as: tannin, sugars, peptide, organic acids, flavone, amino-acids etc.

The isolation of amino-acids can be carried out by different extraction methods on dry material. Previous research mentions such methods as: direct extraction in water, in NaCl 5%, ethylic alcohol 5%, NaOH 0.25% [1]. Another method indicates the extraction of free amino-acids from plants in a methanol- water- hydrochloric acid mixture (18:1:1, v/v) [2]

The amino-acids identification and determination from plants can be carried out with chromatographic methods. Liquid chromatography with reverse phase based on C<sub>18</sub> as a

stationary phase which uses acetonitrile- buffer based on acetate [3], phosphate [2,4], citrate [5] or borate [6,7] as a mobile phase can be used. The detection has been made either by fluorescent detection after derivatization with phthalic anhydride [4,7], dansyl chloride [2,6] or by UV detection.

The thin layer chromatography is also often used for the separation and identification of amino-acids from plants. This method has many advantages, such as: multiple samples can be analysed simultaneously; the short time required, low detection limits [8]. As stationary phases silica gel or modified silica gel [9], polyamide [2] or chromatography paper [1] can be used and the most frequent detection procedure is ninhydrin spraying. In this paper we are presenting the Equisetum sample analysis including the extraction, the separation and the identification of free amino-acids by thin layer chromatography.

## Experimental

### The Extraction of Free Amino-acids

0.5 g dry plant was extracted in 10 mL of 1% hydrochloric acid solution. We added the  $[\text{Na}_3\text{P}(\text{W}_3\text{O}_{10})_4]$  solution for removing the proteins from the extract when these were precipitated. After centrifugation the solution was passed through an ion exchange Amberlite IR 120 H column. The column was eluted with 40 mL of 10% ammonia solution. The solution obtained was evaporated to dry and the residue was taken again in 1 mL of aqueous solution 30% (v/v) i-propanol.

### Separation and Identification of Free Amino-acids by TLC.

The separation and identification of free amino-acids from Equisetum extract are achieved by bidimensional TLC with double elution. The cellulose plates 20 x 20 cm are from Merck. The standard solutions of the eighteen essential amino-acids (1 mg/mL) and the extract solution were applied with some microdropper.

The elution was made 18 cm along in unsaturated N chamber using for the first dimension a n-butanol-acetone-acetic acid-water (35:35:7:23, v/v) mixture [10] and for the second dimension a methanol-water-pyridine (80:20:5, v/v) mixture as mobile phases.

Taking into account that we resorted to a double elution for each dimension after the first elution the plates were dried with hot air, then they were eluted in the same direction, along the same distance and with the same solvent mixture. The detection was carried out after the second elution by spraying the plates with a ninhydrin solution in butanol-acetone (1:1, v/v) then dried at 100-150°C for 10-15 minutes.

The standard solution of amino-acids was eluted in both systems, on different plates, at the same time with the extract sample. The identification of the amino-acids was achieved by comparing the  $R_f$  values.

## RESULTS AND DISCUSSION

The  $R_f$  values of amino-acids from standard and equisetum extract in both elution systems are presented in Table 1 and the separations in Figures 1 and 2.

In Figure 3 the separation of Equisetum extract is presented.

## Study of Free Amino-Acids from Equisetum Extract...

Table 1. The  $R_f$  values for standard amino-acids and Equisetum extract

amino-acid	Standard		Equisetum	
	$R_{f1}$	$R_{f2}$	$R_{f1}$	$R_{f2}$
glutamic acid	0.67	0.58	0,67	0,58
aspartic acid	0.58	0.42	--	--
DL-methionine	0.81	0.78	--	--
glycocoll	0.58	0.50	--	--
DL-alanine	0.44	0.72	0,44	0,72
L-arginine	0.50	0.43	--	--
L-proline	0.42	0.53	0,42	0,53
L-tyrosine	0.33	0.14	0,33	0,14
tryptophan	0.77	0.63	0,77	0,65
DL-asparagine	0.43	0.43	--	--
lysine	0.56	0.73	0,56	0,73
phenylalanine	0.83	0.82	0,83	0,82
L-isoleucine	0.85	0.92	0,85	0,92
L-histidine	0.32	0.30	0,32	0,29
L-leucine	0.88	0.89	--	--
DL-serine	0.53	0.57	0,53	0,57
DL-valine	0.72	0.87	0,72	0,87
DL-threonine	0.51	0.68	0,51	0,68

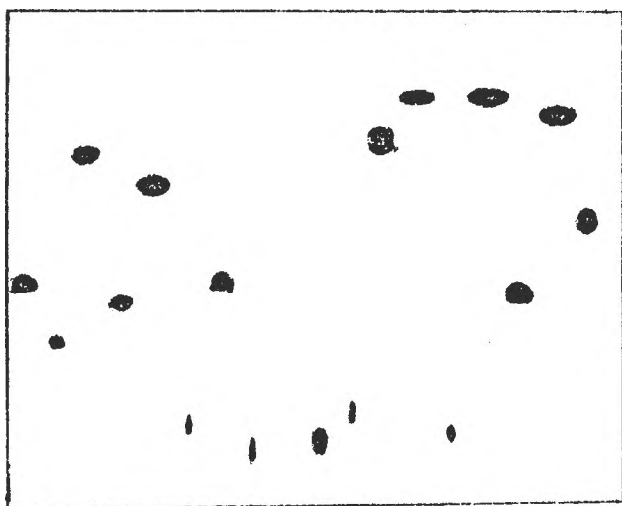


Figure 1. The amino-acids separation in the first solvent system

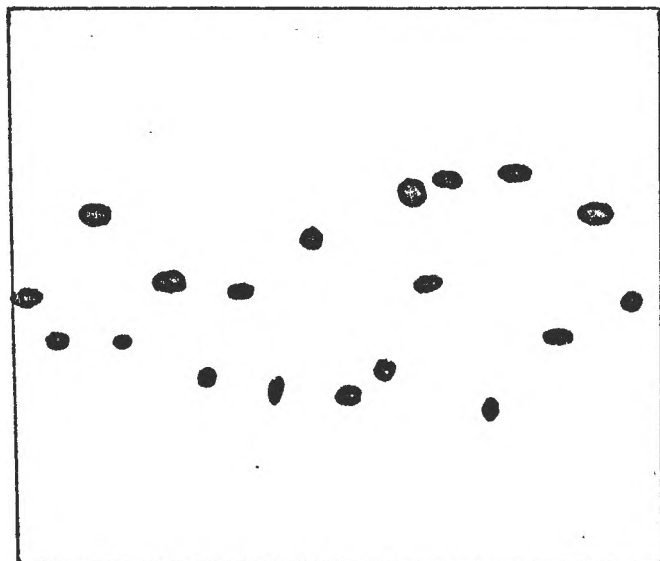


Figure 2. The amino-acids separation in the second solvent system.

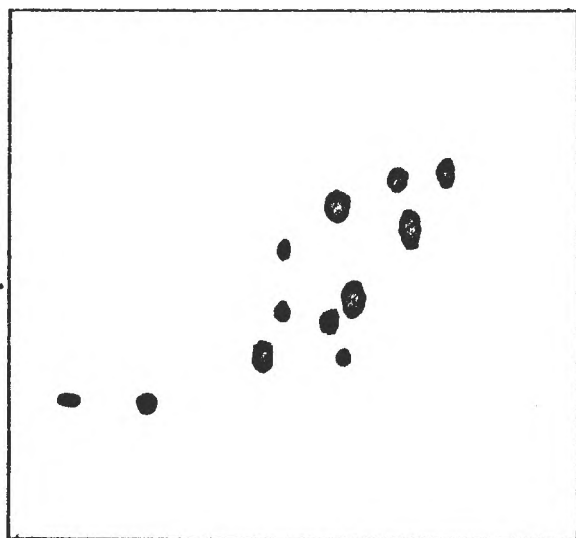


Figure 3. The separation of Equisetum extract

## CONCLUSIONS

The aim of this paper has been to find an efficient method for the separation and identification of free amino-acids from plant extracts. On the basis of the results obtained by TLC it was possible to determine the qualitative composition of amino-acids from plant extracts.

This method offers some advantages comparatively to other methods namely: it is simple, relatively fast, sensitive enough and it is one of the few methods which can be used without a special treatment of the sample

## REFERENCES

1. Ali, M. and Quedry, J., *J. Ind. Chem. Soc.*, 1987, **64**, 230.
2. De los Angeles Barcelon, Maria, *J. Chromatogr.*, 1982, **238**, 175.
3. Chen, Y., Fu, Y., Wang, G., Li, W. and Yang, G., *Yaown Fenxi Zazhi*, 1990, **10**, 149; *Anal Abstr.*, 1991, **53**(3), 3F93
4. Saunders, J.A., Morris, S. and Wyune, S.A., *Chromatogram*, 1988, **9**(1), 2.
5. Mortensen, J.V., *J. Chromatogr.*, 1981, **209**(1), 41.
6. Tsuruta, Y., Date, Y. and Kohashi, K., *J. Chromatogr.*, 1990, **502**(1), 178.
7. Wang, W. and Liu, H., *Fenxi Huaxue*, 1986, **14**(9), 700; *Anal. Abstr.*, 1987, **50**(6), 6D160.
8. York, H., Funk, W., Fischer, W. and Wimmer, H., *Thin Layer Chromatography*, vol. 1a, VCH Verlagsgesellschaft mbH, Weinheim, 1990.
9. Bhusman, R. and Ali, I., *J. Planar Chromatogr.*, 1990, **3**, 85.
10. Krafczyk, F., Helger, R. and Lang, H., *Z. Klin. Chem. u. Klin. Biochem.*, 1969, **7**, 521.

Received: 25.03.1996





## SOLVENT EXTRACTION OF DIOXOURANIUM(VI) WITH DIISOPROPYLDITIOPHOSPHORIC ACID AND TRIPHENIYLPHOSPHINE OXIDE

**Maria Curtui, Ionel Haiduc, Corina Pop**

*Facultatea de Chimie, Universitatea "Babes-Bolyai", Cluj-Napoca*

### ABSTRACT

The extraction of dioxouranium(VI) from aqueous solution with diisopropyldithiophosphoric acid and triphenylphosphine oxide in benzene was investigated. In order to establish the composition of the extracted species, the variation of the distribution ratio versus the parameters of the extraction system was measured. It was established that the organic phase contains a mixed ligand complex  $UO_2(iPrdt)_2TPPO$ . The high solubility of this adduct in benzene explains the synergic increase of the distribution ratio. The extraction constant and stability constant of the synergic adduct were determined. The extraction data are supported by spectral measurements.

### INTRODUCTION

In previous papers [1-7] we have investigated the extraction of dioxouranium (IV) with dialkyldithiophosphoric acids (Hdtp) in different organic solvents. The results show that a neutral complex  $UO_2(dtp)_2$  between dioxouranium(VI) and the dialkyldithiophosphate anion is formed, regardless of the nature of the solvent used. However the donor properties of the solvent are very important for the separation of dioxouranium(IV). When the extraction is carried out with oxygen free solvents, water may coordinate to  $UO_2(dtp)_2$  as demonstrated by Fischer titration by Fitoussi and Musikas[8] making the chelate complex less extractable into organic solvent. In the case of oxygen containing solvents, residual coordination in the chelate complex are occupied by hydrophoric solvent instead of water molecules making the complex more soluble in organic phase. This explains the higher values of the distribution ratios obtained in solvents as butanol and tributylphosphate [6,7]. A remarkable enhancement effect was observed in extraction with Hdtp and TPPO [9].

In the present paper we have investigated the influence of triphenylphosphine oxide (TPFO) on the extraction of dioxouranium(IV) with diisopropyldithiophosphoric acid (iPrdt)

**RESULTS AND DISCUSSION**

The extraction of dioxouranium(VI) aqueous solution with mixtures of HiPrdtp and TPPO in benzene (0.03M) was studied. The distribution ratio D data were obtained by keeping constant the total concentration of HiPrdtp+TPPO in benzene and varying the molar fraction of each extractant. The D values presented in Figure 1. show that HiPrdtp alone in benzene extracts poorly dioxouranium(VI) from aqueous solution of pH 0.7. The extraction of dioxouranium(VI) with 0.03M TPPO without HiPrdtp is negligible. When mixtures of HiPrdtp and TPPO are used, the distribution ratios are enhanced significantly, the maximum D values being obtained for 0.3-0.4 molar fraction of TPPO. The shape of the curve in Figure 1 suggests that a synergic effect takes place.

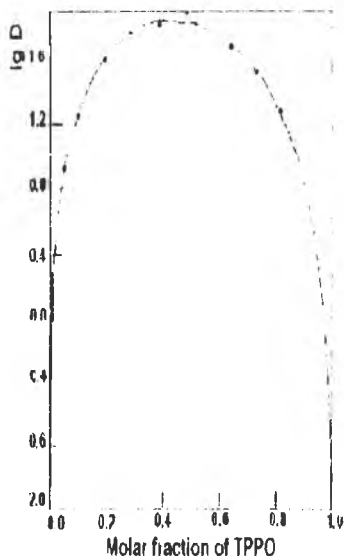
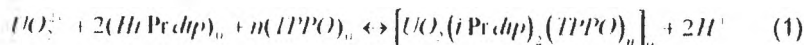


Fig 1 Extraction of dioxouranium(VI) with HiPrdtp - TPPO mixture in benzene  
 $C_{HiPrdtp+TPPO}=0.03M$ ;  $C_U=0.0005M$ ;  $pH=0.7$

Treatment of data

The extraction equilibrium of dioxouranium(VI) with HiPrdtp and TPPO in benzene can be described by equation.



where the index "o" indicates the organic phase

The equilibrium constant called "extraction constant" is given by (2).

$$K = \frac{[UO_2(HiPrdtp)_2(TPPO)_n]_o [H^+]^2}{[UO_2^{2+}] [HiPrdtp]_o^2 [TPPO]_o^n} \quad (2); \quad D = \frac{[UO_2(HiPrdtp)_2(TPPO)_n]_o}{[UO_2^{2+}]} \quad (3)$$

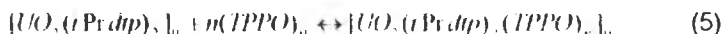
## Solvent Extraction of Dioxouranium(VI)

D is the distribution ratio of dioxouranium(VI) defined as the ratio of the total concentration of the metal in the organic phase and the total concentration of the metal in the aqueous phase. Introducing the distribution ratio D in equation (2) it follows that:

$$\log D = \log K + 2pH + 2\log[H\text{Prdtp}]_0 + n\log[TPPO]_0 \quad (4)$$

The equation (4) expresses the dependence of the distribution ratio versus different parameters of the extraction system, namely the pH of the aqueous phase, the concentration of HiPrdtp and the concentration of TPPO in the organic phase. According to equation (4) an investigation of the distribution ratio versus one of the extraction system parameters maintaining all other parameters constant can provide informations about extracted species.

The formation of the mixed species (synergic adduct) in the organic phase can be represented by the equilibrium



and the stability constant  $\beta$  is given by

$$\beta = \frac{[UO_2(i\text{Prdtp})_2(TPPO)_n]_0}{[UO_2(i\text{Prdtp})_2]_0 [TPPO]_0^n} \quad (6)$$

Distribution ratio D defined above as  $[UO_2^{2+}]_0 / [UO_2^{2+}]$  can be expressed by

$$D = \frac{[UO_2(i\text{Prdtp})_2]_0}{[UO_2^{2+}]_0} \left(1 + \sum_1^n \beta_n [TPPO]_0^n\right) \quad (7)$$

Therefore, the following equation can be derived

$$\frac{D}{D_0} = 1 + \sum_1^n \beta_n [TPPO]_0^n \quad (8)$$

where  $D_0$  denote the distribution ratio of dioxouranium(VI) in the absence of TPPO.

The plot of  $\log D / D_0$  versus TPPO concentration can be used to determine the stability constant of the synergic adduct [10,11].

### influence of the pH

The dependence of distribution ratio D on aqueous phase acidity at constant HiPrdtp concentration and constant TPPO concentration is presented in Figure 2. The slope 2 of the curve (1) shows that in the corresponding concentration range, two molecules of HiPrdtp are involved in the ion exchange mechanism. This result is in agreement with equation (1). The curve 2 in Figure 2 represents the extraction data

of dioxouranium(VI) with HiPrdtp alone. The shift of curve to the lower pH value in the presence of TPPO suggests that a synergic effect occurs.

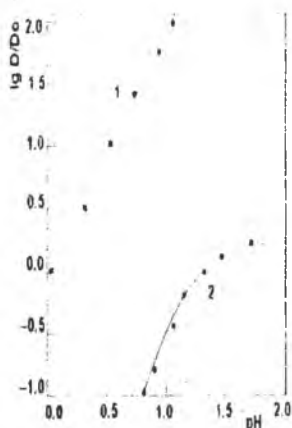


Fig.2 The influence of the pH in the aqueous phase  
HiPrdtp+TPPO curve (1), - HiPrdtp - curve (2)  
 $C_{\text{HiPrdtp}}=0.02\text{M}$ ;  $C_{\text{TPPO}}=0.01\text{M}$ ;  $C_{\text{U}}=0.001\text{M}$

#### Influence of TPPO concentration

The influence of TPPO concentration on the distribution of dioxouranium(VI) at constant pH of aqueous phase and constant HiPrdtp concentration was studied. The results presented in Figure 3 show that the distribution ratio increases linearly with TPPO concentration. The slope 1 of the curve obtained shows that only one TPPO molecule is associated with the extracted species of dioxouranium(VI). For small concentrations of TPPO, when  $[\text{TPPO}] < [\text{UO}_2^{2+}]$  a deviation of the slope unit value was observed because the amount of TPPO is not enough to transform all the  $\text{UO}_2(\text{iPrdtp})_2$  species into the 1:1 complex.

The combination ratio between uranium and TPPO in the complex involved in the extraction process was confirmed with the aid of Job's method of continuous variations adjusted for the ternary system by Ihle and Michael [12] (Fig 4).

#### Extraction mechanism

From the data presented in Figures 2, 3 and 4 it appears that the combination ratio of U:HiPrdtp:TPPO is 1:2:1. The extraction of dioxouranium(VI) with HiPrdtp and TPPO follows the equation (1), where  $n=1$ . The mixed complex  $\text{UO}_2(\text{iPrdtp})_2\text{TPPO}$  is the species responsible for the synergic enhancement of extraction. In fact, this complex was isolated as solid adduct by preparative method and the same combination ratio was established [13]. The IR spectrum of benzene extracts are similar to the spectra obtained for the complex isolated in the solid state.

## Solvent Extraction of Dioxouranium(IV)

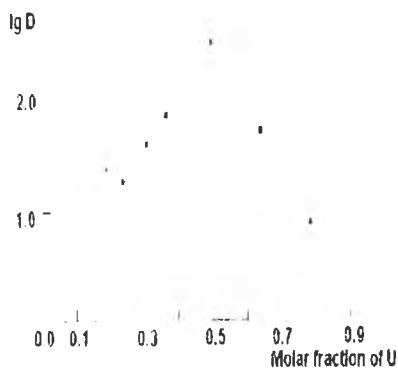
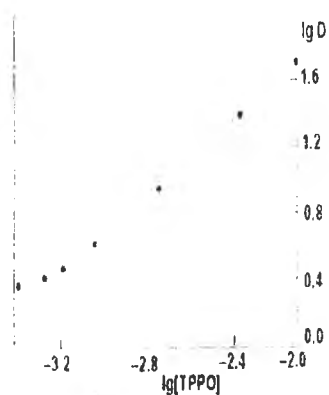


Fig 3 The influence of TPPO in benzene  $C_{\text{HfPrdtp}}=0.02\text{M}$ ,  $C_{\text{U}}=0.001\text{M}$ ;  $\text{pH}=0.7$ . Fig 4 Continuous variation method

The band at  $928\text{ cm}^{-1}$  is due to the asymmetrical stretching vibration of the linear dioxouranium group. The band due to the  $\text{P}=\text{O}$  group stretching in TPPO, which in the spectrum of the free ligand occurs at  $1195\text{ cm}^{-1}$ , is shifted towards lower wave numbers and is split in two sharp components. This confirms the coordination of triphenylphosphine oxide to the metal

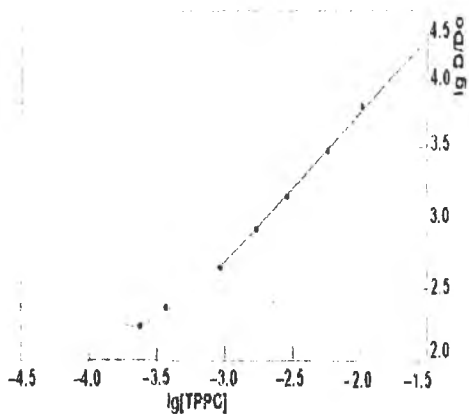


Fig 5 Variation of  $D/D_0$  as a function of TPPO concentration in benzene

### Extraction and stability constants

Using the data presented in Figures 2 and 3 the extraction constants were calculated. The value of  $\log K$  is  $5.8105$ . The plot of  $\log D/D_0$  versus TPPO concentration (Fig 5) was used to determine the stability constant of the synergic adduct. The value of  $\log \beta$  is  $5.85$ . The constants determined are not thermodynamic constants since the activity coefficients were ignored. They can serve only for comparing various extraction systems under similar conditions

## EXPERIMENTAL

**Materials:** The diisopropyldithiophosphoric acid was synthesized by the reaction of tetraphosphorus decasulfide with the appropriate alcohol, according to published procedures and were purified by vacuum distillation [14]. Tetraphosphorus decasulfide, uranium salt and Arsenazo III were supplied by Aldrich Chemie and Ventron A.G., Germany. Triphenylphosphine oxide was prepared by oxidation of triphenylphosphine with  $\text{KMnO}_4$  [14]. All other solvents or reagents were of analytical grade.

The acidity of the aqueous phase was determined with an Orion Model 611 pH meter/milivoltmeter. A Spekol C. Zeiss Jena (DDR) spectrophotometer was used for the colorimetric determination of uranium (VI).

**Operating procedure** - the extractions were carried out in 100 ml separation funnels. Equal volumes (100 ml) of aqueous solutions (0.01-0.0005M uranium) and organic phases containing the appropriate concentration of HiPrdtp and TPPO in benzene were shaken together at room temperature (20±2°C) for 5 min. After the phases were separated, the concentration of uranium in the aqueous phase was determined photometrically with Arsenazo III [15]. In all experiments the ionic strength was kept constant (1 M) with  $\text{HNO}_3$  and  $\text{NaNO}_3$ .

## REFERENCES

1. G. Marcu, M. Curtui, I. Haiduc, *J. Inorg Nucl Chem.*, 1977, **39**, 1415
2. M. Curtui, I. Haiduc, G. Marcu, *J. Radioanal Chem.*, 1978, **44**, 109.
3. M. Curtui, I. Haiduc, *J. Radional Nucl Chem.*, 1984, **86**, 281
4. M. Curtui, M. Diaconeasa, G. Marcu, I. Haiduc, *Studia Univ Babes-Bolyai, Chemia*, 1976, **21**, 63
5. I. Haiduc, M. Curtui, I. Haiduc, *J. Radional Nucl. Chem., Articles*, 1986, **99**, 257
6. G. Marcu, I. Haiduc, M. Curtui, *Studia Univ Babes-Bolyai, Chemia*, 1977, **22**, 49.
7. I. Haiduc, M. Curtui, G. Marcu, *Rev Roum Chim.*, 1977, **22**, 625.
8. R. Fitoussi and C. Musikas, *Sep. Sci. Technol.*, 1980, **15**, 345.
9. M. Curtui, I. Haiduc, *J. Inorg. Nucl. Chem.*, 1981, **43**, 1076.
10. L. G. Sillen, *Acta Chem. Scand.*, 1956, **10**, 186
11. D. D. Durssen, L. G. Sillen., *Acta Chem. Scand.*, 1953, **7**, 663.
12. H. Ihle, H. Michael, A. Murenhof, *J. Inorg. Nucl. Chem.*, 1963, **25**, 734
13. I. Haiduc, M. Curtui, *Syn. Reaci. Inorg. Metal -Org. Chem.*, 1976, **6**, 125
14. K. Sasse, *Methoden der Organischen Chemie* (Huben-Weyl) Band XII, Teil 2, p.684, G. Thieme Verlag, Stuttgart, 1964.
15. S. B. Savin, *Talanta* 1961, **8**, 673

Received: 25.03.1996

## Synthesis of 1,3-Oxathiane and Perhydro-1,3-Thiazine Derivatives

Luminita Muntean, Ion Grosu and Sorin Mager\*

"Babes-Bolyai" University, Organic Chemistry Department, 11 Arany Janos str.,  
RO-3400, Cluj-Napoca, Roumania

**Abstract.** - The results of the exhaustive literature investigations on the methods used in the synthesis of the 1,3-oxathiane and perhydro-1,3-thiazine rings bearing different substituents are critically presented. Some comparisons with the data reported for the synthesis of other saturated heterocycle systems with six membered rings with two heteroatoms are also developed

### INTRODUCTION

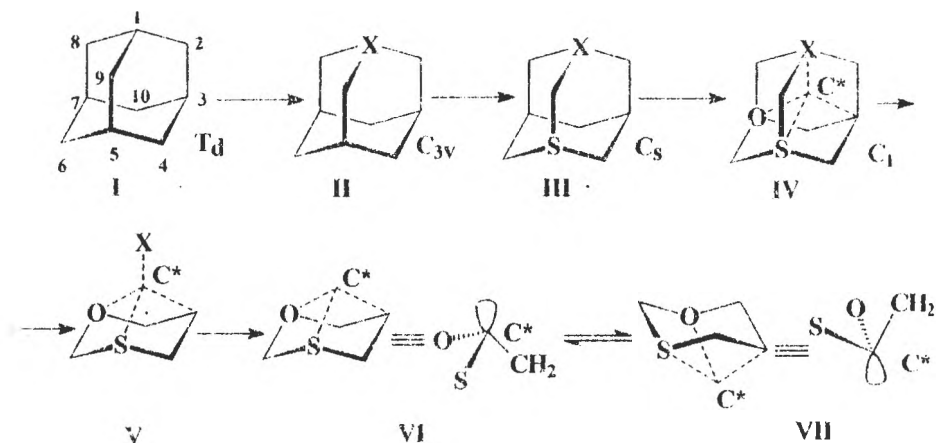
The interest for the syntheses and the investigations on the proprieties of compounds displaying six-membered rings with two different heteroatoms in the positions 1 and 3 is determinate by three main reasons.

These heterocycles (as well as the other six-membered rings bearing heteroatoms in positions 1 and 3) represent an ideal field for investigations on the stereochemistry of saturated six-membered rings [1-8]. The fragmentation of the carbocycle in the positions 1 and 3 makes possible a powerful use of the NMR methods. The magnetic environments of the protons and carbon atoms of the heterocycle are quite different (the signals are dispersed on a large range) and the splitting pattern for the protons is ideal; thus the spectra offer the necessary structural information without being unusually complicated.

A great number of the synthesized compounds showed to be useful in a large domains of interest (e.g. as liquid crystals [9,10], in medicine [11-13], as cosmetics [14,15] in the syntheses of pheromones [16], herbicides [17] or fungicides [18] or as auxiliaries in stereoselective reactions [19-22]).

These types of heterocycles are chiral (recent investigations [23])

explained the chirality of these six-membered rings by the presence of a virtual triligand chiral center obtained by the desymmetrization of adamantane, e.g. 1,3-oxathiane Scheme 1). The possibility to fructify this behavior in stereoselective transformations is taken into account.



Scheme 1

## Discussion

### 1. Synthesis of 1,3-oxathiane derivatives

Despite the significant number of known derivatives of this heterocycle, a limited number of methods were used in their synthesis. The main pathway for a convenient ring closure is the direct reaction of the carbonyl compound with  $\gamma$ -thioalcohols. Compounds bearing different substituents in position 2 or located on the sulfur atom have been obtained by specific reactions carried out on the above obtained 1,3-oxathiane rings

#### 1.1. Direct reaction between $\gamma$ -thioalcohols and carbonyl compounds

The conditions used for the reaction of carbonyl compounds with  $\gamma$ -thioalcohols (as in the cases of acetalization and thioacetalization reactions used for the synthesis of 1,3-dioxane or 1,3-dithiane compounds) are quite different;



## Synthesis of 1,3-Oxathiane and Perhydro-1,3-Thiazine Derivates

they are correlated with the reactivity, solubility and stability of the carbonyl compounds,  $\gamma$ -thioalcohols and the resulted 1,3-oxathiane derivatives.

### 1.1.1 Condensation of aldehydes

The condensation reaction of  $\text{CH}_2\text{O}$  with  $\gamma$ -thioalcohols shows different yields depending on the nature of solvent, catalyst and temperature used in the syntheses. (Scheme 2, Tables 1 and 2).



Scheme 2

Table 1. 1,3-Oxathiane compounds obtained starting from formaldehyde

Compound	R <sub>1</sub>	R <sub>2</sub>	R <sub>3</sub>	R <sub>4</sub>	R <sub>5</sub>	R <sub>6</sub>
1	H	H	H	H	H	H
2	CH <sub>3</sub>	H	H	H	H	H
3	H	H	H	H	C <sub>6</sub> H <sub>5</sub>	H
4	H	H	CH <sub>3</sub>	H	H	H
5	H	H	H	H	CH <sub>3</sub>	H
6	H	H	H	H	CH <sub>3</sub>	CH <sub>3</sub>
7	CH <sub>3</sub>	H	CH <sub>3</sub>	H	CH <sub>3</sub>	H
8	CH <sub>3</sub>	H	H	H	CH <sub>3</sub>	CH <sub>3</sub>
9	CH <sub>3</sub>	CH <sub>3</sub>	H	H	CH <sub>3</sub>	H

The best results were obtained at room temperature using the water as solvent and the sulfuric acid as catalyst. The reaction in benzene as well as in dichloromethane with azeotropic distillation of the water (performed in similar conditions to those used in the synthesis of some 1,3-dioxane derivatives [30])

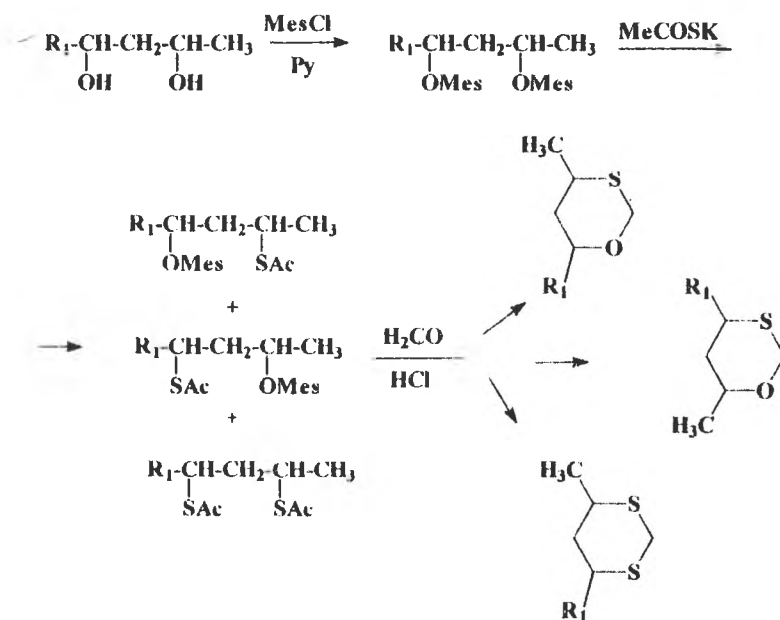
proceeds with very small yields (about 15-20%).

Table 2. Conditions used in the synthesis of compounds 1-9

Compounds	Solvent	Catalyst	Temperature	Yield %	Reference
1-3	benzene	PTSA*	78-80 °C	14-23	[24]
4-7	CH <sub>2</sub> Cl <sub>2</sub>	PTSA	40-42 °C	19-66	[25-28]
8, 9	H <sub>2</sub> O	H <sub>2</sub> SO <sub>4</sub>	-	85-92	[29]

\*PTSA = para-toluenesulfonic acid

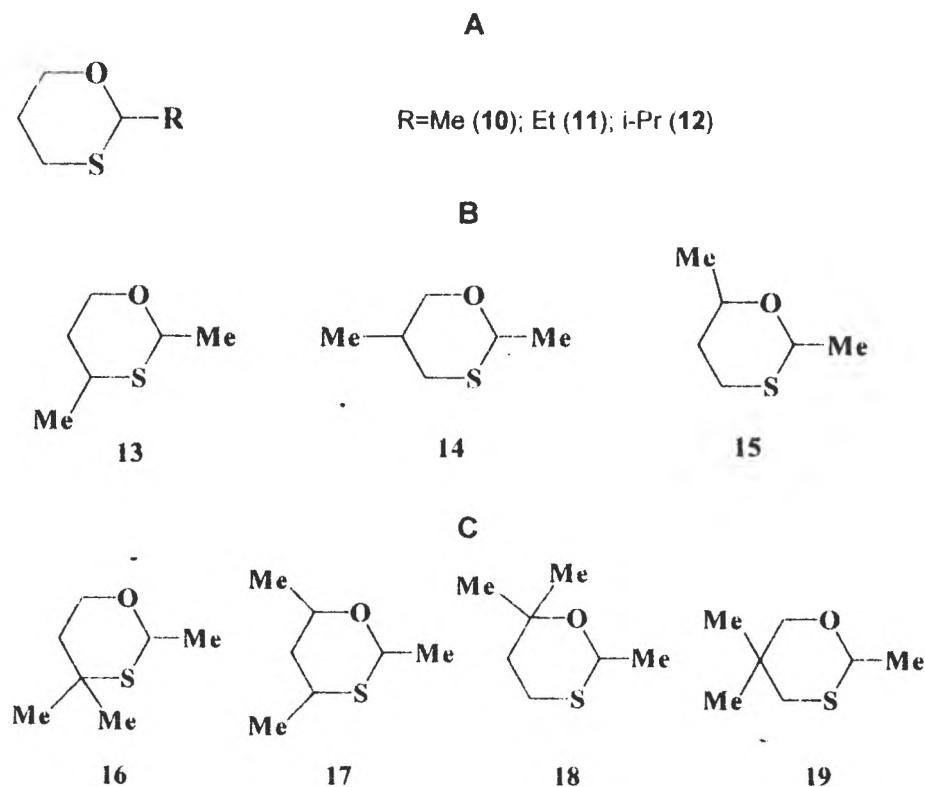
The reactions using protected  $\gamma$ -thioalcohols lead simultaneously to 1,3-oxathiane and 1,3-dithiane derivatives [31]. The derivatives of the two heterocycles can be easily separated by using chromatographic methods. The reactions (Scheme 3) are performed in methanol, with HCl as catalyst and are practically total.



Scheme 3

## Synthesis of 1,3-Oxathiane and Perhydro-1,3-Thiazine Derivates

The reactions with other aliphatic aldehydes have been performed in  $\text{CH}_2\text{Cl}_2$  (at the reflux of the solvent) in acid catalysis (PTSA) separating (by azeotropic distillation) the water formed in the synthesis [25-28]. Some attempts to correlate the values of the yields obtained in the synthesis of the three series of compounds A, B and C (Scheme 4) with the reactivity of the aldehyde or of the  $\gamma$ -thioalcohols were made.



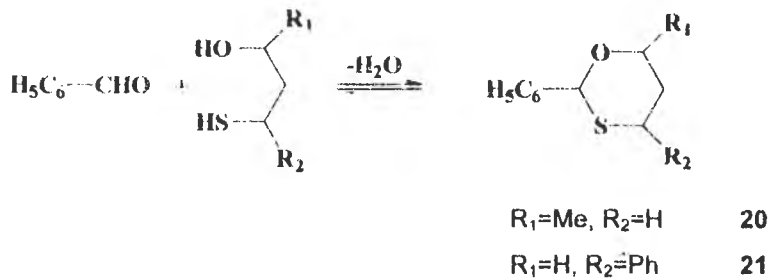
Scheme 4

In A series the increasing of the reactivity of carbonyl compound brings about higher yields for the synthesis of the heterocycle compounds: **10** (77%), **11** (69%) and **12** (60%). The reactivity of the methylated and dimethylated  $\gamma$ -thioalcohols does not significantly influence the yields calculated for the

condensation of these  $\gamma$ -thioalcohols with acetaldehyde resulting into the compounds of B [13 (81%), 14 (90%) and 15 (69%)] and C [16 (42%), 17 (78%); 18 (75%) and 19 (69%)] series. The better results obtained in the synthesis of compound 14 compared with those of compounds 13 and 15 are due to lower steric interactions of the methyl groups in the transition state of the reaction for this compound. The low yield observed in the synthesis of compound 16 (to be compared with the other compounds of the C series) is due probably to the hinderance (in the transition state) associated with the axial methyl group located close to the sulfur atom.

4-Propyl-1,3-oxathiane derivatives were obtained in good yields [32-34] in diethylether using PTSA as catalyst. For removing the water, molecular sieves were used. The reaction showed low yields of only 44%, at room temperature, but at higher temperature (reflux of the solvent) removing the water with a Dean-Stark trap (azeotrop with benzene) and by using PTSA as catalyst, excellent yields, (about 85%) have been obtained. Higher performance (yield 94%) was obtained replacing benzene with cyclohexane and performing the reaction at the reflux temperature of the solvent [14].

The reaction of aromatic aldehydes with the  $\gamma$ -thioalcohols performed in same conditions as those used in the acetalization reaction of 1,3-diols (azeotropic distillation of the water and PTSA as catalyst) showed very small yields, the reaction equilibria being strongly shifted towards the starting compounds (Scheme 5) [24]. In the presence of the  $\text{Et}_2\text{O} \cdot \text{BF}_3$  complex higher yields were reported [10].

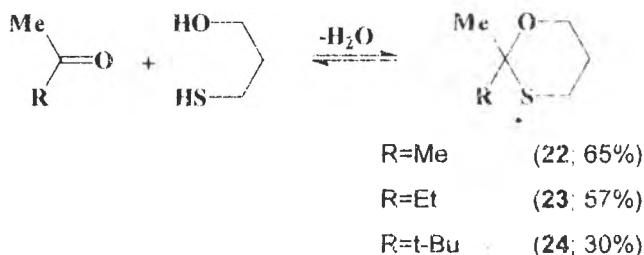


Scheme 5

## Synthesis of 1,3-Oxathiane and Perhydro-1,3-Thiazine Derivates

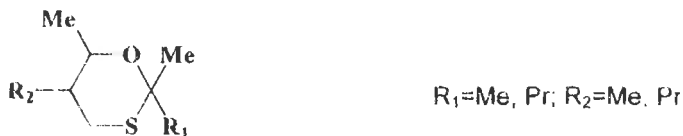
### 1.1.2 Condensation with ketones

The condensation reactions of  $\gamma$ -thioalcohols with ketones are performed in  $\text{CH}_2\text{Cl}_2$ , using PTSA as catalyst and the azeotropic removal of water [25-28]. The yields (32-85%) can be correlated with the reactivity of the ketones as it may be observed for compounds **22-24** (Scheme 6).



Scheme 6

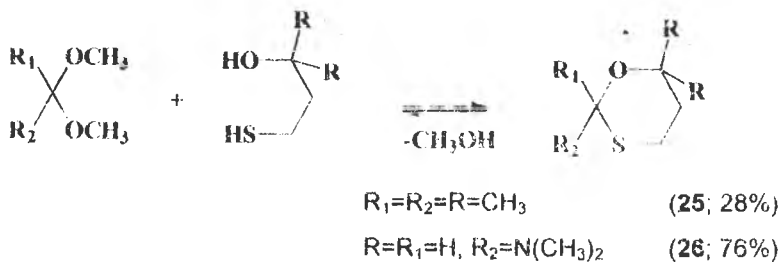
Compounds displaying tetrasubstituted rings (Scheme 7) were obtained by the condensation reaction of some ketones with  $\gamma$ -thioalcohols without solvent but with acidic catalysis (yields 75-82%) [35].



Scheme 7

### 1.2. Reactions of acetals with $\gamma$ -thioalcohols

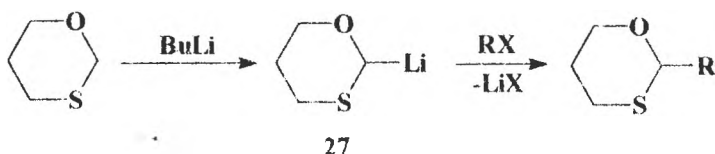
The reaction of the ketals of acetone and DMF with  $\gamma$ -thioalcohols led to 2-substituted-1,3-oxathianes in usual conditions (Scheme 8) [25].



Scheme 8

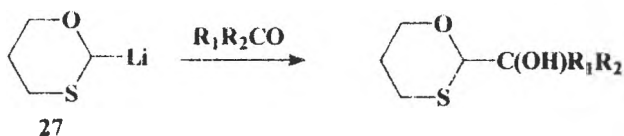
### 1.3. Reactions of lithiated oxathianes with electrophyls

The 1,3-oxathiane derivatives easily react with BuLi to give 2-lithiated-1,3-oxathianes. The reaction of these ones with a large number of electrophilic reagents leads to the corresponding series of the 1,3-oxathiane derivatives bearing substituents in the position 2 of the heterocycle. (Scheme 9).



Scheme 9

Alkylated ( $R=CH_3$ ,  $C_2H_5$ ,  $n-C_3H_7$ ,  $i-C_3H_7$ ,  $i-C_4H_9$ ,  $CH_2-C_6H_5$ ) or acylated ( $R=CH_3CO$ ) compounds were obtained in very good yields (up to 99%) by this procedure. The reactions were performed in THF at  $-78^\circ C$ . Yields have been correlated with the reactivity of the halogenous derivatives in the  $SN_2$  reaction [36, 37]. The reaction of the 2-lithiated-1,3-oxathiane with ketones leads to substituted compounds with a tertiary alcohol group in the ketal part of the heterocycle (Scheme 10).

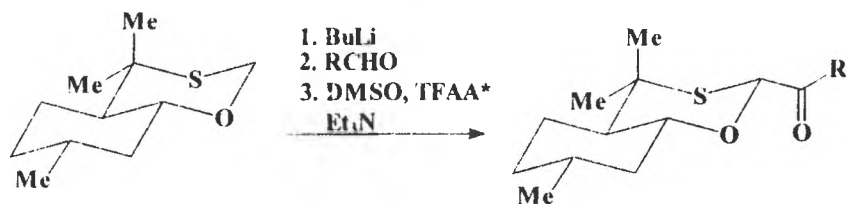


Scheme 10

The unenolizable ketones give the best yields (up to 86%). The reaction of aldehydes (in the presence of DMSO and the anhydride of trifluoroacetic acid) has as intermediate the secondary alcohol which is oxydized to a carbonyl compound (Scheme 11). The synthesized compounds showing a carbonyl group located in the position 2 of the heterocycle were then used in asymmetric synthesis [38,39].

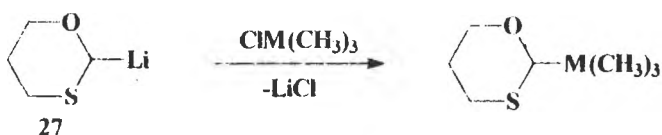
The lithiated compounds were also considered to prepare 2-substituted-1,3-oxathianes with trimethylmetal ligands of elements of the group XIV (Si, Ge,

## Synthesis of 1,3-Oxathiane and Perhydro-1,3-Thiazine Derivates



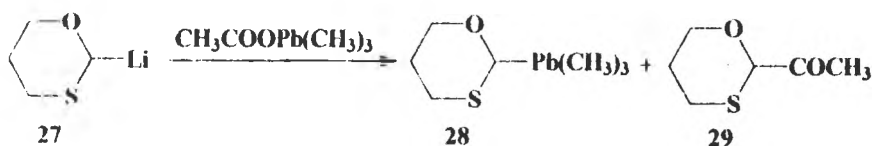
Scheme 11

Sn, Pb; Scheme 12).



Scheme 12

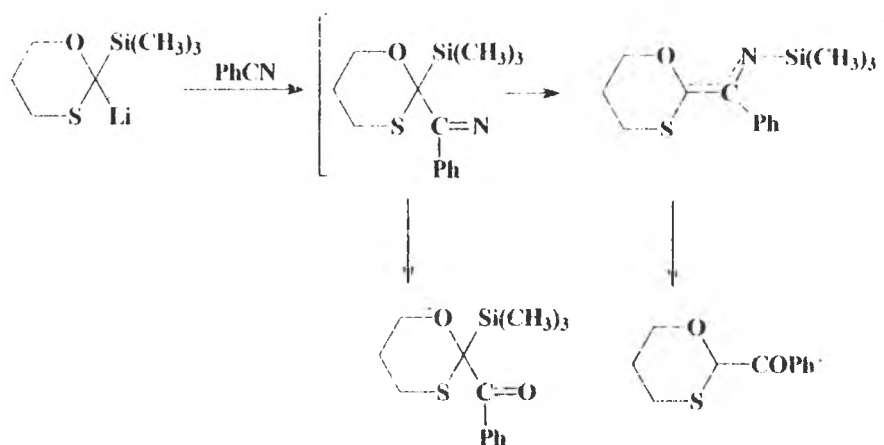
An interesting situation occurs in the reaction of trimethyllead acetate with lithiated 1,3-oxathiane when a mixture of the 2-substituted compounds with trimethyllead and acetyl groups are obtained (Scheme 13) [36].



Scheme 13

The yields calculated for the organometallic and for the acetylated compounds were 70 % and 16%, respectively.

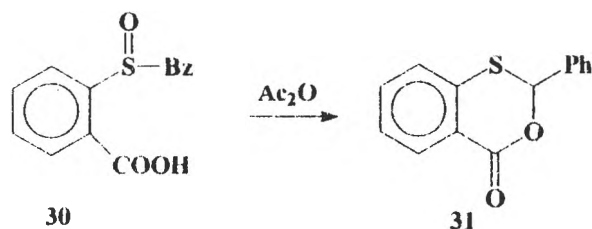
The lithiated trimethylsilyl derivative was transformed with good results (yield 73%) in 2-benzoyl-1,3-oxathiane (Scheme 14) [40].



Scheme 14

2-Methoxy-1,3-oxathiane was obtained starting from the aminotosylated heterocycle in reaction (at room temperature) with methanol (yield 34%) [36].

The intramolecular condensation reaction of 2-S-benzylsulfonylbenzoic acid (Scheme 15) in the conditions of Pummerer [41] reaction ( $130^\circ\text{C}$ , using acetic anhydride) leads to a benzo-1,3-oxathiane substituted with a phenyl group in the position 2 of the heterocycle [41].



Scheme 15

## 2. Synthesis of derivatives of perhydro-1,3-thiazine

The syntheses of a few number of compounds displaying this ring are reported in the literature. The main way of access to this heterocycle is the direct condensation of  $\gamma$ -thioamine with carbonyl compounds. The difficulties

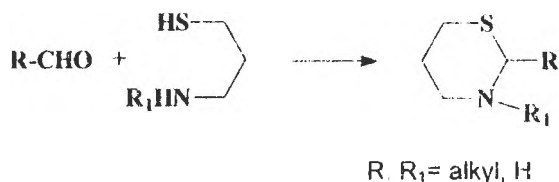


## Synthesis of 1,3-Oxathiane and Perhydro-1,3-Thiazine Derivates

generated by the low reactivity of some carbonyl compounds as well as the low yields of the reactions have determined the investigations for other routes to this purpose. The reduction reaction of some 1,3-thiazine-4-ones and 1,3-dihydro-thiazines showed to be a good solution in some of the cases. The lithiation reaction of some 1,3-thiazine derivatives, followed by the reaction of the lithiated heterocycles with electrophyls resulted into 2-substituted 1,3-thiazines series.

### 2.1. Condensation reactions of $\gamma$ -aminothiols with carbonyl compounds

The reactivity of  $\gamma$ -aminothiols in the ring closure reaction with carbonyl compounds is significantly smaller than the reactivity of 1,3-diols, 3-amino-1-propanols or  $\gamma$ -thioalcohols. The  $\gamma$ -aminothiols react only with aliphatic aldehydes (Scheme 16); no condensation occurred when  $\gamma$ -aminothiols were reacted with aromatic aldehydes or ketones[42-44].



R, R<sub>1</sub> = alkyl, H

Scheme 16

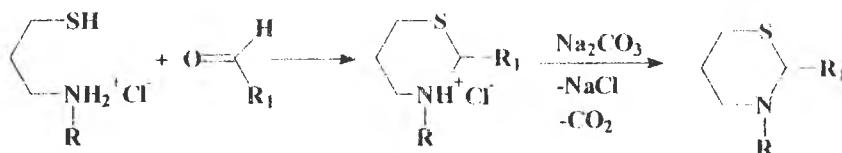
In the presence of  $\gamma$ -aminothiols the aliphatic ketones are transformed into acyclic thioketals; this reaction (Scheme 17) is preferred for the ring closure reaction [45].



Scheme 17

The reaction of formaldehyde carried out in the usual manner, in benzene (in acidic catalysis) with the removal of water by azeotropic distillation,

gives small yields [45]. Contrary, the reaction performed in dried ethanol, using HCl as catalyst shows very good yields (about 99 %) to give the perhydrothiazine hydrochloride (Scheme 18  $R=R^1=H$ ). The free base of thiazine was isolated in reaction with a solution of  $\text{Na}_2\text{CO}_3$  (yield of the separation 77%) [42].



Scheme 18

The reaction of N-alkyl- $\gamma$ -aminothiols with formaldehyde carried out in similar conditions led to N-alkyl-1,3-thiazine (Scheme 18,  $R=\text{Me, Et, Pr}$ ;  $R^1=H$ ) with good yields up to 77 % (free base). Other aldehydes (Scheme 18;  $R=R^1=\text{Me, Et, Pr}$ ) react similarly but the yields are in the range of 21-61% in correlation with the lowest reactivity of the carbonyl compounds and with the steric hindrance introduced by the alkyl group bonded to the nitrogen atom of the heterocycle [e.g. compounds: **32**  $R=H$ ,  $R^1=\text{CH}_3$  (yield 95%); **33**  $R=R^1=\text{CH}_3$  (47%) and **34**  $R=\text{C}_2\text{H}_5$ ,  $R^1=\text{CH}_3$  38%) [50].

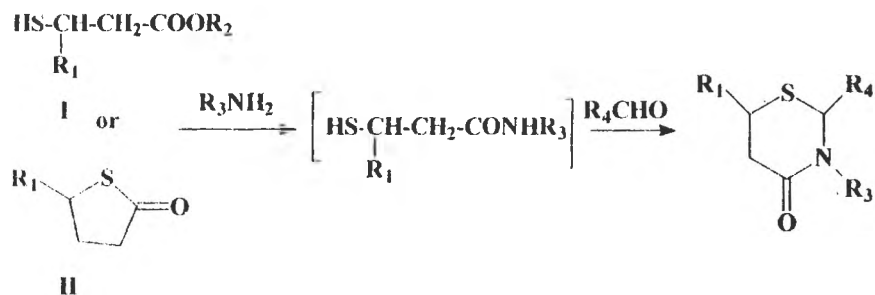
## 2.2. The reduction of the derivatives of perhydro-1,3-thiazine-4-one

The starting perhydro-1,3-thiazine-4-ones can be obtained by the reaction of aldehydes with  $\gamma$ -thiol-amides [these last available from thiol-esters (I) or from cyclic thioamides (II) in reaction with amines]. The reactions are performed in benzene (azeotropic distillation of water) with yields up to 76% (Scheme 19) [45].

2-Phenyl-perhydro-1,3-thiazine-4-ones are obtained by the intramolecular condensation (a Pummerer type reaction) of N-substituted-3-benzyl-sulfinyl-propionamide in the presence of the mixed anhydride of trifluoroacetic and

## Synthesis of 1,3-Oxathiane and Perhydro-1,3-Thiazine Derivates

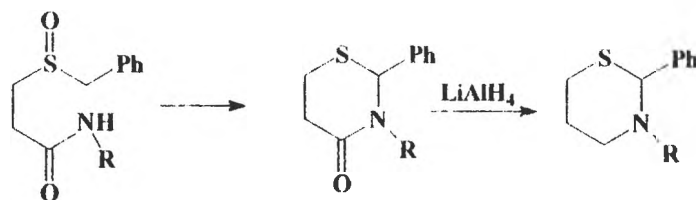
acetic acids ( $\text{CH}_3\text{CO-O-OC-CF}_3$ ) The reaction (Scheme 20) is performed in nitrogen atmosphere at 110-120 °C. The perhydro-1,3-thiazine-4-ones are then reduced (Scheme 20) to the corresponding desoxy-compounds with  $\text{LiAlH}_4$  (yield 45%) [41].



$\text{R}_1 = \text{H, Me; R}_2 = \text{Me, Ph, Bz}$

$\text{R}_3 = \text{H, Me, Ph; R}_4 = \text{Me, Et}$

Scheme 19



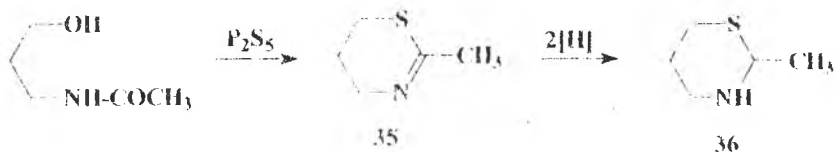
Scheme 20

### 2.3. Reductions of dihydro-1,3-thiazines

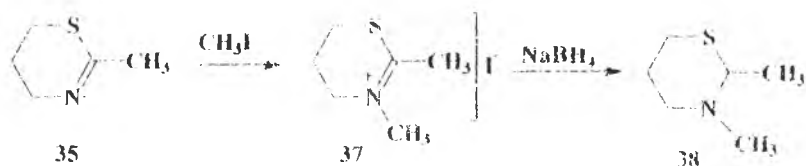
The starting dihydro-1,3-thiazines are obtained by the reaction of N-acylated-3-amino-1-propanols with  $\text{P}_2\text{S}_5$ . The reaction of N-acetyl-3-amino-1-propanol carried out without solvent by heating the mixture of reagents at 145 °C (the reaction is exothermic and finally a temperature of about 220 °C is reached) leads (yield 50 %) to 5,6-dihydro-4H-2-methyl-1,3-thiazine (Scheme 21) [42].

The reduction with aluminum amalgam gives with a very low yield (14%)

the perhydro-1,3-thiazine derivative, while the reduction with other systems as  $H_2/Pt$  or ethanol/ $Na$  gives other type of products.



Scheme 21

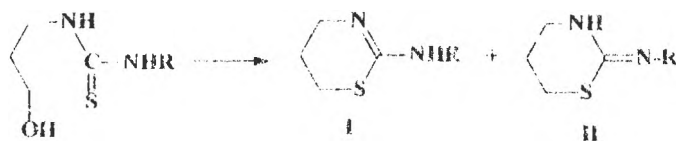


Scheme 22

The N-alkylated-dihydro 1,3-thiazines can be reduced with good yields (up to 97%) using  $NaBH_4$  in methanol at  $-78^\circ C$  (Scheme 22) [42].

#### 2.4. Ring closure reactions of the derivatives of 3-amino-1-propanol

The condensation reactions of the thiocarbamic derivatives of 3-amino-1-propanol can lead to substituted 5,6-dihydro-4H-1,3-thiazine (I) or to perhydro-1,3-thiazine (II) in connection with the nature of the substituent located on the nitrogen atom (Scheme 23) [46].



Scheme 23

## 2.5. N-acylation of perhidro-1,3-thiazines

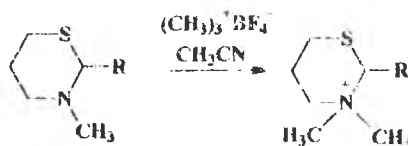
The acylation reaction of the parent heterocycle is performed in benzene with acetylchloride in the presence of  $\text{Et}_3\text{N}$  (Scheme 24) [42]



Scheme 24

## 2.6. N-alkylation reaction of perhidro-1,3-thiazine derivatives

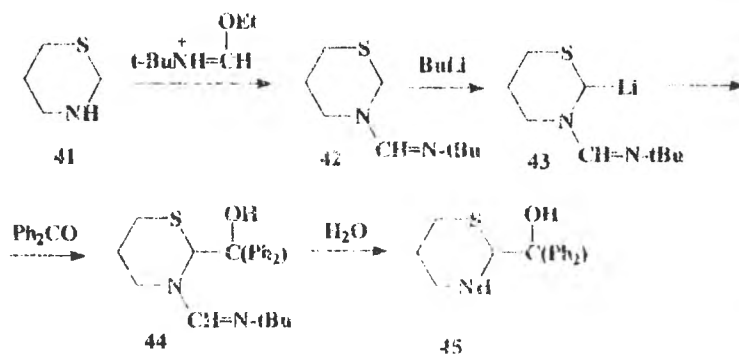
The N-methylation reaction of the heterocycle nitrogen atom is performed using tetrafluoroborate of trimethyloxonium (Scheme 25) [42].



Scheme 25

## 2.6. Lithiation reaction of perhidro-1,3-thiazines

The lithiated perhydro-1,3-thiazines (obtained by using the reaction with

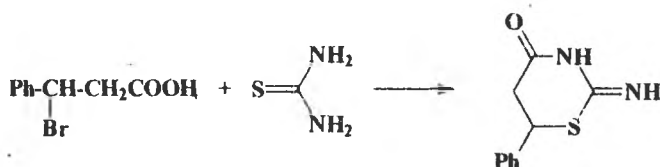


Scheme 26

BuLi) in reaction with ketones arise the access to derivatives of the 1,3-thiazine ring, bearing substituents in the position 2 of the heterocycle (Scheme 26) [47].

## 2.7. Compounds bearing 2-imino-substituents

The reaction (Scheme 27) of  $\beta$ -bromoacids with thiourea leads to derivatives of the 1,3-thiazine substituted with imino groups in the position 2 of the heterocycle [12,48].



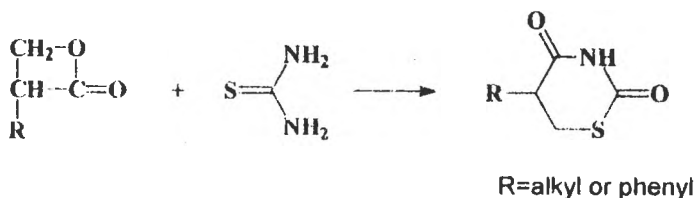
Scheme 27

The use of N-methyl-thiourea in a reaction performed in similar conditions with those employed in the previous reaction (reflux of ethanol and acidic catalysis) results into a compound displaying the 2-methylimino derivative [11].

2-Imino N-substituted derivatives have been obtained in the reaction of  $\beta$ -mercapto-propionic acid with N, S-substituted thiourea [49], as well as in the more efficient reaction (yield 77%) [50] of acryloyl chloride with thiourea when 2-imino-4-oxo-perhydro-1,3-thiazine has been obtained.

## 2.7. Synthesis of perhydro-1,3-thiazine-2,4-dione derivatives

A pathway of access to the title derivatives is the hydrolysis of imino derivatives obtained above [12,48]. Another route is the direct reaction of thiourea with the corresponding lactone (Scheme 28) [51].



Scheme 28

## Synthesis of 1,3-Oxathiane and Perhydro- 1,3- Thiazine Derivates

The use of dithiocarbamates instead of thiourea derivatives permits to obtain compounds belonging to the group of 4-oxo-perhydro-1,3-thiazine-2-thione [17,52].

## REFERENCES

1. E. Juaristi, *Conformational Behavior of Six-Membered Rings*, VCH Publishers, New York, 1995.
2. F. G. Riddell, *The Conformational Analysis of Heterocyclic Compounds*, Academic Press, London, 1980.
3. M.J.O. Anteunis, D. Tavernier, F. Borremans, *Heterocycles*, 1976, **4**, 293.
4. E. L. Eliel, S. H. Wilen, *Stereochemistry of Organic Compounds*. Wiley Interscience, New York, 1994.
5. I. Grosu, S. Mager, G. Plé, R. Martinez, L. Muntean, E. Mesaros, *Heterocycles*, 1995, **41**, 2233
6. I. Grosu, S. Mager, G. Plé, R. Martinez, M. Horn, R. R. Gavino, *Monatsh. Chem.*, 1995, **126**, 1021.
7. I. Grosu, S. Mager, G. Plé, M. Horn, *J. Chem. Soc. Chem. Commun.*, 1995, 167.
8. I. Grosu, S. Mager, G. Plé, *J. Chem. Soc. Perkin Trans. 2.*, 1995, 1351.
9. Y. Haramoto, M. Sano, H. Kamogawa, *Bull. Chem. Soc. Jpn.*, 1986, **59**, 1337.
10. K. Haramoto, H. Kamogawa, *J. Chem. Soc. Chem. Comm.*, 1983, 75.
11. V. W. Gash, K. W. Wheeler, *U.S. 2*, 679, 500, May 25, 1954, CA **49**, 4727g,i
12. K. W. Wheeler, V. W. Gash, *U.S. 2*, 585, 064, Feb. 12, 1952, CA **46**, 7593h
13. K. Okumura, K. Inoue, T. Oda, K. Kondo, *Japan* 70 31, 186 (Cl. C 07d, A 61 k), Oct. 08 1970, CA **74**, 53815d
14. M. Winter, *Ger Offen.*, 2, 534, 162 (Cl. C 07D, A 23L), 12 Feb. 1976, CA **85**, 37096s

- 15 M. Ohwa, E. L. Eliel, *Chemistry Letters*, 1987, 41
- 16 K. Shiokowa, S. Tsuboi, S. Kagaku, K. Moriga, *Eur. Pat., Appl.* EP 192, 060 (Cl C 07 D 401106), 27 Aug. 1986 CA **106**, 28848p.
- 17 J. B. Bowers, I. Benghiat, *U.S.* 2, 727, 035, Dec. 13, 1955, CA **50**, 10800f.
- 18 M. Ohwa, T. Kogure, E. L. Eliel, *J. Org. Chem.*, 1986, **51**, 2599.
- 19 E. L. Eliel, M. T. Alvarez, J. E. Lynch, *New J. Chem.*, 1986, **10**, 749.
- 20 K. Y. Ko, W. J. Frazee, E. L. Eliel, *Tetrahedron*, 1984, **40**, 1333.
- 21 K. Y. Ko, E. L. Eliel, *J. Org. Chem.*, 1986, **51**, 5353.
- 22 A. Solladie-Cavallo, A. D. Vohunle, *J. Org. Chem.*, 1995, **50**, 3494
- 23 I. Grosu, S. Mager, G. Plé, R. Martinez, *Chirality*, 1996, in print
- 24 Y. Allingham, T. A. Crabb, R. F. Newton, *Org. Magn. Resonance*, 1971, **3**, 37
- 25 K. Pihlaja, P. Pasanen, J. Wahalilta, *Org. Magn. Resonance*, 1979, **12**, 331
- 26 P. Pasanen, K. Pihlaja, *Tetrahedron*, 1972, **28**, 2617
- 27 K. Pihlaja, P. Pasanen, *Acta Chem. Scand.*, 1970, **24**, 2257
- 28 P. Pasanen, K. Pihlaja, *Acta Chem. Scand.*, 1971, **25**, 1908
- 29 E. L. Eliel, S. Morris-Natschke, *J. Am. Chem. Soc.*, 1984, **106**, 2937
- 30 A. J. Meskens, *Synthesis*, 1981, 501
- 31 J. Gelan, M. Anteunis, *Bull. Soc. Chim. Belges*, 1970, **79**, 313
- 32 W. Pickenhagen, H. Bronner-Schindler, *Helv. Chim. Acta*, 1984, **67**, 947
- 33 M. Winter, A. Furrer, B. Willhalm, W. Thommen, *Helv. Chim. Acta*, 1976, **59**, 1613
- 34 A. Mosadi, G. Heusinger, *Liebigs Ann. Chem.*, 1985, 1185
- 35 A. M. Turyanskaya, V. A. Bacheribov, A. I. Gren, *Khim. Prom.-st., Ser. Rekl. Osobo Christ. Vashchetva*, 1981, **3**, 3, CA **96**, 104161b
- 36 K. Fuji, M. Ueda, K. Sumi, K. Kajiwara, E. Fujita, T. Iwashita, I. Miura, *J. Org. Chem.*, 1985, **50**, 657
- 37 K. Fuji, M. Ueda, E. Fujita, *J. Chem. Soc. Chem. Comm.*, 1977, 814
- 38 J. E. Lynch, E. L. Eliel, *J. Am. Chem. Soc.*, 1984, **106**, 2943
- 39 K. Bergesen, B. M. Carden, M. J. Cook, *J. Chem. Soc. Perkin Trans. 2*, 1976, 345



Synthesis of 1,3-Oxathiane and Perhydro-1,3-Thiazine Derivates

40. K. Fuji, M. Ueda, K. Sumi, E. Fujita, *J. Org. Chem.*, 1985, **50**, 661
41. S. Wolfe, P. M. Kazmaier, H. Auksi, *Can. J. Chem.* 1979, **57**, 2412
42. J. K. Kim, Y. Souma, N. Bentow, C. Ibbeson, M. C. Caserio, *J. Org. Chem.*, 1989, **54**, 1715
43. A. Katritzky, V. J. Baker, F. M. S. Brito-Palma, I. J. Ferguson, L. Angiolini, *J. Chem. Soc. Perkin Trans 2*, 1990, 1746
44. M. J. Cook, R. A. Y. Jones, A. R. Katritzky, M. M. Manas, A. C. Richards, A. J. Sparrow, D. L. Trepanier, *J. Chem. Soc. Perkin Trans 2*, 1973, 325
45. T. Kametani, K. Kigasawa, M. Huragi, N. Wagatsuma, T. Kohagizawa, H. Inoue, *Heterocycles*, 1978, **9**, 831.
46. J. Rabinowitz, *Helv. Chim. Acta*, 1969, **52**, 255
47. A. I. Meyers, P. D. Edwards, W. F. Rieker, T. R. Bailey, *J. Am. Chem. Soc.*, 1984, **106**, 3270
48. J. Iwao, K. Tomino, T. Ito, *Tanabe Kenkyu Nempo 2*, 1957, **2**, 17, CA **52**, 9138h
49. P. Monforte, *Atti. Soc. Peloritana Sci Fis. Mat. Nat.*, 1964, **10**, 65, CA **64**, 15784g
50. M. Nomura, *Yuki Gosei Kagaku Kyokai Shi*, 1972, **30**, 971, CA **78**, 84342j
51. G. Cignarella, E. Testa, *Brit. 1*, 007 557(CI C 07c, d), Oct. 13, 1965, Appl. June 12, 1963;3 pp. CA **64**, 2101h-2102a
52. J. Weinstock, U.S. 3, 732, 216(CI 260-2434R, C 07d), 08May 1973, Appl. 199, 768, 17 Nov. 1971, CA **79**, 32069b

Received:25.03.1996



## CATALYTIC ANTIBODIES

Florin-Dan IRIMIE, Artemiza MORAR and Mihaela BOJIN

*"Babeș-Bolyai" University of Cluj-Napoca  
Faculty of Chemistry and Chemical Engineering  
11, Arany Janos st. 3400 Cluj-Napoca, Romania*

**Abstracts.** On the basis of the data in literature, a review on the usage of antibodies in the catalysis of the chemical reactions is reported. A systematisation of the chemical reactions catalyzed by antibodies has been made, thoroughly describing reactions mechanisms and the required conditions.

### **Contents**

- 1 Introduction
- 2 Characterization of Antibodies
- 3 Mechanisms of reaction
  - 3.1 General mechanistic considerations
  - 3.2 Entropy effects in antibody catalysis
  - 3.3 Bimolecular reactions
  - 3.4 General acid base catalysis and antibody catalysis
  - 3.5 Medium effects
- 4 Reaction types
  - 4.1 Sigmatropic rearrangements
  - 4.2 Cycloadditions
  - 4.3 Cyclisation reactions
  - 4.4 Decarboxylations
  - 4.5 Hydrolytic reactions
    - 4.5.1 Amide hydrolysis
    - 4.5.2 Ester hydrolysis
    - 4.5.3 Epoxide hydrolysis
    - 4.5.4 Enol ethers hydrolysis
    - 4.5.5 Oligosaccharide hydrolysis
    - 4.5.6 Rearrangement of peptide bond
    - 4.5.7 Group transfer reactions
      - 4.5.7.1 Aminolysis reaction
      - 4.5.7.2 Transesterification reaction
    - 4.5.8 Imine formation
    - 4.5.9 Cis-trans isomerization
    - 4.5.10 Metal chelation
- 5 Extending the scope and increasing activity
- 6 Conclusions
- 7 References
- 8 Appendix : Examples of reactions

## Catalytic antibodies

*The extraordinary power of chemistry consists not only in "classical transformation" of certain substrates, but also in the discovery of new pathways, more and more effective to do it. Besides the progress of catalysis, the biocatalysis has become a tool in the organic synthesis laboratory. The programmed anticorpogenesis, i.e. the design of an artificial enzyme is a challenge of the end of 20<sup>th</sup> century.*

*Apparently, this spectacular technique seems to be simple. It seems clear that chemistry, immunology and biology make the things go round, but nobody can tell where the landmark is between organic chemistry and immunology.*

*The task of organic chemistry is major. The success of strategy depends on the abilities and resourcefulness of its tools because the hapten design is the central point of the strategy. The mechanism of the reaction to be catalyzed, the cognition and the induction of monoclonal antibody are also important.*

*According to estimations, the possibilities offered by the antibody catalysis are astonishing. Basically, any chemical reaction can be catalyzed by an antibody. Moreover, high reaction regioselectivity, stereospecificity, substrate diastereo- or enantioselectivity brought about by this approach make out of the abzymes (see below) a solution for unsolved problems. Still, there is a long way ahead of us.*

### **1. Introduction**

Biological systems are capable of synthesizing, screening enormous chemical diversity and producing molecules with remarkable biological functions. When comparing a cell with a chemical laboratory, the fact that the synthetic chemist is the least skilled at assembling atoms is obvious. Naturally, a question arises: could there exist strategies to use the tremendous possibilities of nature? or are scientists capable of devising ways to make them possible?

In the last few years efforts have been made to develop catalyst with enzyme-like features. These biomolecules, due to their low entropic structure, possess the ability to bind the substrate and, even more powerfully, the transition state of the reaction. On the other hand, the antibodies capacity of binding antigens has suggested a way to create a new type of enzyme-like catalyst. To built an enzyme like substance by means of the cell is, at first sight, a simple problem, since the immune system can generate more than  $10^{12}$  antibodies, can identify and amplify those that bind a given ligand, with high selectivity and specificity. Thus, a big step has been made: the principles and tools of organic chemistry

have been used to exploit the remarkable machinery of the immune system for the generation of antibody catalysts for which the term **abzyme** was suggested. [1]

An important approach that has occurred in the design of catalytic antibodies involves the induction of catalytic groups in antibody combining site via mechanism-based **hapten** design, i.e. a stable molecule, which mimics the structure of the short-timed transition state of the target reaction [2,3a]. After attaching a spacer arm to the hapten and coupling the resulting structure to a carrier protein, the assembly, a real antigen, can be used to produce antibodies. However, the key-element in the synthesis of antibodies-catalysts is the rational design of high selective substrate binding sites. Since the sterical and electronical complementarity is very important for the catalytic ability, the appropriate functionality and geometry of hapten, as transition state - analog, depends on the success of the strategy.

Antibodies elicited to the haptens behave as enzymatic catalysts with the appropriate substrate. Pauling first pointed out that the fundamental difference between enzymes and antibodies lies in the fact that, whereas the former selectively bind transition states, the latter bind ground states. [4,5]

Instead, catalytic antibodies, like enzymes, exhibit rate acceleration, substrate specificity and regio- and stereospecificity, correlated precisely to the structure of the antigen, used to elicit immune response. In fact, the specificity of antibodies for their ligands can exceed that of enzymes for substrates. Moreover, with the advent of *monoclonal antibodies* (antibody molecules secreted by a hybridoma clone; because each such clone is derived from a single B cell, all of antibody molecules are identical.), with the help of protein engineering and efficient catalytic groups available from synthetic chemistry, homogeneous ligand binding sites with enzyme like affinity and specificity can be generated for most biomacromolecules, and for smaller synthetic molecules, as well. Finally, the potential importance of the programmed antibody catalyst as tool in chemistry is obvious.

## **2. Characterization of antibodies**

Antibodies protect organism through their ability to discriminate nonself from self molecules. Selective recognition is achieved through a large number of weak bonding interactions involving hydrogen bonds, Van der Waals and electrostatic interactions, which are not fully understood by chemists yet and are still far from being able to mimic.

## Catalytic antibodies

Antibodies are large proteins assembled in a disulfide cross-linked four chain structure. The major serum antibody, IgG, consists of two identical heavy chains of molecular weight approximately 50,000 and two identical light chains of molecular weight 25,000. Sequence comparison of monoclonal IgG proteins indicates that the carboxyl-terminal half of the light chain and roughly three quarters of the heavy chain from carboxyl end show little **sequence** variation. The antigen combining site of molecule is in the first 100 amino acids of the amino-terminal regions of both light and heavy chains, referred to as  $V_L$  and  $V_H$  domains, which show considerable variation - three such regions in both the heavy and the light chains - associated with antigen recognition and designated as complementary - determining regions. Proteolytic cleavage of the molecule on the carboxy-terminal side of the interstrand disulfide linkage connecting the light and heavy chains generates two  $F_{ab}$  molecules, each containing an antigen-binding region.

Crystallographic studies of  $F_{ab}$  fragments reveal that the immunological fold consists of two twisted, stacked  $\beta$ -sheets, a structural motif characterizing the  $V_H$  and  $V_L$  domains. One sheet has four and the other three antiparallel  $\beta$ -strands related by a pseudo two fold axis. These strands are joined at their ends by six loops of the complementary-determining regions creating a key  $\beta$ -barrel fold that can tolerate sequence and conformational changes in the loop region. On the basis of comparative studies it has been argued that there is a small repertoire of main-chain conformational - "canonical structures" for at least five of the six variable regions of antibodies whose conformation is determined by a few key residues. The area of interaction between the antigen and antibody may be relatively flat and extensive for protein antigen binding to an antibody ( $700 - 750\text{\AA}^2$ ), where as in the case of small organic molecules the binding may occur by way of clefts whose volumes are in excess of  $600\text{\AA}^3$ . For small organic molecules such as fluorescein the dissociation constant of the antigen-antibody complex ranges from  $10^{-4}$  to  $10^{-14} \text{ M}^{-1}$ , which, if totally coupled to drive a chemical transformation would provide a free energy change up to  $20 \text{ kcal}\cdot\text{mol}^{-1}$  sufficient to promote most reactions in aqueous media. The antigen binding brings about no global conformational change in the antibody. The union is rather accommodated by conformational adjustments in the specific amino acid side-chains that improve the weakly binding interactions that involve hydrogen bonds, Van der Waals and electrostatic forces.[3]

B-lymphocytes, the cells of the immune system, which produce antibody molecules, make use of genetic recombination to generate a pool of antibody molecules, each possessing a unique combining site amino acid sequence. The genes encoding each antibody are spliced together out of a battery of gene segments, which enable an organism to mount a primary immune response from a great number of different antibody molecules.

### **3. Reaction mechanisms**

#### **3.1. General mechanistic considerations**

Catalytic antibodies share many mechanistic features found in enzymes. They act as catalysts with rate acceleration on the order of  $10^3$  -  $10^6$  over the uncatalyzed reaction, follow classical Michaelis - Menten kinetics and display substrate specificity. [2b]

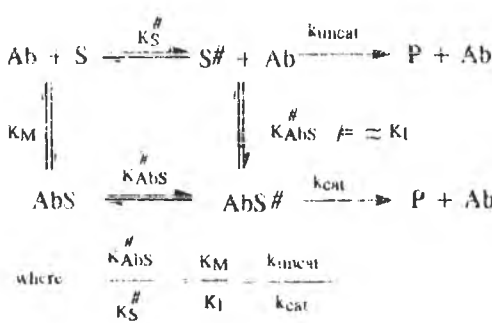
The basic principle of enzymes catalysis states that strong binding interactions are required by enzymes to reduce the energy barriers along the chemical reaction pathway. [1] A mechanism whereby enzymes are believed to act as highly specific catalysts is that they provide an environment complementarity in structure and electronical distribution to a rate limiting transition state of a given reaction, [6], through a combination of substrate destabilization, proximity effects and covalent catalysis mediated by appropriately positioned nucleophiles, general acids and bases, metalions and other cofactors [7]. Thus, the striking parallels between catalytic antibodies and enzymes in the field of mechanistic enzymology are not at all surprising. However, what is particularly remarkable is that the single protein motif (all antibodies possess the same secondary and tertiary principal structure ) can be adopted to accommodate diverse reaction types with noteworthy remarkable efficiency.[8a]

Antibodies have been generated that catalyze a wide array of chemical reactions ranging from one step kinetic pathway through short lived transition state (e.g. pericyclic reactions) to multistep kinetic pathway through intervening covalently bound antibody-intermediate (e.g. hydrolytic reactions, consecutive reactions and group transfer reactions). Since haptens mimic either the transition states or highly energy intermediate [8], the strategies for generating catalytic antibodies include (1) the use of antibody to stabilize negatively and positively charged transition state, (2) the use of antibody as

## Catalytic antibodies

entropic traps, (3) the generation of antibody with catalytic groups and cofactors in their combining sites [2b]

The antibody binds the transition-state analogs considerably more tightly than substrates, i.e. the haptens are potent inhibitors of activity in agreement with their definition as transition state analogs. One indication that antibodies are complementary to rate determining transition-states comes from the comparison of dissociation constants for substrate and transition-state analogs ( $K_M$ , respectively  $K_I$ ) with the rate of antibody-catalyzed reaction over the uncatalyzed reaction ( $k_{cat}/k_{uncat}$ ):



Scheme 1 [2c]-modified

Obs. The  $K_I$  term is presumed to be an approximation of the hypothetical and unmeasurable dissociation constant  $K_{AbS}^\ddagger$  describing the binding of the transition state.

A number of reactions such as unimolecular lactonisation reaction, bimolecular amide bond formation, the hydrolysis of an aryl ester, Diels alder reaction and porphyrin metallation show close agreement between the calculated  $K_{AbS}^\ddagger / K_S$  and the

experimentally derived  $K_M / K_I$  ratio. The binding energy of antibodies induced to a single antigen expressed as a dissociation constant may span 10 orders of magnitude ( $K = 1.0 \cdot 10^{-6} - 1.0 \cdot 10^{-14} \text{ mol}^{-1}$ ) [9]. Note that  $K_M$  parameter may represent an approximate measure for the dissociation of the abzyme substrate complex ( $K_M$  is defined as the concentration of substrate that produces one half of the maximal catalytic rate) [10a]

Just one observation: high affinity of antibodies for the corresponding hapten is no guarantee of catalytic power [10], since, for example, only one out of several antibodies generated against a hapten may show activity against the substrate (as can be seen in the fourth section of herein paper.). The affinity may be a consequence of primary binding interactions to residues on the hapten not central to mimicking transition-state structure [3a]



### 3.2. Entropy effects in antibody catalysis

Antibodies are capable of efficiently catalyzing reactions with unfavorable entropy (high entropy barriers) of activation ( $\Delta S^\ddagger$ ) by acting as "entropy traps" : the binding energy of the antibody is used to freeze out the rotational and translational degrees of freedom necessary to form the activated complex. [2a]. The notion is proper for antibodies catalyzing both unimolecular reactions (such as lactonisation reaction and Claisen rearrangement) and bimolecular reactions (e.g. Diels - Alder reaction and transesterification).

There are few strategies for the use of antibodies in what is called "catalysis by proximity" : bringing the two substrate molecules together in the correct orientation for reaction (Diels-Alder reaction), using the proximity effect in order to restrict the conformation of the transition-state (sigmatropic rearrangement) and inducing fit of the second substrate, to activate the intermediate for subsequent chemical reaction (transesterification).

Since haptens can never mimic transition structure perfectly, antibody raised against imperfect transition-state analogs cannot be expected to reduce free energy of activation in the same extent in which authentic enzymes, designed by nature, do [7]. There are various means of estimating the rate acceleration achieved by restricting the conformational freedom of substrate molecules. One method uses quantum mechanical calculation of entropy loss (presuming  $\Delta H^\ddagger$  is fixed) to determine the effect on rate i.e. the rate constant is proportional to  $\Delta S^\ddagger / R$  [3c]. In addition, a measure of catalytic efficiency is the effective molarity. This value indicates the concentration of the substrate that would be needed in the uncatalyzed reactions to achieve the same rate as that seen in the enzyme complex. For example, the effective molarity for one of antibodies studied in Diels-Alder reaction was determined to be in excess of  $10^2$  M by comparing the pseudo-first order rate constant for the reaction at the antibody active site ( $k_{cat}$ ) with the second order rate constant for the uncatalyzed process in free solution ( $k_{uncat}$ ) [7].

It must be underlined that the diminution of free energy required to reach the transition-state by utilizing binding energy to overcome the entropy requirements may or may not be accompanied by transition-state stabilization or substrate destabilization [9]

### 3.3. Bimolecular reactions

There are two general indices based on steady-state kinetic analysis that are used to assess the catalytic efficiency of an antibody  $k_{cat}/k_{uncat}$  and  $k_{cat}/K_M$  (see scheme 1). As we have already seen, the meaning of the first index is obvious (with observation that for bimolecular reactions  $k_{cat}$  and  $k_{uncat}$  may or may not have same units). The second index of efficiency represents a measure of the encountered kinetic barrier commencing with the combination of antibody and substrate and proceeding along the reaction coordinate to the transition-state of highest energy. This ratio has a limit of approximately  $10^7 \text{ M}^{-1} \text{ s}^{-1}$  when the reaction is limited by the joint diffusion of the substrate and antibody. It is instructive to predict the course of the reactions, based on the kinetic parameters assigned to antibodies. Using a kinetic simulation program [10b], it has been found that  $k_{cat}/k_{uncat}$  ratios of  $> 10^4$  and  $K_M < 0.1 \text{ mM}$  are clearly desirable for antibodies to have practical utility as catalysts, i.e. the efficiency of a given catalytic antibody is sufficient to fit it to determine the outcome of reaction.

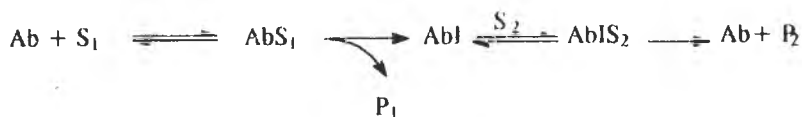
There are two general classifications of kinetic sequence distinguishable by steady-state kinetics for bimolecular enzyme catalyzed reactions

- (1) sequential process is the chemistry of bond formation and bond cleavage which take place within the bisubstrate-enzyme ternary complex. Within the sequential pathways there occur variations dependent upon whether the binding of either substrate is independent or not, which are, at a kinetic equilibrium relative to turnover etc [3]. For example, amide synthesis [9] and imine formation [11] proceed by a random kinetic sequence with respect to the two substrates involving separate binding sites in the antibody (Scheme 2)



Scheme 2

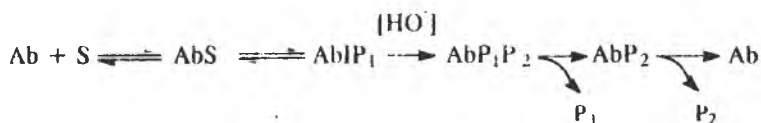
- (2) ping-pong mechanism implies the enzyme acting to shuttle through covalent attachment an isolated fragment of one substrate for chemical union with the second (scheme 3)



**Scheme 3** (adapted from [8b])

In the case of transesterification reaction, the formation of the acyl-antibody intermediate was demonstrated [12]. In addition, such a pathway may also arise from a large difference between the apparent dissociation constants that characterize the two substrates

Transesterification reaction is a formal bimolecular substitution reaction that together with aminolysis reaction must compete with the hydrolysis of the ester. In the case of ester hydrolysis a multistep kinetic pathway, also through an acyl-antibody intermediate is consistent with the experimental data [13] (scheme 4)



**Scheme 4** (adapted from [13])

It is noteworthy that a high  $k_{cat}/k_M$  ratio alone is insufficient for achieving multiple substrate turnovers, but for the antibody, at least a 10-fold weaker product affinity relative to the substrate binding is necessary [8].

There were found and described reoccurring mechanistic themes displaying characteristics previously associated with enzyme behavior, so the utility of antibodies for testing fundamental notions of enzymatic catalysis is confirmed.

### 3.4. General acid-base catalysis and antibody catalysts

Many chemical reactions including condensation, isomerization and hydrolytic reactions (e.g.  $\beta$ -elimination cis-trans isomerization acyl transfer reactions or ester hydrolysis) are accelerated by acid-base catalysis. Appropriate functionalities have been attempted by a "bait and switch" process, in which an additional structural element, for example a charged residue is present in the immunogen, but not in the substrate [3].

Structural features of hapten induce complementary structure feature in the combining site. charged groups are stabilized by oppositely charged entities and

## Catalytic antibodies

hydrophobic groups are surrounded by an apolar environment [2]. Thus, a charged ion may generate an active site that could act as a nucleophile or/and a general acid/base.

For example, the antibody catalyzed hydrolysis of enol ethers, is consistent with general acid catalysis by an ionizable side chain in the active site. To study the pH-dependence on antibody catalysts, an antibody side chain XH with dissociation constant  $K_{XH}$  (eq. 1) was taken into consideration. The antibody substrate complex which can be in two protonation states  $[AbXH \cdot S]$  and  $[AbX^- \cdot S]$ , can react to the product either pH-independent (at low pH, eq. 3) or pH dependent (eq. 4) at high pH. Both processes are kinetically equivalent [14]:

$$K_{XH} = ([AbX^-] \cdot [H_3O^+]) / [AbXH] \quad \text{Eq. 1}$$



$$k_{cat} = ([AbXH] / [Ab_{TOT}]) \cdot k_{XH} \quad \text{Eq. 3}$$

$$k_{cat} = [H_3O^+] \cdot ([Ab_{TOT}] \cdot K_{XH}) \quad \text{Eq. 4}$$

$$K_{XH} = k_{XH} / k_X \quad \text{Eq. 5}$$

$$[Ab_{TOT}] = [AbXH] + [AbX^-] \quad \text{Eq. 6}$$

$$1/k_{cat} = 1/K_{XH} + (1/[H_3O^+]) \cdot (K_{XH} / k_{XH}) \quad \text{Eq. 7}$$

$$1/k_{cat} = 1/K_{XH} \cdot k_X + (1/[H_3O^+]) \cdot (1/k_X) \quad \text{Eq. 8}$$

There were obtained two dependences of the catalytic constant on hydronium ion concentrations in terms of the first order rate law (eq. 7) and the second order rate law (eq. 8). Thus, the antibody reaction can be described as a bimolecular reaction between the antibody substrate complex bearing the negatively charged side chain and the hydronium ion [14].

The "bait and switch" strategy is not limited to charge complementarity. It is possible to induce hydrogen bonds in response to the presence of neutral basic residues on the antigen, or to create a hydrophobic pocket in response to a large patch of nonpolar surface on the antigen. For example, the ability of antibodies to catalyze the decarboxylation reaction is, in a large extent, due to the hydrophobic nature of their binding sites. Another example is provided by enol ether hydrolysis. In this case, antibody catalysis can be explained by the sum of two phenomena: (1) general acid-catalysis by an ionizable side chain, and (2) the interaction of precise hydrophobic interactions between the substrates and the antibody binding pocket. [14a]

### 3.5. Medium effects

Catalytic antibodies have been used to explore the contribution of medium effects to the overall rate of an enzyme-catalyzed reaction. As we have already seen, the kinetic data of unimolecular decarboxylation reflect the kinetic advantage of the low dielectric environment of the binding pocket acting to destabilize the substrate by desolvation and to stabilize the charged-delocalized transition-state through dispersion interactions [15]. In addition, solvent dipolarity and basicity accelerate reaction, most likely by helping to break up hydrogen bonded ion pairs. The solvent dependent property SDP, such as a rate constant or equilibrium constant, is modeled as the linear combination of a polarity term ( $s\pi_1^* + d\delta$ ), hydrogen-bonding terms in which the solvent is the hydrogen-bond acid ( $a\alpha_1$ ), respectively hydrogen-bond base ( $b\beta_1$ ) and cavity term ( $h(\delta_H^2)_1$ )

$$\text{SDP} = \text{constant} + (s\pi_1^* + d\delta) + a\alpha_1 + b\beta_1 + h(\delta_H^2)_1$$

where  $\pi_1^*$ ,  $\alpha_1$  and  $\beta_1$  are known as solvatochromic parameters, which together with multiple linear regression methodology have been used to correlate and rationalize solvent effects on a wide variety of properties and processes [16].

Owing to the inherent complexity of an enzyme catalyzed reaction, the contribution of individual factors to the overall efficiency has been difficult to be measured experimentally. But now, with the advent of catalytic antibody technology, it is possible to examine specific mechanistic issues by using programmed active sites and sensitive reactions to one factor or another [7].

In addition, a comparison between the enzyme- and antibody catalyzed reactions is possible. For instance, like the serine proteases, the antibody catalyzes hydrolytic reaction through a covalent intermediate, which was indicated by three types of evidence (solvent isotope effect studies, substituent effect studies and pH rate studies) [13]. But unlike enzymes, the antibody may use hydroxide ion to cleave the intermediate [17].

In conclusion, the fact that antibody summarizes mechanisms and pathways initially thought to be characteristic of highly evolved enzymes suggests that, since an appropriate binding cavity is achieved, reaction pathways commensurated with the intrinsic chemical potential of protein are succeeded and the ability to direct binding energy allows the chemists to dictate a reaction mechanism which in most cases proves to be a difficult task [12].

#### 4. Reaction Types

In principle, any chemical transformation can be sped by antibodies. As long as the reaction itself is compatible with an aqueous milieu and a protein microenvironment, and as long as a suitable transition state analog can be devised, catalysis can be achieved.[3]. This approach is not only simple and practical, but also appears to be very versatile in terms of reaction types and substrates.[18]

Conceptually, the reactions most susceptible to antibody catalysis would be those originally viewed as "no-mechanism" reactions because their transition states evinced little polar or radical character. These pericyclic processes include electrocyclic reactions, sigmatropic rearrangements and cycloadditions, and generally are not reactions found to be catalyzed by enzymes. Together with cationic cyclisations [19], these are versatile methods available to synthetic chemists for assembling carbon-carbon bonds.[18].

The number of chemical transformations catalyzed by abzymes is rapidly increasing. Antibodies have been shown to catalyse acyl-transfer, eliminations, redox reactions[20]. Well over 60 reactions, including simple hydrolytic reactions, consecutive reactions or chelation of metals have been accelerated by antibodies

##### 4.1. Sigmatropic Rearrangements

The Claisen Rearrangements of allyl enol ethers is a pericyclic reaction of great importance in organic synthesis. Rearrangement of chorismate into prephenate (reactions 1 and 2) is a biologically relevant example of this type of sigmatropic process, representing a key step in the metabolic production of aromatic amino acids in plants and lower organisms. It has been anticipated that the sigmatropic rearrangement would be susceptible to strain and proximity effects, rather than to general acid/base catalysis, and

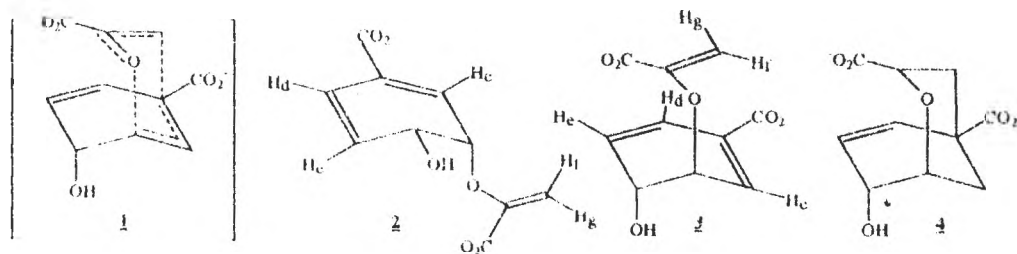


Figure 1

hence particularly susceptible to catalysis by an antibody [16]. Stereochemical studies have established that both enzyme-catalyzed (the enzyme chorismate mutase accelerates the reaction by more than  $10^6$ -fold) and spontaneous reactions occur via a compact, chairlike transition state **1**. In aqueous solution the substrate adopts an extended conformation **2** and must undergo conformational change to position the enolpyruvate side chain properly for reaction. Given this, it has been proposed that the enzyme may increase the probability of reaction by selectively binding and stabilizing the reactive pseudo-diaxial conformer **3** (Figure 1).

Antibody catalyst 11F1-2E9 (Reaction 1) raised against oxabicyclic dicarboxylic acid **4** (Figure 1) show effect a remarkable  $13^4$  fold acceleration of the rearrangement ( $k_{\text{cat}} / k_{\text{uncat}}$ ). The catalytic efficiency is only  $10^2$  times smaller than that achieved by the natural mutase *Escherichia coli* enzyme under identical conditions. A second chorismate mutase antibody 1F7 is roughly  $10^2$  times less active than 11F1-2E9. Despite its relatively sluggish activity, 1F7 is highly enantioselective, showing a > 90:1 preference for the natural (-)-isomer of chorismate, a property that was successfully exploited in the kinetic resolution of the racemic substrate. In contrast to 11F1-2E9, 1F7 achieves its catalytic effect by lowering the enthalpy of activation. The results of NMR study using transferred nuclear Overhauser effects (TRNOE's) are diagnostic for pseudodiaxial conformer and indicate that the antibody pocket is able to preorganise its substrate to an appreciable extent, as dictated by the structure of the templating hapten. The detection of smaller, nonspecific TRNOE's in experiments suggests that 1F7 may not completely reduce the rotational degree of freedom available to bind in enolpyruvyl group. The ability of the substrate to bind in catalytically-unproductive modes may account in part for the antibody's relatively low efficiency compared to 11F1-2E9 and natural chorismate mutase [7].

#### 4.2. Cycloadditions

The Diels Alder reaction provides an example of a transformation proceeding through a highly ordered entropy disfavored, transition state [3b]. One of the simplest ways in which one enzyme can speed such process is to act as an "entropy trap" utilizing binding energy to bring the two substrate molecules to gather in the correct orientation for reaction. This is sometimes referred to as "catalysis by approximation" [7].

While important in laboratory, Diels-Alder reactions are rare in nature, and attempts to isolate enzymes that catalyze such processes have been completely unsuccessful. The development of tailored "Diels-Alderase" antibodies could therefore fill an important niche, particularly, as such catalysts would likely exhibit high regio-, enantio- and diastereoselectivity. Another intriguing possibility would be the use of antibodies to alter the normal endo-exo selectivity of a cycloaddition reaction in a predictable way [18].

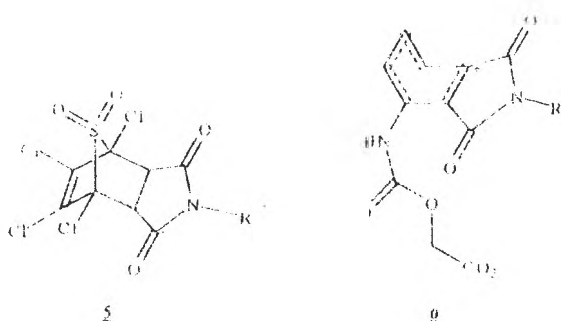


Figure 2

Suitable hapten design is dictated by the boat-like structure of the uncharged, highly ordered Diels-Alder transition state **6** (Figure 2) of reaction 4. The product itself is generally a poor choice of hapten, given the likelihood of seven product inhibition in the

induced binding pockets, and normal strategies must be developed to facilitate catalyst turnover [7].

Two strategies have been created to circumvent this undesirable property: a) catalyze the formation of an initial unstable bicycle intermediate that subsequently rearranges or b) incorporate into the transition-state analog a molecular constraint that restricts the analog to higher energy conformational state than the product. The following approach was used: a) the catalysis of Diels-Alder reaction between tetrachlorothiophene dioxane and N-alkyl maleilimides, (reaction 3), a reaction that occurs in two steps, with the initially formed tricyclic adduct **5** undergoing facile chelotropic elimination of sulfur dioxide to give the phthalimide. [7] Another approach: b) the reaction 4 between the acyclic diene and N-phenylmaleimide. The ethano bridge locks the cyclohexane ring of the hapten that corresponds to **6** into a conformation that resembles the pericyclic transition state for the Diels-Alder reactions, but that corresponds to less favored boat conformation of the product.

The effective molarity for one of antibodies 1E9, elicited to hexachloronorbomane derivative that mimics the high-energy intermediate of reaction 3, was determined to be more than  $10^4$  M, five orders of magnitude more tightly than either reactants.



Antibody 39A11 accelerates the Diels-Alder reaction with multiple turnover. Products bind only 75-100 times more tightly than either substrate, but the catalyst is rather inefficient as judged by its low effective molarity (0.35M). These results indicate poor use of antibody binding energy. However, the use of antigens resembling high energy product conformers or unstable reaction intermediate is likely to be a general solution to the problem of product inhibition in these reactions [7].

### 4.3. Cyclisation reactions

They presents an additional opportunity, namely for general acid base catalysis, as well as a need to reduce the rotational entropy of substrate, in order to maximize the rate of lactonisation. An intramolecular cyclisation was examined, (reaction 5), noting that constraints imposed by the antibody binding pocket should confer a modest degree of rate acceleration, dependent on the reduction of rotational entropy.[21]

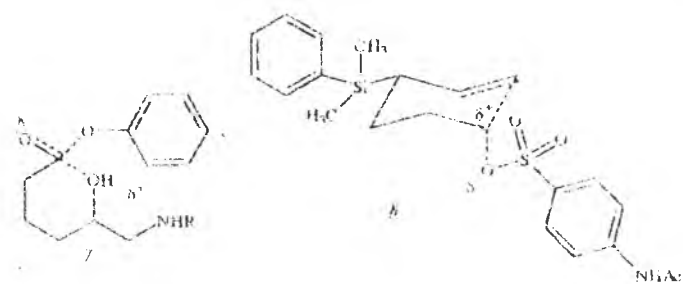


Figure 3

The ring closure in the absence of antibody is specific base catalyzed consistent with nucleophilic attack by alkoxyde ion generated from the hydroxy ester [3]. Formation of a single enantiomer of a

$\delta$ -lactone from the corresponding racemic  $\delta$ -hydroxyester was accelerated by the antibody raised against the hapten that mimics transition-state **7** (figure 3) by about a factor of 170, which permitted isolation of the lactone in an enantiomeric excess of about 94 percent. The system offered another test of the enzyme-like qualities of antibodies; namely a choice between two reaction pathways, which in the absence of a chiral reagent would be equal in free energy (diastereomeric) leading to a specific cyclisation [21].

An antibody has been induced that efficiently catalyzed a cationic cyclisation in which an acyclic olefinic sulphonate ester substrate is converted almost exclusively (98 percent) to a cyclic alcohol (reaction 5). Typically, a cationic cyclisation reaction is initiated by a carbocation formation either by electrophilic addition to double bond or by ionization at

sp<sup>3</sup> hybridized carbon. The reaction is thought to proceed via transition state **8** in which the reactants adopt a quasiciral-like conformation, thereby allowing participation of the olefinic bond in what is essentially a concerted transformation.

The designed hapten induced an antibody that simultaneously facilitates the cleavage of the sulphonate and controls the conformation of the substrate in the transition state such as olefin properly aligned to participate in the reaction. The anionic oxygen should elicit a functionality in the antibody capable of operating by way of a process that is termed "bait and switch" catalysis to stabilize the developing negative charges on the departing sulphonate. The cationic nitrogen is expected to induce an anionic functionality in the antibody combining site, which should stabilize the developing carbocation so that it could not be prohibitively high in energy. In this way, antibody catalysis permits selective control of the mechanism of the solvolysis (reaction 6), thereby reducing the complexity of the reaction and improving the yield of desired products [19]

#### 4.4. Decarboxylations

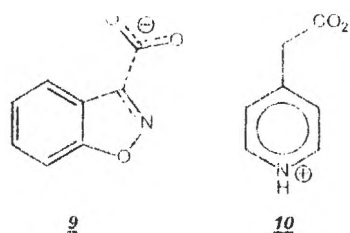


Figure 4

Carboxylation and decarboxylation reactions are crucial components of aerobic and anaerobic metabolism, as exemplified by the fixation of carbon dioxide in photosynthesis and the decarboxylation of  $\alpha$ -ketoacids in the Krebs cycle [7]

The decarboxylation of substituted carboxybenzoxazoles (reaction 7), are unimolecular reactions, which are not susceptible to general acid/base catalysis, but highly sensitive to the microenvironment. The transformation is a concerted, intermediate process that proceeds through the charge delocalized transition state **9** (Figure 4).[22]

The reaction rate increases as much as 10-fold upon transfer the reactant from aqueous solution to aprotic dipolar solvents. This dramatic range of activity has been attributed mainly to two factors: destabilization of the ground state carboxylate upon removal of hydrogen-bonding interactions with water, and concomitant stabilization of charge-delocalized transition-state in organic solvents through dispersion interactions. The rate

retarding effect of ion pairs formation in solvents with low dielectric constant has also been noted. [7]

Specific binding interaction could be utilized to extract the charged substrate from aqueous buffer and force it into the destabilizing environment of an immunoglobulin binding pocket. Therefore to elicit a hydrophobic environment able to exclude water, the apolar naphthalene framework was utilized. Sulphonate groups were included to induce complementary cationic residues within the combining site (the binding site contains positively-charged amino acid residue, such as a protonated lysine or a protonated arginine [16]) to promote binding of the anionic carboxylate of the substrate and to stabilize the incipient phenolate of the product. Thus, the antibody combining site is very hydrophobic and virtually inaccessible to solvent molecules in the presence of bound ligand and the large rate acceleration provided by the antibody (19000 fold over the rate in aqueous buffer) can be ascribed almost entirely to medium effects [18]

The investigation demonstrates that catalytic antibodies can be useful tools for exploring the nature of biological catalysis. Thus, it was established that 4-pyridylacetic acid (reaction 8) is a viable chemical model for pyridoxalphosphate (PLP) utilizing decarboxylases. This compound is known to decompose with a rate dependent on the polarity of the medium. The evolution would incorporate recognition elements and a hydrophobic cavity. The structure of hapten would elicit combining sites possessing a complementary negative charge and a confined region with low dielectric constant. A recent crystal structure of a histidine decarboxylase - substrate analog complex corresponding to **10** ( Figure 4) situates the carboxyl group in a crevasse lined with apolar residue. Clearly, such a medium could support destabilization as a component of catalytic mechanism. The association of antibody and hapten-like molecules is facilitated by classical hydrophobic effects. On the other hand, it requires energy reflected in the high  $K_m$  to induce a charged group into a hydrophobic pocket. The antibody operates by binding the pyridinium moiety through noncovalent interactions to position the carboxylate and therein to promote the loss of carbon dioxide. The  $k_{cat}$  ( $k_{uncat}$  of  $10^5$  might be representative of contributions to catalysis by enzymatic decarboxylases solely as a result of the microenvironment of the active site [23]

## 4.5. Hydrolytic reactions

### 4.5.1. Amide hydrolysis

Catalysts with the ability to cleave specifically peptide bond, would have many potential applications in controlling biological systems. While amide hydrolysis is a thermodynamically favorable process, the reaction possesses an appreciable kinetic barrier. Proteolytic enzymes increase the rate acceleration by factors up to  $10^{10}$ . The reaction proceeds through one or more high-energy tetrahedral transition-states. Substrate analogs in which the reactive carbonyl has been replaced by either a charged tetrahedral phosphorus or a secondary alcohol, so that they could mimic the geometric and electronic characteristics of high-energy intermediates, have found applicability in their rational design of protease inhibitor (the *captopril* drug, as conversion enzyme inhibitor, is a significant example of an inhibitory activity upon substrate analogy [24]). An antigen (hapten) patterned after a protease inhibitor elicits antibodies with amidase activity. [8]

In order to be an effective amidase, an antibody must stabilize the oxyanion and protonate the amide nitrogen for facile expulsion [25]. The kinetic analysis argues the idea that hydrolysis of both amide and esters proceeds through a transient, antibody-bound intermediate which is not accumulated because of an unfavorable equilibrium governing its formation. This intermediate is an acyl-antibody formed by nucleophilic attack of a histidine side chain on the substrate and stabilized by guanidinium group of an arginine side chain by electrostatic and hydrogen bond interactions. [8]

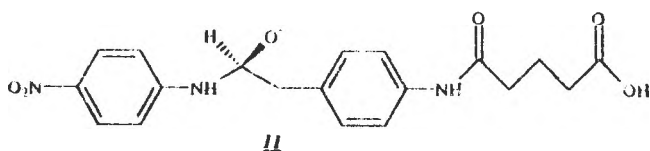


Figure 5

The hapten for reaction 9 was designed as a mimic of tetrahedral intermediate **11** (Figure 5). This antigen might induce an antibody that has a proton in close proximity to

this site that could participate in general acid catalysis. This is an example of "bait and switch" mechanism: the antigen has a group or charge that is missing in the substrate thereby allowing the induced complementary functionality in the antibody to play a different role during catalysis. The nitroaniline and benzylic ring systems impart

immunogenity to the compound. The hapten incorporates the heterofunctional linker appendage due to its easy attachment to carrier protein and proper presentation to the immune system.

#### 4.5.2. Ester hydrolysis

More than 20 acyl transfer reactions have been catalyzed with rate acceleration approaching  $10^8$  M over the uncatalyzed reactions [2], making the corresponding antibody catalysts some of the most efficient enzymes known [8].

The same antibody catalyzes the hydrolysis both of amide and esters [8] (reaction 9 and reaction 10) through an acyl-antibody intermediate, in a multistep pathway [13] and with essentially identical kinetic constants [8]. This antibody (reaction 12) exhibits both similarities to and differences from naturally hydrolytic enzymes. Although its turnover number is less than for its enzyme counterparts, this stereospecificity is exquisite [20]. On the one hand, fairly strict substrate homology to the inducing hapten must be maintained so that the antibody binding energy could manifest itself as catalysis [20]. On the other hand, antibodies can carry out the stereospecific hydrolysis of unactivated esters with an enantiomeric excess greater than 100 : 1. These results are significant because at present there exists no general chemical method for generating stereospecific esterolytic catalysts. Specificities for both the alcohol and the acid components of the esters were demonstrated and for R and S configurations, as well (reactions 15, 16, 17 and 19). [2]

The binding specificities induced by antigen in reaction 15 should be similar to authentic lipases, since phosphonate moiety imparts the oxyanionic and tetrahedral features of the transition state **12** (Figure 6) for ester hydrolysis to the antigen, whereas substitution of the methyl group on the benzylic carbon confers asymmetry of the alcoholic fragment of the molecule. An effective catalytic antibody should stabilize the oxyanion but does not necessarily protonate the leaving group alkoxyde.

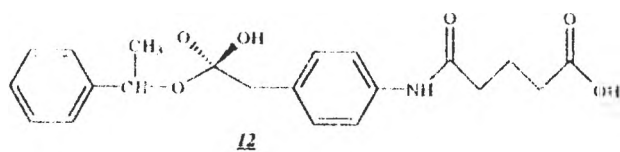


Figure 6

Kinetic studies were performed on 2 out of 11 antibodies (identified as catalysts) chosen on the basis of their rate of reaction and enantiomeric selectivity. In contrast to the

## Catalytic antibodies

(R) stereospecificities of monoclonal antibodies 2H6, 21H3 is completely specific for the hydrolysis of the antipodal (S)- $\alpha$ -methylbenzyl ester. Thus, by performing immunisation with a racemic mixture of antigens, two distinct catalysts can be generated and may be used for selective removal of antipodal blocking groups [26]. The hydrolytic reaction 16 is catalyzed with a greater than 200/1 preference for (R) phenylalanine containing isomer. Hapten was synthesized as a roughly equimolar mixture of the two diastereomers. In spite of this fact antibodies were selective for (D)-phenyl alanine containing isomer. One explanation is that haptens containing D-amino acids (or analogue thereof) are more immunogenic than those containing L amino acids. The pH dependence and hydroxide ion concentration dependence suggest the presence of a catalytic amino acid side chain in antibodies, such as tyrosine residue, which could act as a nucleophile, producing a labile tyrosine ester intermediate [27].

It is possible to isolate four optically pure stereoisomers (> 97-99% ee) in the 19-22% yield by direct optical resolution of 1,2 or 1,3-diastereomeric mixture by an antibody (reaction 21 and reaction 22). Antibody reagent design requires the preparation of haptens with structures that mimic the site catalytic activity, through transition-state analogues. Four stereochemically related haptens were prepared to effect the separation of four stereoisomers [28].

### 4.5.3. Epoxide hydrolysis

Acid catalyzed opening of epoxides may lead to a number of products, depending on the substrate and reaction conditions, and additional aspects of regioselectivity and stereochemistry at the two vicinal carbon centers add to the complexity of this reaction. Enantioselectivity is one of the greatest advantages of antibody catalysis: quaternary ammonium cation as hapten (reaction 28 and reaction 29) could mimic the developing positive charge on one of carbon atoms (**13** and **14**, Figure 7) and antibody catalyzed hydrolysis of epoxide produces trans diols. The aromatic moiety of both substrates is designed to provide most of binding energy to antibody [29].

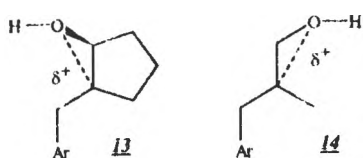


**Figure 7**

The pH- rate profiles of hydrolysis suggest that their reaction appears to depend on the structure of substrates: by contrast with complete kinetic resolution with cyclic substrate (reaction 28), both enantiomers of smaller substrate (reaction 29) are equally reactive with this catalytic antibody 14D9. The

five-membered ring of **13** probably provides a tighter fit to the antibody hydrophobic pocket that complements the piperidinium portion of hapten [29].

#### 4.5.4. Enol ethers hydrolysis

The acid-promoted hydrolysis of alkyl enol ethers can be catalysed by antibodies (reaction 30 and reaction 31) with very high enantioselectivity of rate determining protonation of the  $\beta$ -Carbon [14] to form optically pure carbonyl compounds. Thus, an antibody capable of nearly complete enantioselective protonation of both enol ether isomers (reaction 30) has been obtained from a hapten, where a positively charged tetrahedral nitrogen atom is substituted for a trigonal carbon atom of transition state **15** (Figure 8) [30].

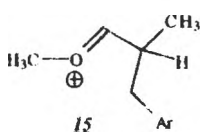


**Figure 8**

Since the quaternary ammonium center in hapten does not contain an exchangeable hydrogen atom to mimic proton transfer and the positively charged nitrogen atom is not substituted for the ether oxygen atom but for the  $\beta$ -carbon undergoing protonation, there are two effects to account for catalysis: (1) the presence of an ionizable protein side chain (neutral in protonated state and negatively charged

as free base, such as aspartate or glutamate, in agreement with active site titrations pH profile and kinetic solvent isotope effect), elicited against the positive charge not to act as a direct proton source but to interact with the  $\alpha$ -carbon center of the electron deficient oxocarbenium ion compatible with transition states **16** and **17** (figure 9), (2) Van der Waals binding interactions to hydrocarbon part of ammonium ion. Thus, the antibody reaction can be described as a bimolecular reaction between the antibody-substrate complex and the hydronium ion (**17**, figure 9).

## Catalytic antibodies

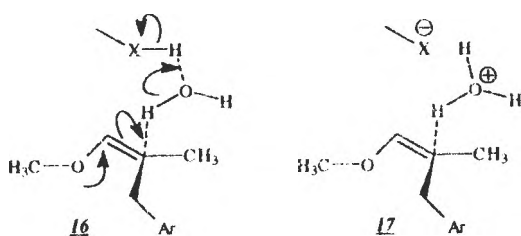


**Figure 9**

The absolute rate of antibody catalyzed reactions 32-38, spans several orders of magnitude depending on the reactivities of the substrates and pH. For pairs of similar substrates, higher substitution at the  $\beta$ -carbon leads to relatively

higher catalyzed reactions compared to background under an effect of the symmetry. Hydrolysis of substrates is significantly catalyzed by 14D9, although the double bond is misplaced relatively to 9, because the  $\alpha$ -carbon center is misplaced relative to the nitrogen center in hapten, in agreement with the figure 9, because the  $\alpha$ -carbon center of the oxocarbenium ion has the same location. Thus, it is possible to obtain catalytic antibodies with versatile substrate specificities (reactions 30-39) [14].

### 4.5.5. Oligosaccharide hydrolysis

For generating glycosidase antibodies (reaction 39 and reaction 40), the positively charged ammonium ion corresponding to the anomeric center of a cyclic acetal can induce functional groups in the antibody combining site which stabilize delocalized positive charge of transition state (**18**, Figure 10) in the hydrolysis and/or assist in the acid catalyzed expulsion of the leaving group.

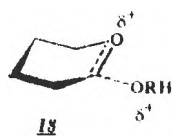


**Figure 10**

The 5-bromoindolyl leaving group (reaction 40) serves as common recognition element between substrate and hapten to ensure substrate binding. The values of  $k_{cat}$  at different pH show that the antibody uses both general acid and base catalysis.[31]

### 4.6. Rearrangement of peptide bond - consecutive reaction (imide formation, imide hydrolysis)

Consecutive reactions, such as rearrangement of chains -an important means in the inactivation of proteins or peptides [32] present the need to encounter and stabilize the transition state [8]. For example, the deamination of an Asn - Gly peptide is known to proceed through a succinimide (reaction 41) and this intermediate can be opened by the



attack of water at either carbonyl [10] (reaction 42). The overall reaction is a two-step process and is rate limited by the initial step of cyclisation to form the succinimide [32]. The inducing racemic hapten - a cyclic phosphinate - contained two tetrahedral mimics of transition states **19** and **20** (Figure 11), which are the phosphinate and the secondary alcohol moiety [8,32].

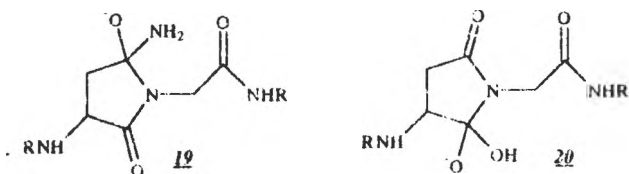


Figure 11

Two classes of antibodies were identified: those that catalyze only the succinimide hydrolysis (39F3 and 14A8 are selective for either L-succinimide or D-succinimide and respectively 23C7 and 40H4 are

selective for both isomers) and those that catalyze both deamination and succinimide hydrolysis (2E4 and 34C3) [8,32].

The rate acceleration is characteristic of rotational restrictions imposed on an intramolecular process [32].

Processing of either L- or D-isomer of the succinimide substrate by an antibody is in a reciprocal relation to isoAsp/Asp = 3.5 background ratio as a consequence of the balance between steric hindrance and an electronic effect [32]. For example, 23C7 produced the largest deviation of isoAsp to Asp. Ratios of 10.9 for L-succinimide and 1.5 for D-succinimide were found as compared to 3.7 for the background reaction. The kinetic constants for the hydrolysis of both isomers indicate that R62-23C7 binds the D-isomer about 4 times better than it binds the L isomer, so it can be inferred that the true hapten was the D-isomer of phosphinate. Thus, the antibody binding site should stabilize both tetrahedral intermediates of D-succinimide and as such, the hydrolysis of both carbonyls is equivalent. In the case of L-isomers hydrolysis to the IsoAsp product is 30 times more likely than hydrolysis to the Asp product [33]. In conclusion, the problem of multiple transition states is dealt with the use of a bifunctional transition state analog [8,32].

#### 4.7. Group transfer reactions

Catalysis of group transfer reactions in general has two mechanistic types: a) direct group transfer between antibody-bound donor and acceptor substrate and (b) indirect group transfer through intervening covalently bound antibody-donor species [8].

##### 4.7.1 Aminolysis reaction (amide bond formation)

The antibody 24B11 elicited to the hapten (reaction 45 and reaction 5) which resembles the tetrahedral intermediate anticipated to form along either the aminolysis from a racemic lactone and an amine (**21**, figure 12) or cyclisation route possesses sufficient binding interaction to promote the bimolecular amide synthesis.

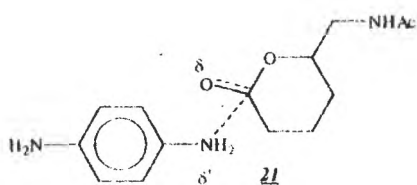


Figure 12

Kinetic data obtained at a range of substrate concentration were in accord with a rapid equilibrium bireactant system and were used to obtain the value of  $K_m$  and  $k_{cat}$ . These show that the binding of one ligand has no effect on the other and the antibody catalysis is enantioselective for (-)

lactone enantiomer (>90% ee) Product appearance ceased after the first 5-10% of reaction, suggesting strong product inhibition ( $K_i = 75nM$ ).

The advantage of the enzyme-promoted reaction may primarily reside in the entropy gain associated with an intra- versus an intermolecular process. This advantage is provided by sequestering lactone plus amine in the antibody binding site in a position favorable for the aminolysis reaction. This process may or may not be accompanied by actual transition state stabilization or further substrate destabilization. For the cyclisation reaction,  $k_{cat}/k_{uncat} = 790$  reflects greater congruence between the analog and the anticipated transition state than that corresponding to the bimolecular reaction [9].

##### 4.7.2. Transesterification reaction (ester bond formation)

The transesterification reaction is formally a bimolecular substitution reaction that must compete with hydrolysis of ester. If transesterification activity had been the initial target, then the hapten should have been a diesterified phosphonate with either similar or dissimilar alcohol moieties. This should provide sufficient space in a programmed binding

site for the simultaneous binding of both ester and alcohol to antibody" [3]. The antibody exhibits an induced fit of the second substrate to activate the acyl intermediate for subsequent chemical reaction [10]

The antibody PCP21H3 catalyzed the reactions 47 to 52 in a mixture of water and 10% DMSO. The kinetic constants are consistent with the ping-pong bi-bi mechanism (product is released between addition of two substrates). Evidence for the covalent antibody intermediate was obtained by measuring the release of p-nitrofenol at different values of PCP21H3 concentration (in reaction 49) and by labelling of ester substrate (also in reaction 49).

Because the mechanism with and without antibody is different (a two chemical steps through an acyl-antibody intermediate, respectively a one-step, base catalyzed process), the analysis of antibody catalytic efficiency is difficult.

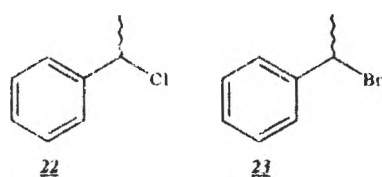


Figure 13

The kinetic behavior of the substrates in reactions 50, 51 and 52 reflects a change in the rate limiting step from deacylation to acylation of the antibody. The enhancement of hydrolysis of vinyl ester by substrate surrogates (**22** and **23**, figure 13) is made by activation of the antibody for a hydrolytic

cleavage in an induced fit model

Thus "the data and observations indicate that monoclonal antibody (PCP21H3 : (I) has both esterase and transferase activities; (II) efficiently catalyzes transesterifications in aqueous media and is capable of reversibility; (III) utilizes an acyl-antibody intermediate; (IV) demonstrates an induced fit of substrate probably as a consequence of the conformation of the acyl intermediate and the need to have the active site congruent to the transition state structure; (V) operates under two general principles, entropy loss and transition state stabilization, which rely on the energy of protein-substrate interaction." [12].

Antibody generated against a neutral phosphonate diester transition-state analog (racemic) containing elements of the acyl acceptor and the leaving group in the tetrahedral geometry is a first step toward aminoacyl tARNs antibodies. Thus, antibody 18R 136.1 was found to catalyze the aminoacylation of 3'-hydroxyl group of thymidine with an alanyl ester (reaction 54) and to have lower affinity for the trigonal product

## Catalytic antibodies

The family of plots constructed for reaction 54 by holding one substrate concentration constant while varying the concentration of the second indicates that the antibody exhibits sequential binding (the binding of one ligand has no effect on the other). The kinetic values for reaction 54e ( $k_{cat} = 1.06 \cdot 10^{-2} \text{ s}^{-1}$  and  $K_m = 0.34 \cdot 10^{-3} \text{ M}$ ) suggest that antibody 18A.136.1 has low selectivity in substrate binding but discriminates the diastereomeric transition states for the transesterification reaction

The antibody has the ability to catalyze acyltransfer to thymidine although the concentration of water exceeds the concentration of alcohol. One mechanistic interpretation is that the amino acid ester is only forced into a transition-state geometry in the presence of thymidine derivative.

In fine, immune system has provided two mechanistic alternatives for similar acyl transfer reaction.[34]

### 4.8. Imine formation

Transamination, important in enzymology and organic chemistry, implies chiral  $\alpha$ -amino acids in a carbanion intermediate reaction and is catalyzed by pyridoxal phosphate (PLP) as enzymatic cofactor.

Antibody 17C5-11C2 raised against the hapten with tetrahedral C-4' (reaction 54), had the affinity and specificity to bind both D-p-nitrophenylalanine substrate and 5'-deoxypyridoxal cofactor in a catalytic orientation proper for stereospecific aldimine intermediate formation

The kinetics of the antibody catalyzed reaction is consistent with a random-binding mechanism. Although the kinetic analysis indicated little or no specificity for L-p-nitrophenylalanine, both D- and L-enantiomers were effective inhibitors. This fact suggests that the antibody discriminates the two diastereomeric transition states, but it doesn't discriminate enantiomers of hapten

Since the design of the hapten doesn't allow the planarity of the delocalized carbanion intermediate (24,

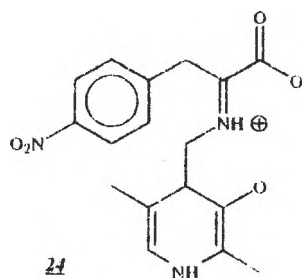


Figure 14

Figure 14), the antibody is not able to catalyze transamination. Improvements in hapten design and mutagenesis or genetic selection may yield catalytic antibodies with desired catalytic capabilities. [35]

#### 4.9. *Cis- trans isomerization*

Antibody catalyzed cis-trans isomerization reaction of carbon-carbon double bond, an important process in -for example- the synthesis of D vitamin and the isomerization of retinal, involves 1,4 nucleophilic addition of an active-site group to the unsaturated substrate, followed by rotation around the resulting  $\alpha,\beta$  - single bond and subsequent collapse of the intermediate.

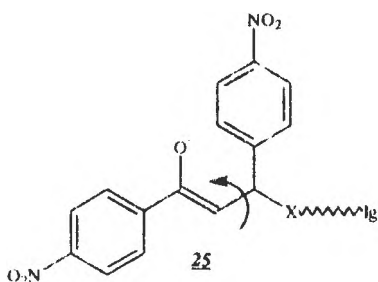


Figure 15

The hapten corresponding to  $\alpha,\beta$  unsaturated ketone (reaction 55) contains a positively charged amino group, so that the induced carboxylate in the antibody combining site may be an active site nucleophile or base. Moreover, the nitrophenyl moieties roughly perpendicular to each other may accommodate the transition state 25 (figure 15) for rotation about  $\alpha,\beta$  -

single bond.

The antibody DYJ10-4 is specific for trans substrate, as it can be inferred from  $K_i$  values for cis and trans substrate ( $K_{i,cis}$  - 1mM,  $K_{i,trans}$ =6.7 $\mu$ M) [36]

#### 4.10. *Metal chelation*

In the catalytic insertion of  $Fe^{2+}$  into protoporphyrin IX by ferrochelatase, the distortion of porphyrin macrocycle resulting from N-alkylation may approximate the transition state of enzymatic reaction. In this model, the exposure of pyrole nitrogen pairs to solvent facilitates metal ion complexation

In addition, antibody 7G12-A10-G1 A12 to N-methylmesoporphyrin IX racemic hapten that mimics a strained , distorted conformation of substrate (reaction 56) was found to catalyze  $Zn^{2+}$ ,  $Cu^{2+}$ ,  $Co^{2+}$ ,  $Mn^{2+}$  incorporation by the planar mesoporphyrin but not  $Ni^{2+}$ .

## Catalytic antibodies

Kinetic studies made for  $Zn^{2+}$  and  $Cu^{2+}$  chelation indicate a value of  $K_{r1}$  almost identical for the two ions. Since no evidence of saturation of antibody by metal was observed between 0.5 and 2.5 mM  $Cu^{2+}$ , it can be inferred that the binding of metal ions by antibody does not contribute significantly to catalysis. Also, it was found that inhibition by metal (III) mesoporphyrins ( $Mn^{3+}$  and  $Fe^{3+}$ ) is greater than that by metal (II) mesoporphyrins ( $Zn^{2+}$  and  $Cu^{2+}$ ) suggesting a closer initiation of the positively charged hapten by metalloporphyrins with more positive charge density at the metal center [37].

Further, the specific, stable complex of the 7G12-A10-G1-A12 antibody with  $Fe^{3+}$  mesoporphyrin IX catalyzed the peroxidation of several substrates (reaction 57) and served for studying the oxidative reactions characteristic of heme enzymes, e.g. horse radish peroxidase (HRP). In all cases, the antibody alone showed no peroxidase activity and the complex catalyzed the peroxidation faster than the iron porphyrin did it alone. The kinetic parameters for antibody-catalyzed peroxidation are comparable:  $k_{cat} / K_M$  is  $233 M^{-1} s^{-1}$  for ABTS,  $122 M^{-1} s^{-1}$  for pyrogallol and  $274 M^{-1} s^{-1}$  for  $H_2O_2$ . Thus, an antibody catalyst with binding site for both cofactor and substrate was obtained [38].

### ***5. Extending the scope and increasing activity***

We must start specifying that antibody catalysis is selected from a large repertoire of structures, initially by screening for antibodies that bind antigen, and then, for activity. The desired active sites can be selected on the basis of antigen affinity coupled with sensitive colorimetric or biologic assays (such as ELISA). Moreover, a high sensitive and generally applicable assay is now available for the detection of low concentration catalysts for bimolecular reactions [39].

Although large rate accelerations have been observed in some cases, most catalytic antibodies exhibit relatively low activities. So, a challenge is required, and this is to achieve access to the precise positioning between substrate and active site residue necessary for increasing catalytic function. Improvements in creating catalytic antibodies can be achieved by both genetic and chemical modifications [3]: (1) site-specific mutagenesis of specific amino acids, (2) replacement of entire loop regions in the antibodies, (3) improvement in hapten design, (4) recruitment of catalytic cofactors; (5) alteration of medium effects, (6) modulation of the binding sites hydrophobic character, (7) selective derivatization of the antibody combining site [36]; (8) obtaining of catalytic

antibodies for combinatorial libraries [40, 41]. Thus, the two major goals for the design of new catalysis, i.e., the facilitation of chemical transformation and the control of product outcome may be successfully achieved.

Side-directed mutagenesis provides a means for evaluating the contributions of various amino acids residues to hapten binding and for improving the catalytic power of antibody [3]. In order to accomplish that modern genetic techniques subject first-generation antibody catalysts to extensive random mutagenesis and identically improved variants by classical genetic selection [7]. A significant example arises. It was identified a permissive chorismate-mutase deficient cell-line following extensive random mutagenesis of the antibody-harboring cells with ethyl methanesulphonate and classical genetic selection. In brief, the genetic selection seems to be a solution of the efficiency.

Since antibody specificity may be programmed through hapten design, improvements in hapten design, which better accommodate the transition state and leaving group structure, will lead to catalysts with novel specificities.

Although some features are clearly programmed by the inducing hapten, others rich in kinetic and stereochemical complexity appear to arise as a consequence of the chemistry within a confined space pocket by a protein [8]. Antibody site chain in the binding pocket can participate directly in some of the reactions. Thus, to increase the catalytic rate production of antibody that present cofactors in proximity to bind antigen was considered.

Catalytic auxiliaries used by enzymes included metal ions, hemes, thiamine, flavins and pyridoxal. But the diversity of immune response should allow to use not only the natural cofactors, but also the unnatural ones, not accessible to enzymes, providing routes to more sophisticated, highly specific and efficient catalysis by operating in a concerted manner.

## Catalytic antibodies

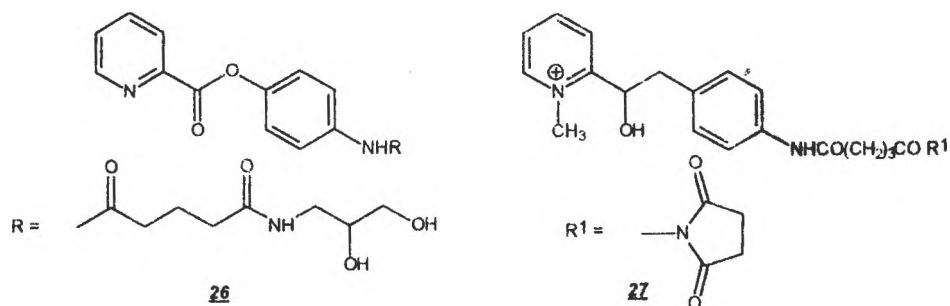


Figure 16

There are three major ways in which this approach could be accomplished. Firstly, the antibody should be elicited to a multisubstrate analog in which binding sites for the cofactor and substrate are generated in a single immunization. Starting with the observation that the strength of metal-ion binding to the reactant and metal-ion promoted  $\text{OH}^-$  attack control the rate of ester and anhydride hydrolysis, a strategy to force immunoglobulin binding to distinct metal entities was developed. The observed rate accelerations in one of the cases show that the presence of the metal is both necessary and sufficient, i.e. the antibody catalyzed hydrolysis of pyridine ester (**26**, figure 16), in the presence of  $\text{Zn}^{2+}$  is >1000 times than the metal catalyzed rate and >10,000 times than the uncatalyzed rate. It is remarkable that the suitable environment for catalysis was provided by a hapten (**27**, figure 16), which does not include a metal ion or a coordination complex. [42]

Secondly, a wide variety of natural and synthetic catalytic groups are likely to be incorporated into antibody combining sites either by generating a cofactor binding site or by a selective derivatization of the antibody combining site. Thus, cofactors are covalently linked to the antibody molecule in close proximity to the substrate binding site through cleavable affinity labels. Further, a selective derivatization of a thiol-containing antibody with imidazole allowed a selective catalyst for ester hydrolysis. Although the antibody MOPC 315 binds initially substituted 2,4-dinitrophenyl ligands, the modified form catalyzes the hydrolysis of coumarin ester with kinetic constants  $K_M = 2.2 \pm 0.2 \mu\text{M}$  and  $k_{\text{cat}} = 0.052 \pm 0.005 \text{ min}^{-1}$  ( $\text{pH}=7.0$ ). The kinetic data are consistent with the presence of a catalytic imidazole acting either as a general base or as a nucleophile. It is noteworthy that the



unique thiol acts as a single handle for the subsequent introduction of catalytic groups into the antibody-combining-site [36].

Thirdly, the existence of two-chained antibodies and combinatorial libraries cofactors can be brought in support of antibody-catalyzed transformations. Within this method, a cofactor binding light chain could be combined with a heavy chain libraries derived from Polymerase Chain Reaction (PCR) products

We must underline that, in fact, large combinatorial libraries of antibody fragments can be generated readily and rapidly using PCR. Such libraries together with semisynthetic libraries, can provide a uniform and reproducible source of antibody molecule as starting materials. Thus, a metalloantibody has been constructed with a coordination site for metals in the antigen binding pocket. Following the metal of the  $Zn^{2+}$  binding site from carbonic anhydrase b, three histidine residues have been placed in the light-chain and evidence for  $Cu^{2+} > Zn^{2+} > Cd^{2+}$  binding in the three histidine site has been brought. By positioning a catalytically active metal next to a specific position of a substrate, antibody catalysis of redox and hydrolytic reactions should be achieved [43].

And last, but not least, light irradiation could be used by an antibody to break two carbon-carbon bonds of a cis - syn thymine dimer (reaction 60). These examples show that antibody catalysts make use of a wide range of cofactors

Further on, the catalytic antibody efficiency may be increased by introducing multiple combination of traits in antibody combining site and having them work in a synergistic manner.

## **6. Conclusions**

The lines above guide the reader toward a natural conclusion: the estimated possibilities offered by antibody catalysis are not only factual, but also amazing. They include synthetic utilities, novel specificities, feasibility of using catalytic antibodies to carry out vital biological transformation "in vivo", to explore the nature of biological catalysts, and also to catalyze reactions not found to be processed by enzymes.

Antibodies should, in principle, be ideal catalysts for initiating and controlling a lot of processes, as they were previously shown to catalyze complex reactions in which claimed to simultaneously neutralize point charges, overcome entropic barriers and to provide chiral building pockets for stereoselectivity. It was already shown that, although unexpected, the antibody induced by a single transition state analogue, carries out its hydrolytic reaction

via two transition states. Then, the advantage of the abzyme-promoted reaction resides in the case of amide synthesis in entropy gain associated with an intra- versus intermolecular process. Aminoacyl transfer synthetases with novel specificities have been accomplished. It was demonstrated the feasibility of catalytic-antibody generation for chemical transformations that require stereochemical control, such as asymmetric synthesis of C-C bond which is difficult to be controlled by using conventional methodologies. It was also possible to isolate four optically pure stereoisomers in the maximum 25% yield by direct optical resolution of a diastereomeric mixture by an antibody.

All the above mentioned are but few examples of what can be made with the help of programmed anticropogenesis. Subsequent applications appear natural, since a lot of resources are available. Nevertheless, there is still much to do.

### 7. References

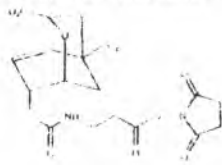
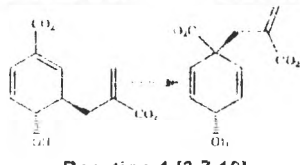
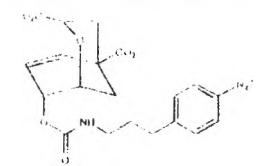
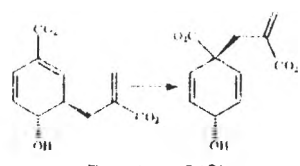
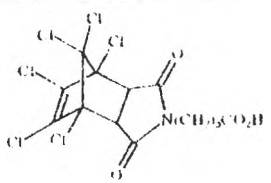
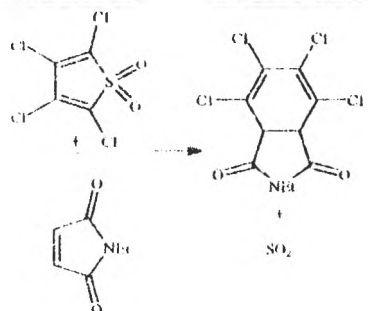
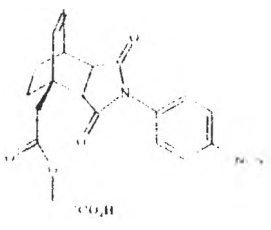
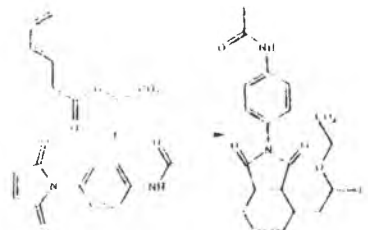
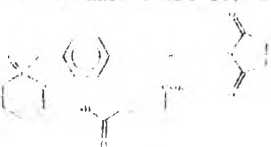

- [1] Tramontano, K.D., Janda, K.D. and Lerner, R. A. *Science*, 1986, **234**, 1566
- [2] Lerner, A.R., Benkovic, S.J. and Schultz, P.G. *Science*, 1991, **252**, 659, 660, 663
- [3] Benkovic, S.J. *Annu. Rev. Biochem.*, 1992, **61**, 31-32, 50, 36, 48
- [4] Pauling, L., *Chem Eng. News*, 1946, **24**, 1376
- [5] Pauling, L., *Am. Scientist* 1948, **36**, 51
- [6] Pollack, S.J., Jacobs, J.W. and Schultz, P.G., *Science*, 1986, **234**, 1570
- [7] Hilvert, D. *Acc. Chem. Res.* 1993, **26**, 552
- [8] Stewart, J.D., Liotta, L.J. and Benkovic, S.J. *Acc. Chem. Res.* 1993, **26**, 396-400
- [9] Benkovic, S.J., Napper, A.D. and Lerner, R.A. *Proc. Natl. Acad. Sci. USA*, 1988, **85**, 5355
- [10] Stewart, J.D. and Benkovic, S.J., *Chemical Society Reviews*, 1993, 214, 217
- [11] Cochran, A.G., Pham, T., Sagasawara, R., and Schultz, P., *J. Am. Chem. Soc.*, 1991, **113**, 6670
- [12] Wirsching, P., Ashley, J.A., Benkovic, S.J., Janda, K.D. and Lerner, R.A., *Science*, 1991, **252**, 680
- [13] Gibbs, R.A., Benkovic, P.A., Janda, K.D., Lerner, R.A. and Benkovic S.J., *J. Am. Chem. Soc.*, 1992, **114**, 3528
- [14] Raymond, J.L., Jahangiri, G.K., Stoudt, C. and Lerner, R.A. *J. Am. Chem. Soc.*, 1993, **115**, 3911, 3915
- [15] Lewis, C., Kramer, T., Robinson, S. and Hilvert, D. *Science*, 1991, **253**, 1019
- [16] Grate, J.W., McGill, R.A. and Hilvert, D., *J. Am. Chem. Soc.*, 1993, **115**, 8578
- [17] Benkovic, S.J., Adams, J.A., Boders, Jr., C.L., Janda and K.D., Lerner, *Science*, 1990, **250**, 1135
- [18] Hilvert, D. *Pure & Appl. Chem* 1992, **64**(8), 1103
- [19] Li, T., Janda, K.D., Ashley, J.A., and Lerner, R.A., *Science*, 1994, **264**, 1289

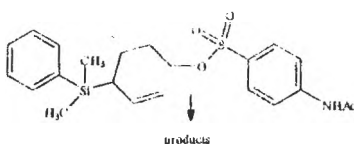
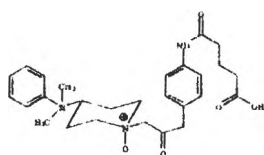
- [20]. Janda, K.D., Ashley, J.A., Jones, T.M., McLeod, D.A., Schloeder, D.M., Weinhouse, M.I., Lerner, R.A., Gibbs, R.A., Benkovic, P.A., Hilhorst R., and Benkovic, S.J., *J. Am. Chem. Soc.*, 1991, **113**, 291
- [21]. Napper, A.D., Benkovic, S.J., Tramontano and A., Lerner R.A. *Science*, 1987, **237**, 1041
- [22]. Lewis, C. Paneh P., O'Leary M.H. and Hilvert, D., *J. Am. Chem. Soc.*, 1993, **115**, 1410
- [23]. Ashley, J.A., Lo C-H.L., McElhaney, G.P., Wirsching, P. and Janda, K.D., *J. Am. Chem. Soc.*, 1993, **115**, 2515
- [24]. Stryer, L. *Biochemistry*, 1995, fourth edition, Freeman & Co, New-York, 236
- [25]. Janda, K.D., Schloeder, D., Benkovic, S.J. and Lerner, R.A. *Science*, 1988, **241**, 1188
- [26]. Janda, K.D., Benkovic, S.J., Lerner, R.A., *Science*, 1989, **244**, 437
- [27]. Pollack, S.J., Hsiun, P. and Schultz, P.G. *J. Am. Chem. Soc.*, 1989, **111**, 5961
- [28]. Kitazume, T., Lin, J.T., Yamamoto, T. and Yamazaki, T. *J. Am. Chem. Soc.*, 1991, **113**, 8573
- [29]. Sinha, S.C. and Keinan, E., *J. Am. Chem. Soc.*, 1993, **115**, 4893
- [30]. Reymond, J.L., Janda, K.D. and Lerner, R.A., *J. Am. Chem. Soc.*, 1992, **114**, 2257
- [31]. Yu, J., Hsieh, L.C., Kochersperger, L., Yonkovich, S., Stephans, J.C., Gallop, M.A. and Schultz, P., *Angew. Chem. Int. Ed. Engl.*, 1994, **33**(3), 339
- [32]. Gibbs, R.A., Taylor, S., and Benkovic, S.J. *Science*, 1994, **258**, 803
- [33]. Liotta, L.J., Benkovic, P.A., Miller, G.P. and Benkovic, P.A. *J. Am. Chem. Soc.*, 1993 **115**, 350
- [34]. Jacobsen, J.R., Prudent, J.R., Kochersperger, L., Yonkovich S. and Schultz, P. *Science*, 1992, **256**, 365
- [35]. Jackson D.Y. and Schultz P., *J. Am. Chem. Soc.* 1991 **113**, 2319
- [36]. Pollack, S.J. and Schultz, P. *J. Am. Chem. Soc.*, 1989 **111**, 1929
- [37]. Cochran, A.G. and Schultz, P., *Science*, 1990, **249**, 781
- [38]. Cochran, A.G. and Schultz, P., *J. Am. Chem. Soc.*, 1990 **112**, 9414
- [39]. Lane, J.W., Hong, X. and Schwabacher, A.W., *J. Am. Chem. Soc.*, 1993 **115**, 2078
- [40]. Chen, Y.C.J., Darion, T., Sastry, L., Mubarak, M., Janda, K. and Lerner, R.A., *J. Am. Chem. Soc.*, 1993 **115**, 357
- [41]. Posner, B., Smiley, J., Lee, I. and Benkovic, S., *TIBS*, 1994, **19**(4), 145
- [42]. Wade, W.S., Ashley, J.A., Jahangiri, G.K., McElhaney, G., Janda, K.D. and Lerner, R.A. *J. Am. Chem. Soc.*, 1993 **115**, 4906
- [43]. Iverson, L.I., Iverson, S.A., Roberts, V.A., Getzoff, E.D., Tainer, J.A., Benkovic, S.J. and Lerner, R.A., *Science*, 1990, **249**, 659

Catalytic antibodies

8. Appendix

Examples of reactions catalyzed by antibodies (adapted from [2])

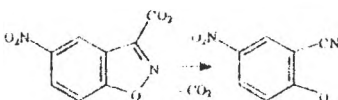
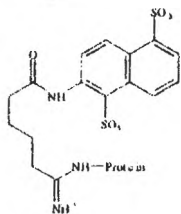
Antigen	Substrates + Products	$k_{cat}/k_{uncat}$	$K_M$
Claisen rearrangement:			
		$10^4$ (11F1-2E9) $10^2$	260  51
Reaction 1 [3,7,18]			
			
Reaction 2 [2]			
Diels-Alder condensation:			
		$10^4$	900 (diene)  583 (dienophile)
Reaction 3 [7,2]			
			
Reaction 4 [7]			
Lactonisation			
		167 25°C, pH=7	76
Reaction 6 [21]			



$k_{cat}$  ( $S^{-1}$ )  
 $3.3 \cdot 10^{-4}$   
 pH 7.0

$K_M$  ( $\mu M$ )  
 230

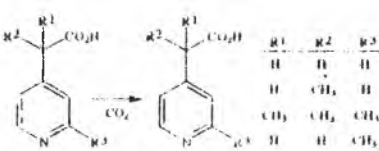
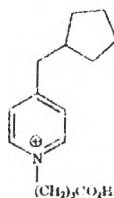
**Reaction 6 [19]**  
 Decarboxylations



$1.9 \cdot 10^4$   
 ( $20^\circ C$ , pH=8)

168

**Reaction 7 [15]**

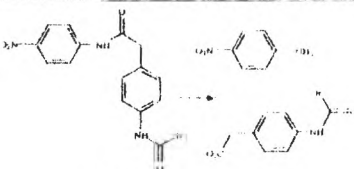
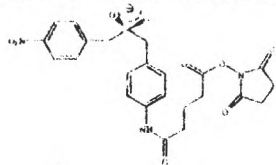


$1.9 \times 10^5$	$144 \times 10^3$
$2.3 \times 10^4$	$91 \times 10^3$
$1.2 \times 10^6$	$41 \times 10^3$
$2.0 \times 10^5$	$70 \times 10^3$

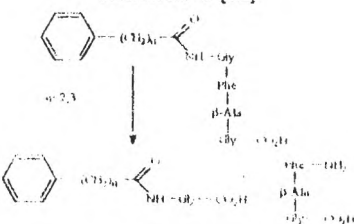
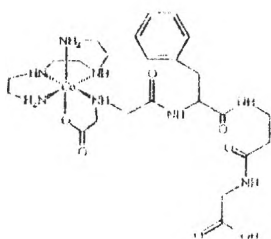
pH = 5.5 ;  $t = 20^\circ C$

**Reaction 8 [23]**

**Amide Hydrolysis**

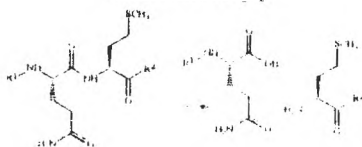


**Reaction 9 [10]**



**Reaction 10 [2]**

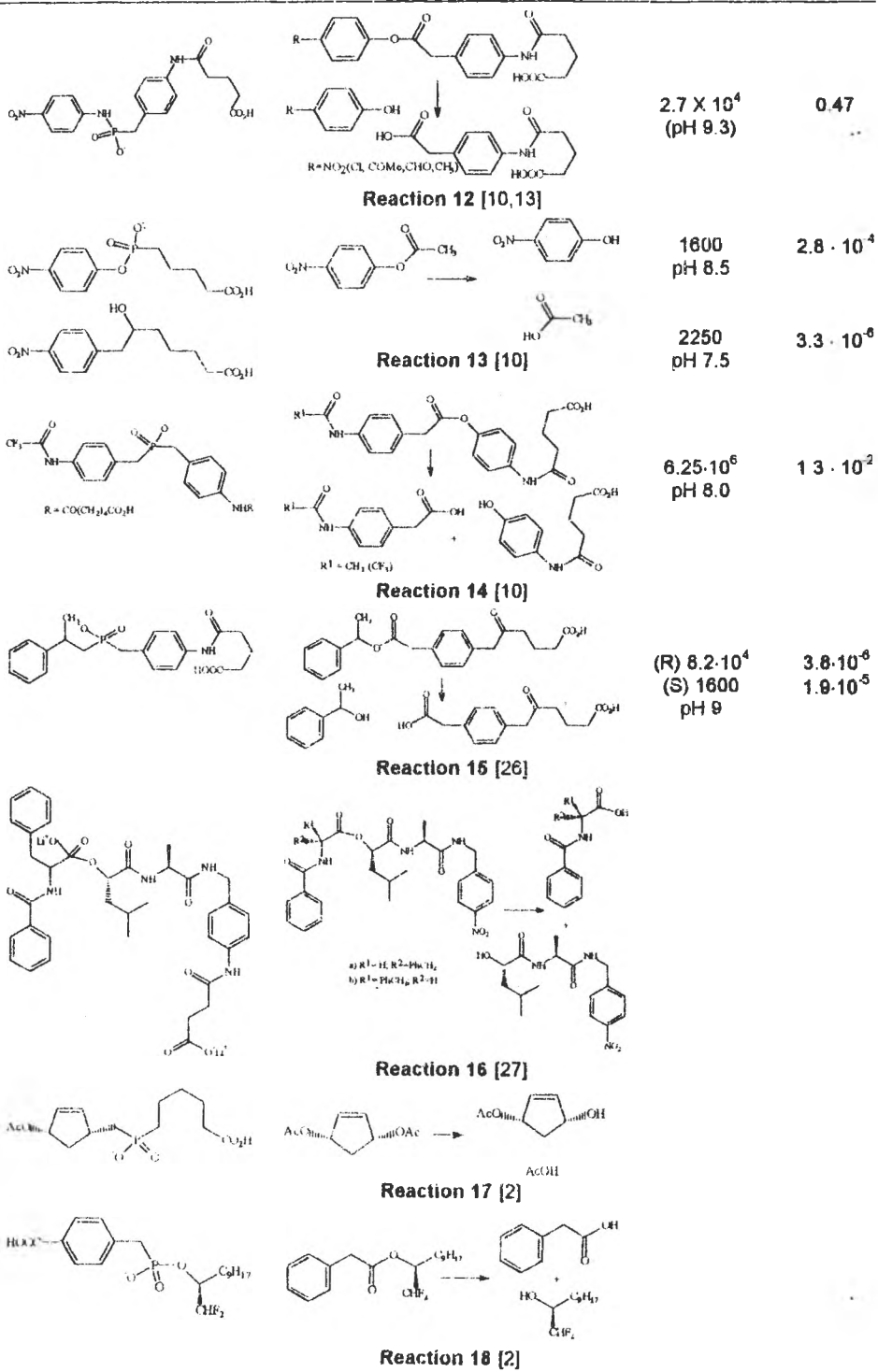
unknown

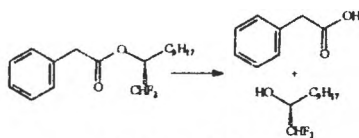
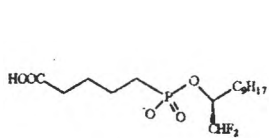


**Reaction 11 [2]**

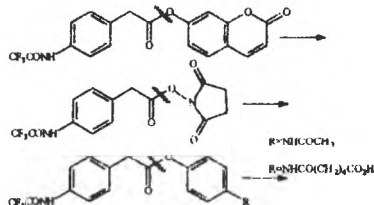
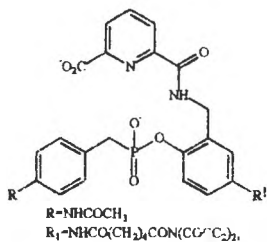
# Catalytic antibodies

## Ester hydrolysis:





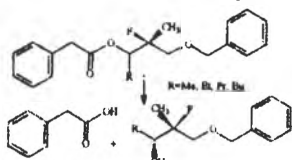
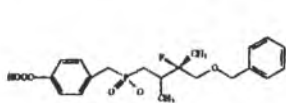
Reaction 19 [2]



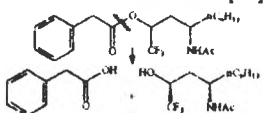
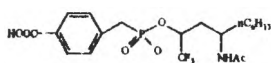
Reaction 20 [1]

960  
210  
pH 8.0

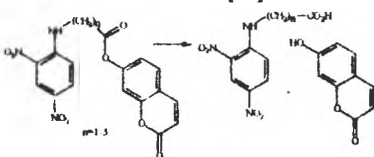
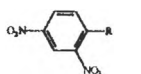
$1.5 \cdot 10^{-2}$   
 $1.3 \cdot 10^{-2}$



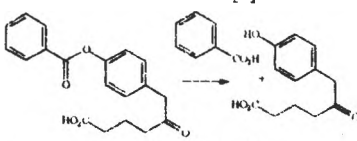
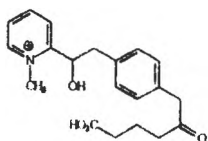
Reaction 21 [28]



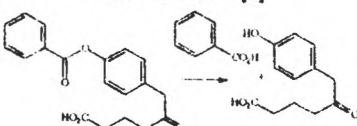
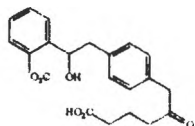
Reaction 22 [28]



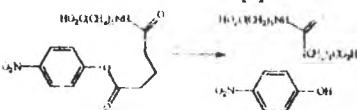
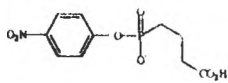
Reaction 23 [2]



Reaction 24-1 [2]

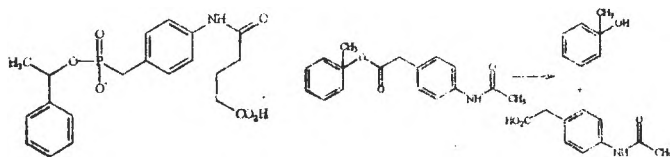


Reaction 24-2 [2]



Reaction 25 [2]

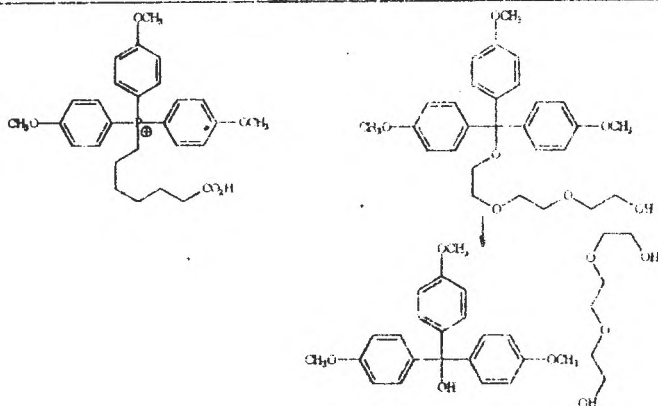
Catalytic antibodies



Reaction 26 [2]

Carbamate reactions (see reactions 43, 44)

Trityl hydrolysis :



Reaction 27 [2]

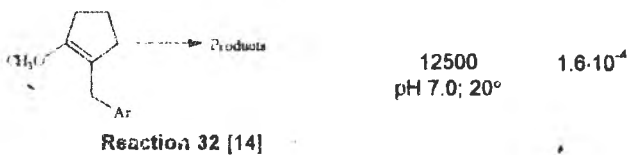
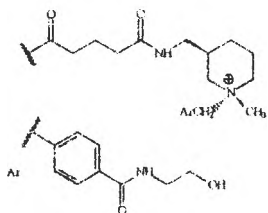
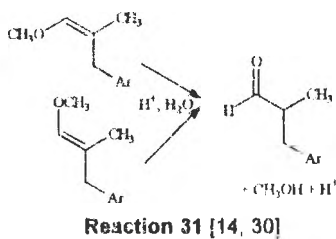
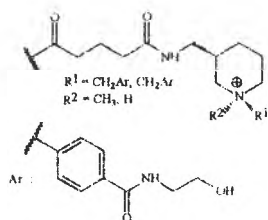
Epoxide hydrolysis :

	$k_{cat}/k_{inert}$	$k_{cat}/K_M$ $\mu M^{-1} s^{-1}$
<p>Reaction 28 [29]</p> <p>R-CH<sub>2</sub>NHCO-linker    Ar :</p>	440 pH 5.8 t=24°C	$0.1 \cdot 10^6$
<p>Reaction 29 [29] see also reaction 64</p> <p>R-CH<sub>2</sub>NHCO-linker    Ar :</p>	(4S): 105 (4R): 100 pH 5.6 t=24°C	$3.6 \cdot 10^7$ $4.4 \cdot 10^7$

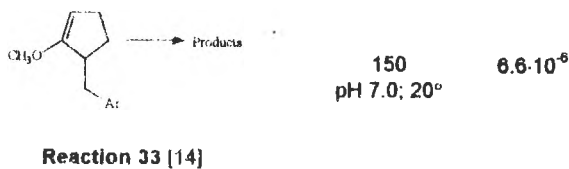
Enol ether hydrolysis :

<p>Reaction 30 [30, 14]</p> <p>R<sup>1</sup> - CH<sub>3</sub> R<sup>2</sup> - CH<sub>2</sub>Ar</p>	2500 pH 5.5 t=37°	$2.7 \cdot 10^7$
<p>Reaction 30 [30, 14]</p> <p>R<sup>1</sup> - CH<sub>3</sub> R<sup>2</sup> - CH<sub>2</sub>Ar</p>	260 pH 5.5 t=37°	$8.3 \cdot 10^7$

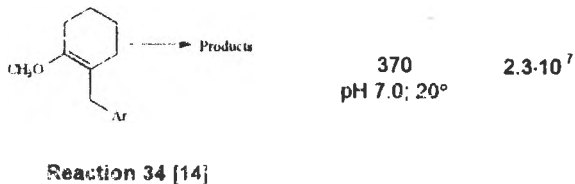




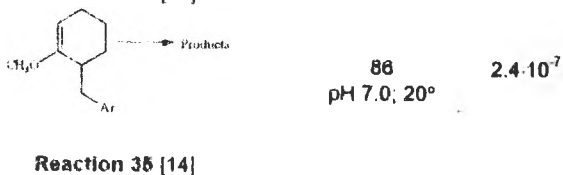
idem



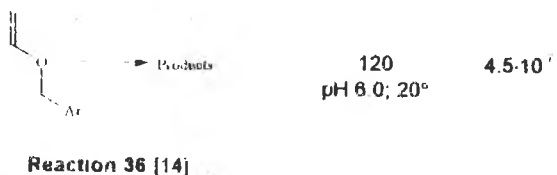
idem



idem



idem



idem

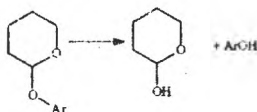
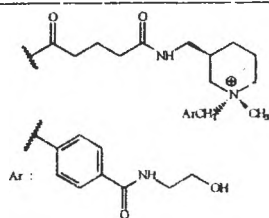


idem

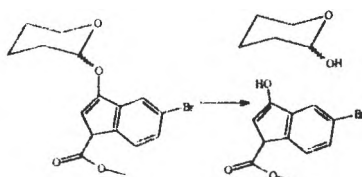
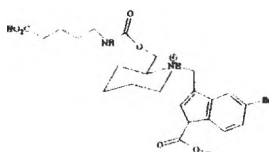


# Catalytic antibodies

## Glycoside hydrolysis

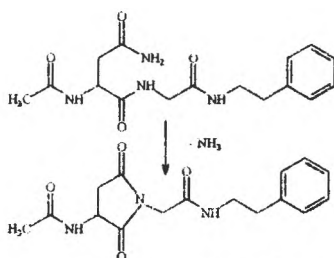
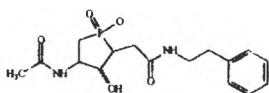


**Reaction 39 [14]**

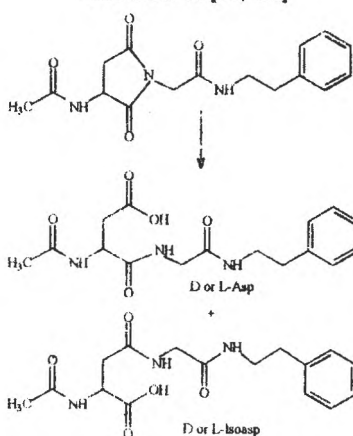
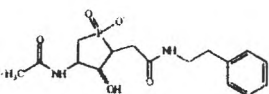


**Reaction 40 [31]**

## Rearrangement of peptide bond:



**Reaction 41 [10, 32]**



**Reaction 42 [10, 32,33]**

$k_{cat}/k_{uncat}$

$k_{cat}/K_M$   
 $\mu M^{-1} \cdot s^{-1}$

(D) 70  
pH 8.5

$6.3 \cdot 10^{-7}$

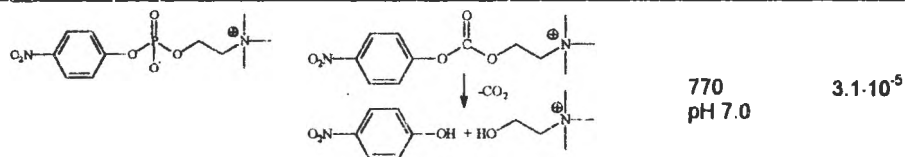
(D) 70  
(Isoasp)

$3.6 \cdot 10^{-2}$

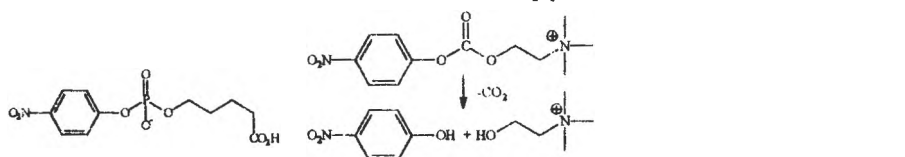
90  
(Asp)

$3.9 \cdot 10^{-2}$

Carbonate hydrolysis:

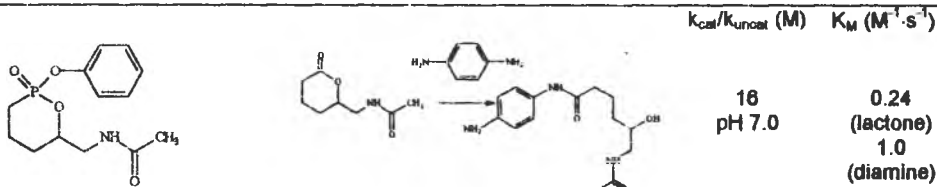


Reaction 43 [6]

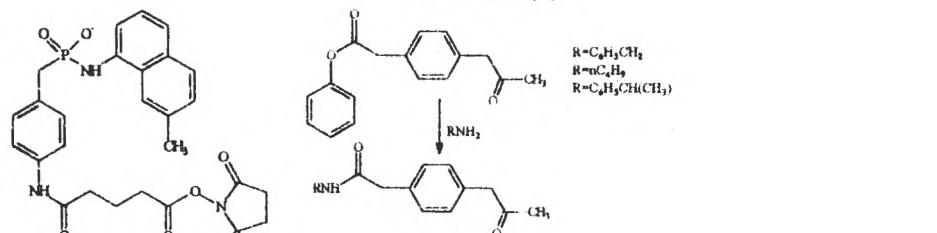


Reaction 44 [2]

Amide bond formation:

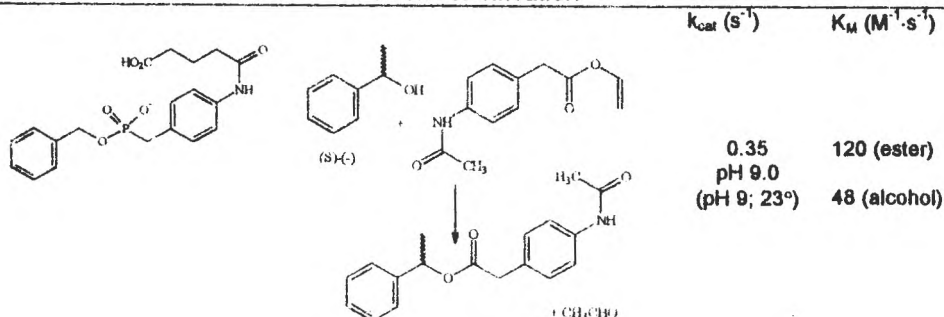


Reaction 45 [9]



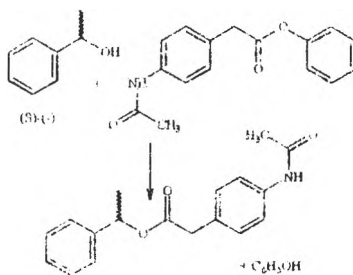
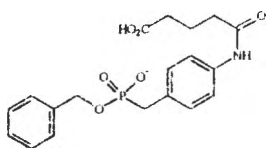
Reaction 46 [2]

Transesterification



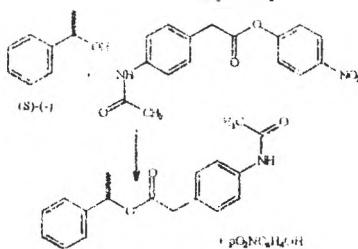
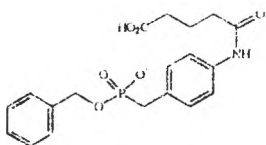
Reaction 47 [8, 12]

## Catalytic antibodies



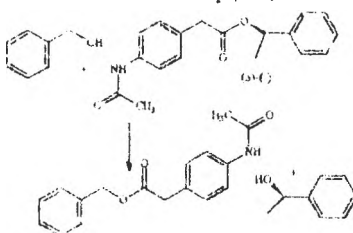
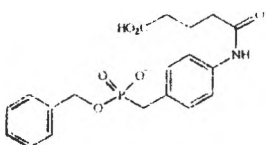
0.32  
pH 9.0  
(pH 9; 23°)  
1700 (ester)  
64 (alcohol)

**Reaction 48 [8, 12]**



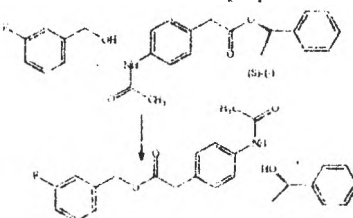
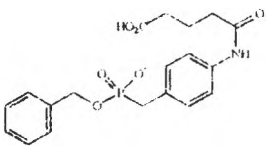
$5.5 \cdot 10^{-3}$   
pH 9.0  
(pH 7; 23°)  
140 (ester)  
0.42 (alcohol)

**Reaction 49 [8, 12]**



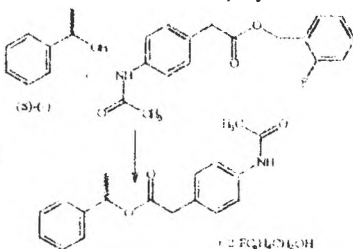
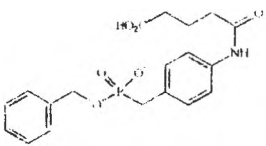
0.072  
pH 9.0  
(pH 9; 23°)  
5.43 (ester)  
37.5 (alcohol)

**Reaction 50 [12]**



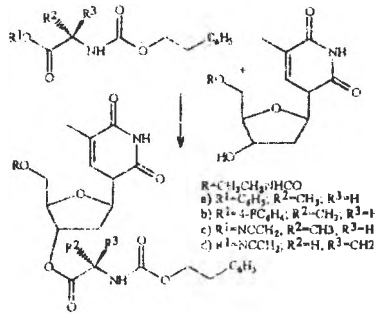
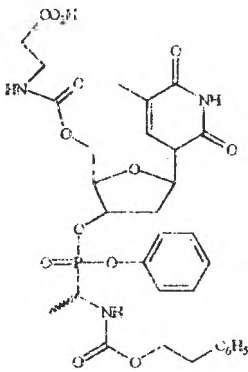
0.075  
pH 9.0  
(pH 9; 23°)  
10.86 (ester)  
37.05 (alcohol)

**Reaction 51 [12]**



0.075  
pH 9.0  
(pH 9; 23°)  
17.91 (ester)  
46.07 (alcohol)

**Reaction 52 [12]**



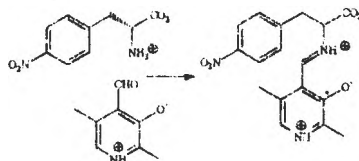
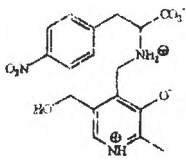
Reaction 53 [28]

0.075  
pH 9.0  
(pH 9; 23°)

17.91 (ester)

46.07  
(alcohol)

Imine formation



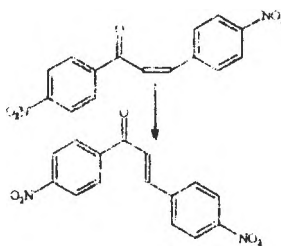
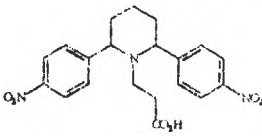
Reaction 54 [11]

0.21  
pH 9.0  
(pH 7 25°)

$2.5 \cdot 10^3$   
(aminoacid)

$4.2 \cdot 10^2$   
(piridoxal)

Cis - trans izomerisation:



Reaction 55 [44]

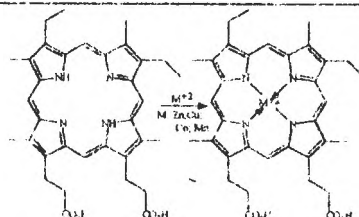
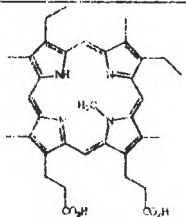
$k_{cat}/k_{uncat}$

$K_M (\mu\text{M}^{-1} \cdot \text{s}^{-1})$

$1.5 \cdot 10^4$   
pH 7.5; 25°

220

Metal chelation



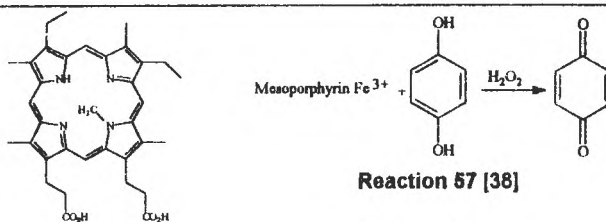
Reaction 56 [38]

Zn: 2600  
Cu: 1700

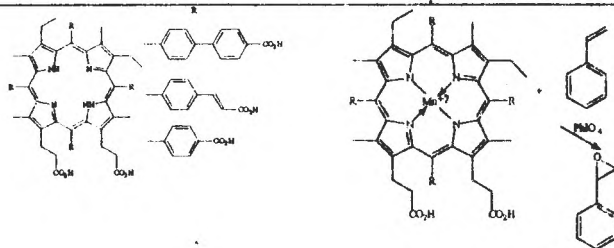
49  
50

## Catalytic antibodies

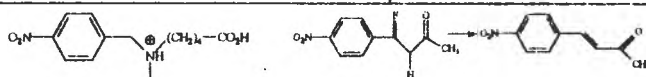
### Oxidation



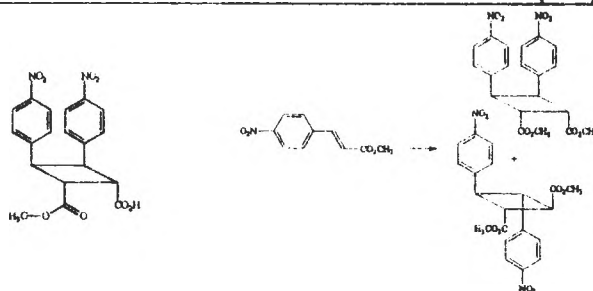
### Epoxidation



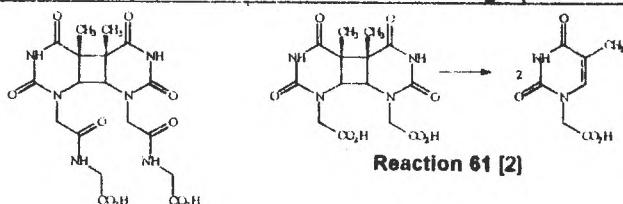
### Reaction 59 [2] β-elimination



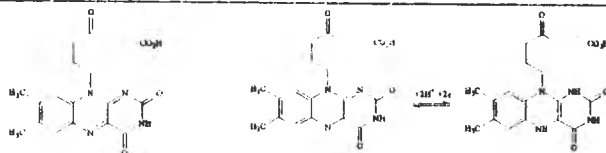
### Reaction 60 [2] Photoinduced dimerization (2+2)

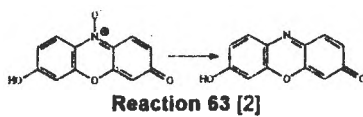
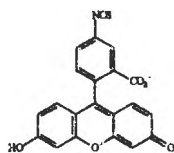


### Reaction 61 [2] Photoinduced cleavage (retro 2+2)



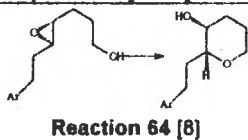
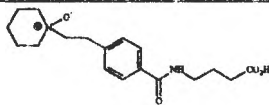
### Reaction 62 [2] Redox reactions





---

**Epoxide hydrolysis**



Book review

**Roger N. Reeve**, *Environmental Analysis*, John Wiley & Sons, Chichester, New York, 1994, 263 pages, ISBN 0 471 93833 5 (A book in the "Analytical Chemistry by Open Learning" Series).

Environment protection is not simply a fashionable subject nowadays, but it responds to real needs of mankind. Analytical chemistry is an important actor in this process, since it provides the knowledge and means required for the identification, quantitative measurement and monitoring of polluting agents in our water, soil and atmosphere. There is no wonder that in recent years a considerable number of books dealing with this subject have been published. Why then a new one ? The answer is simple: because it is different!

The book reviewed here is part of a series "Analytical Chemistry by Open Learning" and is designed for those studying in "a more flexible way than traditional institute attendance". As a result this book is conceived for self-training, clearly written, with simple explanations and provided with self-assessment questions and responses after each chapter. This is not intended to eliminate a study supervisor or tutor, but is of great help for the reader who tries to do by itself as much as possible of the study. Thus, the book starts with a short chapter explaining "*How to use an open learning book*", which contains good and useful advice. As one of the suggestions is to familiarize yourself with the book and flip through pages before really reading it, then comes the table of *Contents*, followed by a *Study Guide*, a list of suggested experiments as *Supporting Practical Work*, and *Bibliography*. Only after this introductory material is presented the book proceeds to discuss in detail its theme..



The subjects treated in a chapter each, are the following: Transport of pollutants in the environment; Water analysis - major constituents; Water analysis - trace pollutants; Analysis of solids; Atmospheric analysis - gases; Atmospheric analysis - particulates; and Ultra-trace analysis. Each group of analyses is clearly described, with attention paid to sampling, storage of samples, pretreatment, extraction and/or concentration of the analyte and the most recommended analytical methods and techniques.

The present reviewer feels that the book could be extremely useful not only for self-study, but also as teaching guide in traditional courses, in which a textbook like this, can be a useful link between the teacher and his (her) students. A good part of this book will be used by this reviewer in her course on Environmental analytical chemistry.

In our opinion books like this deserve a wide-spread distribution and even translation in other languages. In Eastern Europe environment pollution is a problem of great concern, and availability of a book like this can be regarded as an excellent type of assistance from western colleagues, which are more experienced in distance learning and have produced excellent teaching aids and textbooks for this purpose.

Iovanca Haiduc  
Chemistry Department  
"Babes-Bolyai" University  
RO-3400 Cluj-Napoca



In cel de al XL-lea an (1995) *Studia Universitatis Babeş-Bolyai* apare în următoarele serii:

matematică (trimestrial)  
fizică (semestrial)  
chimie (semestrial)  
geologie (semestrial)  
geografie (semestrial)  
biologie (semestrial)  
filozofie (semestrial)  
sociologie-politologie (semestrial)  
psihologie-pedagogie (semestrial)  
ştiinţe economice (semestrial)  
ştiinţe juridice (semestrial)  
istorie (semestrial)  
filologie (trimestrial)  
teologie ortodoxă (semestrial)  
educaţie fizică (semestrial)

In the XL-th year of its publication (1995) *Studia Universitatis Babeş-Bolyai* is issued in the following series:

mathematics (quarterly)  
physics (semesterily)  
chemistry (semesterily)  
geology (semesterily)  
geography (semesterily)  
biology (semesterily)  
philosophy (semesterily)  
sociology-politology (semesterily)  
psychology-pedagogy (semesterily)  
economic sciences (semesterily)  
juridical sciences (semesterily)  
history (semesterily)  
philology (quarterly)  
orthodox theology (semesterily)  
physical training (semesterily)

Dans sa XL-e année (1995) *Studia Universitatis Babeş-Bolyai* paraît dans les series suivantes:

mathematiques (trimestriellement)  
physique (semestriellement)  
chimie (semestriellement)  
géologie (semestriellement)  
géographie (semestriellement)  
biologie (semestriellement)  
philosophie (semestriellement)  
sociologie-politologie (semestriellement)  
psychologie-pédagogie (semestriellement)  
sciences économiques (semestriellement)  
sciences juridiques (semestriellement)  
histoire (semestriellement)  
philologie (trimestriellement)  
théologie orthodoxe (semestriellement)  
éducation physique (semestriellement)

43870